

**Development of T cell based therapeutic strategies for
childhood cancer neuroblastoma**

Aysha Patel

University College London

A dissertation submitted to University College London in
candidature for the degree of Doctor of Philosophy

2017

I, Aysha Patel, confirm that the work presented in this thesis is my own. Where information has been derived from other sources, I confirm that this has been indicated in the thesis.

Aysha Patel

Abstract

High risk neuroblastoma poses a significant clinical problem in paediatric oncology and new treatment strategies are needed. Antibody-derived bispecific T cell engagers (BiTEs) and chimeric antigen receptors (CARs) are novel treatment options that redirect a patient's own T cells to recognise and eliminate tumour cells; both have demonstrated promise in clinical trials for haematological malignancies. In this study I explored an empirical approach to BiTE design in order to identify the optimal format for redirecting T cell cytotoxicity against neuroblastoma cells. GD2 was used as a target antigen, based on its high level of expression across neuroblastoma tumours and limited expression on healthy tissues. BiTEs were designed with different single chain variable fragments (scFv) to bind GD2 and CD3 (T cell) antigens. We demonstrated that a high affinity for GD2 was determinant of improved cytotoxicity of T cells against neuroblastoma cell lines and an optimal linker length between the two scFvs impacted tumour cell targeting. The secretion of interferon- γ and proliferation by activated T cells occurred in a CD3-specific and GD2-specific manner, confirming target specificity of the BiTEs.

In a second strategy; as an attempt to reduce the on-target off-tumour toxicity of targeting GD2, novel antigen O-acetyl-GD2 was explored as an improved target antigen due to its restricted tumour expression pattern. The latter is a requirement when aiming to induce a persistent anti-tumour response with CAR T-cell therapy. An O-acetyl-GD2 specific CAR was generated which showed selective specificity to the O-acetylated form of GD2.

Finally, as a pre-clinical approach to develop BiTE and CAR T cell therapy for neuroblastoma *in vivo*, pilot experiments were performed in a transgenic neuroblastoma mouse model which has co-expression of the ALK^{F1174L} mutation and *MYCN* oncogene. This work indicated that this murine model appears suitable to develop T cell based immunotherapy into an effective therapeutic approach for neuroblastoma.

Acknowledgements

There are many people I am grateful to for their encouragement and support throughout the duration of this PhD project. First and foremost, I would like to thank my supervisor Dr Karin Straathof for allowing me to work under her supervision. Together with my supervisor Professor John Anderson who have both offered endless guidance, support and encouragement throughout my PhD. Thank you to Dr Martin Pule, who conceived many of the project ideas and has always offered guidance, resources and expertise.

Next, I would like to thank Christine Thevanesan, who has helped set up the assays and never-ending replicates for this project. I think we make a great team and the constant enthusiasm always kept the project going. Thank you to Giulia Agliardi and Jack Barton for performing the animal work. Also, a huge thank you to Ayad Eddaoudi and Stephanie Canning from the ICH Core Flow facility, for all their help and expertise with flow cytometry.

I would like to extend my thanks to the rest of the Straathof and Anderson labs, in particular to Anna Capsomidis, Yvonne Majani, Barry Flutter, Rebecca Wallace, Jon Fisher and Pierre Abramowski for making it an enjoyable four years. Thank you to members of the Cancer Institute who have always helped with troubleshooting and given project advice. Thank you to Jenny Yeung who has offered endless help and guidance on my project and to Gordon Cheung for helping me with all my cloning problems.

I would not be where I am today without the amazing support from my family. A special thank you to my mum and dad, for their unconditional love and on-going support throughout my studies and life in general. I feel fortunate to have the support of my sister Asma who, no matter what the time or the situation has always been there for me. Thank you to the rest of my family and friends for being truly amazing and supporting me through this journey. Last but definitely not least, I would like to thank my husband and best friend, Asjad. I could not have wished for a more loving, caring and supportive person to share my life with.

Contents

Abstract	3
Acknowledgements	4
List of Figures	11
List of Tables	14
Abbreviations	15
CHAPTER 1: INTRODUCTION	20
1.1 Childhood cancer neuroblastoma	21
1.1.1 Neuroblastoma genetic predisposition	21
1.1.2 Neuroblastoma staging system	22
1.1.3 Current treatment of high-risk neuroblastoma.....	25
1.1.4 Neuroblastoma cell surface antigens	27
1.2 Adaptive immunity: a focus on T cells.....	38
1.2.1 T cell development.....	38
1.2.2 TCR signalling.....	41
1.2.3 T cell activation	43
1.2.4 CD8 ⁺ T cell mediated cytotoxicity	44
1.2.5 Cancer immunoediting.....	47
1.3 Immunotherapy for neuroblastoma	49
1.3.1 Monoclonal antibody therapy	49
1.3.2 Redirected T cell-based therapy	51
1.3.2.1 Bispecific antibodies.....	52
1.3.2.1.1 Bispecific T cell engagers (BiTEs).....	55
1.3.2.2 Chimeric antigen receptors (CARs).....	59
1.3.2.3 Comparisons of BiTEs and CARs	62
1.4 Hypotheses	64

1.5 Aims and objectives	65
CHAPTER 2: MATERIALS AND METHODS	66
2.1 Reagents and Buffers.....	67
2.1.1 Reagents.....	67
2.2 Molecular biology techniques	70
2.2.1 SFG γ -retroviral vector for gene transfer.....	70
2.2.2 Construction of BiTE variants	74
2.2.2.1 Generation of scFvs by PCR assembly of overlapping nucleotides	75
2.2.2.2 Purification of PCR product	77
2.2.2.3 Amplification of assembled overlapping nucleotides by PCR	77
2.2.2.4 Detection of PCR product by agarose gel electrophoresis	77
2.2.3 Construction of anti-O-acetyl-GD2 specific antibody 8B6 heavy and light chains by overlap extension PCR	77
2.2.4 Digestion of PCR product or SFG vector using restriction endonucleases	79
2.2.5 Construction of GD2 and OAcGD2 specific CARs	80
2.2.6 DNA extraction from agarose gel.....	80
2.2.7 Ligation.....	80
2.2.8 Transformation of chemically competent Escherichia coli with plasmid DNA.....	80
2.2.9 Small scale plasmid preparation (Miniprep).....	81
2.2.10 Medium scale plasmid preparation (Midiprep)	81
2.2.11 Quantification of DNA	81
2.2.12 DNA sequencing.....	81
2.3 Cell culture techniques	82
2.3.1 Transient transfection of 293T cells	82
2.3.2 Retroviral vector production.....	82
2.3.3 Human peripheral blood mononuclear cell isolation.....	83
2.3.4 Activation and expansion of human T cells.....	83

2.3.5 Enrichment of human T cells.....	83
2.3.6 Production of Retronectin coated plates	84
2.3.7 Retroviral transduction	84
2.3.8 CD56 depletion.....	85
2.3.9 Labelling of cells with CFSE.....	85
2.3.10 Single cell cloning by limiting dilution	86
2.3.11 Large scale antibody production using a bioreactor	86
2.4 Protein purification and analysis	87
2.4.1 Protein purification	87
2.4.2 Quantification of protein.....	87
2.4.3 Dialysis of purified protein into PBS.....	87
2.4.4 Concentration and storage of purified protein	87
2.4.5 Preparation of protein samples for SDS-PAGE.....	88
2.4.6 Protein separation by SDS-PAGE	88
2.4.7 Coomassie Blue staining method.....	88
2.4.8 Protein transfer to nitrocellulose membrane.....	88
2.4.9 Western Blotting analysis	89
2.4.10 Protein thermal stability measurements using differential scanning fluorimetry	89
2.5 In vitro functional assays.....	90
2.5.1 Cytotoxicity assay by flow cytometry	90
2.5.2 T cell proliferation assay by flow cytometry	90
2.5.3 ⁵¹ Cr release cytotoxicity assay	91
2.5.4 Interferon gamma (IFN- γ) detection by ELISA	91
2.6 In vivo animal work	92
2.6.1 Animals.....	92
2.6.2 Total body irradiation	92
2.6.3 Intravenous injection of mice	92
2.6.4 Bioluminescence imaging of mice.....	92

2.6.5 Magnetic Resonance Imaging.....	92
2.7 Flow cytometry.....	93
2.7.1 Antibodies.....	93
2.7.2 Staining for cell surface markers	94
2.7.3 Measure of transfection/transduction by detection of eBFP2/eGFP2	94
2.7.4 Detection of BiTE staining to cell lines.....	94
2.7.5 Quantification of cell surface epitopes by flow cytometry.....	94
2.7.6 Disaggregation of tumours from ALK ^{F1174L} /MYCN transgenic mice.....	95
2.8 Statistical analysis	95
CHAPTER 3: RESULTS (I).....	96
3.1 Introduction	97
3.2 Results	100
3.2.1 Target validation on reference cell lines.....	100
3.2.2 Target validation on neuroblastoma cell lines	100
3.2.3 Target validation on primary neuroblastoma cell lines	104
3.2.4 Detection of GD2 and OAcGD2 on reference SupT1 cell lines using immunohistochemistry.....	108
3.2.5 Antigen quantification on reference and neuroblastoma cell lines.....	110
3.3 Discussion	116
CHAPTER 4: RESULTS (II).....	118
4.1 Introduction	119
4.1.1 Bispecific T cell Engagers (BiTE).....	119
4.1.2 Selection of GD2 specific scFvs.....	120
4.1.3 Selection of CD3 specific scFvs	121
4.1.4 Selection of a linker	122
4.2 Results	125
4.2.1 Cloning of 18 GD2/CD3 specific BiTE variants	125

4.2.2 BiTE production by transient transfection of 293T cells.....	125
4.2.3 BiTE purification using immobilised metal ion affinity chromatography (IMAC)	125
4.2.4 Measurement of BiTE thermal stability by differential scanning fluorimetry	
4.2.5 BiTEs have specificity for GD2 and CD3 antigens.....	138
4.3 Discussion	141
CHAPTER 5: RESULTS (III)	143
5.1 Introduction	144
5.2 Results	145
5.2.1 Set up of a flow cytometry based cytotoxicity assay.....	145
5.2.2 BiTEs redirect T cells to lyse GD2.SupT1 cells and not SupT1 cells	150
5.2.3 BiTEs mediate specific killing of neuroblastoma cells	153
5.2.4 T cells are activated and secrete IFN- γ upon co-culture with neuroblastoma cells and BiTEs	156
5.2.5 Cytokine production	158
5.2.6 T cells proliferate upon co-culture with neuroblastoma cells and BiTE ..	161
5.2.7 Neuroblastoma patient T cells are able to lyse GD2 ⁺ targets in the presence of BiTE	166
5.3 Discussion	168
CHAPTER 6: RESULTS (IV)	171
6.1 Introduction	172
6.2 Results	175
6.2.1 Recombinant mAb 8B6-IgG2a shows similar specificity for OAcGD2 as the parental mAb 8B6.....	175
6.2.2 8B6 mAb shows differential binding to GD2.SupT1 cells.....	178
6.2.3 OAcGD2 specific CAR T cells secrete IFN- γ and lyse OAcGD2 ⁺ cell lines	
6.3 Discussion	182

CHAPTER 7: RESULTS (V)	183
7.1 Introduction	184
7.1.1 Mouse model with overexpression of ALK ^{F1174L} /MYCN oncogenes	185
7.2 Results	187
7.2.1 ALK ^{F1174L} /MYCN tumours express neuroblastoma antigens GD2, OAcGD2 and ALK	187
7.2.2 Development of murine BiTEs targeting GD2 and CD3.....	190
7.2.3 Generation of murine CARs targeting GD2	192
7.2.4 Functional testing of GD2-specific murine CARs in vitro	192
7.2.5 GD2-specific CAR T cells migrate to the tumour site in vivo in ALK ^{F1174L} /MYCN transgenic mice	196
7.2.6 Effect of GD2-specific CAR T cells on tumour growth in vivo.....	200
7.3 Discussion	202
CHAPTER 8: DISCUSSION	203
8.1 Target validation of neuroblastoma antigens	205
8.2 Development of GD2/CD3 specific BiTEs	208
8.3 Novel targeting of OAcGD2 with CAR T cells	212
8.4 T cell therapy for solid tumours	213
8.5 Final conclusions	215
REFERENCES.....	216

List of Figures

Figure 1.1: Kaplan-Meier estimate of overall survival in neuroblastoma patients.	24
Figure 1.2: Kaplan–Meier estimates of overall survival of high-risk neuroblastoma patients treated with immunotherapy or standard therapy alone	26
Figure 1.3: Biosynthesis and structure of Disialoganglioside GD2.....	31
Figure 1.4: Structure of <i>O</i> AcGD2.....	34
Figure 1.5: Structure of anaplastic lymphoma kinase.....	37
Figure 1.6: $\alpha\beta$ -T cell development in the thymus	40
Figure 1.7: T cell receptor signalling	42
Figure 1.8: Formation of an immunological synapse.....	46
Figure 1.9: Two main bispecific antibody formats.	54
Figure 1.10: BiTE mediated immunological synapse formation between a T cell and tumour cell.	58
Figure 1.11: Evolution of Chimeric Antigen Receptors.	61
Figure 2.1: Engineering of γ -retroviral vector system.	72
Figure 2.2: Oncoretroviral SFG vector.	73
Figure 2.3: Construction of a DNA fragment by assembly PCR.....	76
Figure 2.4: Overlap extension PCR	78
Figure 3.1: An approach to target validation and quantification of neuroblastoma antigens.	99
Figure 3.2: Expression of neuroblastoma antigens on reference SupT1 cell lines ...	102
Figure 3.3: Expression of GD2, <i>O</i> AcGD2 and ALK on neuroblastoma cell lines. ..	103
Figure 3.4: Gating strategy for phenotyping of primary neuroblastoma cell lines by flow cytometry.	106
Figure 3.5: Antigen expression on primary neuroblastoma cell lines.....	107
Figure 3.6: Detection of GD2 and <i>O</i> AcGD2 on frozen cell lines by immunohistochemistry.....	109
Figure 3.7: Generation of low and high levels of antigen expression on reference cell lines.	110

Figure 3.8: Antigen expression quantified by interpolation of a standard curve generated using calibration beads with known antigen levels and MFI values.	112
Figure 3.9: GD2, OAcGD2 and ALK antigen density on reference SupT1 cell lines.	113
Figure 3.10: GD2, OAcGD2 and ALK density on neuroblastoma cell lines.....	115
Figure 4.1: Detection of eBFP expression in 293T cells transfected to express BiTE variants.	127
Figure 4.2: Determination of optimal imidazole concentration in elution buffer for maximum elution of BiTEs from His-Trap column.....	129
Figure 4.3: Confirmation of BiTE purification by Coomassie Blue staining on SDS-PAGE gel.	131
Figure 4.4: Confirmation of BiTE purification by Western Blot analysis.....	132
Figure 4.5: Thermal stability of BiTEs determined by differential scanning fluorimetry.....	135
Figure 4.6: Measurement of binding specificity of GD2/CD3 specific BiTEs to GD2.	139
Figure 4.7: Measurement of binding specificity of GD2/CD3 specific BiTEs to CD3.	140
Figure 5.1: T cell enrichment from healthy donor PBMCs	146
Figure 5.2: Measurement of target cell cytotoxicity by T cells after 16 hours co-culture using flow cytometry.	148
Figure 5.3: Measurement of target cell viability at different time points after co-culture with T cells and 0-1 $\mu\text{g/ml}$ BiTE.	149
Figure 5.4: Comparison of BiTE variants in mediating target cell death by T cells after 16 hours co-culture.	151
Figure 5.5: Comparison of the activity of BiTEs with different CD3 binders and different linkers.	153
Figure 5.6: GD2/CD3 BiTEs redirect T cell cytotoxicity to neuroblastoma cell lines.	155
Figure 5.7: Production of IFN- γ by activated T cells in the presence of GD2 ⁺ /GD2 ⁻ target cells and BiTE.....	157

Figure 5.8: Production of cytokines by activated T cells in the presence of GD2 ⁺ /GD2 ⁻ target cells and BiTE.....	160
Figure 5.9: Measure of T cell proliferation after co-culture with GD2 ⁺ Lan-1 cells and BiTE (0-1000 ng/ml).....	163
Figure 5.10: CD4 ⁺ T cell proliferation in response to co-culture with target cells and BiTE.....	164
Figure 5.11: CD8 ⁺ T cell proliferation in response to co-culture with target cells and BiTE.....	165
Figure 5.12: Patient T cells are redirected by BiTEs to lyse GD2 ⁺ tumour cells.	167
Figure 6.1: Production and purification of OAcGD2 specific mAb 8B6-IgG2a.	176
Figure 6.2: 8B6-IgG2a mAb has specificity to OAcGD2.....	177
Figure 6.3: OAcGD2 ⁺ and OAcGD2 ⁻ GD2.SupT1 cells obtained by fluorescence activated cell sorting.	178
Figure 6.4: Transduction of activated T cells to express CARs.....	180
Figure 6.5: OAcGD2-specific CAR T cells have specificity to OAcGD2.	181
Figure 7.1: Phenotyping of ALK ^{F1174L} /MYCN transgenic mouse tumours.....	188
Figure 7.2: GD2, OAcGD2 and ALK antigen expression on tumour samples from ALK ^{F1174L} /MYCN transgenic mice.....	189
Figure 7.3: Generation of murine BiTE constructs.....	191
Figure 7.4: Murine CAR expression vectors and transduction efficiencies.....	194
Figure 7.5: GD2-specific CAR T cells are cytotoxic to GD2.CT26 cells.....	195
Figure 7.6: Expression of GD2-specific MuK666 CAR in transduced splenocytes. Mouse s	196
Figure 7.7: Experimental timeline for GD2-specific CAR T cell administration and monitoring.....	198
Figure 7.8: Bioluminescence imaging (BLI) of GD2-specific CAR T cell treated mice.....	199
Figure 7.9: In vivo imaging of mice by MRI to monitor the effect of GD2-CAR T cell treatment on tumour growth.....	201

List of Tables

Table 1. 1 Candidate cell surface targets for MHC non-restricted immunotherapy of neuroblastoma	28
Table 2. 1 Buffers and solutions	68
Table 2. 2 Cell lines	69
Table 2. 3 Components of humanised BiTEs.....	74
Table 2. 4 Components of murine BiTEs.....	75
Table 2. 5 Antibodies and HRP-conjugates used for Western Blotting analysis.....	89
Table 2. 6 Antibodies used for flow cytometry.....	93
Table 3. 1 Summary of neuroblastoma tumour characteristics.....	105
Table 4. 1 Reported GD2 specific mAbs and corresponding binding affinities	120
Table 4. 2 CD3 specific mAbs and corresponding binding affinities	121
Table 4. 3 Linkers considered in the BiTE design	123
Table 4. 4 Structure of eighteen GD2/CD3 specific BiTE variations with short, medium or long linkers	126
Table 4.5 Yield of individual BiTEs obtained after purification	133
Table 4. 6 Melting temperature of BiTE variants (n=3)	137
Table 5. 1 Maximum percentage killing of GD2.SupT1 by T cells at 16 hours incubation (mean \pm SD)	150
Table 5. 2 BiTE EC ₅₀ values for killing of GD2.SupT1 cells by T cells at 16 hours incubation.....	152
Table 5. 3 BiTE EC ₅₀ (ng/mL) values for T cell proliferation after 6 days co-culture with target cells	162

Abbreviations

2-ME	2-mercaptoethanol
ADCC	Antibody dependent cell mediated cytotoxicity
ADCP	Antibody dependent cellular phagocytosis
ALK	Anaplastic lymphoma kinase
ALL	Acute lymphoblastic leukaemia
APC	Allophycocyanin
APC	Antigen presenting cell
Bio	Biotin
BiTE	Bispecific T cell engager
BLI	Bioluminescence imaging
BsAb	Bispecific antibody
CASD1	CAS1 domain containing 1
CAR	Chimeric antigen receptor
CD	Cluster of differentiation
CDC	Complement dependent cytotoxicity
CDR	Complementarity determining region
CERT	Ceramide transfer protein
CFSE	Carboxyfluorescein succinimidyl ester
CHO	Chinese Hamster Ovary
CNS	Central nervous system
CTL	Cytotoxic T lymphocyte
DAG	Diacylglycerol
DAPI	4',6-diamidino-2-phenylindole
DC	Dendritic cell
DD H ₂ O	Double distilled water
DMEM	Dulbeccos modified eagle medium
DN	Double negative
DNA	Deoxyribose nucleic acid
DNTP	Deoxynucleotide triphosphate

DP	Double positive
EBFP	Enhanced blue fluorescent protein
EBV	Epstein-Barr virus
ECMV	Encephalomyocarditis Virus
EDTA	Ethylamine diamine tetra acetic acid
EGFP	Enhanced green fluorescent protein
ELISA	Enzyme linked immunosorbent assay
EMA	European Medicines Agency
EpCAM	Epithelial cell adhesion molecule
ER	Endoplasmic reticulum
Fab	Fragment antigen binding
FACS	Fluorescence activated cell sorting
FAM150A	Family with sequence similarity 150A
FAM150B	Family with sequence similarity 150B
FBS	Foetal bovine serum
Fc	Fragment crystallisable
FCS	Foetal calf serum
FDA	Food and drug administration
FITC	Fluorescein isothiocyanate
Fp	Forward primer
GEM	Glycolipid enriched microdomain
GlcCer	Glucosyl ceramide
GMP	Good manufacturing practice
GM-CSF	Granulocyte macrophage colony stimulating factor
GOI	Gene of interest
GWAS	Genome wide association studies
HGF	Hepatocyte growth factor
His	Histidine
HLA	Human leukocyte antigen
HNG	IgG1 hinge region

HRP	Horseradish peroxidase
ICAM-1	Intercellular adhesion molecule 1
IFN- γ	Interferon gamma
Ig	Immunoglobulin
IL – 2	Interleukin-2
IMAC	Immobilised-metal affinity chromatography
IMDM	Iscoves modified Dulbecco medium
IP ₃	Inositol-trisphosphate
IRES	Internal ribosome entry site
ITAMs	Immune-receptor tyrosine-based activation motifs
Kb	Kilobases
KDa	Kilo Daltons
LB	Lysogeny broth
LBD	Ligand binding domain
LFA-1	Lymphocyte function-associated antigen 1
LTR	Long terminal repeat
Luc	Luciferase
MAb	Monoclonal antibody
MAP	Mitogen activated protein
MDSC	Myeloid derived suppressor cell
MHC	Major histocompatibility complex
MMLV	Maloney murine leukaemia virus
MOPS	3-(N-morpholino)propanesulfonic acid
MRD	Minimum residual disease
MRI	Magnetic resonance imaging
MYCN	V-Myc Avian Myelocytomatosis Viral Oncogene Neuroblastoma Derived Homolog
NB	Neuroblastoma
NCAM	Neural cell adhesion molecule
NFAT	Nuclear factor of activated T cells

NK	Natural killer
NKG2D	Natural-killer group 2, member D
NPM	Nucleolar phosphoprotein
OAcGD2	O-acetylated GD2
OAcGD3	O-acetylated GD3
ORF	Open reading frame
Ori	Origin of replication
PAMPs	Pathogen associated molecular patterns
PBMC	Peripheral blood mononuclear cell
PCR	Polymerase chain reaction
PE	Phycoerythrin
PI	Propidium iodide
PIP ₂	Phosphatidylinositol bisphosphate
PLC	Phospholipase C
PSA-NCAM	Polysialated neural cell adhesion molecule
Rp	Reverse primer
RTK	Receptor tyrosine kinase
scFv	Single chain variable fragment
SDS	Sodium dodecyl sulphate
SDS-PAGE	SDS-polyacrylamide gel electrophoresis
SMAC	Supramolecular activation cluster
SP	Single positive
TAA	Tumour associated antigen
TAE	Tris-acetate EDTA
TBS	Tris-buffered saline
TBS-T	Tris-buffered saline-Tween
TCR	T cell receptor
TGF- β	Transforming growth factor beta
T _m	Melting temperature
TM	Transmembrane domain

TNF	Tumour necrosis factor
UV	Ultraviolet
V _H	Variable heavy
V _L	Variable light
ZAP-70	Zeta-chain-associated-protein-70

CHAPTER 1:
INTRODUCTION

1.1 Childhood cancer neuroblastoma

Neuroblastoma is the most common extracranial solid tumour in childhood and the most frequently diagnosed neoplasm during infancy (Maris et al., 2007). The tumour arises from the aberrant growth of neural crest progenitor cells of the sympathetic nervous system. The most common sites of tumour origin tend to be the adrenal medulla of the kidney or paraspinal sympathetic ganglia and as a result tumours present as masses in the abdomen, chest or neck (Maris, 2010). Clinical manifestations of neuroblastoma can vary depending on the site of presentation and commonly include abdominal pain, weight loss, fatigue and bone pain (Adair et al., 1994). Neuroblastoma is most common in children under five years of age, with a median age of 17 months at diagnosis. The disease accounts for 7% of malignancies in patients younger than 15 years and is disproportionately related to around 15% of all paediatric oncology deaths due to a high rate of relapse after therapy (Smith, 2010).

1.1.1 Neuroblastoma genetic predisposition

A number of underlying genetic events drive neuroblastoma tumourigenesis. A small subset of neuroblastoma cases (1-2%) are inherited in an autosomal dominant pattern while the majority of cases are sporadic. Genome-wide association studies (GWAS) have identified a number of genomic loci which are significantly associated with neuroblastoma predisposition (Bosse, 2016). In particular, patients with metastatic disease harbour driver oncogenes that are essential in maintaining tumourigenicity in established tumours (Bosse, 2016). The most common focal genetic lesion in sporadic neuroblastoma is the amplification of the V-Myc Avian Myelocytomatosis Viral Oncogene Neuroblastoma Derived Homolog (*MYCN*) gene. *MYCN* amplification occurs in approximately 25% of cases and correlates with clinically aggressive advanced stage disease and treatment failure (Brodeur et al., 1984, Seeger et al., 1985). *MYCN* encodes a transcription factor which activates the transcription of downstream target genes involved in multiple cellular processes including proliferation (Tweddle et al., 2001), metastasis (Zaizen et al., 1993) and angiogenesis (Meitar et al., 1996). Although *MYCN* is a major oncogenic driver, there are currently

no clinical trials targeting *MYCN* directly due to the difficulty of developing molecular targeted therapies to transcription factors. Much attention is being directed to the therapeutic targeting of molecules that modulate the activities of this potent oncoprotein (Huang, 2013).

Gain-of-function mutations in the anaplastic lymphoma kinase (*ALK*) gene have been found in approximately 50% of familial and 7% of sporadic neuroblastoma cases (Mosse et al., 2008, Janoueix-Lerosey et al., 2008). *ALK* is a receptor tyrosine kinase (RTK) which acts as a major oncogenic driver by activating signal transduction pathways involved in proliferation, migration and cell survival as a result of kinase domain mutations (described further in section 1.1.4) (Soda et al., 2007). Several other genomic alterations including DNA ploidy and chromosomal gains and deletions impact patient prognosis (Bosse, 2016).

1.1.2 Neuroblastoma staging system

One of the hallmark features of neuroblastoma is the remarkable heterogeneity of the disease, this may account for the broad spectrum of clinical presentation, response to treatment and overall patient prognosis. In order to determine the appropriate level of therapy and care a patient will require; neuroblastoma is risk stratified into categories using the international neuroblastoma staging system. Prognostic factors taken into account include patient age at diagnosis, stage of disease, *MYCN* oncogene amplification, DNA ploidy and specific recurrent segmental chromosomal aberrations. Based on these factors patients are stratified into three broad categories, consisting of low risk, intermediate risk and high risk disease.

Low risk disease

Patients with low risk neuroblastoma lack *MYCN* amplification and have localised tumour which can mostly or completely be removed by surgery. The five year event-free survival rates are >85% and 75 – 85% for very low risk and low risk patients respectively. A unique group of neuroblastoma cases termed special neuroblastoma or stage MS (formally 4S) also fall into the low risk category. Metastases in stage 4MS neuroblastoma are restricted to the bone marrow, liver or skin. The uniqueness about

this sub-group is the spontaneous regression of the tumour and cure of the patient without the need of therapy.

Intermediate risk disease

Patients with intermediate risk disease lack *MYCN* amplification and include localised tumours in which < 50% of the tumour mass is removable by surgery and require additional chemotherapy. This group includes tumours that have started to spread to surrounding areas near the tumour or to other organs such as the bone marrow, liver or skin in children younger than 18 months. Patients typically have a 50 – 75% five-year event free survival.

High risk disease

At the time of diagnosis, up to 60% of cases are classified as high-risk due to metastatic disease and/or the presence of *MYCN* oncogene amplification. High risk disease is typically found in children 18 months or older. Despite intensive combination therapies available, the five-year even free survival for patients with high risk disease is less than 50% (**Figure 1.1**).

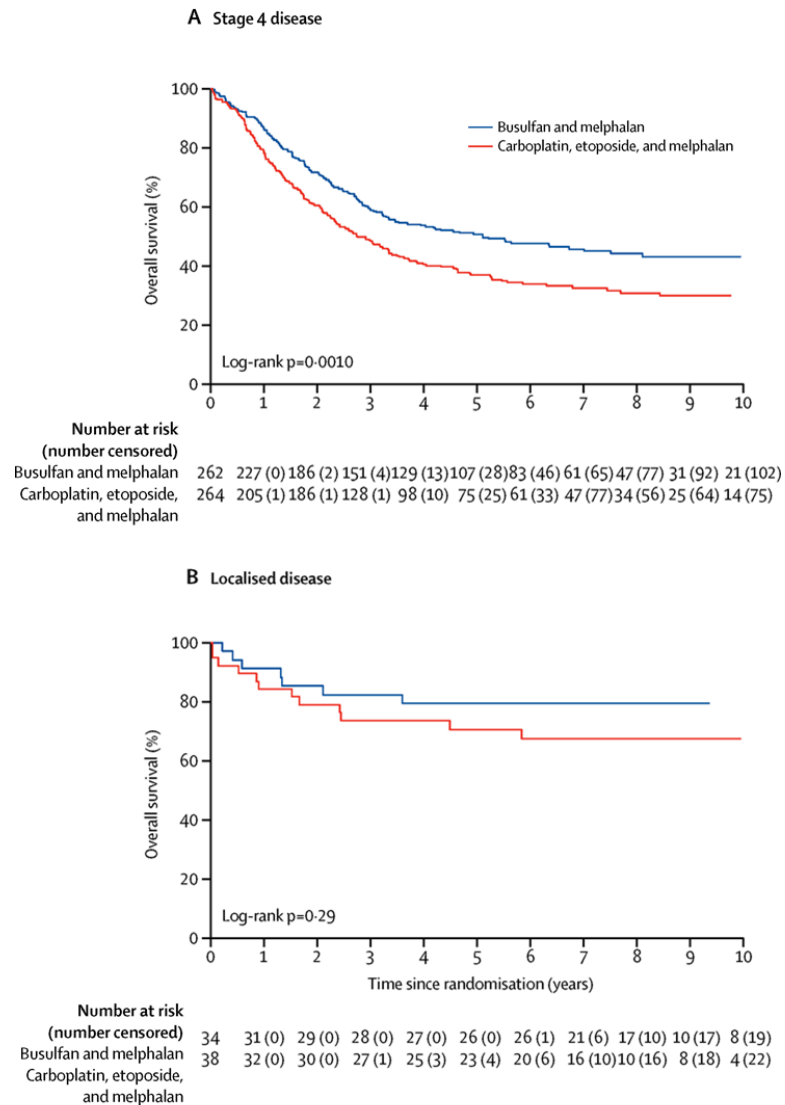


Figure 1.1: Kaplan-Meier estimate of overall survival in neuroblastoma patients. Overall 10 year survival of children with (A) Stage 4 (high risk) or (B) localised neuroblastoma after treatment with high dose chemotherapy with busulfan and melphalan compared with carboplatin, etoposide and melphalan. Figure taken from (Ladenstein et al., 2017).

1.1.3 Current treatment of high-risk neuroblastoma

High-risk neuroblastoma patients are treated with multi-modal therapies which each have their own associated toxicities. During the treatment regimen patients initially receive induction chemotherapy for a period of 4-6 months. This involves alternating regimens of several drugs including cisplatin and cyclophosphamide which help to reduce the size of the primary tumour and any metastatic lesions present. Following chemotherapy the tumour mass is removed by surgery. The patient then receives consolidation therapy involving high dose chemotherapy and radiation therapy to remove remaining cancerous cells. High dose chemotherapy has the side effect of destroying the bone marrow and so this treatment is followed by autologous haematopoietic stem cell transplantation which enables bone marrow recovery. The stem cells are normally harvested from the patient during induction chemotherapy.

Despite the majority of the tumour being removed with this multi-modal approach, low or undetectable levels of cancer cells that remain put the patient at risk of relapse. At this stage of minimum residual disease (MRD), two modes of maintenance therapies are available to sustain remission. Firstly, 13-cis retinoic acid (isotretinoin) is a vitamin A derivative which is taken orally over a period of 6 months. 13-cis retinoic acid induces differentiation of rapidly dividing neuroblastoma cells into mature nerve cells. However, greater than 40% of children develop recurrent disease during or after 13-cis retinoic acid treatment (Sonawane, 2014).

A second form of maintenance therapy is cancer immunotherapy which targets tumour cells using the immune system's cytotoxic mechanisms. Monoclonal antibodies (mAb) (described further in section 1.3) recognise tumour cells by detection of a specific cell surface antigen and upon binding to the antigen can initiate an anti-tumour immune response. In a randomised phase III clinical trial, high risk neuroblastoma patients treated with a mAb, ch14.18, specific for neuroblastoma antigen disialoganglioside GD2 and combined with the cytokines GM-CSF and IL-2 plus isotretinoin had a significantly improved event-free and overall survival compared to patients who received isotretinoin treatment alone (66% vs. 46% at 2 years) (Yu et al., 2010) (**Figure 1.2**). These results led to the regulatory approval of

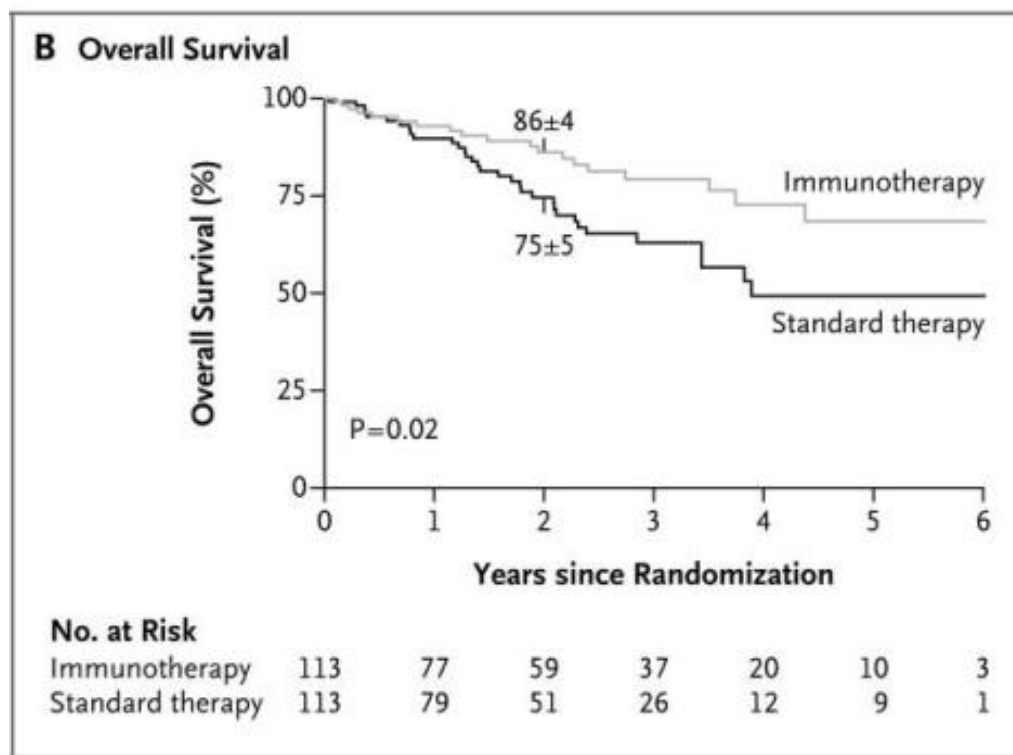


Figure 1.2: Kaplan–Meier estimates of overall survival of high-risk neuroblastoma patients treated with immunotherapy or standard therapy alone. Immunotherapy includes anti-GD2 mAb ch14.18, cytokines IL-2 and GM-CSF in addition to isotretinoin. Standard therapy includes isotretinoin alone. Taken from (Yu et al., 2010).

dinutuximab by the US Food and Drug Administration (FDA) and European Medicines Agency (EMA) in 2015 for treatment of patients with high-risk neuroblastoma. This treatment and associated side effects will be further discussed in section 1.3.

Clinical studies like this as well as others (Pule et al., 2008, Gargett et al., 2016) have highlighted the potential of harnessing the patient immune system in the treatment of neuroblastoma. Such tumour specific therapies require the presence of a cell surface antigen in abundance on the tumour cell with limited or absence of expression on normal and healthy tissues. The immune system is then manipulated to recognise the tumour cells through identification of a specific tumour antigen. The next section focusses on antigens specific to neuroblastoma which are favourable targets for immunotherapy.

1.1.4 Neuroblastoma cell surface antigens

Neuroblastoma cells have been shown to express defined tumour associated antigens which represent potential targets for immunotherapy. A discussion of all possible antigens expressed on neuroblastoma is beyond the scope of this thesis. **Table 1.1** provides a summary of selected antigens alongside their function and tumour vs. normal tissue expression. Antigens GD2, *O*-acetyl-GD2 and ALK which are abundantly expressed on neuroblastoma with limited or absence of expression on normal tissues are further described in this section.

Disialoganglioside GD2

The disialoganglioside GD2 is abundantly expressed on the surface of a broad spectrum of human cancers including neuroblastoma (Cheung et al., 1985), melanoma (Hersey et al., 1988), small cell lung cancer (Yoshida et al., 2001), glioblastoma (Longee et al., 1991), osteosarcoma and breast cancer (Chang et al., 1992, Orsi et al., 2017). The limited expression of GD2 in normal tissue, which is largely limited neurons (Marconi et al., 2005), skin melanocytes and peripheral nerve fibres makes GD2 a favourable target for cancer immunotherapy (Lammie et al., 1993).

Table 1. 1 Candidate cell surface targets for MHC non-restricted immunotherapy of neuroblastoma

Antigen	Function / description	Tumour expression (examples)	Normal expression	References
Disialoganglioside GD2	Sialic acid containing glycosphingolipid that functions to repair and maintain the nervous tissue	Neuroblastoma Melanoma Osteosarcoma Soft-tissue sarcoma Neuroectodermal tumours	Neuronal tissues (including peripheral sensory nerve fibres), melanocytes and the CNS	(Ohmi, Tajima et al. 2011) (Kushner et al 2011)
<i>O</i> -Acetyl GD2	Derived from a 9-O Acetyl post-translational modification of GD2. <i>O</i> AcGD2 is normally expressed during neuronal development, very little is known about its role.	Neuroblastoma Melanoma Osteosarcoma Soft-tissue sarcoma Neuroectodermal tumours	Faint expression on Purkinje cells, Bergmann glia cells in the cerebellum and dorsal horns in the spinal cord.	(Alvarez-Rueda, Desselle et al. 2011)(Fleurence et al., 2016)
Anaplastic lymphoma kinase (ALK)	A receptor tyrosine kinase expressed as a transmembrane protein during neuronal development. ALK is down regulated soon after birth.	Neuroblastoma Melanoma Glioblastoma Non-Hodgkin's lymphoma Neuroectodermal tumours	Restricted CNS expression limited to rare neurons, pericytes and endothelial cells.	(Webb, Slavish et al. 2009)
B7H3 (CD276)	Functions as both a T cell co-stimulator (through the TLT-2 receptor on CD8 T cells) and a T cell co-inhibitor.	Neuroblastoma Non-small cell lung cancer Prostate cancer	Mature dendritic cells	(Modak, Kramer et al. 2001)(Altan et al., 2017, Yuan et al., 2011)
PSA-NCAM	Cell surface glycan with a large hydrated volume that serves to modulate the distance between cells by promoting neural plasticity	Neuroblastoma Glioblastoma Small-cell lung carcinoma Renal cell carcinoma	Embryonic nervous system and adult nervous system including specific regions of the olfactory system, visual system and hypothalamus.	(Rutishauser 2008) (Bonfanti 2006)
L1CAM	Neural cell adhesion molecule. Plays an important role in nervous system development including neuronal migration and differentiation	Neuroblastoma Ovarian cancer Breast cancer Melanoma	Foetal brain Amniocyte Frontal cortex	(Novak-Hofer 2007)

GD2 is a sialic acid containing glycosphingolipid. The glycosphingolipid consists of a ceramide backbone made of sphingomyelin and cholesterol, which anchors GD2 into the plasma membrane. This lipid anchor enables the formation of membrane microdomains which play important roles in cell – cell communication and signal transduction. The oligosaccharide portion of the glycosphingolipid which contains two sialic acid residues is exposed as a pentasaccharide head group on the surface of the cell (Furukawa et al., 2002).

GD2 biosynthesis begins in the endoplasmic reticulum and involves the stepwise addition of monosaccharides to ceramide (**Figure 1.3 A**). The ceramide is synthesised first by the ceramide transfer protein, CERT, and is subsequently transferred to the Golgi apparatus where it is converted to glucosylceramide (Glc-Cer) by addition of a glucose sugar residue. Next, the addition of galactose to Glc-Cer forms lactosylceramide (Lac-Cer / Gal-GlcCer). This is the basic framework of the majority of gangliosides. Addition of a sialic acid residue to LacCer by sialyltransferase I, also called GM3 synthase forms GM3, an a-series ganglioside. A second sialic acid is then added by sialyltransferase II or GD3 synthase to form the b-series ganglioside GD3, the precursor of GD2. Finally, the addition of N-acetylneuraminic acid to LacCer by the enzyme GM2/GD2 synthase converts GD3 to GD2. Upon completion of synthesis, GD2 undergoes vesicle sorting and fusion with the plasma membrane (Suzuki and Cheung, 2015). The structure of GD2 is depicted in **Figure 1.3 B**.

In embryonic development, GD2 is involved in neural differentiation and proliferation, but the precise function of GD2 remains unclear. After birth, GD2 expression is limited to a few cell types and is thought to play a role in the maintenance and repair of nervous tissues in humans (Svennerholm et al., 1989). Ganglioside biosynthesis in tumour cells is controlled by a network of enzymes, the key members of which for induction of GD2 are GM2 and GD3 synthases and the availability of the precursor ganglioside lactosyl ceramide. Neuroblastoma cells have high levels of GM2/GD3 synthase transcripts and thus increased GD2 expression (Yamashiro et al., 1993). As a component of the glycolipid enriched microdomain (GEM) / rafts on the cell membrane, GD2 is able to promote proliferation, invasion

and motility in tumour cells by activation of tyrosine kinase signalling. In GD2 positive breast cancer, GD2 induces tyrosine phosphorylation of the hepatocyte growth factor (HGF) receptor in the absence of HGF, leading to the activation of c-Met, engaging MEK/ERK and PI3K/Akt pathways, resulting in increased proliferation and cell migration (Furukawa et al., 2012).

In osteosarcoma, GD2 induces the phosphorylation of either the focal adhesion kinase or Lyn kinase, a member of Src family of tyrosine kinases. This leads to the activation of paxillin, a signal transduction protein, and subsequently the inhibition of integrin-mediated cell adhesion resulting in enhanced cell migration (Shibuya et al., 2012). Given the abundant expression of GD2 on neuroblastoma, the interaction of GD2 with integrins in GEM / rafts is likely to be important for controlling the malignant potential of the disease (Wu et al., 2008).

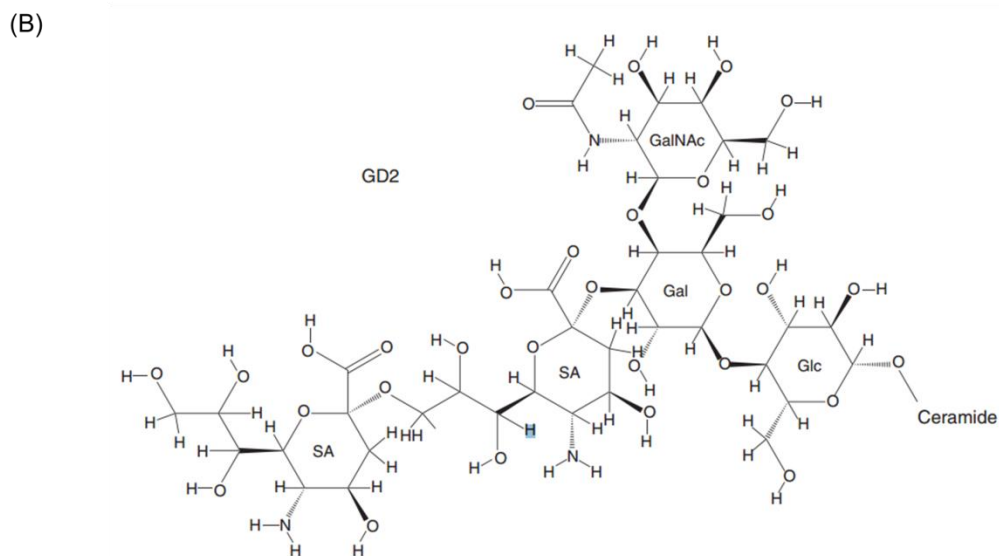
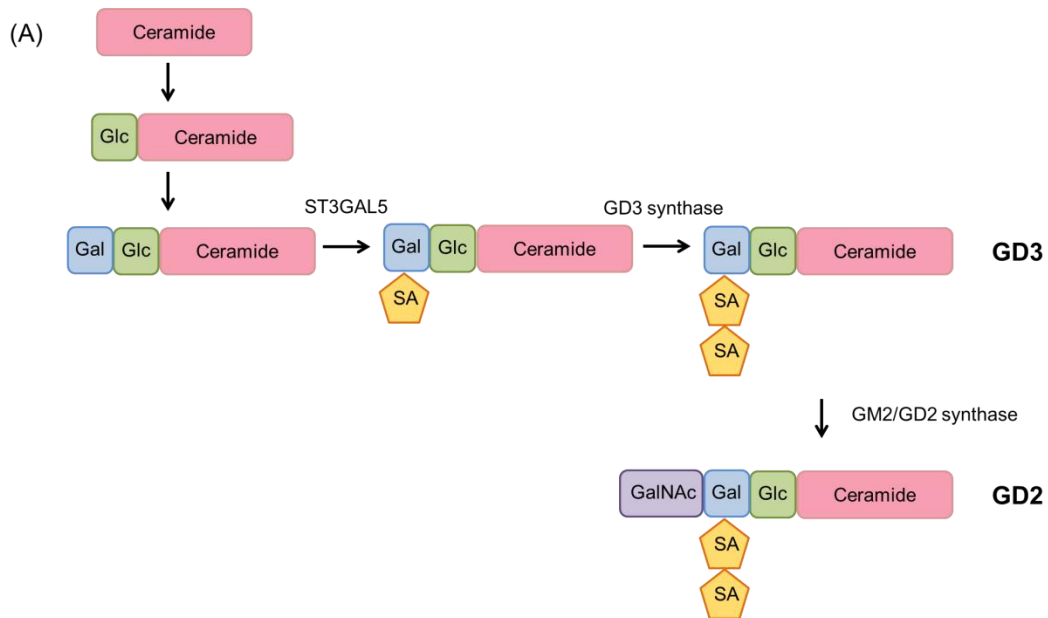


Figure 1.3: Biosynthesis and structure of Disialoganglioside GD2. (A) Biosynthesis of GD2 and (B) structure of GD2, Glc: glucose, Gal: galactose, SA: sialic acid, NAc: N-acetylneuraminic acid. Adapted from Suzuki and Cheung, 2015.

O-Acetyl-GD2

The accumulation of tumour-associated gangliosides in malignant cells is associated with aberrant acetylation of the sialic acid side chains. *O*-acetyl GD2 (*O*AcGD2) is the *O*-acetyl derivative of the GD2 ganglioside and is expressed alongside GD2 on the tumour cell surface (Ye and Cheung, 1992). The outer negatively charged α 2-8 linked sialic acid residue of GD2 is modified on the C7 and/or C9 hydroxyl group in the Golgi apparatus. The reaction is catalysed by the CASD1 sialate *O*-acetyltransferase via a covalent acetyl-enzyme intermediate (**Figure 1.4**) (Sjoberg et al., 1992, Arming et al., 2011, Baumann et al., 2015). The spontaneous migration of the *O*-acetyl group from the C7 to C9 position is observed when *O*-acetylated sialic acids are exposed to mild alkaline conditions. Thus it can be easy to lose the *O*-acetylation during sample collection and stringent control of buffer pH and temperature are required (Kamerling et al., 1987).

The *O*-acetyl group modifies a number of chemical properties of the ganglioside acceptor, such as a decrease in the polarity and hydrophobicity of the ganglioside but does not affect the overall conformation (Siebert, 1996). The synthesis of *O*AcGD2 can be regulated by the amount of acetyl CoA concentrations within the Golgi apparatus and as a result, the presence of GD2 and level of *O*-acetylation present on tumour cells varies. The ratio between the amounts of *O*AcGD2 to GD2 is between 10 - 50% (Higa et al., 1989, Kaneko et al., 2010).

The biological and functional roles of *O*AcGD2 are not yet known, however functional roles for *O*AcGD3 are well defined as *O*AcGD3 was the first identified member of the *O*-acetyl family. Understanding the roles of *O*AcGD3 may provide an insight into the roles of *O*AcGD2. Araujo *et al.* studied the impact of blocking *O*AcGD3 signalling on dorsal root ganglion neurons using the anti-*O*AcGD3 Jones mAb *in vitro*. The results indicated that blocking induced microtubule depolarisation both in growth cones and neurites and thus *O*AcGD3 was concluded to be involved in modulating growth cone motility and axonal branch formation (Araujo et al., 1997).

Further, the induction of O-acetylated sialoglycoproteins on lymphoblasts of childhood acute lymphoblastic leukaemia (ALL) cell lines promoted survival of lymphoblasts by preventing apoptosis (Erdmann et al., 2006, Mukherjee et al., 2007). Due to the close relation of the *OAcGD2* and *OAcGD3* gangliosides, it is likely that *OAcGD2* has similar roles in promoting tumour cell survival, although the mechanisms are not yet known.

Unlike *GD2*, *OAcGD2* is reportedly expressed on tumour tissue and not on peripheral nerves. Alvarez-Rueda *et al.* studied the distribution of *OAcGD2* expression across a range of malignant and healthy tissue samples by immunohistochemistry. *OAcGD2* expression was detected on 35/35 glioblastoma samples 12/12 *GD2* positive neuroblastoma samples and 3/4 melanoma and small cell lung cancer samples. On healthy tissue *GD2* expression was detected on 12 peripheral nerve samples tested whilst *OAcGD2* expression was not. Thirty-two other normal tissues recommended for screening by FDA guidelines, including the skin, spleen and brain were also negative for *OAcGD2* expression. Only a few cell types such as Purkinje cells, the Bergmann glia in the cerebellum, and the dorsal horns in the spinal cord showed faint staining for *OAcGD2*. The staining results indicated that targeting *OAcGD2* with immunotherapy may have a safer reactivity profile in comparison to targeting *GD2* by avoiding on-target off-tumour toxicities (Alvarez-Rueda et al., 2011, Fleurence et al., 2016).

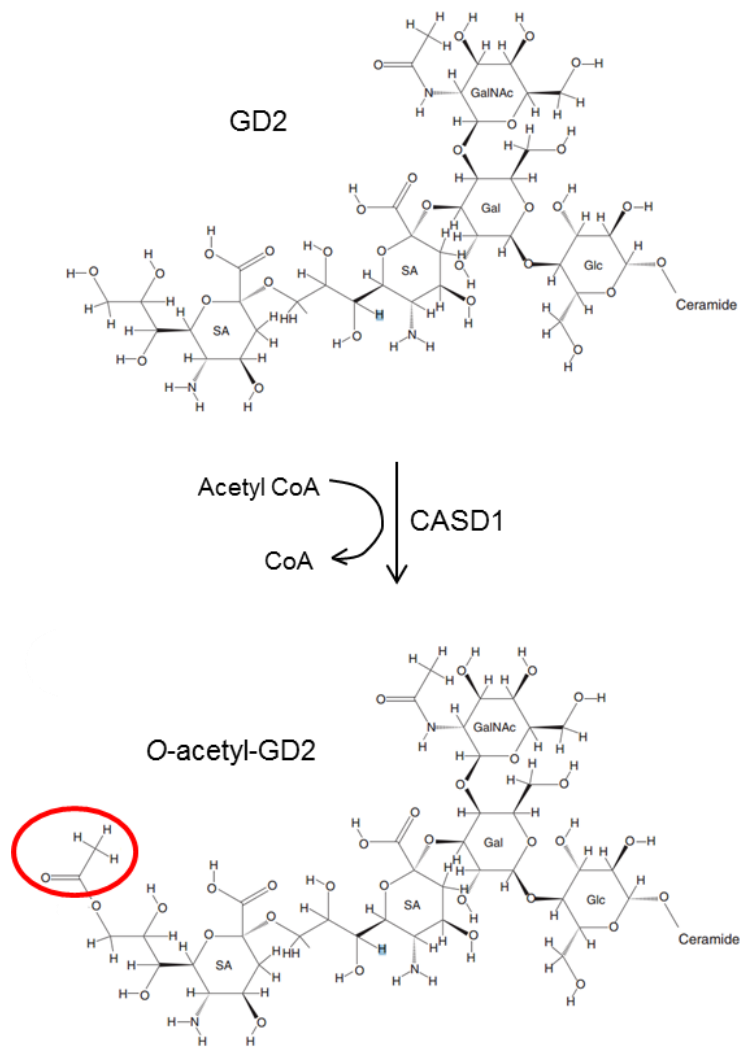


Figure 1.4: Structure of OAcGD2. *O*-acetylation of GD2 occurs on the outer sialic acid residue by the CASD1 sialate *O*-acetyltransferase via a covalent acetyl-enzyme intermediate. Glc: glucose, Gal: galactose, SA: sialic acid, NAc: N-acetylneuraminic acid, red circle: acetyl group. Adapted from (Suzuki and Cheung, 2015).

Anaplastic lymphoma kinase (ALK)

ALK is a RTK kinase belonging to the insulin receptor superfamily. ALK was first described as a fusion partner in the t(2;5)(p23;q35) chromosomal rearrangement. This rearrangement fuses the cytoplasmic domain of ALK to the N-terminal portion of the nucleolar phosphoprotein NPM in anaplastic large cell lymphoma (ALCL) (Morris et al., 1994). ALK was subsequently found to be rearranged, mutated or amplified in a series of tumours including lymphoma, neuroblastoma and non-small cell lung cancer (Soda et al., 2007).

The full length ALK RTK consists of an extracellular ligand-binding domain, a transmembrane domain and an intracellular tyrosine kinase domain (**Figure 1.5**) (Iwahara et al., 1997, Wellstein and Toretsky, 2011). ALK becomes activated only upon ligand-induced homo-dimerisation, and inactivated through de-phosphorylation by receptor protein tyrosine phosphatase beta and zeta complex (PTPRB/PTPRZ1) when there is no stimulation by a ligand. Reported ligands for ALK include the family with sequence similarity 150A (FAM150A) and family with sequence similarity 150B (FAM150B) (Guan et al., 2015). Proteins midkine and pleiotropin have also been reported as ligands of ALK, but this remains controversial (Perez-Pinera, 2007).

ALK is highly conserved across species and is transiently expressed in specific regions of the central and peripheral nervous systems and in the developing sympatho-adrenal lineage of the neural crest (Iwahara et al., 1997). Although the normal function of full length ALK is not entirely clear, mammalian ALK is believed to play roles in the development and function of the nervous system as mRNA is detected throughout the nervous system during mouse embryogenesis (Vernersson et al., 2006).

Dominant germline mutations in ALK have been identified in approximately 50% of familial neuroblastoma cases (Mosse et al., 2008). Three distinct germline mutations, R1275Q, R1192P and G1128A have been described, with R1275Q being the most frequent (Janoueix-Lerosey et al., 2008, Mosse et al., 2008). Additionally, somatic

activating mutations have been identified in conserved positions in the tyrosine kinase domain; and R1275 and F1174 are the two major mutational hotspots. Both are associated with constitutive phosphorylation of ALK and of downstream targets such as ERK, STAT2 and AKT leading to proliferation and differentiation (Chen et al., 2008). ALK is also amplified in the absence of mutations in approximately 2% of neuroblastoma cases (De Brouwer et al., 2010).

ALK may provide an ideal target for immunotherapy due to its reported expression on the cell surface of most neuroblastoma tumours and restricted distribution in normal tissues.

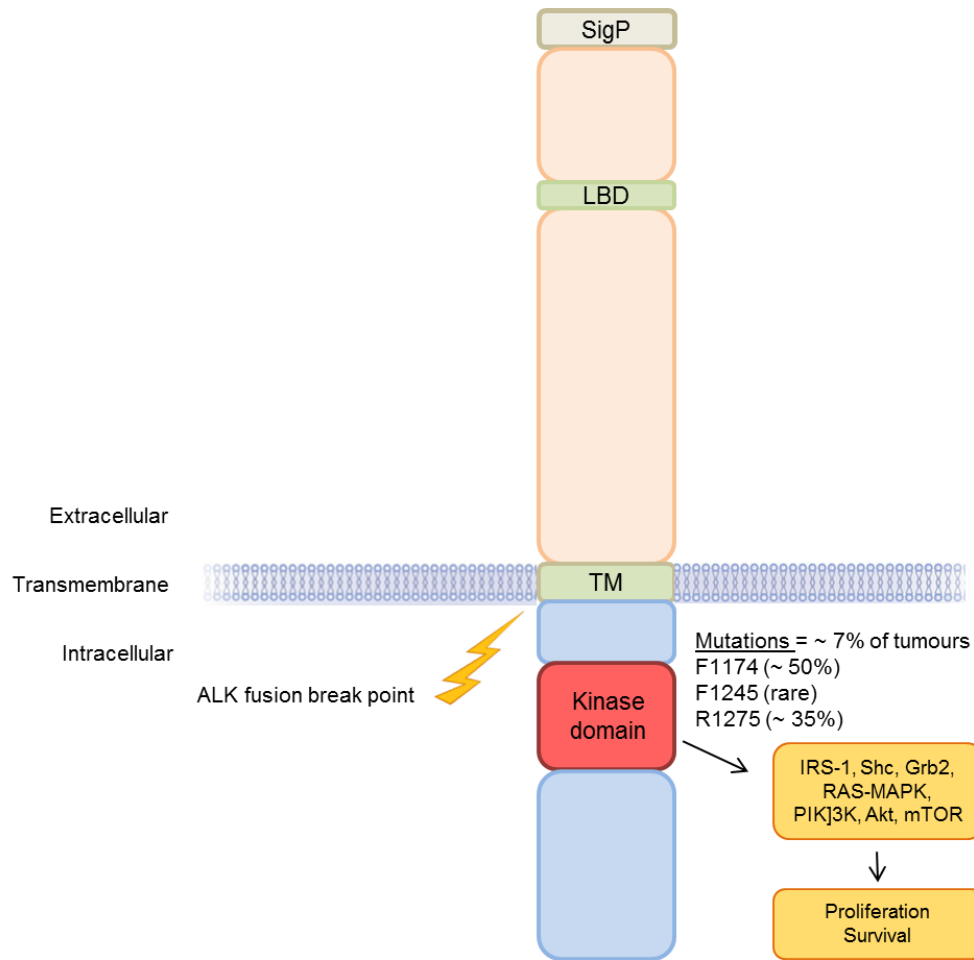


Figure 1.5: Structure of anaplastic lymphoma kinase. The RTK consists of an extracellular ligand binding domain (LBD), transmembrane domain (TM) and intracellular kinase domain. The major mutations found in the kinase domain and their relative frequencies are shown. Adapted from (Wellstein and Toretzky, 2011)

1.2 Adaptive immunity: a focus on T cells

The major aim of the work described in this thesis is to develop an improved immunotherapeutic approach for the treatment of high-risk neuroblastoma. Mechanisms employed by neuroblastoma tumours to actively avoid detection by the immune system and how this can be overcome through targeted therapy using T cells is described in the following sections, beginning with a focus on T cell development and function.

The human immune system comprises both innate (non-specific) and adaptive (specific) defence mechanisms to eliminate a wide variety of pathogens. One of the most important features of the immune system required for host defence is the ability to distinguish between the structural aspects of a pathogen (non-self) and its own host tissue (self). Whilst the innate arm specialises in the recognition and elimination of pathogens containing pathogen associated molecular patterns (PAMPs) (Medzhitov and Janeway, 2002), the adaptive arm comprises B and T lymphocytes which are capable of rearranging their genomic elements to create clonotypic antigen receptors (B and T cell receptors) that mediate humoral and cellular immune responses.

1.2.1 T cell development

The majority of peripheral T cells contain the $\alpha\beta$ T cell receptor (TCR) and are the main population of interest in the context of this thesis. $CD8^+$ T cells are cytotoxic lymphocytes which are capable of detecting and eliminating virally infected or neoplastic cells. $CD4^+$ T cells on the other hand, are helper T lymphocytes which can be classified into four subsets, Th1, Th2, Th17 and Thf and play a central role in immune protection. Major roles include their capacity to help B cells make antibodies and induce macrophages to develop enhanced microbial activity.

During T cell development (**Figure 1.6**), committed lymphoid progenitors arise in the bone marrow and migrate to the thymus (Scimone et al., 2006). Early committed T cells lack the expression of co-receptors CD4 and CD8 and are termed double negative (DN) thymocytes. These are subdivided into a further four stages (DN1 - DN4) based on the expression of the CD44 adhesion molecule and the CD25

interleukin-2 receptor chain (Aifantis et al., 2008, Naito et al., 2011). As cells progress through the DN2 - DN4 stages, they express the pre-TCR, composed of the non-rearranging pre-T α chain and a rearranged TCR β -chain (von Boehmer and Fehling, 1997).

Successful pre-TCR expression leads to substantial cell proliferation and transition to a double positive (DP) stage where cells have a CD4⁺CD8⁺ phenotype. DP cells subsequently undergo positive and negative selection by interacting with cortical epithelial cells that express a high density of MHC class I and class II molecules associated with self-peptides. Too little or too much signalling results in negative selection and apoptosis of the DP cell, while an intermediate level of signalling results in positive selection (von Boehmer et al., 1989). Thymocytes become single positive (SP) CD8⁺ T cells upon recognition of self-peptide-MHC class I complexes and become SP CD4⁺ T cells upon recognition of self-peptide-MHC class II complexes. T cells are then ready for migration out of the thymus to the peripheral lymphoid organs.

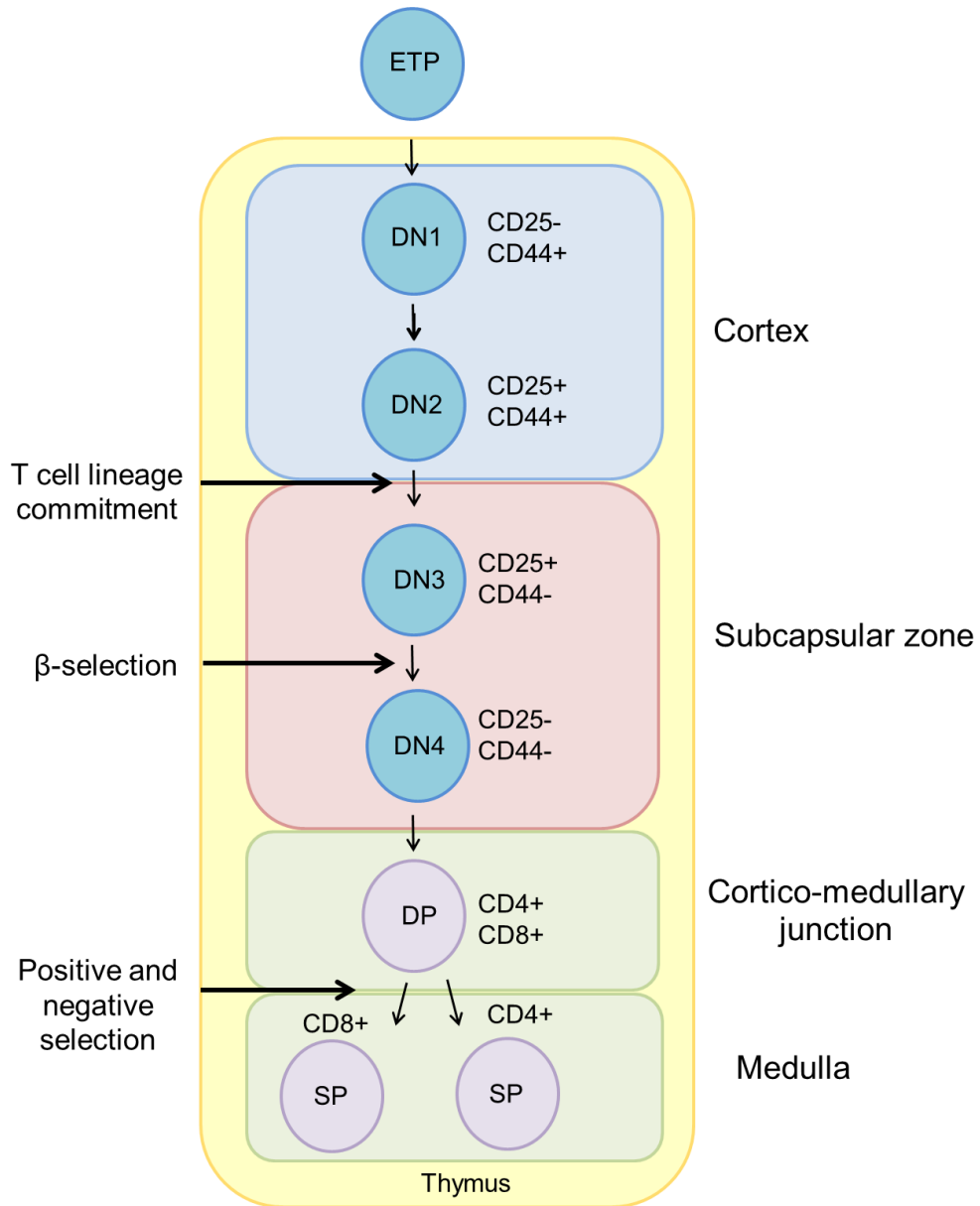


Figure 1.6: $\alpha\beta$ -T cell development in the thymus. Early thymocyte progenitors (ETP) undergo transition from double negative (DN) to double positive (DP) thymocytes through regulation of markers CD44, CD25, CD4 and CD8. Positive and negative selection tests thymocyte interaction with self-peptide-MHC complexes and further divides cells into single positive (SP) CD8⁺ or CD4⁺ T cells. Adapted from Fayard et al, 2010.

1.2.2 TCR signalling

The ability of T cells to respond to their specific antigen is central to adaptive immunity. Although the $\alpha\beta$ TCR has exquisite specificity to antigen, it is unable to initiate signalling within the T cell alone. The TCR is associated with invariant accessory proteins to form the TCR complex that initiates signalling when the receptor binds antigen. Together with signalling from co-receptors and co-stimulatory receptors, full lymphocyte activation can be achieved.

As part of the TCR complex the $\alpha\beta$ TCR heterodimer is associated with the CD3 signalling complex comprised of CD3 γ , CD3 δ and CD3 ϵ chains and the ζ chain which is present as a disulphide-linked heterodimer (**Figure 1.7**) (Janeway, 2001). The cytoplasmic regions of the CD3 ζ chains contain immune-receptor tyrosine-based activation motifs (ITAMs) which are phosphorylated by the lymphocyte specific protein tyrosine kinase Lck upon TCR engagement with peptide-MHC. Lck is found constitutively associated with the cytoplasmic regions of the CD4 and CD8 co-receptors which cluster to the TCR by binding invariant regions of the MHC molecule (Kersh et al., 1998).

Phosphorylated ITAM residues become docking sites for the tyrosine kinase ZAP-70 (ζ -chain-associated protein). Once ZAP-70 is recruited to the receptor complex, it is phosphorylated and activated by Lck (Chan et al., 1995). ZAP-70 is then able to phosphorylate both the scaffold protein LAT (linker of activated T cells), a transmembrane protein with a large cytoplasmic domain and another adaptor protein, SLP-76 which are then both linked by adaptor protein Gads. The subsequent steps in the T cell signalling pathway involve the activation of Phospholipase C- γ (PLC- γ), a key signalling protein. PLC- γ is recruited to the inner leaflet of the plasma membrane by binding to PIP₃ (formed by phosphorylation of PIP₂ by PI 3-kinase) where it is then able to bind to phosphorylated LAT and SLP-76 and is subsequently activated by the membrane-associated tyrosine ItK (Berg et al., 2005).

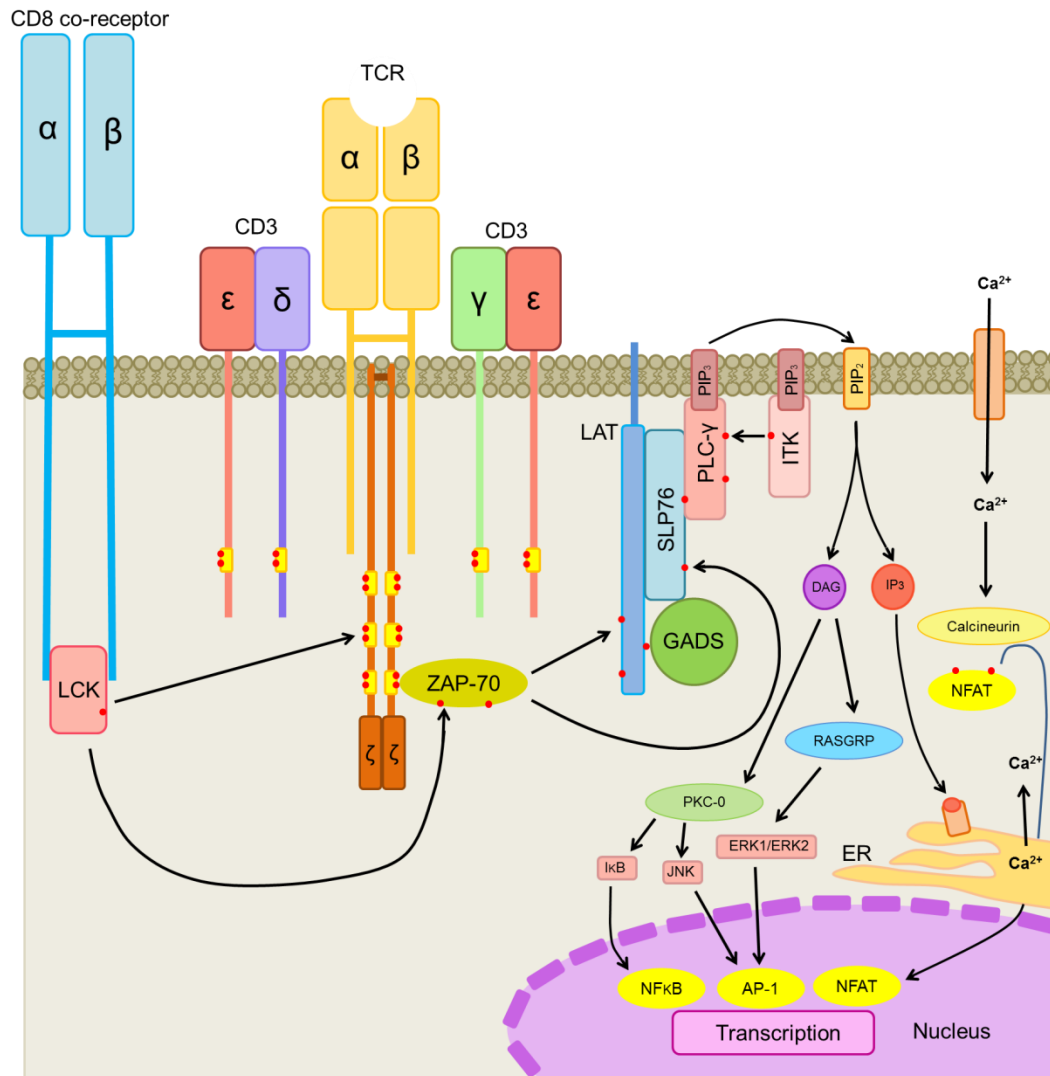


Figure 1.7: T cell receptor signalling. Upon engagement of a TCR with a peptide-MHC complex, Lck phosphorylates ITAMs on intracellular regions of CD3ζ chains, leading to recruitment and phosphorylation of ZAP-70. ZAP-70 in turn phosphorylates LAT and SLP76, to which PLC-γ binds and is activated by ITK. PIP₂ is cleaved by PLC-γ to yield IP₃ and DAG which subsequently lead to the translocation of NFκB, AP-1 and NFAT transcription factors in to the nucleus to induce gene transcription leading to cell proliferation and differentiation. Adapted from (Schwartzberg et al., 2005)

Activated PLC- γ cleaves phosphatidylinositol bisphosphate (PIP₂) to yield the membrane lipid diacylglycerol (DAG) and the diffusible second messenger inositol-trisphosphate (IP₃). This subsequently leads to three distinct branches of the TCR pathway. In one branch of the pathway, IP₃ diffuses through the cytosol and binds to ligand gated Ca²⁺ channels on the endoplasmic reticulum (ER) membrane. Ca²⁺ is released from membrane sequestered calcium stores, leading to a rapid increase in cytosol Ca²⁺ concentration. The cytosolic Ca²⁺ binds a ubiquitous calcium dependent regulatory protein called calmodulin, which in T cells targets the protein phosphatase calcineurin. Calcineurin dephosphorylates the NFAT (nuclear factor of activated T cells) transcription factor which then enters the nucleus and is able to turn on many genes crucial for T cell activation (Hogan et al., 2003).

A second branch of signalling leading from PLC- γ is activation of RasGRP by DAG. RasGRP is a guanine-nucleotide exchange factor which activates Ras and in turn activates the mitogen activated protein (MAP) kinase cascade. Erk is the final kinase of this pathway and acts indirectly to generate the AP-1 transcription factor. The third branch of signalling involves the activation of PKC- θ which activates the scaffold protein CARMA leading to the activation of the NF κ B transcription factor. All three transcription factors: NFAT, AP-1 and NF κ B induce specific gene transcription leading to cell proliferation and differentiation (Leevers and Marshall, 1992, Matsumoto et al., 2005).

1.2.3 T cell activation

Naïve T cells (which have not yet encountered antigen) require two signals delivered by antigen presenting cells (APC) for activation to occur. The interaction of TCR with peptide-MHC complex on the APC delivers signal 1 and secondary co-stimulation delivers signal 2. Signal 1 involves the activation of intracellular signalling pathways as described above, however signal 1 alone is not sufficient to activate a T cell and when delivered solely can result in T cell anergy (Valitutti, 2012).

For activation and proliferation to occur, co-stimulation is required and is achieved by engagement of T cells with co-stimulatory receptors on APCs. The two main receptor

families are: the CD28 family, including CD28 and ICOS, which interact with CD80/CD86 and B7-H2 and the TNF receptor superfamily including 41BB, CD27 and OX40 which interact with 4-1BBL, CD70 (CD27L) and OX40L on APCs. These signals enable a number of effects on the T cell including survival, effector function and memory formation. Upon antigen priming, resting naïve T cells undergo dramatic changes in metabolism and proliferation. Once a T cell is activated, signal 2 is no longer required upon subsequent encounter of antigen.

1.2.4 CD8⁺ T cell mediated cytotoxicity

Cytotoxic CD8⁺ T cells kill their target cells by inducing apoptosis (programmed cell death). To achieve this, T cells need to be in direct contact with their target cell through a TCR and peptide-MHC interaction and have efficient formation of an immunological synapse (**Figure 1.8**). The immunological synapse is also known as the supramolecular activation cluster (SMAC) which is composed of three concentric rings, each containing segregated clusters of proteins.

All nucleated cells express MHC class I molecules, which present processed intracellular peptide from pathogens that reside in the cytosol. Once the TCR engages a peptide-MHC complex, TCRs begin to cluster around the site of contact along with co-stimulatory receptors (e.g. CD28), tyrosine kinases (Lck and ZAP70), serine kinases (PKC- θ) and adaptor molecules (LAT, SLP76) to form the central-SMAC (cSMAC) (Varma et al., 2006, Monks et al., 1998).

Next, the binding of LFA-1 on T cells to ICAM-1 on APCs creates a molecular seal that surrounds the TCR and its co-receptor, this is known as the peripheral SMAC (pSMAC). The pSMAC is surrounded by a more distal ring (dSMAC), containing membrane proteins with large ectodomains such as phosphatases CD45 and CD148. The phosphatases are excluded from the synapse and allow TCR induced tyrosine phosphorylation to be initiated (Leupin et al., 2000).

The clustering of TCRs signals a reorientation of the cytoskeleton that polarises the CD8⁺ T cells and allows the release of pre-formed cytotoxic granules containing the cytotoxic proteins perforin and granzyme B. Perforin enables the formation of pores

in the target cell membrane and allows entry of granzyme B into the target cell. Granzyme B cleaves and activates caspase 3 to trigger a proteolytic cascade, ultimately leading to DNA degradation. Apoptotic cells are ingested by phagocytic cells which detect phosphatidylserine expressed on the outer leaflet of the plasma membrane (Heusel et al., 1994) . T cells also release cytokines such as IFN- γ and TNF- α . IFN- γ inhibits viral replication directly and induces the increased expression of MHC class I. Both IFN- γ and TNF- α recruit macrophages to the site of infection.

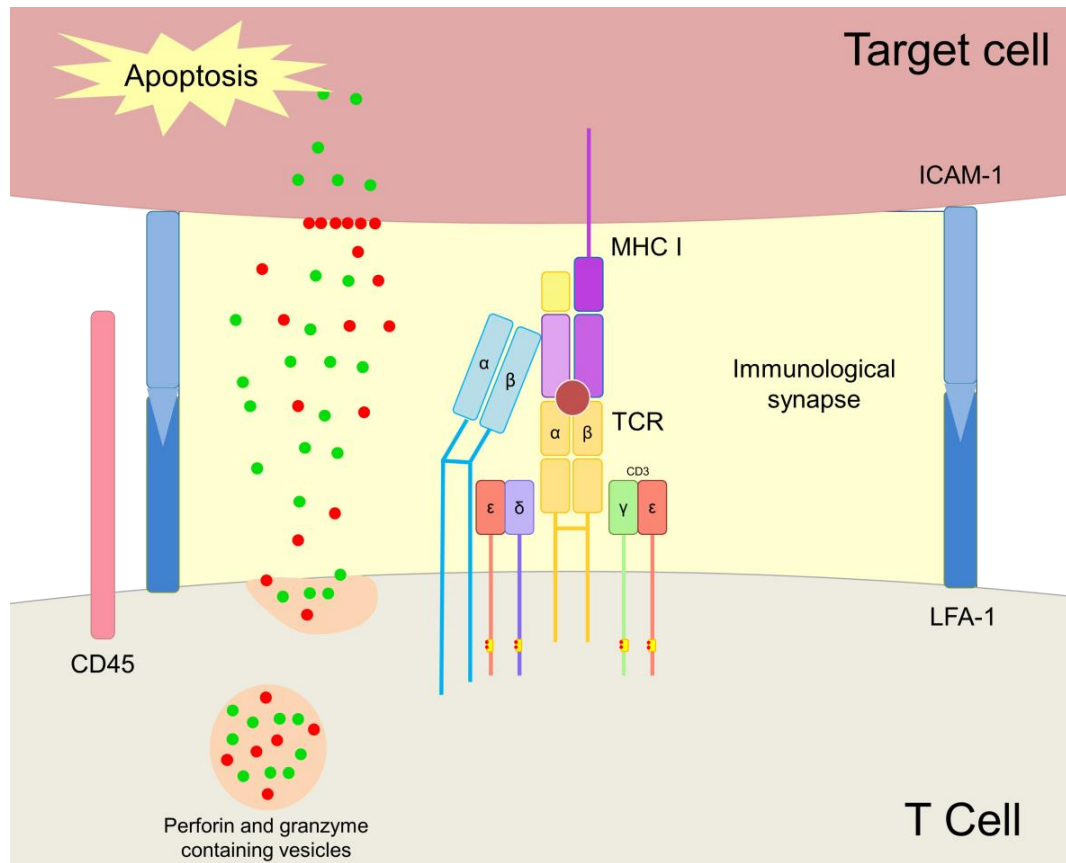


Figure 1.8: Formation of an immunological synapse. After a TCR binds to peptide-MHC, interactions between LFA-1 and ICAM-1, exclude larger phosphatases like CD45 from the forming synapse to allow sufficient downstream signalling. The synapse allows controlled release of perforin and granzymes from cytotoxic granules within the T cell to the target cell. Perforin forms pores in the target cell membrane and allows the entry of granzyme B which cleaves caspases and subsequently leads to DNA fragmentation and apoptosis of target cell.

1.2.5 Cancer immunoediting

The concept that the immune system is able to recognise and eliminate developing tumour cells was originally proposed by Burnet and Thomas in 1957. Now, several decades later, this concept has developed to appreciate the dual role the immune system plays in cancer, of not only suppressing tumour growth but also promoting tumour progression, and is termed cancer immunoediting (Dunn et al., 2002, Schreiber et al., 2011).

The importance of T cells in immune surveillance has been demonstrated by a number of studies showing that patients appear to live significantly longer if their tumours are infiltrated by T cells. A landmark study by Naito *et al.* analysed the distribution of CD8⁺ T cells within or around colorectal cancer cell populations and demonstrated that T cells specifically infiltrating cancer cell nests were most significantly associated with a better survival of patients (Naito et al., 1998). Subsequent studies in colon cancer, melanoma and ovarian cancer demonstrated the distribution patterns of infiltrating T cells were critical determinants of prognosis (Sato et al., 2005, van Houdt et al., 2008, Galon et al., 2006). In addition, there is a reportedly increased incidence of tumours in patients with primary immunodeficiency and those who are immunosuppressed after organ transplant (von Boehmer et al., 2013).

Despite the crucial role of T cells in eliminating tumour cells, the ability of T cells to recognise tumour antigens leads to immunological destruction or sculpting of the antigen, and thus promotes outgrowth of pre-existing clones that may not be recognised by T cells (Matsushita et al., 2012). A study of relapsed melanoma patients demonstrated that immunoediting occurs as a consequence of immunotherapy, resulting in absence of the initial target antigen in the relapsed tumour (von Boehmer et al., 2013).

The cancer immunoediting hypothesis is composed of three phases: Elimination; Equilibrium and Escape. During the elimination phase, both the innate and adaptive immune systems actively detect and destroy nascent transformed cells before they become clinically detectable. In the equilibrium phase, which is likely the longest

phase, the immune system and surviving tumour cell variants enter into a dynamic equilibrium in which tumour cells are maintained in a state of dormancy. In the escape phase tumours that have acquired the ability to circumvent immune recognition and or destruction through genetic or epigenetic changes, proliferate in an unrestricted manner leading to clinically apparent tumours (Schreiber et al., 2011).

Neuroblastoma escapes the immune system

Neuroblastoma cells have developed sophisticated mechanisms to evade detection by the host immune system. In particular, tumour cells down regulate HLA (MHC in humans) to evade T cell recognition (Raffaghello et al., 2005). Further, there is downregulation or release of NKG2D ligands, which bind the NKG2D activating immunoreceptor expressed by cytotoxic T cells and natural killer (NK) cells. NK cells belong to the innate arm of the immune system and are able to recognise and eliminate stressed or infected cells, independent of MHC expression (Raffaghello et al., 2004).

Neuroblastoma tumours have developed a highly immunosuppressive microenvironment. The production of pro-inflammatory cytokines such as membrane bound TNF- α , TGF- β and IL-10 enable recruitment of tumour associated macrophages which produce chemokines to disable infiltrating lymphocytes (Liu et al., 2012). Myeloid derived suppressor cells (MDSC) are a major component of the tumour microenvironment. MDSCs can use enzymes involved in L-arginine metabolism to deplete arginine from the tumour microenvironment (Mussai, 2015). L-arginine plays a central role in regulating cell cycle progression in T cells and is correlated with cell cycle arrest, impaired proliferation and reduced activation (Rodriguez et al., 2007, Zea et al., 2004).

In addition, neuroblastoma cells carry high levels of gangliosides on their surface which contribute to migration, adhesion and metastasis (Dong et al., 2011). Li *et al.* demonstrated that the presence of GD2 on the tumour surface has an immunosuppressive function. *In vivo* studies in mice showed that transplanted GD2⁺ tumour cells were not efficiently killed by the local immune system in comparison to

a GD2⁻ control and was due to downregulation of the cellular immune response (Li et al., 1996).

1.3 Immunotherapy for neuroblastoma

Immunotherapy has evolved over the last few decades as a tool to redirect and utilise the immune system to control and eliminate malignant cells. Both humoral and cellular components of the immune system can be employed to enhance an anti-cancer response through recognition of tumour associated antigens.

1.3.1 Monoclonal antibody therapy

An immunoglobulin is a four-chain structure consisting of two identical heavy and light chains. Fragment antigen binding (Fab) regions mediate antigen recognition through variable heavy (V_H) and variable light (V_L) chains containing hypervariable complementarity determining regions (CDRs). A fragment crystallisable (Fc) region interacts with cell surface receptors.

The advent of mAb production by Köhler and Milstein in 1975 paved the way for the development of novel and effective cancer immunotherapies. By 1997, FDA approval was given to the first mAb for the treatment of cancer (anti-CD20 Rituximab for non-Hodgkin's lymphoma); subsequently many other mAbs have been developed and received FDA approval.

Upon binding to a target antigen, mAbs can elicit multiple mechanisms to eliminate malignant cells. Apoptosis can be induced by the direct binding of a mAb to a tumour antigen. The Fc portion of the mAb is able to trigger complement dependent cytotoxicity (CDC), NK cell or myeloid cell mediated antibody dependent cell mediated cytotoxicity (ADCC) and monocyte mediated antibody dependent cellular phagocytosis (ADCP). Many tumour target antigen specific antibodies can bind target antigen but lack cytolytic capacity. In this scenario, antibodies can instead be used as a vehicle to deliver a payload to the cell, examples include antibody drug conjugates (Lode et al., 1998), immunotoxins and targeted nano-particles (Thomas et al., 2002, Pastorino et al., 2013).

GD2 as a target antigen for monoclonal antibody therapy

In the treatment of neuroblastoma, GD2 has been used as a successful target antigen in mAb therapy for over two decades. A number of GD2-specific mAbs have been developed and tested in clinical trials, details of various anti-GD2 mAbs that have recently been under pre-clinical or clinical testing are reviewed by Ahmed and Cheung, 2013. The first anti-GD2 mAbs to be tested in patients with neuroblastoma were of murine nature and elicited human anti-mouse antibody (HAMA) responses, which limited dose escalations and compromised the clinical efficacy of the therapeutic.

Chimerisation and/or humanisation efforts were made to overcome the intrinsic immunogenicity of murine-based mAbs. Chimerisation involves the engraftment of the antibody binding domains ($V_H - V_L$) on to human IgG constant domains leading to a significant reduction in immunogenicity. However, HAMA responses can still occur due to the murine antibody variable regions. Humanisation involves engraftment of the complementarity determining regions (CDR), directly involved in antigen recognition, and a few structurally significant residues (if necessary) on to human IgG constant domains. One of the limitations of this approach is often a reduction in avidity, however this is not always significant.

To date the most significant clinical results in mAb therapy for neuroblastoma have been seen with a chimeric anti-GD2 mAb: ch14.18 (dinutuximab). As described earlier, high-risk neuroblastoma patients treated with immunotherapy (ch14.18 mAb, IL-2, GM-CSF) and isotretinoin in a randomised phase III clinical trial had an improved event-free and overall survival compared to patients who received isotretinoin treatment alone (Yu et al., 2010).

Toxicities associated with GD2 targeted mAbs

Treatment with anti-GD2 mAbs is often associated with acute toxicities. Within the ch14.18 mAb phase III trial, the main toxicity associated with antibody treatment was pain in over a third of patients, the abdomen being the most common site of pain. Non-target antigen related side effects included fever, hypotension and capillary leak

syndrome in the treated group compared with minimal side effects observed in the group receiving standard therapy. These toxicities were more severe when mAb therapy was combined with IL-2 (Yu et al., 2010). A recent study also reported that 3 high-risk neuroblastoma patients receiving dinutuximab developed transverse myelitis during or after the second cycle of immunotherapy. The study theorised this was possibly due to an anti-idiotypic reaction, patients were discontinued from dinutuximab therapy and recovered after receiving corticosteroid therapy (Ding et al., 2017).

The acute toxicities associated with anti-GD2 mAbs are thought to be due to the on-target off-tumour binding of mAbs to GD2-positive sensitive nerve fibres, followed by complement activation. The complement cascade involves the production of inflammatory peptides which increase the symptoms of pain. In an attempt to reduce complement activation, Sorkin *et al* have shown that the specific point mutation K332A in the Fc region of the humanised form of mAb 14.18 (hu14.18) resulted in a significant reduction in antibody induced pain in a rat model. Further studies in rats have demonstrated that complement activation can be avoided by disruption of the binding of C1q by the Fc portion of the antibody through incubation of the antibody at 56 °C for 30 minutes (Sorkin et al., 2010).

1.3.2 Redirected T cell-based therapy

Several strategies have been used to enhance the efficacy of antibody-based immunotherapy. In particular, the antigen specific portion of a mAb ($V_H - V_L$) can be expressed as a single polypeptide chain by joining V_H and V_L with a short flexible linker to form a single chain variable fragment (scFv). The scFv can be used to redirect T cell specificity to tumour cells and will be the focus of the remainder of this thesis.

There are a number of advantages of using T cells as an effective tool for cancer therapy, these include: (1) The specificity of the T cell response through the native receptor or an engineered antigen specificity allows potential differentiation between healthy and cancerous cells; 2) Following activation in response to antigen, there is a robust clonal expansion; 3) T cells are able to infiltrate effectively throughout the

body and identify areas where the antigen of interest is expressed; 4) Memory T cells are able to mount an antigen specific response upon re-encounter of the antigen at a later time point, resulting in ongoing tumour surveillance.

1.3.2.1 Bispecific antibodies

Bispecific antibodies (bsAb) are bivalent molecules which combine the specificities of two mAbs to enable simultaneous binding of two antigens located on different cell types. Their most promising use is their ability to redirect T cells to recognise and eliminate tumour cells.

There are three methods for producing bispecific antibodies: 1) chemically cross-linking by chemical conjugation 2) fusion of two different hybridoma cell lines by quadroma technology and 3) genetic approaches using recombinant DNA technology (Graziano and Guptill, 2004, Milstein and Cuello, 1983). The latter approach has yielded the greatest range of bsAbs through artificial manipulation of genes and represents the most diverse approach for bsAb generation. This method overcomes some of the limitations of the former approaches, including purity, large scale production of homogeneous batches, poor stability and decreased avidity of the antibodies.

BsAbs largely fall into two main categories: IgG-like and small bispecific formats, a comprehensive description of all formats is beyond the scope of this work. Both trifunctional antibodies (triomabs) which are an IgG-like format and bispecific T cell engagers (BiTEs) which represent a type of small bispecific format were the two earliest types of bsAb to yield responses in clinical trials (**Figure 1.9**).

Trifunctional antibodies combine the halves of two separate mAbs, ideally a tumour antigen specific mAb and CD3-specific mAb. They have the ability to engage the tumour cell, T cell and through the Fc region, Fc receptor expressing cells such as NK cells and macrophages, combining both innate and adaptive immunity. Catumaxomab combines a rat anti-human CD3 Fab with a murine anti-human EpCAM Fab resulting in a rat/murine Fc fusion. Catumaxomab received clinical approval in 2009 and has

been licensed for malignant ascites for patients with EpCAM positive tumours (Seimetz et al., 2010).

Surek is a GD2 and CD3 specific trifunctional antibody. Initial studies of Surek were unable to demonstrate activity similar to catomaxomab. Further studies identified the requirement of dendritic cells (DC) in order to improve tumour rejection in murine melanoma models, with the proposal of combining both Surek and DC based vaccines as a vaccination strategy (Ruf et al., 2012, Deppisch et al., 2015).

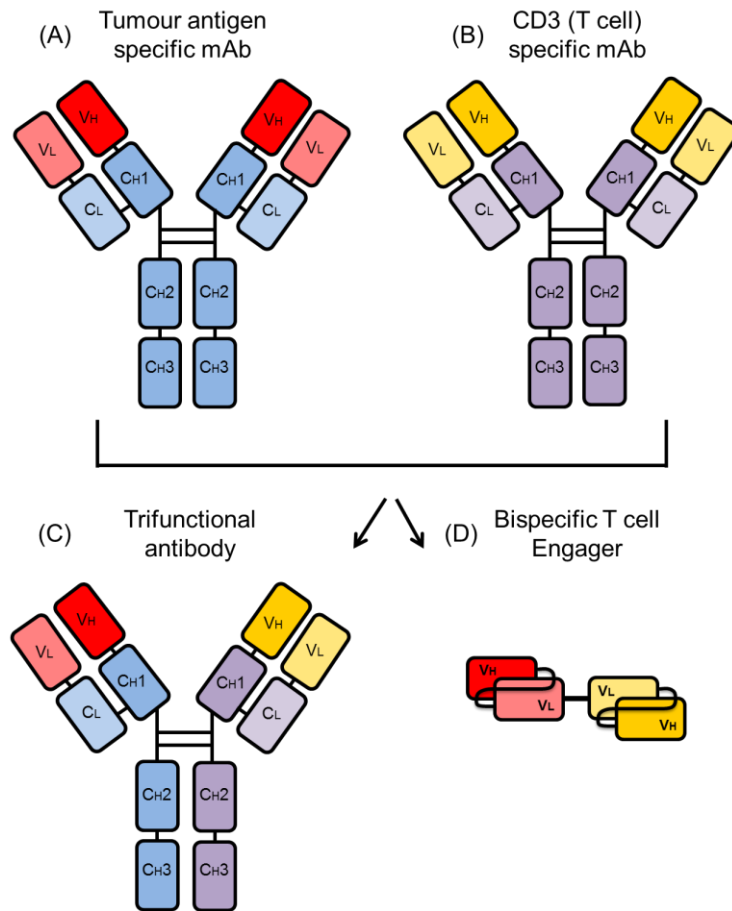


Figure 1.9: Two main bispecific antibody formats. (A) A tumour antigen-specific mAb and (B) a CD3-specific mAb are combined to form (C) a trifunctional antibody. (D) A Bispecific T cell Engager is derived from combining the variable regions of two mAbs in the form of single chain variable fragments.

1.3.2.1.1 Bispecific T cell engagers (BiTEs)

BiTEs are bivalent molecules that combine the specificity of two mAbs in the form of tandem scFvs linked by a short flexible linker. The entire BiTE is expressed as a single polypeptide chain and is approximately 55 kDa in size. One scFv has specificity for a tumour antigen and the second scFv has specificity for the invariant CD3 ϵ component of the TCR signalling complex on T cells. By simultaneously binding to both antigens, BiTEs can bring T cells and target cells into close proximity, resulting in T cell activation, proliferation and T cell induced target cell lysis. Out of the plethora of recombinant CD3 bsAb formats that exist, BiTEs have demonstrated the most promising efficacy in their ability to redirect T cells (Byrne *et al.*, 2013).

BiTEs are able to redirect both CD4⁺ and CD8⁺ T cell subpopulations (with the exception of naïve T cells) in a polyclonal manner without the requirement of co-stimulation. CD28 co-stimulation is thought to be fundamental for early activation of naïve T cells; but of less significance in memory and effector T cell responses. Although the reason for lack of co-stimulation requirement is unclear, one possibility is that BiTEs lead to an increase in the number of TCRs clustering with the induced immunological synapse, triggering more potent signalling than with physiological TCR engagement (Huehls, 2015). Another explanation is that memory T cells may be the predominant effector cells in BiTE mediated cytotoxicity. Dreier *et al.* have demonstrated that CD8⁺/CD45A⁺ naïve T cells do not mediate tumour cell lysis in the presence of BiTE while CD8⁺/CD45O⁺ memory T cells respond rapidly in the presence of BiTE (Dreier *et al.*, 2002).

BiTE constructs bypass MHC I restriction and thus may overcome some of the evasion mechanisms commonly employed by tumour cells. Brandl *et al.* demonstrated that upon engagement of BiTE with resting peripheral T cells, there is upregulation of activation markers CD69 and CD25 on the cell surface, upregulation of cell adhesion molecules such as CD2 and the transient release of inflammatory cytokines such as IFN- γ , TNF α , IL-2, IL-6 and IL-10. Moreover, this can be achieved at low nanomolar concentrations, without the need for co-stimulation (Brandl *et al.*,

2007). BiTE-mediated T cell activation is only observed in the presence of target cells expressing the antigen of interest and is one of the hallmark features of the therapeutic.

Upon engagement of T cells with tumour cells, the BiTE is able to mediate the formation of an immunological synapse (**Figure 1.10**). Hoffmann *et al.* used video-assisted microscopy to further understand the mechanism of T cell engagement by BiTE. Individual T cells were highly motile and able to serially eliminate multiple target cells, inducing nuclear fragmentation and membrane blebbing after a few hours of co-culture. The binding of BiTE antibody to target cells alone was not sufficient to lead to tumour cell death and specifically required the presence of cytotoxic T cells expressing granzymes and perforin (Hoffmann *et al.*, 2005).

Gruen *et al.* also demonstrated that cytotoxic T cells were the main mediators of tumour cell killing after engagement with BiTE antibody. The study showed that the presence of an extracellular calcium chelator in co-culture medium was able to prevent BiTE mediated tumour cell lysis by T cells. Calcium ions are needed for both T cell signalling and assembly of perforin subunits into functional pores after their secretion, suggesting that redirected lysis predominantly lies in cytotoxic vesicle fusion by T cells (Gruen *et al.*, 2004).

The benchmark BiTE: blinatumomab

Blinatumomab is a CD19/CD3 specific BiTE which received FDA approval in 2014 for the treatment of relapsed and/or refractory Philadelphia chromosome negative acute lymphoblastic leukaemia (ALL). The initial *in vitro* studies performed with blinatumomab demonstrated the half maximal concentration for redirected lysis of CD19⁺ target cells was 10-100 pg/mL *in vitro*, which was unprecedented for any other type of bsAb format at the time (Dreier *et al.*, 2002).

Initial phase I clinical trials involved short intravenous infusions of blinatumomab to treat patients with CD19⁺ malignancies such as non-Hodgkin's lymphoma. However, clinical studies were terminated early due to toxicity, mainly neurotoxicity which were caused by T cell cytokine release (Nagorsen *et al.*, 2012). Further studies

involved continuous infusion to sustain plasma levels of blinatumomab and balance the rapid on-going clearance. A dosing strategy was used to determine the maximum tolerated dose (MTD) alongside treatment with corticosteroids to manage toxicities.

Subsequently, a phase I clinical trial of adults with relapsed non-Hodgkin's lymphoma (NHL) showed a 69% overall response rate (Goebeler et al., 2013). More recently a large randomised phase III trial named the TOWER study demonstrated that a subset of ALL patients treated with blinatumomab had a significantly longer overall survival compared to patients who received standard of care chemotherapy (Kantarjian et al., 2017). BiTEs targeting solid tumours are also in clinical development (Fiedler et al., 2012, De Vries et al., 2015).

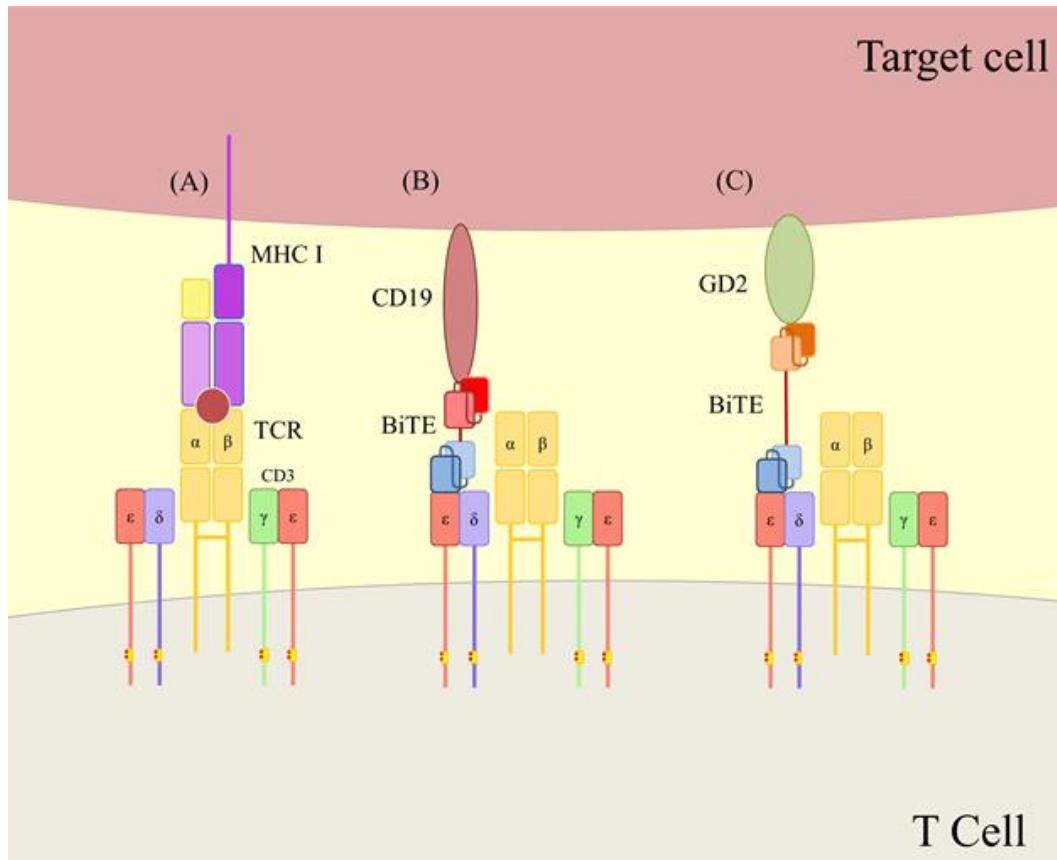


Figure 1.10: BiTE mediated immunological synapse formation between a T cell and tumour cell. T cell mediated tumour cell lysis through formation of a cytolytic immunological synapse induced by TCR/peptide-MHC interaction (A) or BiTE action (B and C). Variations in BiTE linker length may facilitate optimal synapse formation for different target antigens.

1.3.2.2 Chimeric antigen receptors (CARs)

Chimeric antigen receptors (CARs) are artificial T cell receptors which combine an scFv against a tumour associated antigen with the intracellular activation domain of the TCR. These receptors are transduced into T cells and are able to recognise intact membrane antigens irrespective of MHC restriction or antigen processing. Upon binding to their ligand, CAR transduced T cells are activated in a similar way to that of the endogenous TCR. CARs typically consist of four components:

- 1) An antigen binding domain: A scFv derived from the variable portion of an antibody, the choice of scFv can vary in affinity or antigen epitopes recognised, which can lead to marked differences in the immunological properties of the CARs (Chmielewski et al., 2004, Hudecek et al., 2013).
- 2) Linker/spacer region: The linker anchors the scFv to the membrane and mediates the formation of a synapse between a CAR and target cell, this is influenced by the scFv's epitope location and the spacer region, relative to the distance from the tumour cell's plasma membrane (Hudecek et al., 2013). The length and flexibility has implications for antigen engagement and clustering of the CARs, longer linkers may allow access to membrane proximal epitopes which may not be accessible to shorter linkers (Moritz and Groner, 1995, Hombach et al., 2000, Guest et al., 2005).
- 3) Transmembrane domain: This is normally derived from the linker or membrane-proximal endodomain. The transmembrane domain is responsible for keeping the CAR membrane bound and for stable CAR expression (Bridgeman et al., 2010).
- 4) Intracellular activation domain: Required to initiate downstream signalling and T cell activation as described below.

Evolution of CAR generations

The first generation of CARs contained CD3 ζ as part of their intracellular activation domain. These proved to be sufficient to induce signals with similar potency to normal TCR/CD3 signalling. Initial clinical outcomes however were disappointing due to the failure of the CAR expressing T cells to persist in the recipient (Till et al.,

2008). This was likely due to the inadequate signal strength provided by the CD3 ζ endodomain alone.

To enable effective activation and T cell proliferation, co-stimulation was necessary. The fusion of the CD3 ζ chain and the cytoplasmic portions of co-stimulatory receptors including CD28, 4-1BB and OX40 led to the creation of second and third generation CARs (**Figure 1.11**). The CD28 signalling domain was first introduced as a co-stimulatory moiety and demonstrated that T cells transduced with this construct showed enhanced activation, proliferation and cytokine production by CAR T cells *in vitro* (Finney et al., 1998, Friedmann-Morvinski et al., 2005).

The most successful demonstration of a CAR based immunotherapy to date has been in the treatment of CD19⁺ B cell tumours. In a Phase I/IIA study, T cells expressing a second generation anti-CD19 CAR bearing CD3 ζ and 41BB induced complete remission in 90% of relapsed ALL patients, with responses sustained over 6 months in 67% of patients (Maude et al., 2014).

The first GD2 specific CAR was developed by Rossig *et al.* based on an scFv derived from mAb 14G2a and was tested in a Phase I clinical trial (Pule et al., 2008, Louis et al., 2011). The trial evaluated a first-generation GD2-specific CAR in children with relapsed/refractory neuroblastoma and compared safety, persistence and anti-tumour persistence of two effector cell populations: activated T cells (ATC) and Epstein-Barr virus specific cytotoxic T lymphocytes (EBV-CTLs) (Pule et al., 2008). No dose limiting toxicity was found, the therapy was well tolerated, and some patients had long-term complete tumour regression. The GD2-CAR expressing EBV-CTLs persisted significantly longer and were associated with better anti-tumour efficacy (Louis et al., 2011).

Given the limited persistence of adoptively transferred GD2 CAR T cells, development of second and third generation CARs consisting of additional co-stimulatory domains have shown the ability to release cytokines, proliferate and kill tumour cells *in vitro* (Ahmed and Cheung, 2014, Thomas et al., 2016).

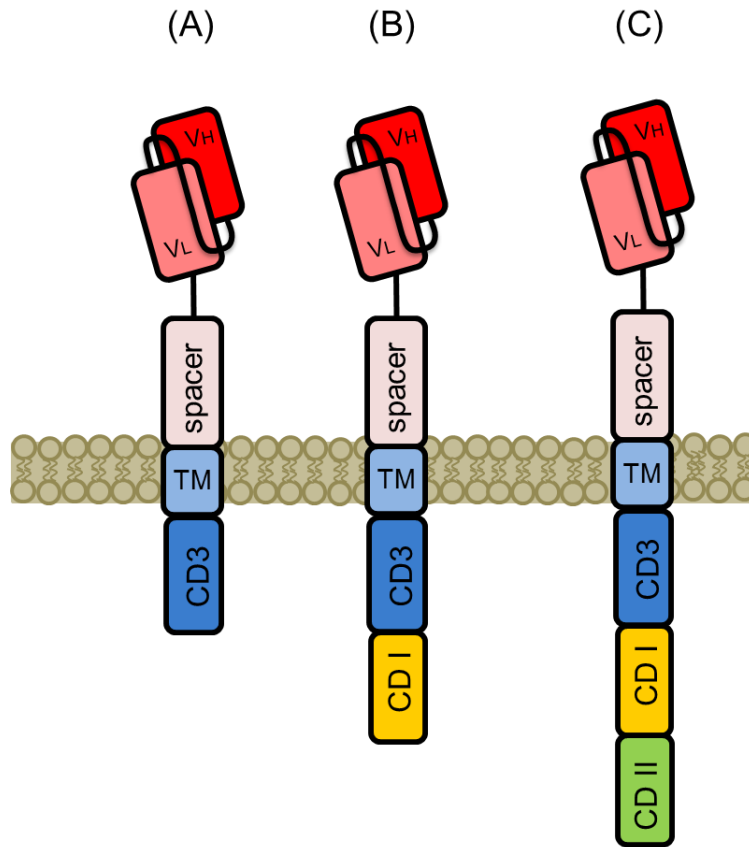


Figure 1.11: Evolution of Chimeric Antigen Receptors. (A) First generation CARs incorporate a CD3 ζ activation domain. (B) Second generation CARs additionally have a costimulatory domain (CD I), either CD28 or 4-1BB. (C) Third generation CARs have two co-stimulatory domains CD28/4-1BB/OX-40. TM: transmembrane domain.

1.3.2.3 Comparisons of BiTEs and CARs

Both BiTE and CAR therapeutics are evolving technologies that have demonstrated promise in the clinical setting, in particular with haematological malignancies. Due to the differences in therapeutic strategy and production; both have unique advantages that may be optimal for treatment of a particular disease setting, such as solid tumour or MRD. Compared to CARs, BiTEs have the advantage of being easier to produce as a readily available off-the-shelf therapeutic. The production of CAR T cells requires the use of Good Manufacturing Practice (GMP) facilities and bespoke manufacture for each patient. If CAR T cells demonstrate promising clinical efficacy, this may outweigh many manufacturing issues.

The small size of BiTEs gives the potential to infiltrate solid tumours and redirect resident lymphocytes to mediate cytotoxicity. Infiltrating lymphocytes may however be tolerised or exhausted under conditions of the tumour microenvironment. Conversely, adoptively transferred CAR-expressing T cells are conditioned *in vitro*, away from tolerising influences and could be further transformed to deliver immunostimulatory factors upon activation to counteract tumour mediated-immunosuppression. Although one of the great advantages of CARs is the potential long-term persistence of effector T cells, the short half-life of BiTEs may also serve as a safety mechanism allowing immediate therapeutic withdrawal in the event of treatment related toxicity.

The choice of therapeutic for a particular disease setting (i.e. liquid vs solid tumour or localised vs. metastatic disease) can be influenced by numerous factors including choice of target tumour antigen. Stone *et al.* performed a direct comparison of the *in vitro* sensitivity of BiTEs and CARs directed against a tumour-specific glycopeptide epitope on the transmembrane glycoprotein OTS8. The study demonstrated that CAR T cells had greater sensitivity to a low number of epitopes per target cell in comparison to BiTE-targeted T cells. The study concluded that CARs might be an appropriate therapeutic for tumour specific epitopes, when epitope densities are low, or when down regulation of targeted epitopes is known to limit effectiveness (Stone *et al.*, 2012).

In contrast, BiTE based approaches may be best used in scenarios where a particular therapeutic window is available to select between normal and malignant cells. Other studies have demonstrated that the avidity of CAR transduced T cells is also determined by the density of CAR expression on the T cells. High levels of CAR expression lead to T cells being triggered by both low and high expressed tumour antigens, whereas low levels of CAR expression lead to CAR T cells being unable to lyse the target cells (Walker et al., 2017).

1.4 Hypotheses

The overarching aim of this project is to investigate both BiTE and CAR T cell mediated immunotherapy for neuroblastoma by targeting the GD2 or *OAcGD2* antigens. For the design of a BiTE we hypothesise that the binding affinity of GD2 and CD3 specific scFvs will impact T cell mediated tumour cell lysis. Firstly, a low-affinity CD3-specific scFv may resemble natural peptide:MHC-TCR interactions while a high-affinity GD2 specific scFv will ensure optimal tumour cell specific binding. In addition, we hypothesise that the length of the linker between the GD2 and CD3-specific scFvs will influence the formation of an optimal immunological synapse between the T cell and tumour cell, and the optimal linker length of the linker may be influenced by the size of the tumour target antigen. As a second strategy, to avoid on-target off-tumour toxicity associated with targeting GD2, we hypothesise that *OAcGD2* may serve as a more tumour specific target antigen which will be tested using CAR T cell therapy.

1.5 Aims and objectives

1. To investigate the expression of neuroblastoma antigens GD2, *OAcGD2* and ALK on neuroblastoma cell lines and patient derived primary neuroblastoma cell lines in order to explore the clinical utility of targeting these antigens.
2. To determine the optimal format of a GD2 and CD3 targeted BiTE by comparing BiTE production, stability, T cell-mediated cytolytic function, T cell proliferation and cytokine release.
3. To explore novel antigen *OAcGD2* as a target for immunotherapy using a CAR approach.
4. To develop a suitable *in vivo* model of neuroblastoma to study T cell based immunotherapy approaches.

Chapter 3 details an approach to target validation of neuroblastoma antigens. Chapter 4 describes the design, production, purification and characterisation of GD2 and CD3 targeted BiTEs. Chapter 5 describes the *in vitro* functional comparisons of different BiTE formats and the ability of BiTEs to redirect T cells to lyse neuroblastoma cell lines. Chapter 6 focusses on an approach to reduce on-target off-tumour toxicity of targeting GD2 by targeting *OAcGD2* with CAR therapy. Lastly, an approach to compare BiTE and CAR therapeutics in a transgenic mouse model for neuroblasatoma is described in chapter 7.

CHAPTER 2:
MATERIALS AND METHODS

2.1 Reagents and Buffers

2.1.1 Reagents

Chemicals and all tissue culture reagents were purchased from Sigma Aldrich, Dorset, United Kingdom. Restriction enzymes and PCR reagents were purchased from New England Biolabs LTD, United Kingdom. Oligonucleotides were purchased from Integrated DNA Technologies, Glasgow, United Kingdom.

Formulations of buffers and solutions are provided in **Table 2.1**. Details of cell lines used in this study, and culture methods are provided in **Table 2.2**.

Table 2. 1 Buffers and solutions

Buffer or solution	Final concentration of components
Antibody staining buffer for Western Blot	5% non-fat milk in TBS-T
Blocking buffer for Western Blot	5% non-fat milk in TBS
Coomassie Blue staining solution	0.1% Coomassie Blue R250, 10% acetic acid, 50% methanol, 40% H ₂ O
De-stain solution	10% acetic acid, 50% methanol, 40% H ₂ O
FACs staining buffer	Phosphate buffered saline (PBS) containing 0.5% bovine serum albumin (BSA) and 2.5mM EDTA
LB broth	1.0% tryptone, 0.5% yeast extract, 1.0% NaCl, pH 7.0
TBS	50 mM Tris base and 150 mM NaCl, pH 7.5
TBS-T	50 mM Tris base, 150 mM NaCl and 0.05% Tween-20, pH 7.5
TAE buffer	40mM Tris-acetate and 1mM EDTA pH 8.3
MOPS SDS running buffer	50 mM MPS, 20 Mm Tris Base, 0.1% SDS, 1 mM EDTA, pH 7.7
Protein transfer buffer	25 mM Bicine, 25 mM Bis-Tris, 1 mM EDTA, pH 7.2
Histrap HP binding buffer	20 mM sodium phosphate, 0.5 M NaCl, 20 mM imidazole, pH 7.4
Histrap HP wash buffer	20 mM sodium phosphate, 0.5 M NaCl, 40 mM imidazole, pH 7.4
Histrap HP elution buffer	20 mM sodium phosphate, 0.5 M NaCl, 10 – 500 mM imidazole, pH7.4
Histrap HP stripping buffer	20mM sodium phosphate, 0.5 M NaCl, 50 mM EDTA, pH7.4
Histrap HP recharging solution	0.1 M NiSO ₄
Protein A binding buffer	20 mM sodium phosphate
Protein A elution buffer	0.1 M sodium citrate, pH 3.4
Protein A neutralisation buffer	1 M Tris-HCL, pH 9

Table 2. 2 Cell lines

Cell line, origin	Culture method	Source
293T, human embryonic kidney	DMEM with 10% FBS, 37 °C, 5 % CO ₂	ATCC
A204, rhabdomyosarcoma	RPMI with 10% FBS, 37 °C, 5 % CO ₂	ATCC
CT26, colon carcinoma	RPMI with 10% FBS, 37 °C, 5 % CO ₂	Gift from Martin Pule (University College London)
GD2.CT26, colon carcinoma	RPMI with 10% FBS, 37 °C, 5 % CO ₂	Gift from Martin Pule (University College London)
IMR32, neuroblastoma	RPMI with 10% FBS, 37 °C, 5 % CO ₂	Gift from Andrew stoker (University College London)
Jurkat, T cell lymphoma	RPMI with 10% FBS, 37 °C, 5 % CO ₂	Gift from Martin Pule (University College London)
Jurkat TCR ko, T cell lymphoma	RPMI with 10% FBS, 37 °C, 5 % CO ₂	Gift from Martin Pule (University College London)
K562, T cell lymphoma	RPMI with 10% FBS, 37 °C, 5 % CO ₂	ATCC
Lan-1, neuroblastoma	RPMI with 10% FBS, 37 °C, 5 % CO ₂	ECACC
SKNDZ, neuroblastoma	RPMI with 10% FBS, 37 °C, 5 % CO ₂	ATCC
SKNSH, neuroblastoma	RPMI with 10% FBS, 37 °C, 5 % CO ₂	ATCC
SupT1, T cell lymphoma	RPMI with 10% FBS, 37 °C, 5 % CO ₂	ECACC
GD2.SupT1, T cell lymphoma	RPMI with 10% FBS, 37 °C, 5 % CO ₂	Gift from Martin Pule (University College London)
ALK.SupT1, T cell lymphoma	RPMI with 10% FBS, 37 °C, 5 % CO ₂	Generated by Maria Alonso- Ferrero (University College London)
Phoenix human embryonic kidney	DMEM with 10% FBS, 37 °C, 5 % CO ₂	Gift from Martin Pule (University College London)

2.2 Molecular biology techniques

2.2.1 SFG γ -retroviral vector for gene transfer

Retroviruses including γ -retroviruses, are capable of reverse transcribing their single stranded RNA genome into double stranded DNA, which will be stably integrated into the host cell genome (Temin and Mizutani, 1970). Retroviruses can be manipulated and utilised as a delivery tool to introduce a desired gene-of-interest (GOI) into a host cell. Steps have been taken to avoid the generation of replication competent retrovirus and ensure their safety of use. This includes placing the genes encoding the structural and replication proteins (*gag/pol*) and envelope glycoproteins (*env*) from the retroviral genome in different vectors, whilst incorporating the GOI into the γ -retroviral vector containing the remaining features of the retroviral genome (Maetzig et al., 2011).

As shown in **Figure 2.1** the γ -retroviral vector contains long terminal repeats (LTR) which consist of transcriptional enhancer and promoter sequences. A U3 region functions as a promoter, the R region is where transcription begins and the U5 region is involved in reverse transcription followed by a primer binding site (PBS) and major splice donor (SD). Retroviral vectors can be transiently expressed in a cell line by transfection, or stably expressed by co-expression with both Gag/Pol and Env.

The tropism of a virus for a target cell is determined by the viral envelope, for transduction of human cells we have selected the RD114 envelope (Gift of Mary Collins, University College London) (Cosset et al., 1995). In the making of γ -retroviral particles, only the retroviral vector contains the MMLV Ψ packaging signal (derived from the Maloney murine leukaemia virus) and so viral structural proteins only recognise the Ψ -containing retroviral vector leading to preferential packaging of retroviral vector genomes into infectious particles. After entry of the particle into the target cell, only nucleic acid of the retroviral vector construct is reverse transcribed and stably integrated into the host genome. Since *gag/pol* and *env* are only transferred in the form of proteins (and not nucleic acid) the generation of replication competent retroviral vector progeny is prevented (Maetzig et al., 2011).

The splicing oncoretroviral SFG vector which is based on the Maloney Murine Leukaemia Virus was the vector used for either transiently or stably expressing the DNA constructs described in this thesis from the human embryonic kidney 293T packaging cell line (Riviere et al., 1995). The complete design of the vector is shown in **Figure 2.2**. In addition to the features described in **Figure 2.1**, the vector also contains the following components:

- 1) The ampicillin resistance gene β lactamase, which is expressed when bacteria are transformed with the retroviral vector and enables selection of successfully transformed clones of bacteria growing on LB agar plates with ampicillin.
- 2) The open reading frame (ORF) which contains two constructs that are co-expressed from a single transcript incorporating ECMV IRES sequence (Bochkov and Palmenberg, 2006); these are the GOI and the enhanced green fluorescent protein (eGFP) or enhanced blue fluorescent protein 2 (eBFP2) reporter genes (Ai et al., 2007). The constructs are separated by a sequence which encodes a cleavable peptide derived from the Foot & Mouth 2A virus, which is cleaved during post translational modification of the synthetic protein.
- 3) The origin of replication (*ori*) gene is where replication is initiated. SFG vectors containing different ORF sequences are designated characters MP and assigned a unique identification number e.g. MP15587.

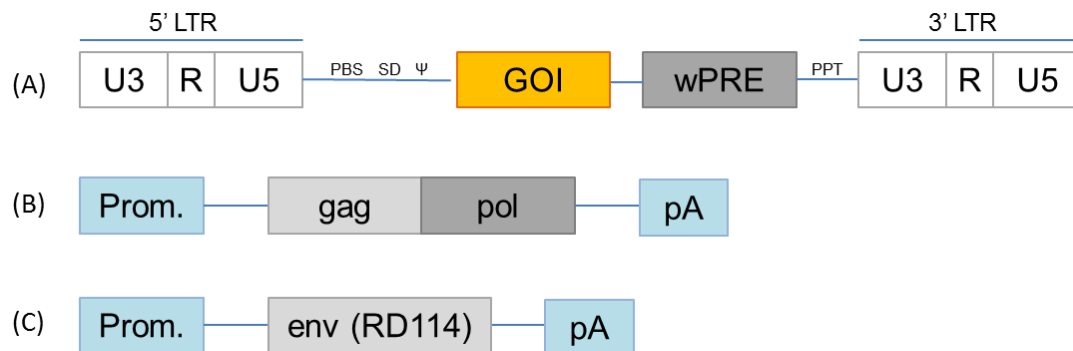


Figure 2.1: Engineering of γ -retroviral vector system. (A) The gene of interest (GOI) is placed in the retroviral vector with long terminal repeats (LTR) containing transcription and enhancer sequences and the MMLV Ψ packaging signal. (PBS: primer binding site, SD: splice donor) (B) Gag/pol and (C) env (pseudotyped RD114) are placed in a heterologous DNA context (Prom: promoter, pA: polyA signal). Adapted from (Maetzig et al., 2011)

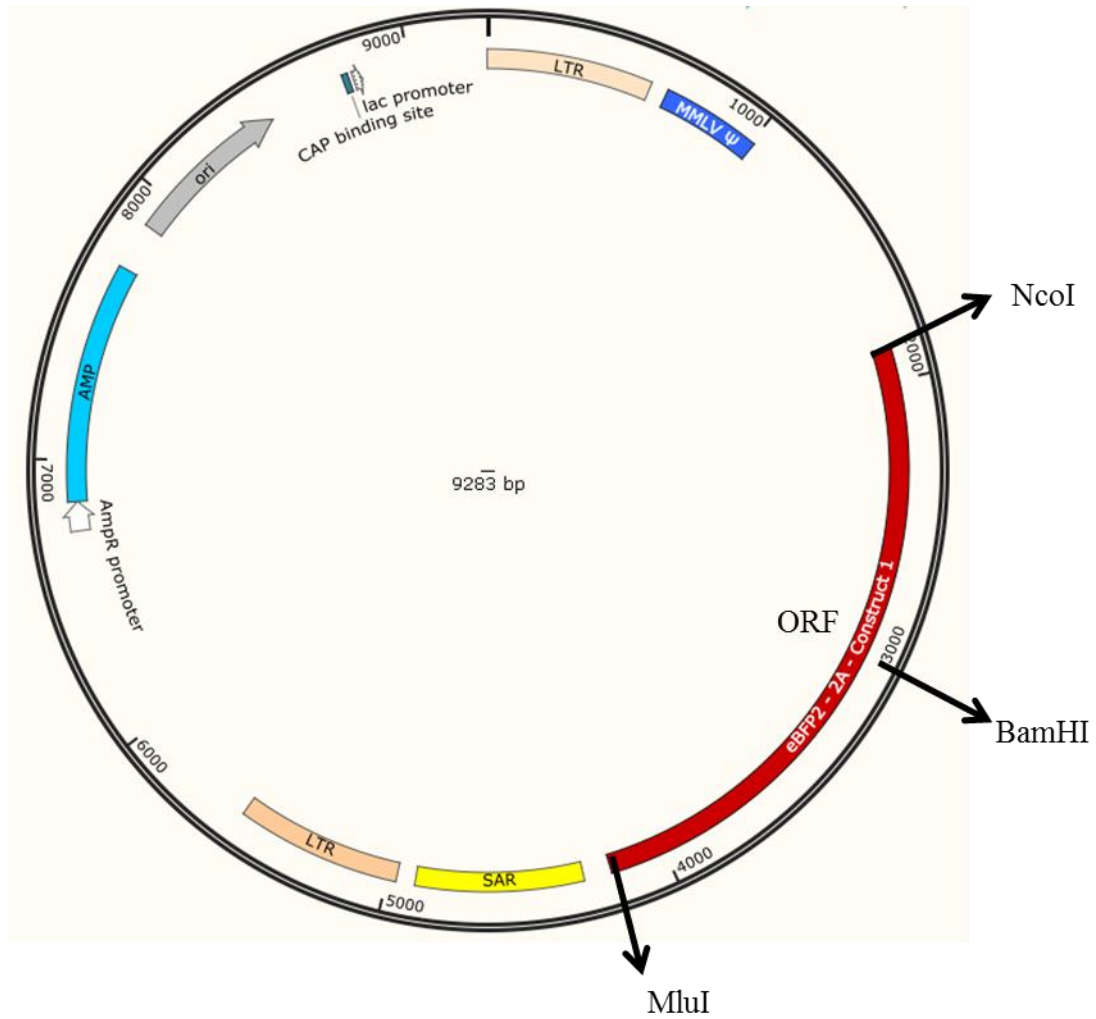


Figure 2.2: Oncoretroviral SFG vector. Features include LTRs containing promoter and transcription elements, MMLV Ψ packaging signal, ORF: open reading frame, SAR: scaffold attachment region, AMP: ampicillin resistance and ori: origin of replication. The *NcoI*, *BamHI* and *MluI* restriction sites allow for cut and paste of various DNA fragments in to the ORF.

2.2.2 Construction of BiTE variants

BiTEs are expressed as a single polypeptide chain consisting of two scFvs joined by a flexible linker (see **Figure 1.9 D**). 18 humanised BiTE variants were generated by combination of two GD2-specific scFvs, three CD3-specific scFvs and three linkers ranging in size and sequence. The scFv and linker combinations are described in **Table 2.3**. 6 murinised BiTEs were also generated and components are described in **Table 2.4**.

Table 2. 3 Components of humanised BiTEs

Portion	scFv clone / linker	Reference / sequence
GD2 specific scFvs	huK666	(Nakamura et al., 2001)
	hu14.18	Patent: US7767405 B2
Linkers	Short linker: glycine - serine linker	GGGGSGGGSGGGGS (15 amino acids)
	Medium linker: IgG1 hinge	DPAEPKSPDKTHTCPPCKDPK (22 amino acids)
	Long linker: CD8 stalk region	SDPTTTPAPRPPTPAPTIASQPLSLR PEACRPAAGGAVHTRGLDFACD (48 amino acids)
	CD3 specific scFvs	huOKT3 (Adair et al., 1994)
	huUCHT-1 (Shalaby et al., 1992)	
	huYTH (Routledge et al., 1991)	

Key: hu = humanised

Table 2. 4 Components of murine BiTEs

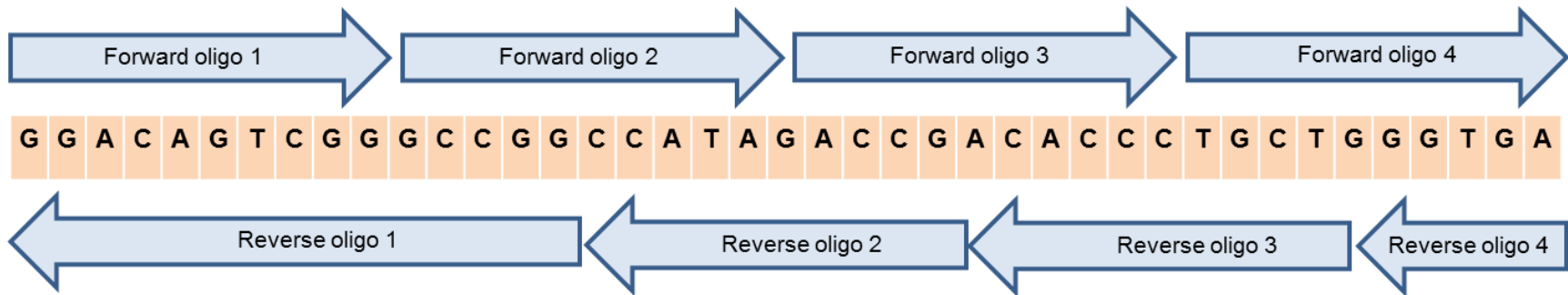
Portion	scFv clone / linker	Reference / sequence
GD2 specific scFvs	MuK666	(Nakamura et al., 2001)
	14.18	(Gillies et al., 1989)
Linkers	Short linker: glycine - serine linker	GGGSGGGSGGGGS (15 amino acids)
	Medium linker: IgG1 hinge	RGPTIKPCPPKCCPAPNLLGGP (22 amino acids)
	Long linker: CD8 stalk region	SDPTTTKPVLRTSPVHPTGTSQP QRPEDCRPRGSVKGTGLDFA (44 amino acids)
	CD3 specific scFv	17A2 (Adair et al., 1994, Alegre et al., 1995)

2.2.2.1 Generation of scFvs by PCR assembly of overlapping nucleotides

All three humanised CD3-specific scFvs (huOKT3, huUCHT-1 and huYTH) and one GD2-specific scFv (hu14.18) in combination with short, medium or long linkers were generated by *de novo* gene synthesis using PCR assembly of overlapping nucleotides (IDT DNA) briefly described in **Figure 2.3**.

HuK666 scFv DNA was available in the SFG vector designated MP15587, MuK666 scFv was available in vector MP5945 and 17A2 scFv in vector 14375. To assemble the DNA fragment, PCR reactions were set up using three concentrations of each of the overlapping nucleotides (25 μ M, 12.5 μ M and 6.25 μ M) in a reaction volume of 50 μ L containing 36.5 μ L nuclease-free water, 10 μ L 5x Phusion HiFid buffer, 1 μ L 10 mM dNTPs, 0.5 μ L of 2000 units/mL Phusion hot-start polymerase and 2 μ L of pooled overlapping nucleotides. Thermal cycling conditions were as follows: 98 °C for 2 minutes, 98 °C for 1 minute, 65 °C for 45 seconds, 72 °C for 60 seconds, steps 2 – 4 repeated 35 times and 72 °C for 10 minutes.

(A) Construction of a DNA fragment by assembly PCR of overlapping oligonucleotides



(B) Amplification of assembled DNA by PCR using first forward and last reverse oligonucleotides



Figure 2.3. Construction of a DNA fragment by assembly PCR. (A) The desired DNA sequence (pink boxes) is assembled by splicing overlapping forward and reverse oligonucleotides in to a larger polynucleotide using ligation by PCR. (B) A second PCR further amplifies the DNA fragment using the first forward and last reverse oligonucleotides.

2.2.2.2 Purification of PCR product

The PCR product was purified using a PCR purification kit (Qiagen) according to the manufacturer's instructions. Briefly, the PCR product was mixed with a high-salt binding buffer (PB) and applied to a spin column containing a silica membrane to absorb the nucleic acids. The columns were centrifuged at 17,900 x g for 60 seconds in a microcentrifuge at room temperature, followed by a second spin in wash buffer (PE) to remove impurities (primers, enzymes etc.) from the PCR product. A third spin allowed removal of residual buffer and a final spin eluted the DNA from the column after addition of 30 μ L nuclease-free H₂O and incubation of the column for 1 minute at room temperature.

2.2.2.3 Amplification of assembled overlapping nucleotides by PCR

Purified DNA was further amplified (**Figure 2.3**) in a 50 μ L reaction volume containing 35.5 μ L nuclease-free water, 10 μ L Phusion HiFid buffer, 1 μ L of purified DNA, 1 μ L 25 μ M first (forward) primer and 1 μ L 25 μ M last (reverse) primer (from the overlapping oligonucleotides), 1 μ L dNTPs and 0.5 μ L Phusion polymerase. Thermal cycling conditions were as described in 2.2.2.1.

2.2.2.4 Detection of PCR product by agarose gel electrophoresis

To determine the optimal oligonucleotide concentration (25 μ M, 12.5 μ M or 6.25 μ M) required to achieve the highest PCR yield; 12 μ L of PCR product was mixed with 3 μ L 5x DNA loading buffer and run by electrophoresis on a 1% agarose gel at 100 V for 1 hour. PCR fragments were detected under UV light and the optimal oligonucleotide concentration selected. The assembly and amplification PCRs were repeated with an additional 3 tubes using the optimal oligonucleotide concentration. These three tubes were then pooled with PCR product from the original PCR and cleaned using the PCR purification kit as described in 2.2.2.2 and eluted in 80 μ L nuclease-free H₂O.

2.2.3 Construction of anti-*O*-acetyl-GD2 specific antibody 8B6 heavy and light chains by overlap extension PCR

To generate the 8B6 antibody heavy (V_H - C_H) and light (V_L - C_L) chains, the variable and constant regions were amplified individually by overlap extension PCR and then

fused together in a subsequent ‘fusion’ PCR. Overlap extension PCR introduces 5’ overhangs at the junction where two DNA fragments are to be joined (**Figure 2.4**). The overhang is created by using primers which are extended at their 3’ ends to contain a complementary sequence to the 5’ end of the other DNA fragment. When the primers anneal to the DNA template during the PCR, the DNA is extended by a new sequence which is complementary to the molecule it is to be joined to. In a second PCR, known as a fusion PCR, the overlapping complementary sequences introduced serve as primers and the two sequences are fused.

A first round of PCR amplified the DNA fragments. Reactions were carried out in 50 μL volume consisting of 35.5 μL nuclease-free H_2O , 10 μL 5 X HiFid buffer, 1 μL dNTPs, 0.5 μL Phusion polymerase, 1 μL DNA template and 1 μL each of forward and reverse primers. Thermal cycling conditions were as described in 2.2.2.1. After confirmation of correct PCR fragment sizes on a 1% agarose gel, remaining PCR product was purified using a PCR purification kit (as described in 2.2.2.2) and variable and constant regions fused ($V_H - C_H$) or ($V_L - C_L$) in a second amplification PCR using the first and last primers to generate the heavy and light chains (as described in 2.2.2.3).

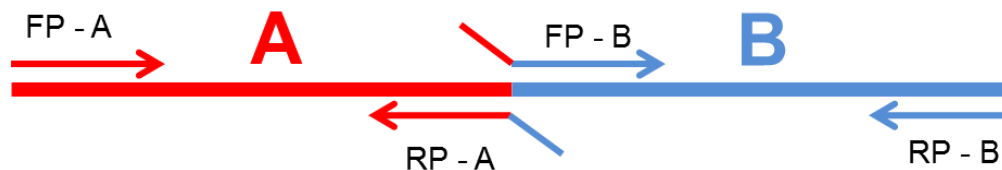


Figure 2.4: Overlap extension PCR. Fragment A and B are amplified individually by respective forward and reverse primers (FP and RP). The central primers (RP-A and FP-B) are extended at their 3 primer ends (diagonal lines) to include sufficient DNA from the opposite DNA fragment and allow extension of the DNA fragments for subsequent fusion.

2.2.4 Digestion of PCR product or SFG vector using restriction endonucleases

The cloning sites outside the open reading frame in the SFG vector are *NcoI* and *MluI*. The DNA fragment of interest has the same restriction sites at the start and end of the sequence and allows a convenient cut and paste method of inserting the DNA into the vector. Both PCR fragment and vector were digested with identical enzymes in a 100 µL reaction volume. The reaction mixture contained 10 µL 10x buffer (New England Biolabs), 5 µL enzyme 1, 5 µL enzyme 2, 5 µg vector DNA / 80 µL purified PCR product and the appropriate volume of nuclease-free H₂O to total 100 µL. Reactions were incubated at 37 °C for 2 hours.

2.2.4.1 Digestion of GD2/CD3 specific scFvs for generation of BiTEs

To clone BiTE constructs into the SFG vector, the GD2-specific and CD3-specific scFv PCR fragments are flanked with *NcoI/BamHI* and *BamHI/MluI* restriction sites respectively to enable combinations of the two scFvs to be assembled in the vector. To clone the linker-anti-CD3 scFvs into vector MP15587 (containing huK666 scFv), both MP15587 and purified PCR product were digested with *BamHI/MluI* restriction endonucleases. To later generate the GD2-specific hu14.18 scFv based BiTEs, vectors containing huK666-scFv in combination with three CD3 specific scFvs were digested with *NcoI/BamHI* restriction endonucleases.

2.2.4.2 Digestion of 8B6 antibody heavy and light chain PCR fragments

To clone the 8B6 antibody heavy chain into an SFG vector (MP3279) containing co-expression of enhanced green fluorescent protein (eGFP2), digestion with *NcoI/MluI* restriction nucleases occurred as described in 2.2.4. Likewise the 8B6 antibody light chain and SFG vector (MP3593) with co-expression of enhanced blue fluorescent protein (eBFP2) were digested with the same enzymes. The newly synthesised antibody heavy and light chain plasmids are designated MP14603 and MP14604 respectively.

2.2.5 Construction of GD2 and OAcGD2 specific CARs

SFG vectors containing GD2-specific (MP13311) and OAcGD2-specific (MP5421) second generation humanised CARs (scFv-CH₂CH₃-CD28-CD3ζ) were provided by Martin Pule (Department of Haematology, Cancer Institute).

GD2-specific murine CARs were generated by cloning GD2-specific scFvs (MuK666 from vector MP5945 and 14.18 from vector MP24845) into vector MP20493 containing a second generation murine CAR (scFv-CD8 stalk-CD28-CD3ζ) or vector MP20504 containing CAR and co-expression of luciferase. The vectors were digested with *NcoI/BamHI* restriction endonucleases as described in 2.2.4.

2.2.6 DNA extraction from agarose gel

Digested PCR and/or vector DNA were run on a 1% agarose gel (100 V, 1 hour). The bands of interest were cut from the gel under a blue light transilluminator and DNA extracted using a gel extraction kit (Qiagen), according to the manufacturer's instruction.

2.2.7 Ligation

The digested PCR product (insert DNA) and vector were ligated at ratios 3:1 and 5:1 using amounts obtained from the formula:

$$\frac{(\text{kb of insert}) \times (\text{ng of vector})}{(\text{kb of vector})} \times \frac{3}{1} (\text{ratio}) = \text{ng of insert needed for a 3:1 molar ratio.}$$

The reactions consisted of 10 μL 2 X quick ligase buffer, appropriate volumes of digested vector and insert DNA at 3:1 and 5:1 ratios and addition of nuclease-free H₂O to a total volume of 20 μL. 1.5 μL of quick ligase was added to join the vector and insert DNA strands together by catalysing the formation of a phosphodiester bond between the cohesive ends. The reaction was left at room temperature for 5 minutes and then kept on ice prior to transformation.

2.2.8 Transformation of chemically competent *Escherichia coli* with plasmid DNA

To introduce the newly ligated plasmid into *E. coli* cells (NEB5-α, high efficiency), 2 μL of ligation reaction mix was added to 25 μL of *E. coli* competent cells and incubated

on ice for 30 minutes. The competent cells were heat shocked by incubation at 42 °C for 35 seconds and subsequently transferred to ice for 5 minutes. The cells were then added to 250 µL SOC medium and shaken at 200 rpm at 37 °C for 40 minutes. Transformed bacteria were spread on to ampicillin (100 µg/mL) containing agar plates and cultured at 37 °C for 16 hours.

2.2.9 Small scale plasmid preparation (Miniprep)

3 mL of LB broth with ampicillin was inoculated with a bacterial colony and cultured overnight at 37 °C with shaking at 200 rpm. Plasmid DNA was extracted from 1.5 mL of bacterial culture by an alkaline lysis method using QIAprep Spin Miniprep Kit (Qiagen) according to the manufacturer's instructions.

2.2.10 Medium scale plasmid preparation (Midiprep)

100 mL of LB broth with ampicillin was inoculated with 100 µL bacterial miniculture (from 2.2.11) and cultured overnight at 37 °C with shaking at 200 rpm. Plasmid DNA was extracted from 100 mL of bacterial culture using a plasmid midiprep kit (NucleoBond Xtra, Machery Nagel) according to the manufacturer's protocol. The final DNA pellet was air dried for 5 minutes followed by resuspension in 300 µL nuclease-free H₂O.

2.2.11 Quantification of DNA

The absorbance of final midiprep solution was measured on a spectrophotometer (Nanodrop ND1000) set to record at 260/280 nm wavelength. To determine the purity of DNA a ratio of $A_{260}/A_{280} > 1.8$ was pursued.

2.2.12 DNA sequencing

DNA sequencing was carried out by Sanger Sequencing Service, Source Bioscience, 1 Orchard Place, Nottingham Business Park, Nottingham, NG8 6PX, United Kingdom. Forward primer: TTACACAGTCCTGCTGACCACC, reverse primer: CAAGCGGCTT CGGCCAGTAAC.

2.3 Cell culture techniques

2.3.1 Transient transfection of 293T cells

Human embryonic kidney derived 293T cells were plated at a density of 1.5×10^6 cells per 10 cm diameter tissue culture plate in 10 mL IMDM, supplemented with 10% FBS and 5 mM L-glutamine. Cells were cultured at 37 °C in a 5% CO₂ incubator and transfected when 60% confluency was reached (after approximately 30 hours). First 470 µL IMDM and 30 µL Genejuice transfection reagent (Novagen) were mixed and incubated at room temperature for 5 minutes, followed by addition of 12.5 µg plasmid DNA and incubation for a further 15 minutes. The transfection mixture was added dropwise to the plated cells.

BiTE production

For experiments requiring non-purified BiTEs, supernatant was harvested from the transfected cells after 72 hours, centrifuged at 400 x g for 10 minutes and filtered through both 0.45 µm and 0.22 µm filters and stored at -20 °C.

For experiments requiring purified BiTEs, five 10 cm diameter plates were transfected per BiTE construct. After 16 hours of transfection, the media was removed and the cells gently washed with 5 mL PBS. The media was replaced with 5 mL phenol-free X-VIVO-15 (Lonza) and cells cultured for a further 48 hours before harvest of the BiTE containing supernatant. A total of 25 mL supernatant was centrifuged (400 xg, 10 minutes) and filtered through both 0.45 µm and 0.22 µm filters and stored at -20 °C.

2.3.2 Retroviral vector production

Retrovirus for transduction of human cells

293T cells were chosen as the packaging cell line for the production of the retroviral particles due to their ease of transfection. Vectors were produced by transient transfection into 293T cells. Cells were plated at a density of 1.5×10^6 cells per 10 cm diameter tissue culture plate in 10 mL IMDM, supplemented with 10% FBS and 5 mM L-glutamine, cells were cultured at 37 °C in a 5% CO₂ incubator. The cells were

transfected when 60% confluence was reached (after approximately 30 hours). First 470 μL IMDM and 30 μL Genejuice transfection reagent (Novagen) were mixed and incubated at room temperature for 5 minutes followed by addition of 12.5 μg plasmid DNA (4.75 μg envelope RD114, 4.75 μg gag/pol and 3.75 μg transfer vector). Supernatant was harvested twice at 48 and 72 hours after transfection and, after snap freezing the samples (in ethanol and dry ice) to remove any remaining live cells; samples were stored at $-80\text{ }^{\circ}\text{C}$.

Retrovirus for transduction of mouse splenocytes

Retrovirus was made by transfection of Phoenix cells. The process was as described above with the following modifications: 1.3×10^6 Phoenix cells were plated and DNA added to the transfection mixture consisted of 2.6 μg pCL-Eco retrovirus packaging vector and 4.68 μg transfer vector.

2.3.3 Human peripheral blood mononuclear cell isolation

Peripheral blood mononuclear cells (PBMCs) were isolated from whole blood using Ficoll density centrifugation. An equal volume of blood was mixed 1:1 with plain RPMI-1640 and 20 mL blood/RPMI mix layered on 10 mL ficoll (Stem Cell technologies). After centrifugation at $750 \times g$ for 40 minutes at $25\text{ }^{\circ}\text{C}$, mononuclear cells were collected using a Pasteur pipette and washed twice in 30 mL RPMI-1640 at $400 \times g$ for 5 minutes. Cells were counted and again centrifuged as above followed by resuspension in RPMI containing 10% FBS at a density of 1×10^6 cells/mL and plated at 2 mL / well of a 24 well tissue culture plate.

2.3.4 Activation and expansion of human T cells

For experiments requiring stimulated T cells, PBMCs were activated with 1 $\mu\text{g}/\text{mL}$ anti-CD3/anti-CD28 antibodies (Miltenyi Biotec). After 24 and 48 hours cells were fed 100IU/mL recombinant human Interleukin--2 (Proleukin, Novartis).

2.3.5 Enrichment of human T cells

For experiments requiring unstimulated T cells, T cells were enriched from PBMCs by depletion of B cells and monocytes using a human T cell enrichment column (R&D

systems) following the manufacturer's instruction. Up to 100×10^6 cells were applied to the columns which are coated with anti-immunoglobulin (Ig) and Ig beads to bind B cells and monocytes. A 30 - 40 % yield was usually achieved.

2.3.6 Production of Retronectin coated plates

In order to improve T cell and cell line (e.g. K562) transduction, 24 well plates were pre-treated with Retronectin[®] (Takara), a recombinant human fibronectin fragment. 8 μ L of Retronectin (at concentration 1 mg/mL) was resuspended in 1 mL PBS for every 2 wells of a non-tissue culture treated 24 well plate and 500 μ L added to each well. Plates were then incubated for 24 hours at 4 °C.

2.3.7 Retroviral transduction

Transduction of human PBMCs

Forty-eight hours after activation, T cells were transduced on Retronectin coated plates. 250 μ L retroviral supernatant was added to each well and incubated at room temperature for 30 minutes and then removed. Activated T cells were counted by trypan blue exclusion and 500 μ L of viable cells at a concentration of 6×10^5 /mL added to each well along with 1.5 mL retroviral supernatant and 100 IU/mL IL-2. Plates were centrifuged for 40 minutes at 1000 x g and cells were subsequently incubated for 60 hours. Cells were then pooled and centrifuged at 400 x g for 5 minutes and transferred to tissue-culture treated plate at 1×10^6 /mL along with 50 IU/mL IL-2.

Transduction of K562 cells

To generate an 8B6 antibody secreting cell line, K562 cells were co-transduced with retroviral supernatant for the 8B6 antibody heavy and light chains. The transduction method was as described in 2.3.6.1 with the following modifications: IL-2 was omitted and 0.75 mL each of 8B6 heavy chain and 8B6 light chain retroviral viral supernatant were used to transduce the cells.

Activation and transduction of mouse splenocytes

For *in vivo* mouse experiments, CAR-T cells were prepared by transduction of mouse splenocytes. Spleen was obtained from mice of 129/SvJ strain and mechanically disaggregated using the plunger of a 1 mL syringe and passed through a 70 μ M cell strainer. Cells were incubated in 3 mL ACK lysis buffer (Lonza) for 5 minutes followed by 3 mL RPMI, 10% FBS. Cells were washed twice in PBS and centrifuged at 400 \times g for 5 minutes. To activate T cells, cells were cultured at 1×10^6 cells/mL concentration in RPMI containing concanavlin A, IL-7 and β -mercaptoethanol.

Splenocytes were transduced 24 hours after activation, 2×10^6 cells were mixed with 1.25 mL retroviral supernatant per well of a retronectin coated non-tissue culture treated 24 well plate. Retronectin coated plates were incubated with 2% BSA in PBS for 30 minutes prior to use. Plates were centrifuged at 2000 RPM for 90 minutes at 32 °C. Wells were supplemented with 0.75 mL complete RPMI with IL-2.

2.3.8 CD56 depletion

To prevent non-specific target cell killing, proliferation or cytokine production by natural killer cells (NK cells) in the PBMC preparation used for transduction, cultures were depleted for CD56 expressing cells using CD56 Microbeads (Miltenyi Biotec), according to the manufacturer's protocol. Depletion was performed one day prior to set up of further *in-vitro* functional testing, corresponding to 5 days post transduction.

2.3.9 Labelling of cells with CFSE

CFSE is a fluorescent cell staining dye used for cell identification and proliferation studies. CFSE readily crosses intact cell membranes, where the CFSE acetate groups are cleaved to yield the fluorescent molecule and the succinimidyl ester group reacts with primary amines within the cell to crosslink the dye to intracellular proteins allowing CFSE to be retained in the cell. Cell divisions result in sequential halving of fluorescence and can be detected by flow cytometry. 5×10^6 unstimulated T cells / cell lines were labelled with a CFSE cell division assay kit (Cayman Chemical) according to the manufacturer's instruction. After labelling cells were resuspended between 1×10^5 to 5×10^5 cells/mL RPMI, 10% FBS.

2.3.10 Single cell cloning by limiting dilution

Transduced cells can express a varying amount of desired transcript. At times, a cell line of very homogenous expression is desired and one way to achieve this is by single cell cloning. Transduced K562 cells were counted by trypan blue exclusion and resuspended at 1×10^6 /mL in RPMI containing 10% FBS. Dilution 1 was made by adding 39 μ L of this cell suspension to 30 mL media, obtaining a concentration of 1.293×10^4 /mL. 39 μ L of dilution 1 was added to 30 mL media to obtain dilution 2 of concentration 1.67 cells /mL. Each 30 mL of dilution 2 is sufficient for seeding one 96 well plate with 200 μ L/well. The plates were incubated at 37 °C in a 5% CO₂ incubator and inspected after 1 week followed by daily inspection. Once a single cell clone occupied 25% of the well, 100 μ L was removed and inspected by flow cytometry to determine all cells were from a single clone. The remaining 100 μ L was transferred to culture in 24 well plates followed by transfer to T25 and T75 flasks upon expansion.

2.3.11 Large scale antibody production using a bioreactor

K562 cells transduced to secrete the 8B6 antibody were cultured in a bioreactor (Wilson-Wolf, CELLline) for antibody production. The bioreactor consists of two compartments: a top nutrient media compartment of 1 L capacity and a bottom cell compartment of 15 mL capacity. The design allows cells to grow to at a very high concentration and produce concentrated antibody in the cell compartment with sufficient diffusion of nutrients from the nutrient compartment and diffusion of oxygen through the bottom of the cell compartment.

To inoculate the bioreactor, 50 mL phenol-free IMDM was added to the nutrient compartment to equilibrate the dialysis membrane and then removed. 1×10^8 K562 cells were centrifuged at 400 x g for 5 minutes and resuspended in 15 mL phenol-free IMDM containing 375 μ L ultra-low FBS. Cells were added slowly to the cell compartment and 950 mL phenol-free IMDM supplemented with ultra-low FBS added to the nutrient compartment. After 1 week the antibody rich supernatant was harvested from the bioreactor and centrifuged twice, first at 400 x g for 5 minutes to remove the pelleted cells and next at 4000 x g for 10 minutes to remove remaining cell debris. The supernatant was sterile filtered through 0.45 μ M and 0.22 μ M and stored at -20 °C.

2.4 Protein purification and analysis

2.4.1 Protein purification

Protein purification was performed using two types of purification column: HisTrap HP columns (GE Healthcare) for purification of BiTEs by capture of the C-terminal 6 x his tag by metal ion affinity chromatography (IMAC) and HiTrap Protein A HP columns (GE Healthcare) for purification of 8B6 antibody by capture of the antibody Ig. For buffer formulations see **Table 2.1** under section 2.1.

Protein was purified according to the manufacturer's instruction. Briefly, protein containing supernatant was mixed 1:1 with binding buffer and passed through the appropriate purification column at a rate of 1 mL/minute using a peristaltic pump (Econo pump, Bio-Rad). The column was subsequently washed with 15 mL wash buffer / binding buffer, followed by elution of the bound protein by addition of 10 mL elution buffer and collection in 1 mL aliquots. A further 10 mL elution buffer was applied to the column to ensure efficient removal of protein and the column washed with 5 mL binding buffer before storage at 4 °C in 20% ethanol.

2.4.2 Quantification of protein

The absorbance of final purified protein was measured on a spectrophotometer (Protein A280, Nanodrop ND1000) set to record at 280 nm wavelength. Final protein concentration was obtained by division of the reading with the respective protein extinction coefficient value (ExPasy ProtParam online tool).

2.4.3 Dialysis of purified protein into PBS

Eluted protein fractions 2 - 4, which consistently had the highest protein concentration were pooled and dialysed into PBS using a 3 mL capacity dialysis cassette (Slide-A-Lyzer). 3 X 1.5 L PBS washes at 4 hours, overnight and a final 4 hours were performed at 4 °C with gentle mixing.

2.4.4 Concentration and storage of purified protein

Purified and dialysed protein was sterile filtered through a 0.22 µM filter and concentrated from 3 mL to 0.5 mL using a centrifugal filter column (Millipore)

according to the manufacturer's instruction. Briefly, 3 mL purified protein was applied to the column filter and centrifuged at 4000 x g for 2 minutes 2-3 times at 4°C. Protein was stored in 50 - 100 µL aliquots at -80°C.

2.4.5 Preparation of protein samples for SDS-PAGE

Protein samples were mixed with 4x Laemmli sample buffer (Bio-Rad) containing 10% 2-ME and denatured by incubation at 95 °C for 10 minutes. Samples were stored at -20 °C.

2.4.6 Protein separation by SDS-PAGE

Purified protein was resolved by electrophoresis in 4-12% Bis - Tris precast gels (NuPAGE, Invitrogen). SDS-PAGE was carried out using Mini Protean III apparatus (BioRad) and gels were electrophoresed in NuPage running buffer (**Table 2.1**) at 160 V for 1 hour.

2.4.7 Coomassie Blue staining method

To detect all proteins present in the samples; gels were stained with 10 mL Coomassie Brilliant Blue R-250 dye (Thermo Scientific) (**Table 2.1**) and microwaved for 1 minute, followed by gentle shaking on an orbital rotor for 10 minutes. Three washes in 10 - 20 mL de-stain solution (**Table 2.1**), removed excess Coomassie Blue dye from the gel and allowed visualisation of individual bands present in the sample.

2.4.8 Protein transfer to nitrocellulose membrane

Proteins were transferred from the precast gels on to a nitrocellulose membrane (Amersham Biosciences) in protein transfer buffer (**Table 2.1**) using a BioRad Mini Trans-Blot Electrophoretic Transfer system. Gels were transferred at 360 mA for 1 hour.

2.4.9 Western Blotting analysis

Table 2. 5 Antibodies and HRP-conjugates used for Western Blotting analysis

Name	Catalogue no.	Manufacturer	Dilution
Penta-his-biotin	34440	Qiagen	1:50,000
Streptavidin-HRP	N100	Thermo-Fisher Scientific	1:20,000
Anti-mouse IgG-HRP	43C-CB1569-FIT	Stratech	1:2000

Membranes were washed in TBS (**Table 2.1**) for 10 minutes and blocked in blocking buffer containing 5% non-fat milk for 1 hour at room temperature followed by two additional washes in TBS-T (**Table 2.1**). Membranes were incubated with primary antibody (**Table 2.5**) for 1 - 2 hours at room temperature or 4 °C overnight and washed twice in TBS-T for 10 minutes each at room temperature. Membranes were incubated in appropriate detection secondary antibody (**Table 2.5**) for 1 - 2 hours at room temperature and washed four times in TBS-T for 10 minutes each at room temperature. Proteins were visualised using a chemiluminescent film after incubation in 1 mL ECL substrate solution (GE healthcare).

2.4.10 Protein thermal stability measurements using differential scanning fluorimetry

The thermal stabilities of the BiTE variants were measured by differential scanning fluorimetry using the Protein Thermal Shift assay (Life Technologies, Grand Island, NY). BiTEs (0.2 mg/mL) were mixed with SYPRO Orange dye (1:1000) in a 40 µL volume in optical 96 well plates (Thermofisher) and fluorescence monitored using a StepOnePlus quantitative PCR machine (Applied Biosystems, Foster City, CA) with a 1% thermal gradient from 25 °C to 99 °C. Data were analysed using Protein Thermal Shift Software (Applied Biosystems, Foster City, CA) to calculate the T_m using the Derivative method (Niesen et al., 2007).

2.5 *In vitro* functional assays

2.5.1 Cytotoxicity assay by flow cytometry

The ability of BiTEs to redirect effector cells (unstimulated T cells) to kill CFSE labelled target cells (SupT1, GD2.SupT1, Lan-1, SKNDZ, IMR32, A204) was studied by flow cytometry. Cells were co-cultured in 96 well plates at a 5:1 effector: target ratio with an increasing concentration of BiTEs (0-1000 ng/mL), in a total volume of 200 μ L RPMI containing 10% FBS. Each condition was set up in duplicate wells. After 16, 24, 40, 48 or 64 hours, target cell death was analysed by measurement of apoptosis and necrosis of CFSE labelled cells. Plates were first centrifuged at 400 x g for 5 minutes and supernatant removed by pipetting. After two washes in 200 μ L FACs buffer (**Table 2.1**) and centrifugation as above, cells were washed with 200 μ L Annexin buffer (eBioscience) and subsequently incubated in 0.5 μ L Annexin V, 0.5 μ L PI (eBioscience) and 10 μ L Annexin buffer per well for 15 minutes in the dark at room temperature. Wells were supplemented with 195 μ L annexin buffer and 5 μ L counting beads (CountBright Absolute counting beads, Invitrogen) before analysis on BD FACS Calibur using the Cell Quest software. Specific lysis was calculated as follows:

$$100 - \frac{(\text{viable cells of treatment group}) \times 100}{(\text{viable cells of control group})} = \% \text{ lysis}$$

EC₅₀ values were calculated by non-linear regression using Prism v5 software.

2.5.2 T cell proliferation assay by flow cytometry

T cell proliferation induced by engagement of T cells with BiTEs and GD2 positive target cells was measured by detection of CFSE using flow cytometry. Assays were prepared as described in 2.5.1 including the following modifications: T cells were labelled with CFSE and target cells were irradiated one day prior to experimental set up. After 5 days co-culture, cells were stained with CD4 and CD8 specific antibodies (**Table 2.6**) for identification of T cell subsets and the 7-AAD viability dye (eBioscience). Wells were analysed as described in 2.5.1.

2.5.3 ⁵¹Cr release cytotoxicity assay

Standard ⁵¹Cr release assays were performed to determine cytotoxic activity of GD2 and OAcGD2 specific CAR T cells against GD2+ / OAcGD2+ SupT1 cell targets as well as a GD2 negative target SupT1. 1 x 10⁶ target cells were labelled with 20 μL ⁵¹Cr (Perkin Elmer) for 1 hour at 37 °C during which cells were intermittently flicked to improve the exposure to ⁵¹Cr. Cells were washed five times in 4 mL complete media and co-cultured with effector cells at the following effector: target ratios 32:1, 16:1, 8:1 and 4:1 in 96 well v-bottom plates. Untransduced T cells served as a negative control. After 4 hours of co-culture at 37 °C in a 5% CO₂ incubator, plates were centrifuged as above and 150 μL of supernatant transferred to High Binding Isoplate-96 HB96-well plates (Perkin Elmer). Wells were supplemented with of 50 μL scintillation liquid (Perkin Elmer) and the plates were incubated overnight. ⁵¹Cr release was counted in assay supernatants a 1450 MicroBeta TriLux (Perkin Elmer). Specific cell lysis was calculated as follows:

$$\frac{(\text{Experimental release} - \text{spontaneous lysis}) \times 100}{(\text{maximum lysis} - \text{spontaneous lysis})} = \% \text{ lysis}$$

2.5.4 Interferon gamma (IFN-γ) detection by ELISA

The presence of IFN-γ in co-culture supernatant was detected using a human IFN-γ ELISA kit (Biolegend). 100 μL supernatant was harvested after 24 hours co-culture between effector and target cells and stored at -80 °C. 96 well ELISA plates were coated with human IFN-γ specific capture antibody and stored overnight at 4 °C. After blocking plates for 1 hour, the ELISA was performed according to the manufacturer's instructions. Human IFN-γ standards were used to generate a standard curve of range 0 - 500 pg/mL. Absorbance was read at 450 nm on a microplate reader (Tecan).

2.6 *In vivo* animal work

2.6.1 Animals

Both *Th-ALK^{F1174L}* mice (derived from *CBA* × *C57BL/6J* mice) and *Th-MYCN* mice of the 129/SvJ strain were a gift from Louis Chesler (Institute of Cancer Research, UK). The two mouse strains were genetically crossed to generate *ALK^{F1174L}/MYCN* transgenic mice which were used in the experiments. Tail DNA of all animals was analysed for *ALK* and *MYCN* transgenes by qRT-PCR (Transnetyx, Inc.). All animal experiments were performed under a project license approved by the UK Home Office following University College London Biological Services Ethical Review. Animal experiments were designed in line with the AcoRD principles.

2.6.2 Total body irradiation

Unless otherwise stated, mice received 3.1 Gy total body irradiation.

2.6.3 Intravenous injection of mice

After irradiation, mice were heated for 15 minutes in a warming box to facilitate vasodilation of the tail veins. Intravenous inoculation with 6×10^6 bulk splenocytes (6 days post-transduction) was done in a volume of 0.2 mL PBS with a 1 mL syringe and 29G needle.

2.6.4 Bioluminescence imaging of mice

Mice were anaesthetised with isoflurane and given 0.1 mL (10 mg/mL) Luciferin (Strattech) by intraperitoneal injection. Mice were scanned after 15 minutes using a PhotonIMAGERTM optical imaging system (Biospace Lab).

2.6.5 Magnetic Resonance Imaging

Images were acquired on a low magnetic field small animal 1T ICON MRI (Bruker) scanner. Images were acquired using a T2 weighted sequence, slice thickness = 0.5 mm, 15 or 30 averages were acquired with an acquisition time of 6 or 13 minutes, depending on number of averages. Differences in structure and the higher water content of the tumour translate in longer relaxation time (T2).

2.7 Flow cytometry

2.7.1 Antibodies

Table 2. 6 Antibodies used for flow cytometry

Specificity	Clone	Isotype	Manufacturer	Fluorochrome	Dilution
ALK	13	Mouse IgG1	Gift from Marc Vigney	N/A	1:100
CD4	OKT4	Mouse IgG2b, κ	Biolegend	PE	1:100
CD4	RM4-5	Rat IgG2a, κ	BD Biosciences	Pacific Blue	1:100
CD8	SK1	Mouse IgG2a, κ	Biolegend	APC	1:100
CD8	SK1	Mouse IgG2a, κ	Biolegend	FITC	1:100
CD11b	M1/70	Rat IgG2b, κ	Biolegend	BV 711	1:100
CD14	Sa14-2	Rat IgG2a, κ	Biolegend	PE	1:100
CD16	3G8	Mouse IgG1 κ	Biolegend	PerCP	1:100
CD19	HIB19	Mouse IgG1 κ	Biolegend	APC	1:100
CD34	RAM34	Rat IgG2a, κ	eBioscience	FITC	1:100
CD45	30-F11	Rat IgG2b, κ	Tonbo biosciences	PE-Cy7	1:100
GD2	14G2a	Mouse IgG2a, κ	Biolegend	PE	1:100
GD2	14G2a	Mouse IgG2a, κ	Biolegend	N/A	1:100
OAcGD2	8B6	Mouse IgG2a	Made in-house	AF-647	10:100
Anti-mouse IgG	polyclonal	Goat	Stratech	FITC	2.5:100
Anti-mouse F(ab)2	polyclonal	Goat	Stratech	AF-647	2.5:100
Penta-his			Qiagen	AF-647	1:100
Annexin V			eBioscience	APC	10:100
Annexin V			eBioscience	FITC	10:100
Fixable viability dye			Life technologies	APC-Cy7	1:1000

2.7.2 Staining for cell surface markers

Immunostaining of 1×10^5 to 1×10^6 cells was performed with antibodies at dilutions stated in **Table 2.6**. Cells were stained for 30 minutes on ice and washed twice in cold FACs buffer. Cells were fixed in 100 μ L fixation buffer (eBioscience) for 20 minutes at room temperature. Cells were washed twice in FACs buffer and subsequently analysed on the LSR II flow cytometer using BD FACSDiva software 6.0. Acquired data was analysed on FlowJo v8.

2.7.3 Measure of transfection/transduction by detection of eBFP2/eGFP2

To enable measurement of transfection or transduction efficiencies; the expression of eBFP2 / eGFP2 co-expressed in the SFG vector was measured by flow cytometry using the Pacific blue / FITC channels respectively. 2.5×10^5 cells were washed twice with 1 mL FACs buffer (**Table 2.1**) and centrifuged at 400 x g for 5 minutes. Cells were analysed on the LSRII flow cytometer using BD FACSDiva software 6.0. Acquired data was analysed on FlowJo v8.

2.7.4 Detection of BiTE staining to cell lines

To detect binding of BiTEs to cell lines, supernatants were harvested from 293T cells transiently transfected with constructs encoding the BiTE variants. 1×10^5 target cell lines (SupT1, GD2.SupT1, Jurkat and Jurkat TCR ko) were incubated with 250 μ L harvested supernatants for 30 minutes at room temperature. Cells were subsequently washed in FACs buffer and stained 1:100 with penta-his-Alexa Fluor 647 secondary antibody for 30 minutes on ice. After washing twice in FACs buffer cells were analysed on FACs Calibur flow cytometer using Cell quest Software. Acquired data was analysed on FlowJo v8.

2.7.5 Quantification of cell surface epitopes by flow cytometry

The expression levels of cell-surface antigens on a cell lines were quantified by flow cytometry using an antigen quantification kit (QIFIKIT, Dako). Cell lines were stained with 10 μ L of purified anti-GD2, anti-OAcGD2 or anti-ALK antibodies (**Table 2.6**) at 4 °C for 1 hour. Cells were washed twice with FACs buffer (**Table 2.1**) with centrifugation at 400 x g for 5 minutes. Cells and calibrated mouse IgG-binding beads

were stained for one hour on ice with a fluorescein-labelled goat anti-mouse IgG antibody (Dako North America, Inc.). The cells and beads were washed three times in 2 mL FACs buffer and resuspended in 200 μ L FACs buffer immediately prior to analysis by flow cytometry (CYAN analyser). Quantification of bound antibodies per cell was accomplished by comparing the increase in fluorescence between antibody labelled cells and isotype control. A calibration curve determined by the increase in fluorescence for the IgG-binding beads related to the number of IgG molecules bound per peak.

2.7.6 Disaggregation of tumours from *ALK^{F1174L}/MYCN* transgenic mice

Tumours were cut into small pieces using a scalpel and further disaggregated using the flat-end of a plunger from a 1 mL syringe. Cells were passed through a 70 μ m cell strainer and washed twice in 5 mL RPMI; cells were centrifuged at 400 x g for 5 minutes. Cells were resuspended in 5 mL RPMI and 3 mL Histopaque (Sigma) layered below the media using a 1 mL pipettor. Cells were centrifuged at 700 x g for 30 minutes with no break. The cells in the interphase between the RPMI and histopaque were removed and washed twice in FACs buffer. Cells were stained for cell surface antigens as described in 2.7.2.

2.8 Statistical analysis

All statistical analyses were performed in GraphPad Prism v5. Unless otherwise stated, data were expressed as mean \pm SEM. EC₅₀ values for cytotoxicity or proliferation assays were determined by non-linear regression and statistically compared using the comparison of Fits (F) test. Statistical analyses of in vitro assays were undertaken by 1-way ANOVA with donor matching and Bonferonni's post-test for multiple comparisons. Statistical significance was indicated as follows in the figures **p<0.001 and *p<0.01.

CHAPTER 3:

Results (I)

An approach to target validation of neuroblastoma antigens for T cell immunotherapy

3.1 Introduction

The choice of tumour associated antigen (TAA) in cancer immunotherapy can influence the efficacy and toxicity profile of a particular T cell based therapy (Offringa, 2009). Ideally, a suitable target antigen is expressed homogeneously and abundantly on the tumour cell surface and has a minimal level or absence of expression on healthy tissues to avoid on-target off-tumour toxicities (Scott et al., 2012). It is also optimal that the TAA be essential to tumour cell survival, as this decreases the likelihood of immune editing and tumour escape, through its downregulation (Goldberger et al., 2008).

In neuroblastoma, GD2 provides an attractive target antigen for immunotherapy due to its high level of expression across several tumour types and restricted expression pattern on normal tissues (Suzuki and Cheung, 2015). The National Cancer Institute pilot programme for the prioritisation of cancer antigens ranks GD2 in place 12 out of 75 potential targets for cancer therapy. The criteria include therapeutic function, immunogenicity, role of antigen in oncogenicity, specificity to tumour cells, stem cell expression and cellular location of antigen expression (Cheever et al., 2009). Despite this, the main problems associated with targeting GD2⁺ tumours with immunotherapy are the on-target off-tumour toxicities associated with the minimal but restricted level of GD2 expression on healthy tissues (Lammie et al., 1993).

More recently, novel antigen *OAcGD2* has been described to have a highly tumour specific expression pattern. Targeting *OAcGD2* as opposed to GD2 may overcome some of the limitations associated with GD2-specific therapies (Alvarez-Rueda et al., 2011). In addition ALK may also serve as a favourable target for therapy as it is overexpressed in some neuroblastoma tumours (Lamant et al., 2000).

A crucial step in the development of any T cell based immunotherapy is target validation; this indicates whether a target antigen is a suitable TAA based on expression profiles across both tumour and healthy tissue samples. We have developed an approach to explore the expression pattern of tumour antigens across neuroblastoma cell lines and clinical samples by flow cytometry; the process is outlined in **Figure 3.1**.

The first step of our target validation process involves the confirmation of antigen expression on reference cell lines which have been modified to express our antigen of interest (described in section 3.2.1). This first step confirms the antibodies being used detect the respective antigen. The subsequent steps determine antigen expression on materials which to an increasing extent reflect the actual neuroblastoma tumour, whilst at the same time becoming a more limited resource. These include established neuroblastoma cell lines, primary neuroblastoma cell lines and ultimately fresh neuroblastoma tumour samples and healthy paediatric tissue samples. Target validation described in this chapter is limited to work on cell lines.

As a second arm of the validation process, the amount of antigen on reference and neuroblastoma cell lines was quantified to determine and compare the range of expression between GD2, OAcGD2 and ALK. The level of antigen expression can influence the sensitivity and efficacy of T cell therapies including approaches using BITEs and CARs (Weijtens et al., 2000, Stone et al., 2012)

Aims

1. To set up an approach to target validation by measuring expression of GD2, OAcGD2 and ALK antigens on established neuroblastoma cell lines and primary neuroblastoma cell lines by flow cytometry
2. To quantify the levels of antigen expressed across neuroblastoma cell lines

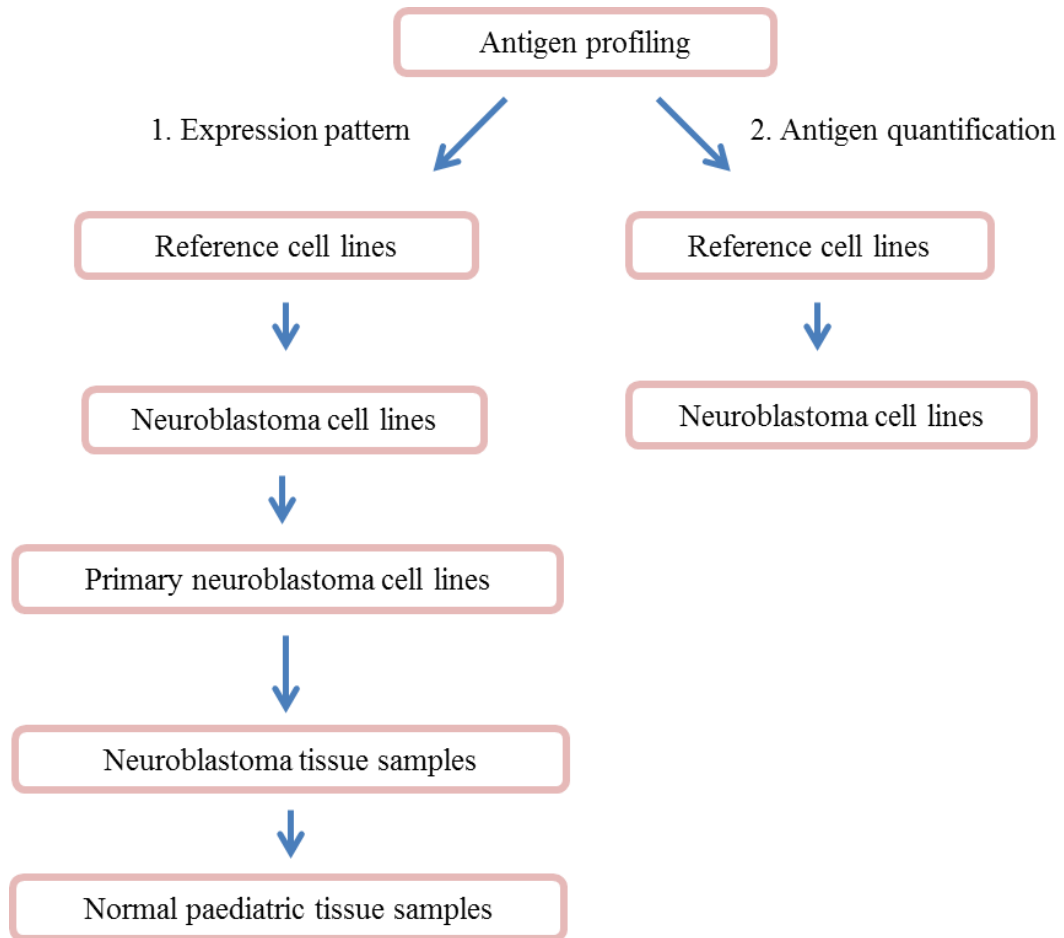


Figure 3.1: An approach to target validation and quantification of neuroblastoma antigens. This step-by-step approach enables the optimisation of antigen detection using flow cytometry and/or immunohistochemistry.

3.2 Results

3.2.1 Target validation on reference cell lines

As part of the target validation process, SupT1 lymphoma cells were used as a reference cell line. These cells have been transduced to express antigens of interest on the cell surface and can be used as positive or negative controls for detection of GD2, *O*AcGD2 or ALK expression by flow cytometry, immunohistochemistry and other immunological methods.

SupT1 cells positive for GD2 expression (and named GD2.SupT1) were generated by transduction of cells with the oncoretroviral SFG vector encoding both GD3 synthase and GM2/GD2 synthase separated by a cleavable in-frame 2A peptide. The enzymes work in sequence to convert membrane expressed GM3 to GD3 and subsequently to GD2 (GD2 biosynthesis is described in section 1.1.4). The cell line was generated by the Martin Pule group (UCL Cancer Institute). GD2 expression was confirmed on GD2.SupT1 cells by flow cytometry (**Figure 3.2 A**), additionally *O*AcGD2 was also detected on approximately 50% of GD2.SupT1 cells (**Figure 3.2 B**), indicating active *O*-acetylation on GD2.

SupT1 cells positive for ALK expression (and named ALK.SupT1) were produced by transduction of cells with the SFG vector encoding the ectodomain and transmembrane domain of ALK; leading to ALK expression on the cell surface and absence of the RTK intracellular signalling domains. The cell line was generated by Maria-Alonso Ferrero (UCL Great Ormond Street Institute of Child Health). ALK expression was detected on ALK.SupT1 cells (**Figure 3.2 C**). These staining results confirmed the antibodies used for flow cytometry are appropriate for antigen detection.

3.2.2 Target validation on neuroblastoma cell lines

For the next step of the target validation process; the presence of GD2, *O*AcGD2 and ALK were determined on neuroblastoma cell lines Lan-1, SKNDZ, SKNSH and IMR32 (**Figure 3.3**). Cells were incubated in equal quantities of primary unconjugated

antibody, followed by detection of antibody binding with FITC-conjugated anti-mouse IgG.

GD2 expression was the brightest (approx. MFI 30,000 - 75,000) on Lan-1, SKNDZ and IMR32 cell lines, whereas dim or absence of expression was detected on SKNSH. The presence of *OAcGD2* was also detected on the three GD2 bright cell lines (approx. MFI 10,000) and dim or absence of expression on SKNSH. In comparison to GD2 and *OAcGD2*, ALK stained more dimly (approx. MFI 200 - 600) on all cell lines. This demonstrates that our antigens of interest are uniformly expressed across 3/4 of our neuroblastoma cell lines.

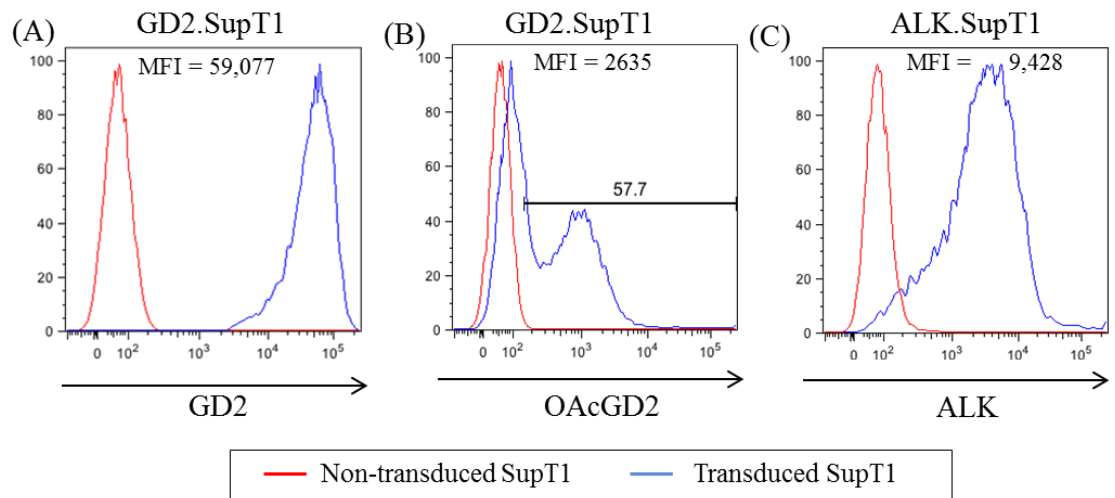


Figure 3.2: Expression of neuroblastoma antigens on reference SupT1 cell lines. Detection of (A) GD2 and (B) *OAcGD2* expression on SupT1 cells transduced with GD3/GD2 synthase enzyme (GD2.SupT1). Detection of (C) ALK on SupT1 cells transduced with a gene encoding the ALK ectodomain and transmembrane domain (ALK.SupT1). Non-transduced SupT1 cells were used as a control for staining. Cells were stained with primary unconjugated antibody (anti-human GD2, anti-human *OAcGD2* and anti-ALK purified antibodies) and antibody binding detected with FITC-conjugated anti-mouse IgG secondary antibody by flow cytometry. Mean fluorescence intensity (MFI) is shown for transduced SupT1 cells.

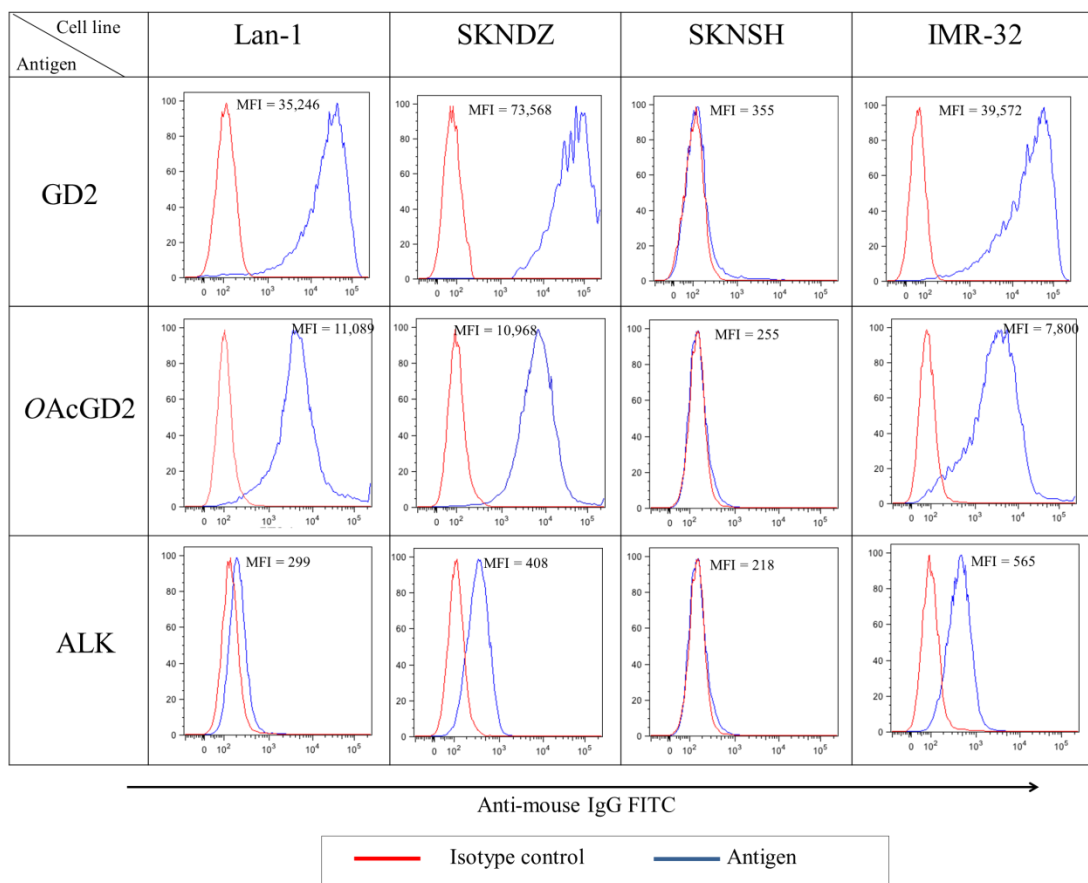


Figure 3.3: Expression of GD2, OAcGD2 and ALK on neuroblastoma cell lines. Neuroblastoma cell lines Lan-1, SKNDZ, SKNSH and IMR32 stained for GD2 expression (top panel), OAcGD2 expression (middle panel) and ALK expression (bottom panel). Cells were stained with primary unconjugated antibody (anti-human GD2, anti-human OAcGD2 and anti-ALK purified antibodies) and antibody binding detected with FITC-conjugated anti-mouse IgG secondary antibody by flow cytometry. MFI values are shown for blue graphs.

3.2.3 Target validation on primary neuroblastoma cell lines

For the third part of the target validation process; antigen expression on material that more closely resembled the neuroblastoma tumour was determined. Primary neuroblastoma cell lines derived from patient biopsy or resection tumour samples at Great Ormond Street Hospital were established and cultured as neurospheres in stem cell media by Katherine Pacey and Tessa Kasia (UCL GOSH ICH). **Table 3.1** provides a summary of tumour characteristics for 10 patient samples received between 2014 -2016. 6/10 samples were from a patient biopsy and 4/10 were from a post-chemotherapy resection. 5/10 samples had confirmed CD56 (NCAM) expression by immunohistochemistry, CD56 is uniformly expressed and strongly positive in neuroblastoma cells (Krishnan et al., 2009). 2/10 samples had detectable levels of *MYCN* amplification. In total all primary cell lines underwent less than three cell culture passages.

Unlike established cell lines, the primary cell lines have a mixed, heterogeneous cell population. To detect neuroblastoma tumour cells in the cell mixture, cells were stained with both CD56 and CD45-specific antibodies. CD56⁺/CD45⁻ cells were identified as the neuroblastoma population and expression of antigens GD2, *OAcGD2* and ALK were subsequently measured by flow cytometry. **Figure 3.4** provides an example of the gating strategy used to analyse neuroblastoma cells and **Figure 3.5** provides a summary of the staining results on the 10 primary neuroblastoma cell lines. Both GD2 and *OAcGD2* expression were detected on 10/10 primary cell lines, indicating that both antigens are favourable targets for therapy. Dim ALK expression was only detected on 2/10 primary cell lines. This confirms findings reported in the literature of GD2 being abundantly expressed on neuroblastoma tumours but only a subset of tumours overexpress ALK (Lammie et al., 1993, De Brouwer et al., 2010).

Table 3. 1 Summary of neuroblastoma tumour characteristics

No	Pathology number	Histological diagnosis	Nature of sample	Diagnosis or relapse?	Histology report
1	4669	Neuroblastoma, poorly differentiated	Biopsy, abdominal tumour	Diagnosis	CD56 ⁺ , NB84 ⁺ , CD99 ⁻ , MYCN amplified, 1p loss, 17q gain, no 11q imbalance
2	4566	Neuroblastoma, poorly differentiated	Biopsy, suprarenal tumour	Diagnosis	CD56 ⁺ , NB84 ⁺ , CD99 ⁻ , S100 ⁻ , MYCN amplified, 1p.1q imbalance, 11q imbalance, 17q gain
3	3544	Neuroblastoma, differentiating	Resection, abdominal tumour	Diagnosis	MYCN not amplified, no 1p/q imbalance, no 11q imbalance, no 17q imbalance
4	4433	Neuroblastoma, poorly differentiated	Resection, suprarenal tumour	Diagnosis	CD56 ⁺ , NB84 ⁺ , 1p/q imbalance, MYCN not amplified, no 11q imbalance, inconclusive 17p/17q imbalance
5	5045	Ganglioneuroblastoma, intermixed	Resection, abdominal tumour	Post chemotherapy resection	No staining or molecular analysis described
6	4519	Neuroblastoma, poorly differentiated	Biopsy, abdominal tumour	Diagnosis	CD56 ⁺ , NB84 ⁺ , no 1p/1q imbalance, MYCN not amplified, 11q imbalance, 17q imbalance
7	2006	Neuroblastoma	Resection, suprarenal tumour	Post chemotherapy resection	No staining or molecular analysis described
8	4544	Neuroblastoma, poorly differentiated	Resection, paraspinal tumour	Post chemotherapy resection	No staining or molecular analysis described
9	1315	Neuroblastoma, poorly differentiated	Biopsy, suprarenal tumour	Diagnosis	CD56 ⁺ , NB84 ⁺ , 1p/q imbalance, MYCN not amplified, no 11q imbalance, 17q imbalance
10	4467	Neuroblastoma	Resection, adrenal tumour	Post chemotherapy resection	No staining or molecular analysis described

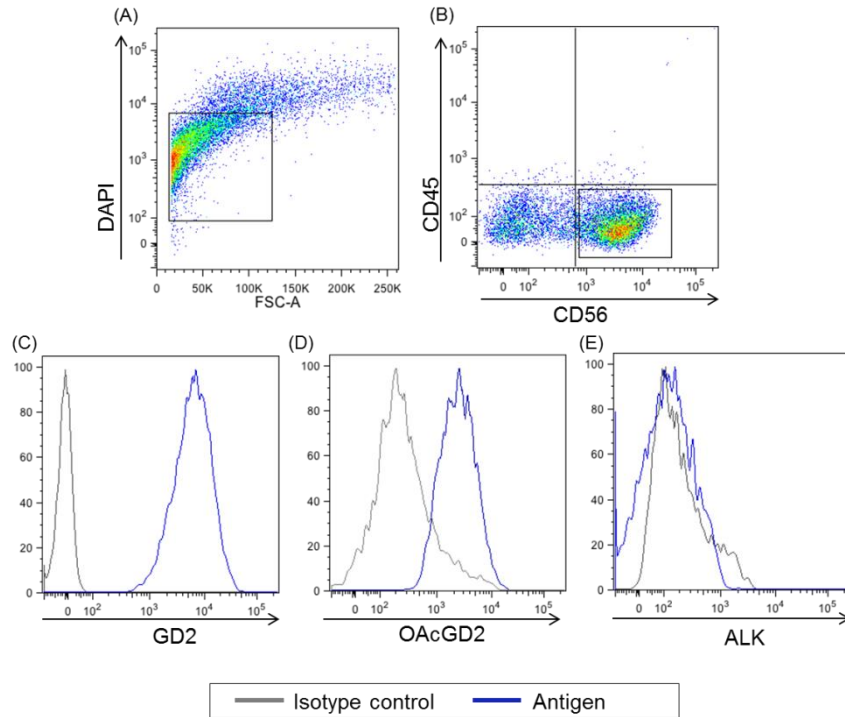


Figure 3.4: Gating strategy for phenotyping of primary neuroblastoma cell lines by flow cytometry. (A) Live cells were identified by exclusion of DAPI. (B) Neuroblastoma cells were determined to be the CD56⁺/CD45⁻ population. Surface expression of (C) GD2 (D) OAcGD2 and (E) ALK on the CD56⁺/CD45⁻ neuroblastoma cells were subsequently assessed. Cells were stained with anti-GD2-PE or primary unconjugated antibody and antibody binding detected with APC-conjugated anti-mouse IgG secondary antibody by flow cytometry.

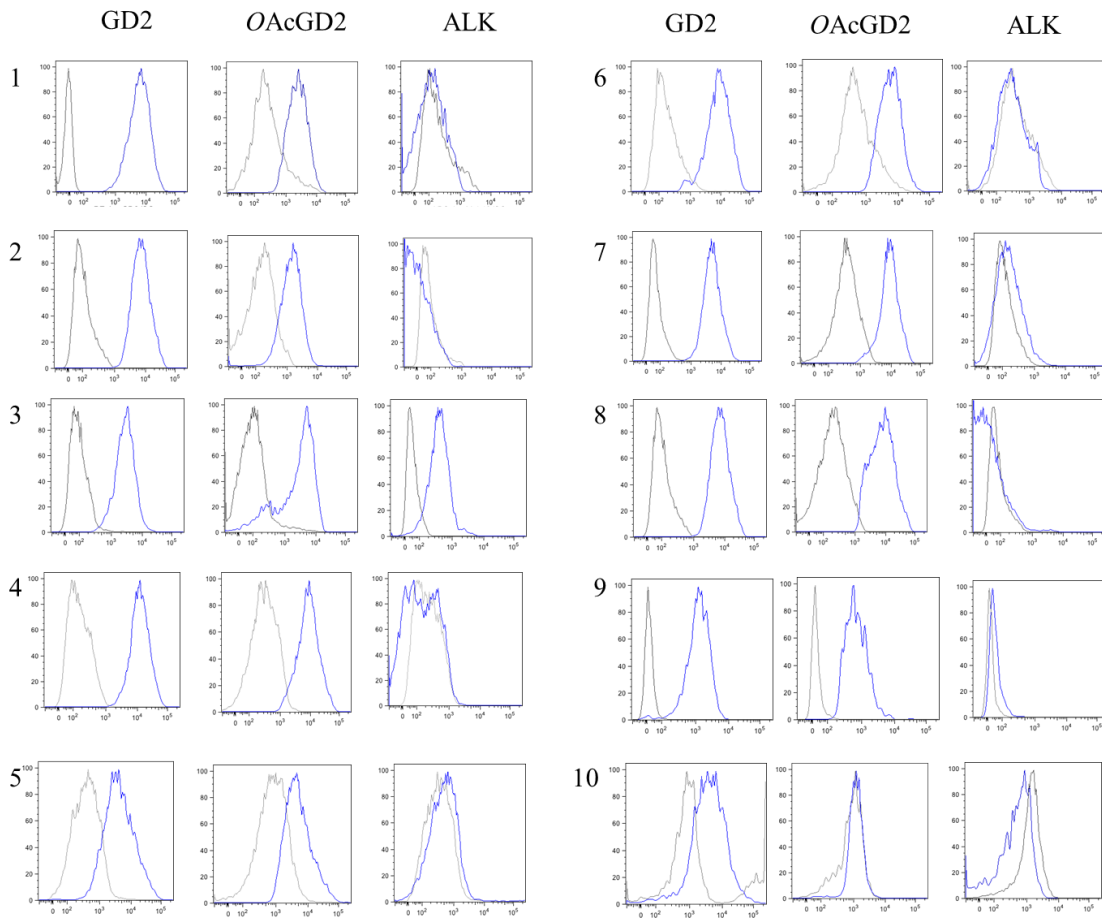


Figure 3.5: Antigen expression on primary neuroblastoma cell lines. Antigen expression determined on live, CD56⁺/CD45⁻ primary cell lines 1 - 10 by flow cytometry. Expression of GD2, OAcGD2 and ALK (blue line) in comparison to isotype control (grey line). Cells were stained with anti-GD2-PE or primary unconjugated antibody and antibody binding detected with APC-conjugated anti-mouse IgG secondary antibody by flow cytometry, n=10.

3.2.4 Detection of GD2 and OAcGD2 on reference SupT1 cell lines using immunohistochemistry

The next step in the target validation approach is to determine antigen expression on frozen neuroblastoma tissue sections. This approach will provide a more accurate representation of antigen expression profiles on cells that have not been cultured in the laboratory, which can potentially influence antigen expression. To set up this validation process, our reference cell lines SupT1 and GD2.SupT1 were pelleted and snap frozen. Cells pellets were sectioned and stained for GD2 and OAcGD2 expression by immunohistochemistry. Staining was performed by the Histopathology department at GOSH (**Figure 3.6**).

Cell pellets were Expression of both GD2 and OAcGD2 was determined by detected on the surface of GD2.SupT1 cells. Positive (brown) staining was present on the surface of all cells incubated with an anti-GD2 antibody (14G2a) (**Figure 3.6B**), confirming the 100% GD2 positive expression on GD2.SupT1 detected by flow cytometry (**Figure 3.2 A**).

Less than 50% of cells stained positive for OAcGD2 expression (mAb 8B6) (**Figure 3.6 D**) which correlates with the approximately 50% level of detection of OAcGD2 on GD2.SupT1 measured by flow cytometry (**Figure 3.2 B**). The flow cytometry and immunohistochemistry data combined, confirm the presence of GD2 and OAcGD2 on our reference target GD2.SupT1 cell lines. GD2 and OAcGD2 were not detected on non-transduced SupT1 cells (**Figure 3.4 A, D**). This approach has demonstrated it is possible to detect antigens GD2 and OAcGD2 by immunohistochemistry and will lead to the future set up of staining frozen neuroblastoma tissue sections.

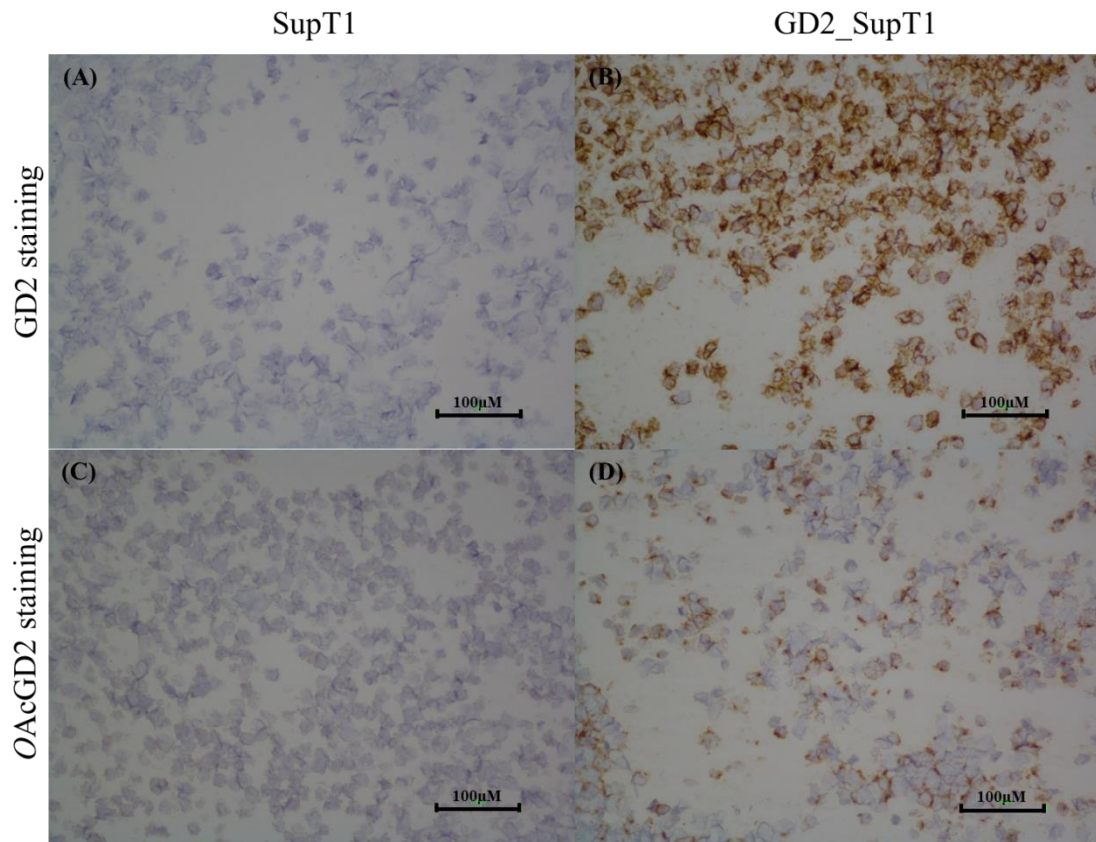


Figure 3.6: Detection of GD2 and OAcGD2 on frozen cell lines by immunohistochemistry. GD2 expression on (A) Non-transformed SupT1 (negative control) and (B) GD2.SupT1 cell pellets. OAcGD2 expression on (C) SupT1 cells (negative control) and (D) GD2.SupT1 cells. Cells were stained with purified anti-GD2 or anti-OAcGD2 antibody followed by an anti-mouse IgG-horseradish peroxidase conjugated antibody. Positive staining is determined by brown staining upon addition of DAB substrate solution.

3.2.5: Antigen quantification on reference and neuroblastoma cell lines

Another part of the validation process is to quantify the levels of antigen expressed on our cell lines. This can give an indication of the type of T cell based therapy that may be more appropriate to target a given antigen with a specific expression (Stone et al., 2012). It is important to have reference cell lines that have a range of antigen densities which can be used to determine the upper and lower limits of antigen detection. This can be achieved using fluorescence activated cell sorting. Reference ALK.SupT1 cell lines that have been sorted into high and low ALK expression have been produced in the lab (**Figure 3.7**).

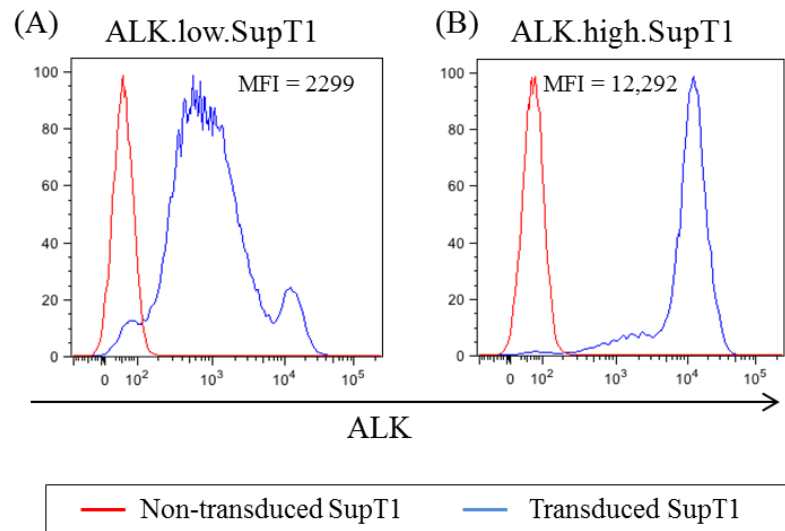


Figure 3.7: Generation of low and high levels of antigen expression on reference cell lines. ALK.SupT1 cells were sorted into (A) low and (B) high levels of ALK expression by fluorescence activated cell sorting. For sorting cells were stained with for ALK expression immediately after being sorted. MFI values are shown for blue graphs.

To quantify the level of antigen expression on our cell lines an antigen quantification kit was used (QIFIKIT®), this kit provides quantitative analysis of indirect immunofluorescence staining in flow cytometry. To perform the assay, both reference SupT1 and neuroblastoma cell lines were labelled with an unconjugated antigen-

specific primary mouse mAb at saturating concentrations (e.g. anti-GD2, anti-*OAcGD2* or anti-ALK mAb). The number of bound antibody molecules corresponds to the number of antigenic sites. To detect the binding of the primary antibody; cells were labelled with saturating amounts of FITC-conjugated anti-mouse IgG secondary antibody and binding (MFI) measured by flow cytometry.

To correlate the MFI with the corresponding number of antigenic sites per cell a set of calibrated beads coated with different but well-defined quantities of mouse IgG mAbs were labelled with the same secondary antibody and used to construct a calibration curve by correlating the MFI with the corresponding number of antigen molecules per bead. The number of antigenic sites on a given cell line were determined by interpolation of the calibration curve (**Figure 3.8**).

Antigen density was first quantified on the SupT1 reference cell lines. GD2.SupT1 cells have approximately 1×10^6 GD2 molecules expressed on their cell surface (**Figure 3.9 A**) and approximately 30,000 *OAcGD2* molecules (**Figure 3.9 B**) on cells positive for *OAcGD2* expression (**Figure 3.9 B**). ALK.low.SupT1 and ALK.high.SupT1 have approximately 30,000 and 170,000 ALK molecules expressed on the cell surface respectively (**Figure 3.2 C**). GD2, *OAcGD2* and ALK were not detected on non-transduced SupT1 cells (**Figure 3.9 A-C**).

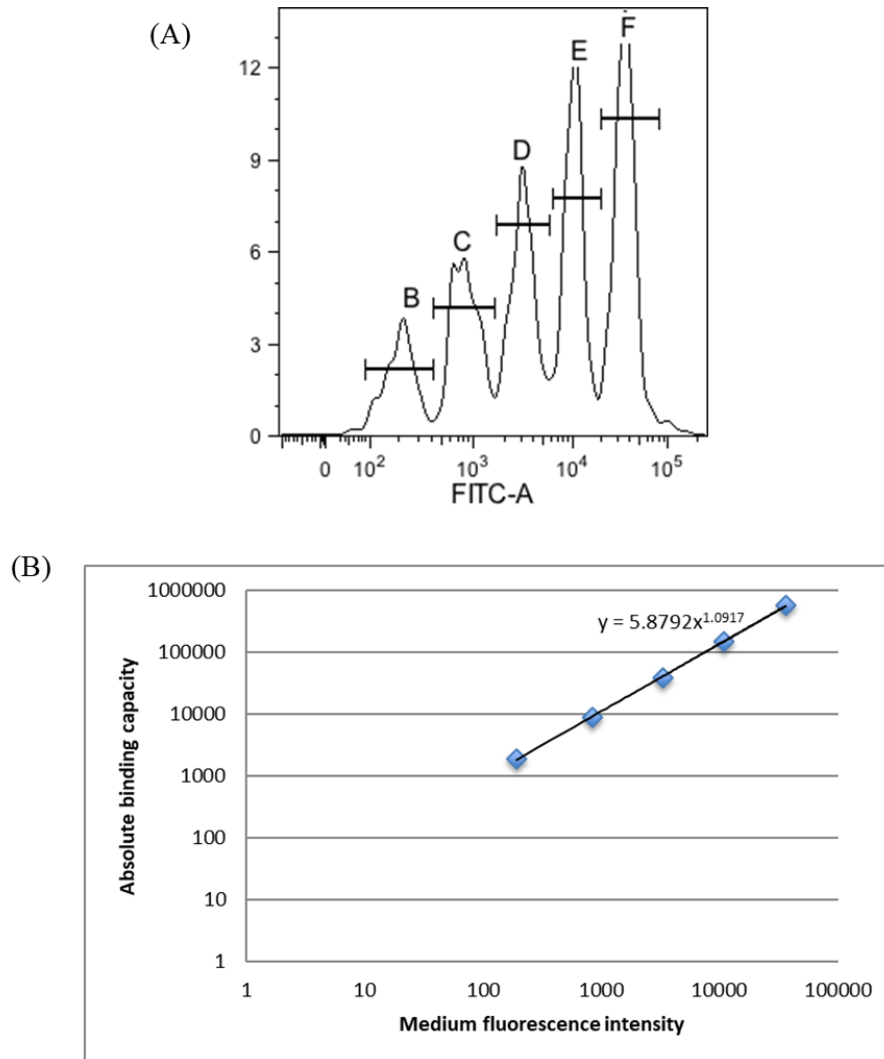


Figure 3.8: Antigen expression quantified by interpolation of a standard curve generated using calibration beads with known antigen levels and MFI values. (A) Calibration beads B – F with increasing and quantified levels of mouse IgG on the surface were incubated with saturating amounts of FITC-anti-mouse-IgG antibody and MFI values measured by flow cytometry. **(B)** Antigen quantity and MFI values for beads B – F were used to generate a standard curve for subsequent calculation of antigen quantity on cells after antibody labelling.

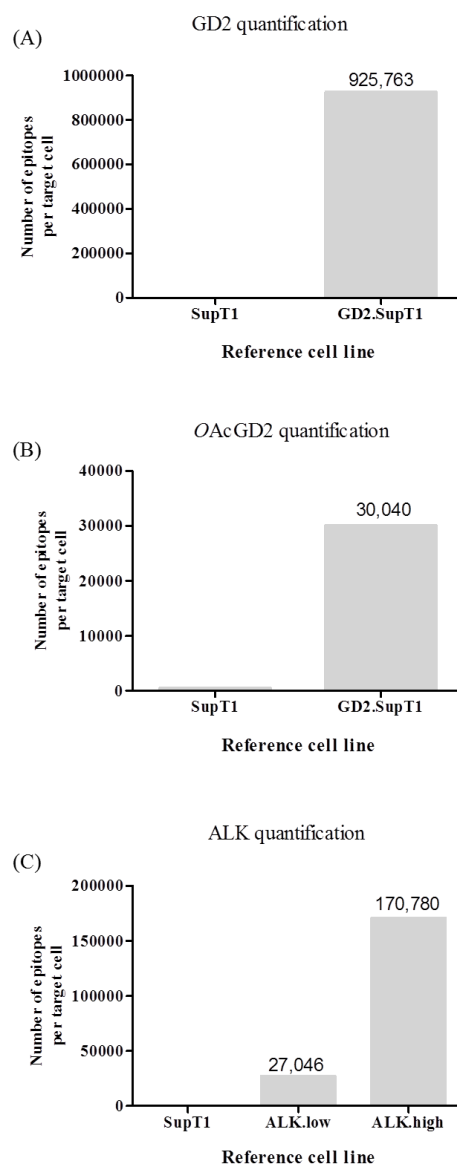


Figure 3.9: GD2, OAcGD2 and ALK antigen density on reference SupT1 cell lines. Quantification of antigens GD2 (A) and OAcGD2 (B) on the GD2.SupT1 cell line and ALK (C) on ALK.low.SupT1 and ALK.high.SupT1 cell lines using the QIFIKIT antigen density kit. Cells were stained with saturating amounts of unconjugated anti-GD2, anti-OAcGD2 or anti-ALK antibody and saturating amounts of FITC-anti-mouse IgG secondary antibody. Cells were analysed by flow cytometry and MFI values used to determine antigen density by interpolation of a standard curve, n=1.

Next, the level of antigen expression was determined on Lan-1, SKNDZ, IMR32 and SKNSH neuroblastoma cell lines. The GD2 expression levels for these cell lines ranged from approximately 500,000 – 1,000,000 molecules per cell. SKNDZ cells had the highest level of GD2 expression (1,177,544 molecules per cell) similar to reference cell line GD2.SupT1. Lan-1 and IMR32 cells had 524,870 and 596,524 molecules of GD2 per cell respectively and SKNSH had a dim GD2 expression (2421 molecules per cell) (**Figure 3.10A**).

The density of OAcGD2 on the neuroblastoma cell lines was five to ten-fold less in comparison to GD2, with a range of approximately 80,000 – 150,000 molecules per cell. Both Lan-1 and SKNDZ had approximately 150,000 OAcGD2 molecules per cell and IMR32 cells had 81,529 molecules per cell. SKNSH appeared negative for OAcGD2 expression (1,185 molecules per cell) in comparison to the other cell lines (**Figure 3.10 B**).

Expression of ALK was the lowest and ranged between 500 – 5000 antigen molecules per cell. ALK expression was the highest in the IMR32 cell line (4785), followed by SKNDZ (2978), Lan-1 (844) and SKNSH (489) (**Figure 3.10 C**). This data highlights the differences in levels of antigen expression for a given antigen across a panel of cell lines.

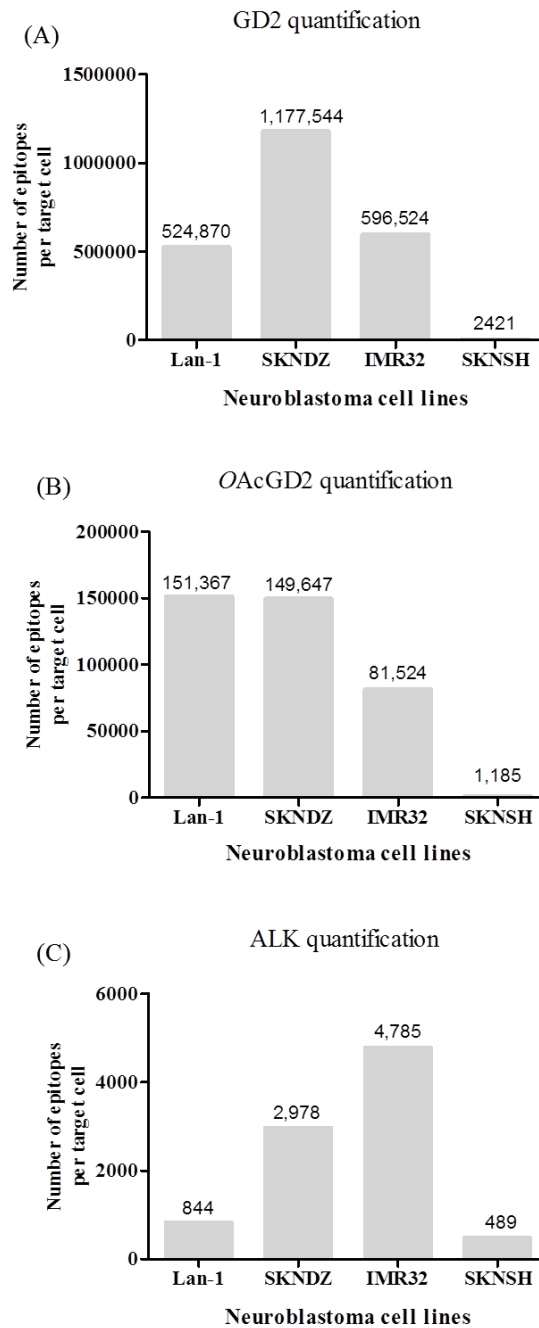


Figure 3.10: GD2, OAcGD2 and ALK density on neuroblastoma cell lines.

Quantification of antigens (A) GD2, (B) OAcGD2 and (C) ALK on Lan-1, SKNDZ, IMR32 and SKNSH using the QIFIKIT antigen density kit. Cells were stained with saturating amounts of unconjugated anti-GD2, anti-OAcGD2 or anti-ALK antibody and saturating amounts of FITC-anti-mouse IgG secondary antibody. Cells were analysed by flow cytometry and MFI values used to determine antigen density by interpolation of a standard curve, n=1.

3.3 Discussion

An approach to target validation was used to determine the expression of antigens GD2, *OAcGD2* and ALK across neuroblastoma cell lines and patient derived primary cell lines. This work has shown that both GD2 and *OAcGD2* are uniformly expressed across neuroblastoma samples. GD2 is a highly expressed antigen, with up to 1×10^6 molecules per cell across neuroblastoma cell lines. The reported expression on neuroblastoma tissue is up to 1×10^7 molecules per cell (Wu et al., 1986). *OAcGD2* has a lower level of expression than GD2, the antigen density across cell lines was 5 - 10 fold lower in the range 80,000 - 150,000, SKNSH was the only GD2/*OAcGD2* dim cell line, which has been previously reported (Biedler et al., 1973). ALK was expressed at low levels across all neuroblastoma cell lines, but was only detected on 2/10 primary cell lines.

This work supports both GD2 and *OAcGD2* as promising targets for immunotherapy. ALK is also a potential target but will not be pursued further in this project. One of the important features of a target antigen is the maintenance of expression after therapy. A number of studies have demonstrated the continued high level of expression of GD2 across tumour samples after multi-modal therapies including chemotherapy and radiotherapy and in particular after GD2-targeted treatment with antibodies. The loss of GD2 expression has only been described as a rare event (Kramer et al., 1998, Schumacher-Kuckelkorn et al., 2005, Poon et al., 2015). Antigen maintenance after therapy is yet to be explored for *OAcGD2*.

One of the limitations of measuring antigen expression on cultured cell lines/primary cell lines is the potential change in the antigen expression profile over time. Cell lines may therefore not be truly representative of the original tumour sample. One of the ways to overcome this problem is to determine antigen expression on tumour samples by flow cytometry as soon as fresh tumour samples are received.

Another approach is to preserve tumour tissue and measure antigen expression using immunohistochemistry. Fixation is a standard procedure during sample preparation in immunohistochemistry; however this process can mask epitopes of interest including

GD2. An alternative approach is to snap freeze tissue samples which will enable preservation and allow antibody access to potential antigens. We have demonstrated that snap freezing cell lines, preserves the GD2 and *OAcGD2* antigens on GD2.SupT1 cells in a form that is readily detectable using available antibodies. Detection of ALK on ALK.SupT1 cell lines was not measured as the ALK detection antibody (mab13) is not compatible with this technique.

Based on the high level of GD2 expression on tumour and minimal expression across healthy tissues, we explored GD2 as a target for BiTE therapy. Few GD2-specific BiTE approaches have been reported, in comparison to GD2-specific CAR studies (Yankelevich et al., 2012, Cheng et al., 2015, Pule et al., 2008, Prapa et al., 2015).

We also explored *OAcGD2* as a novel target for CAR T cell therapy based on the lower expression levels of *OAcGD2* in comparison to GD2. Current targets of CAR T cell therapy have a low expression pattern on tumour cells. For example the median density of CD22 in ALL blasts was reported to be 3500 sites per cell, and the expression of CD19 on CLL cells was reported to be 13,000 sites per cell (Haso et al., 2013) (Ginaldi et al., 1998).

Future directions

The next step in this target validation approach will be to screen tumour samples as well as healthy paediatric tissues to test presence or absence of antigen expression. Reference cell lines can be used to set up this approach, in particular, selective expression and a range of antigen densities across a reference cell line can help determine the limit of detection, this work is currently ongoing.

Based on the set up of the target validation approach described in this chapter, flow cytometry on fresh tumour samples from neuroblastoma biopsy or resection samples is now routinely performed to assess GD2 and *OAcGD2* expression.

CHAPTER 4:

Results (II)

Development and characterisation of GD2 and CD3 targeted Bispecific T cell Engagers (BiTE)

4.1 Introduction

4.1.1 Bispecific T cell Engagers (BiTE)

This chapter describes the generation and characterisation of a series of BiTEs to redirect T cells to target GD2 positive tumours. An empirical approach to BiTE design was explored to determine the optimal BiTE format. In particular the choice of scFvs and linker sequence, which can impact the properties and pharmacodynamics (such as production, stability and affinity) of a BiTE therapeutic, were considered (Dreier et al., 2002, Cheng et al., 2015).

A high binding affinity of an scFv to the respective tumour target antigen has been demonstrated to be a key requirement for achieving tumour cell killing by T cells at low BiTE concentrations (<10 pg/mL *in vitro*) and is one of the features of FDA approved BiTE Blinatumomab (Dreier et al., 2002). In contrast, a low binding affinity of an scFv to CD3 ϵ on T cells is required to mimic the binding interaction of a TCR and its target MHC peptide complex to achieve efficient T cell signalling (Hoffmann et al., 2005). Additionally, the formation of an immunological synapse and subsequent potency of redirected T cell lysis is affected by epitope distance to the target cell membrane and antigen size (Bluemel, 2010) (**Figure 1.10**). We therefore investigated differences in linker size between the two scFvs in the BiTE molecule to determine the effects on redirecting T cell cytolytic activity.

In the context of antigen-antibody interactions, binding affinity is the strength of the binding interaction between an epitope and an antibody's antigen binding site, this is described by the equilibrium dissociation constant (K_D). The K_D can further be described as a ratio between the association (K_a) and dissociation (K_d) rate of an

antibody-antigen complex. $K_D = K_d/K_a$, the smaller the K_D the greater the binding affinity.

4.1.2 Selection of GD2 specific scFvs

To select GD2 specific scFvs to compare in the BiTE design, the reported binding affinity of five GD2 specific monoclonal antibodies along with their chimerised (ch) and/or humanised (hu) versions were studied from the literature and are reported in **Table 4.1**. The two scFvs selected to study in the BiTE design are derived from mAbs hu14.18 and huK666. Hu14.18 is derived from parental mAb 14.18 of which 14.G2a is an IgG2a-class switch variant (Mujoo et al., 1989). Hu14.18 was selected based on the proven efficacy of ch14.18 in the clinical setting (Yu et al., 2010); variations of this mAb under clinical testing are documented by Ahmed *et al*, 2014.

Table 4. 1 Reported GD2 specific mAbs and corresponding binding affinities

GD2 specific mAb	Affinity (K_D)	References
3F8	5 nM	(Cheung, 2012)
Ch.3F8	13 nM	(Cheung, 2012)
Hu.3F8	11 nM	(Cheung, 2012)
14.G2a	77 nM	(Cheung, 2012)
14.18	35 nM	(Mujoo et al., 1987)
Hu.14.18	Not reported	
Ch.14.18	Not reported	
ME36.1	19 nM	(Cheung, 2012)
MuK666	100 nM	(Nakamura et al., 2001)
HuK666	149 nM	(Nakamura et al., 2001)
60C3	212 nM	(Alvarez-Rueda et al., 2007)
Chimeric 60C3	206 nM	(Alvarez-Rueda et al., 2007)

Ch = chimeric; Hu = humanised

Although the affinity of the hu14.18 mAb is not reported, the parental 14.18 mAb has a reported binding affinity of 35 nM. HuK666 derived from murine mAb muK666 was selected to compare against hu14.18 as it has a lower binding affinity to GD2 and would be useful to observe differences in the ability of redirecting T cells (Nakamura et al., 2001).

4.1.3 Selection of CD3 specific scFvs

It is well established that mere binding of different anti-CD3 mAbs trigger mitogenesis in T cells and induce the production of immune mediators like IFN- γ and IL-2 (Van Wauwe et al., 1980). In the context of a BiTE; the monomeric binding of the BiTE to the CD3 ϵ subunit of the TCR complex in the absence of binding a target cell antigen is insufficient to allow robust T cell signalling and activation. This feature is desirable and avoids non-specific T cell activation (Dreier et al., 2002).

In T cell biology, the duration of the TCR and peptide-MHC binding is a critical parameter in T cell activation. The upper limit of natural TCR affinity correlates to a dissociation constant (K_D) of around 1 - 50 μ M. To select a panel of scFvs to be tested in the BiTE format, the reported binding affinities of a selection of mitogenic CD3 specific mAbs were studied from the literature and are reported in **Table 4.2**.

Table 4. 4 CD3 specific mAbs and corresponding binding affinities

CD3 specific mAb	Affinity (K_D)	References
L2K	*260 nM	(Dreier et al., 2002)
OKT3	1.2 nM	(Adair et al., 1994)
HuOKT3	1.4 nM	(Adair et al., 1994)
UCHT-1	2.2 nM	(Hexham et al., 2001)
HuUCHT-1	2.5 nM	(Beverley and Callard, 1981)
YTH12.5	not reported	
HuYTH	not reported	
TR-66	36 nM	(Jacobs et al., 1997)
BMA030	8 nM	(Jacobs et al., 1997)
SP34	150 nM	(Hexham et al., 2001)

*Reported affinity of scFv

The three humanised scFvs chosen to compare in the BiTE format were derived from mAbs huOKT3, huUCHT-1 and huYTH 12.5 (Adair et al., 1994, Shalaby et al., 1992, Routledge et al., 1991). OKT3 is highly mitogenic and has a reported binding affinity to CD3 of 1.2 nM, the affinity of huOKT3 is 1.4 nM. Both forms have shown

the ability to bind and activate T cells in a number of bispecific antibodies directed at tumour antigens such as HER2. (Sen et al., 2001, Yoshida et al., 2003, Zhou et al., 2006, Cheng et al., 2015)

Parental mAb UCHT-1 and huUCHT-1 have reported binding affinities of 2.2 nM and 2.5 nM respectively (Beverley and Callard, 1981). The ability of UCHT-1 to retarget cytotoxic T cells efficiently has been demonstrated in a number of bispecific antibody formats (Shalaby et al., 1992, Kim et al., 2012, Durben et al., 2015). Both OKT3 and UCHT-1 monoclonal antibodies recognise the same epitope on CD3 (Burns et al., 1982, Van Wauwe et al., 1984). Other studies have also demonstrated overlap between the binding sites of both antibodies (Arnett et al., 2004).

The third CD3 specific scFv is derived from mAb clone YTH12.5 (Clark et al., 1989), of which we refer to the humanised form as huYTH (Routledge et al., 1991). The avidity of the humanised mAb is 1.3 fold down compared to the parental antibody format, this is reported to compare favourably with changes in avidity and affinity observed after the reshaping of other antibodies (Routledge et al., 1991). Although the binding affinity of YTH12.5 and huYTH have not been reported, the mAbs have demonstrated the ability to redirect T cells to kill tumour target cells in the bispecific antibody format (Haagen et al., 1992, Haagen et al., 1995).

4.1.4 Selection of a linker

A non-immunogenic linker sequence is used to link the two scFvs of the BiTE molecule in tandem. The linker determines the distance between the two scFvs and is expected to allow a high degree of rotational flexibility as may be needed for simultaneous binding of the scFvs to two epitopes positioned on cell membranes of two separate cells (**Figure 1.10**).

Bluemel *et al.* studied the impact of epitope distance and antigen size on the potency of target cell lysis by human cytotoxic T cells that were redirected by BiTE antibodies (Bluemel, 2010). The study demonstrated that despite a similar binding affinity of BiTE variants to the melanoma chondroitin sulphate proteoglycan (MCSP) tumour antigen; respective BiTE formats greatly differed in their potency of

redirected lysis of target CHO cells displaying various MCSP truncations. MCSP-specific BiTE antibodies binding the most membrane proximal domain of MCSP were the most potent. A stepwise increase in the distance of domains to the plasma membrane of target cells decreased BiTE potency and this was concluded to be due to the ability to form an immunological synapse. The results indicated the synapse formation or function may be more efficient, the closer T cell and target cell membranes can adhere to each other. (Bluemel, 2010).

An immunological synapse is typically 15 nm wide and although a BiTE induced immunological synapse has not been measured; the size of the synapse can be influenced by the length of the linker between the two scFvs. The length and sequence of the linker can impact BiTE stability as well as function. The most common protein linkers contain a combination of glycine and serine residues to provide flexibility and protease resistance (Huston et al., 1988). Other factors including oligomeric state and level of glycosylation can affect the stability, solubility and function of the BiTE. Reported BiTEs tend to have a short glycine-serine (Gly₄-Ser) linker of 5 or 15 amino acids. Blinatumomab has a five amino acid Gly₄-Ser linker; as CD19 has a large extracellular component, this size is thought to be efficient for optimal immunological synapse formation (Dreier et al., 2002). GD2 has a smaller membrane component; it is possible that an increased linker size can influence the efficient formation of an immunological synapse.

Table 4. 7 Linkers considered in the BiTE design

Linker	Abbreviation	Sequence	Length
Glycine- serine	(G ₄ S) ₃ / S	GGGGSGGGGSGGGGS	15
IgG1 hinge region	HNG / H	DPAEPKSPDKTHTCPPCKDPK	22
CD8α stalk region	CD8-STK / C	SDPTTTPAPRPPTPAPTIASQPLS LRPEACRPAAGGAVHTRGLDF ACD	48

Table 4.3 describes the three short (glycine-serine), medium (IgG1 hinge) and long (CD8 stalk) linkers used to join the GD2 and CD3 specific scFvs in the BiTE design which differ in their origin and sequence. Glycine-serine linkers are found natural occurring in many proteins and can be considered as independent proteins that do not affect the function of proteins to which they attach. As small amino acids, both glycine and serine provide flexibility and maintain stability of the linker structure (Argos, 1990).

The IgG1 hinge linker is 15 amino acids in length; in this study extra amino acids have been incorporated at the start and end of the linker. The hinge region forms a flexible linker between the Fab arms and the Fc part of an IgG1 antibody and is the most flexible out of the hinge regions in the various IgG subclasses (IgG1 -IgG4) (Roux et al., 1997). The stalk region of the CD8 α chain from the CD8 co-receptor found on cytotoxic T cells is 30 - 50 residues long and has a high degree of flexibility (Merry et al., 2003).

Aims

1. To generate 18 GD2/CD3 targeted BiTE variants by combination of two GD2-specific scFvs, three linkers and three CD3-specific scFvs.
2. To optimise production and purification of the BiTE variants.
3. To characterise the BiTE variants by measurement of thermal stability.

4.2 Results

4.2.1 Cloning of 18 GD2/CD3 specific BiTE variants

The 18 GD2/CD3 specific BiTE variants are shown in **Table 4.4**. 17 out of 18 of the BiTEs were successfully cloned into SFG retroviral vectors which co-express eBFP2. The GD2 specific scFvs were oriented as V_H - V_L and the CD3 specific scFvs as V_L - V_H. A hexa-histidine tag was positioned at the C-terminus to facilitate purification.

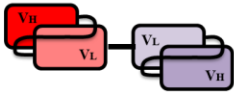
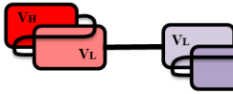
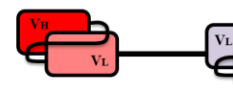
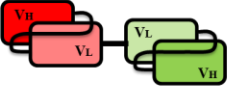
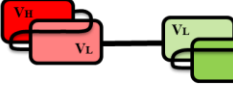
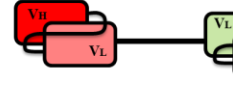
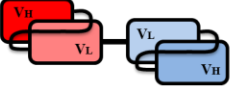
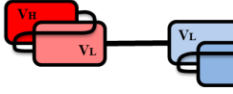
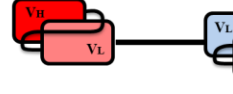
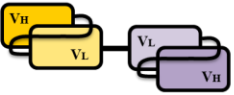
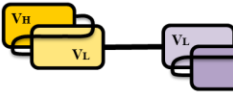
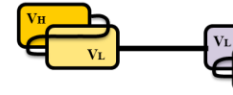
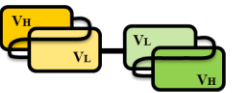
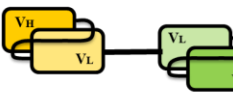
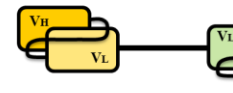
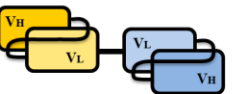
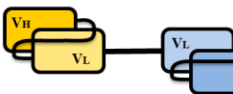
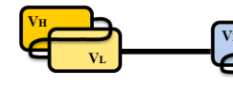
4.2.2 BiTE production by transient transfection of 293T cells

A small-scale production system was set up to generate the different BiTE variants. The BiTEs were produced by transient transfection of 293T cells followed by a harvest of BiTE containing supernatant at 72 hours post transfection. Successful transfection of the 293T cells was measured by detection of the co-expressed eBFP2 protein using flow cytometry (**Figure 4.1 A-B**). Transfection efficiencies were consistently between 60-80% for the 17 constructs tested (**Figure 4.1 C**).

4.2.3 BiTE purification using immobilised metal ion affinity chromatography (IMAC)

A column coated with nickel sepharose beads (His-trap HP) was used to purify the BiTEs from the cell culture supernatant by affinity purification. The BiTEs were captured on the nickel (II) via their C-terminal hexa-histidine tag. The imidazole side chain of histidine has a specific binding affinity for metal ions and facilitates this binding interaction to nickel (II); any non-specific proteins passed through the column and were discarded. Subsequent elution of the BiTE protein from the column was achieved by applying an elution buffer with a high concentration of imidazole to the column. The concentration of imidazole required in the elution buffer for efficient protein displacement is protein dependent. To determine the optimal concentration of imidazole required to elute the BiTEs from the column, elution buffers (formulations in **Table 2.1** of Materials and Methods) containing increasing concentrations (10 mM, 300 mM or 500 mM) of imidazole were applied consecutively and the eluates tested for presence of BiTEs by using an indirect flow cytometry based detection method.

Table 4. 8 Structure of eighteen GD2/CD3 specific BiTE variations with short, medium or long linkers

	Short linker (G4S) ₃	Medium linker HNG	Long linker CD8-STK	
Anti-GD2 scFv hu14.18	 14-S-O	 14-H-O	 14-C-O	Anti-CD3 scFv huOKT3
	 14-S-U	 14-H-U	 14-C-U	Anti-CD3 scFv huUCHT1
	 14-S-Y	 14-H-Y	 14-C-Y	Anti-CD3 scFv huYTH
Anti-GD2 scFv huK666	 K6-S-O	 K6-H-O	 K6-C-O	Anti-CD3 scFv huOKT3
	 K6-S-U	 K6-H-U	 K6-C-U	Anti-CD3 scFv huUCHT1
	 K6-S-Y	 K6-H-Y	 K6-C-Y	Anti-CD3 scFv huYTH

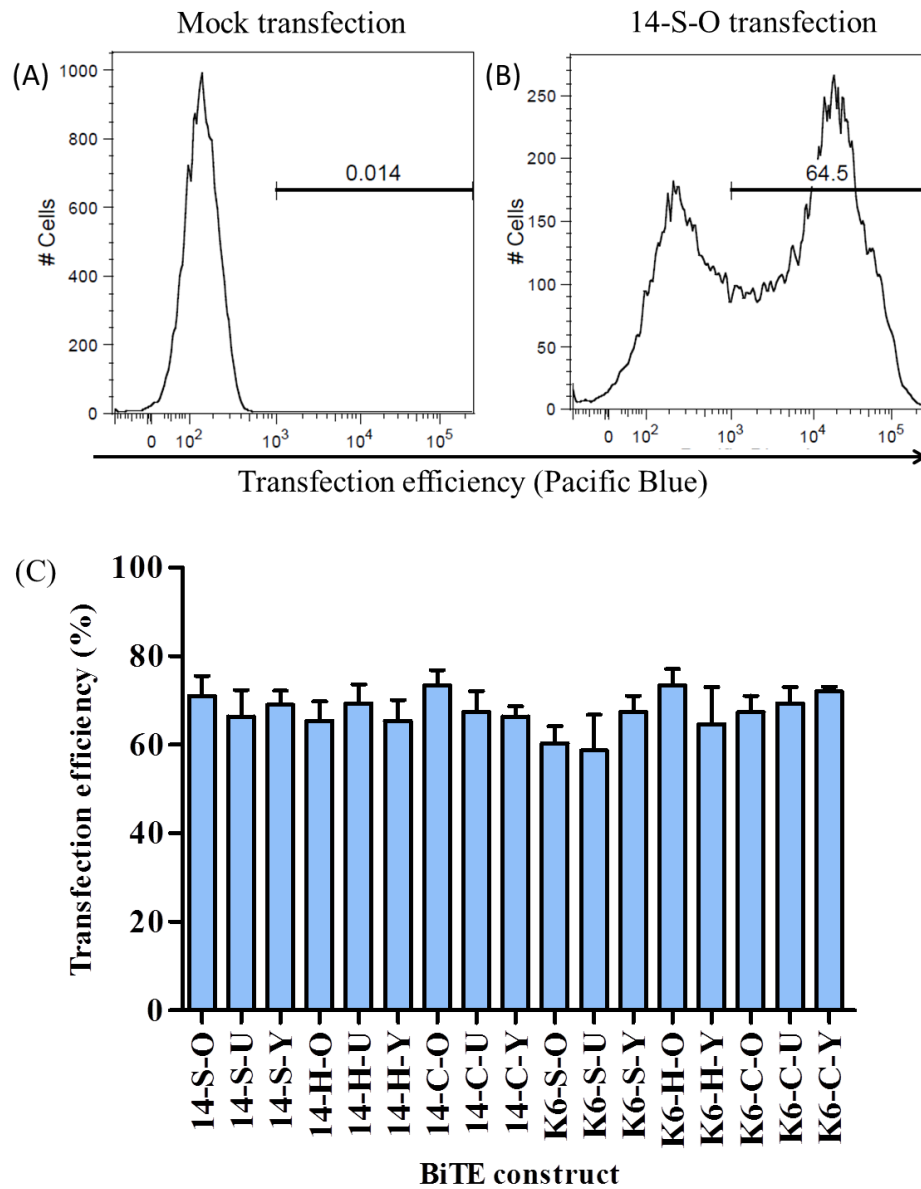


Figure 4.1: Detection of eBFP expression in 293T cells transfected to express BiTE variants. EBFP expression used as a measure of transfection efficiency and detected by flow cytometry using the Pacific Blue channel in (A) Mock transfected and (B) BiTE (14-S-O) transfected 293T cells. (C) Average transfection efficiencies of 293T cells for 17/18 of the BITE variants (n=3).

First, the eluates were dialysed into PBS to remove salts from the protein solution and subsequently, GD2.SupT1 cells were incubated with equal volumes of the eluates. The presence of BiTE in the eluate was confirmed by detection of BiTE staining on GD2.SupT1 cells using an Alexa-Fluor 647-conjugated polyclonal anti-F(ab)₂ antibody, staining was measured by flow cytometry. An increased staining of GD2.SupT1 cells (compared to cells stained with a PBS control) was seen in conditions with 300 mM imidazole (86% positive stain) and 500 mM imidazole (17% positive stain) (**Figure 4.2 A – D**). The experiment was repeated twice and confirmed most of the BiTEs were eluted when 300 mM imidazole was used in the elution buffer (**Figure 4.2 E**).

To confirm the optimal imidazole concentration for the elution buffer was 300 mM and not between 300 mM – 500 mM; a further range of imidazole concentrations in increments of 50 mM were tested in a similar experiment and confirmed that 300 mM was the optimal concentration (data not shown).

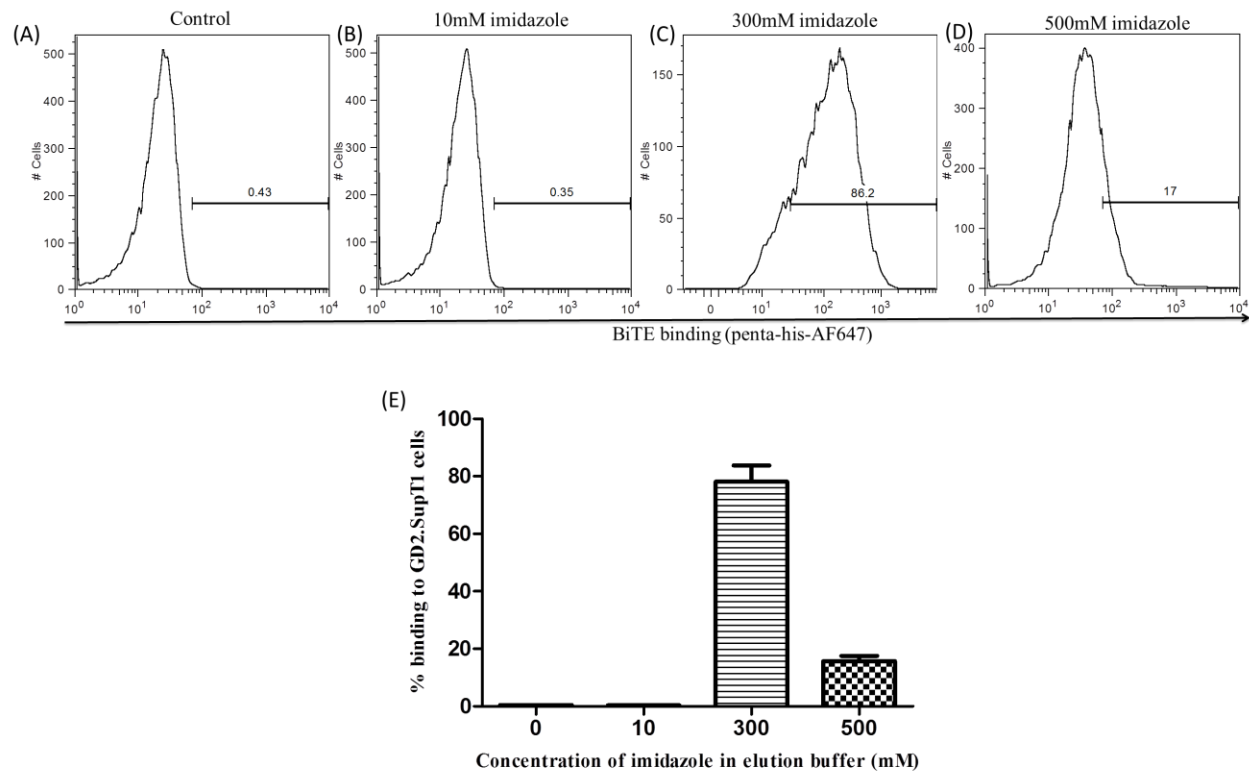


Figure 4.2: Determination of optimal imidazole concentration in elution buffer for maximum elution of BiTEs from His-Trap column. Detection of BiTEs in eluants after purification measured by staining GD2⁺ GD2.SupT1 cells with eluants containing (A) Control (PBS) (B) 10 mM imidazole (C) 300 mM imidazole and (D) 500 mM imidazole. BiTE binding detected using AF647-conjugated penta-his antibody by flow cytometry. (E) Average percentage binding to GD2.SupT1 cells from 3 experiments.

Coomassie Blue staining and Western Blotting analyses were used to directly confirm the purification of BiTEs from the His-trap HP column. During the purification process, BiTEs were eluted from the column in 1 mL aliquots called fractions and in total 10 fractions were eluted from the column. Fractions 2 - 4 which consistently had the highest protein concentration were pooled and dialysed into PBS for each BiTE separately. Samples from all stages of the purification process were resolved on a gel by SDS-PAGE.

Coomassie Blue staining confirmed the BiTE was the only protein present after purification. **Figure 4.3 A** is a representative example for BiTE K6-C-Y where a single band at 60 kDa is seen after purification. As a control, supernatant from non-transfected 293T cells was also purified using the His-trap HP column, Coomassie Blue staining did not detect any protein bands after purification (**Figure 4.3 B**).

Western Blotting analysis confirmed the single band purified was BiTE protein by detection with a his-tag specific antibody (**Figure 4.4 A**). All 17 BiTE variants were subsequently purified using the same IMAC method, 14 of 17 BiTE variants were successfully purified (**Figure 4.3 B**). The sizes of the BiTE variants are 56 kDa, 58 kDa and 60 kDa for BiTEs containing short ((G₄S)₃), medium (HNG) and long (CD8-STK) linkers respectively. Hu14.18/huOKT3 based BiTEs: 14-S-O, 14-H-O and 14-C-O were not detected after purification indicating the protein was not secreted by the 293T cells, despite successful transfection of the cells (**Figure 4.1 C**). m

The total yield (μg) of BiTE obtained after purification is reported for each BiTE variant in **Table 4.5**. The table reports an average of three separate purifications which varied in yield by $\pm 20 \mu\text{g}$. HuUCHT1 scFv-based BiTEs had a yield in the range of 60-190 μg , while huYTH scFv-based BiTEs had a yield in the range of 60-150 μg . However, the yield for huOKT3 scFv-based BiTEs was consistently poor in comparison (22-36 μg).

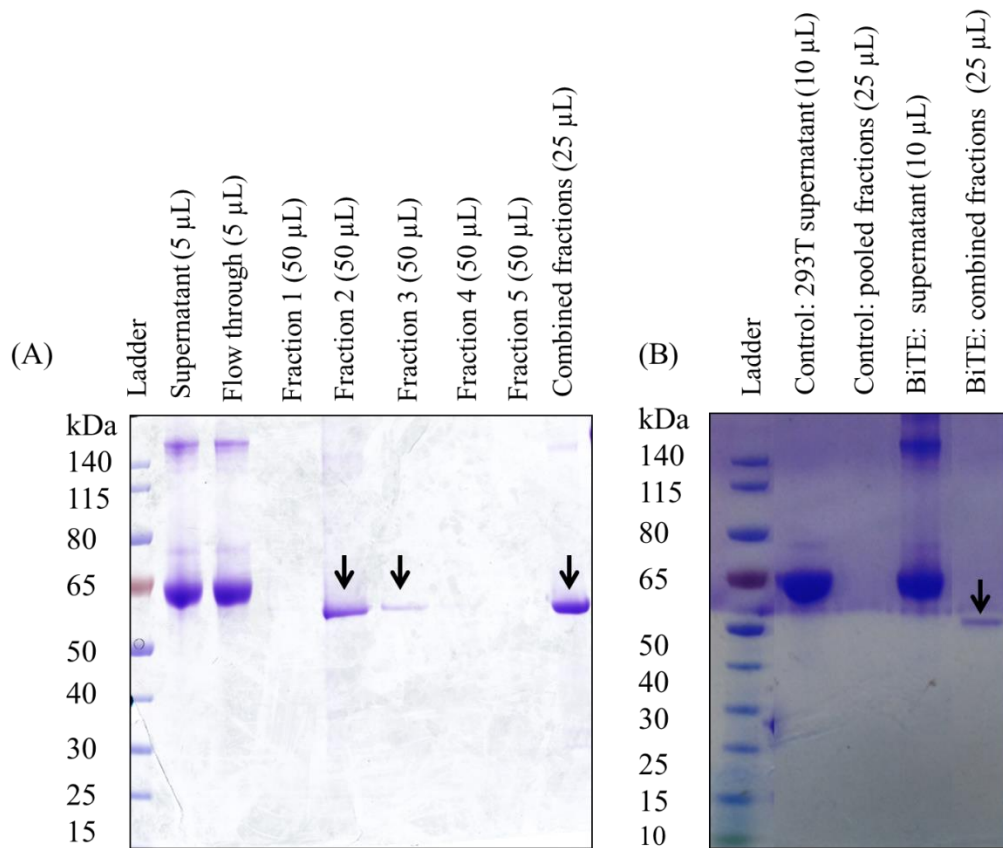


Figure 4.3: Confirmation of BiTE purification by Coomassie Blue staining on SDS-PAGE gel. (A) Samples from different stages of IMAC purification process were run on an SDS-PAGE gel, the gel was stained with Coomassie Blue stain to detect BiTE protein after purification. (B) Comparison of non-purified and purified samples from non-transfected 293T cells and transfected 293T cells secreting BiTE K6-C-Y. Black arrows indicate the purified BiTE K6-C-Y at 60 kDa.

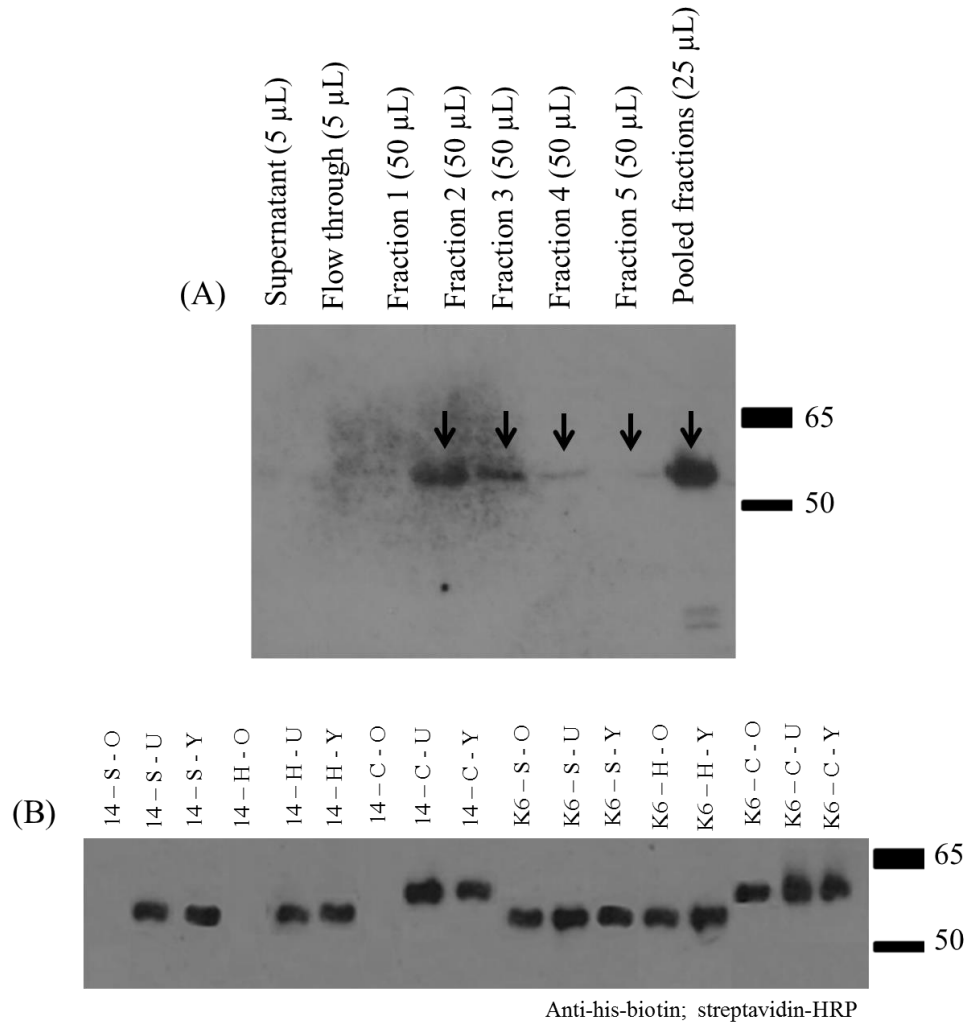


Figure 4.4: Confirmation of BiTE purification by Western Blot analysis. (A) Detection of purified BiTE K6-C-Y (black arrow) at 60 kDa in elution fractions 2-5 and in the pooled fractions. (B) Analysis of all 17 BiTEs purified from transfected 293Ts. BiTEs were detected using anti-his-biotin antibody and streptavidin-HRP. Expected BiTE sizes are 56 kDa, 58 kDa or 60 kDa 14 = hu14.18 scFv, K6 = huK666 scFv, S = (G₄S)₃ linker, H = hinge linker, C = CD8 stalk linker, O = huOKT3 scFv, U = huUCHT1 scFv, Y = HuYTH scFv.

Table 4. 5 Yield of individual BiTEs obtained after purification

	BiTE	Total yield from 25ml media (µg)
1	14-S-U	170.0
2	14-S-Y	41.4
3	14-H-U	182.3
4	14-H-Y	114.1
5	14-C-U	158.6
6	14-C-Y	108.2
7	K6-S-O	22.5
8	K6-S-U	80.1
9	K6-S-Y	60.9
10	K6-H-O	35.7
11	K6-H-Y	61.4
12	K6-C-O	33.5
13	K6-C-U	190.0
14	K6-C-Y	130.3

Values are an average of three purifications which had SD \pm 20 µg.

4.2.4 Measurement of BiTE thermal stability by differential scanning fluorimetry

The thermal stability of individual scFv domains in a bispecific antibody has shown to be correlated with increased antigen binding affinity and improved cytotoxicity of T cells against tumour cells at low BiTE concentrations. (Cheng et al., 2015). A high thermal stability is often associated with high expression level and other desired properties including solubility and reduced protein aggregation (Michaelson et al., 2009). Factors that have been described to influence thermal stability include the orientation of scFv $V_H - V_L$ domains, linker length and scFv sequence (Willuda et al., 1999)

To compare the thermal stability of individual BiTE variants used in this study, a differential scanning fluorimetry (DSF) assay was used. DSF involves exposure of the protein of interest to an increasing temperature gradient. The stability of a protein is related to its Gibbs free energy of unfolding ΔG_u , which is temperature dependent. As the protein unfolds, the ΔG_u decreases and becomes zero at equilibrium where the concentrations of folded and unfolded protein are equal, this point is considered as the melting temperature (T_m). The assay is performed in the presence of a fluorescent dye which binds to exposed hydrophobic sites of unfolded proteins and fluoresces. In DSF, fluorescence intensity is plotted as a function of temperature; this generates a sigmoidal curve; the inflection point of the transition curve is the T_m and is calculated using the Boltzmann equation:

$$y = LL + \frac{(UL - LL)}{1 + \exp\left(\frac{T_m - x}{a}\right)}$$

UL and LL are values of minimum and maximum intensities respectively and a denotes the slope of the curve within T_m . An alternative and easier way to calculate T_m is to calculate the maximum of the first derivative, which is performed by the Protein Thermal Shift Software.

Melt curve analysis was performed for 11/14 of the BiTE variants; BiTEs with a CD3-specific huOKT3 scFv were not produced in sufficient quantity to be included in the assay. A representative melt curve and derivative plot for BiTE 14-S-U is shown in

Figure 4.5. In the melt curve two T_m peaks are seen which will be assumed to correspond to differences in melting temperatures of the GD2-specific scFv and CD3-specific scFv in the BiTE. A summary of scFv T_m values are provided in **Table 4.6**. To determine the corresponding T_m for each scFv, the melting curves for each BiTE variant were compared. We found that T_m values of approx. 72 °C were only found when huUCHT1 scFv was present in the BiTE while a T_m of approx. 60 °C were found when huYTH scFv was present in the BiTE. Therefore, in **Figure 4.5**, the first T_m (T_m A) was inferred to correlate with the GD2-specific scFv and the second T_m (T_m B) inferred to correlate with the CD3-specific scFv in each BiTE variant.

Both hu14.18 and huK666 scFv-based BiTEs had similar melting temperatures of approximately 55 °C, only in the combinations 14-S-U, K6-S-U and K6-C-U were the melting temperatures 2 - 6 °C lower. In contrast, BiTEs containing huUCHT1 and huYTH scFv-based BiTEs differed in T_m regardless of GD2 binder and linker combinations. Two combinations, K6-S-Y and K6-H-Y had a slightly lower T_m of 56 - 57.3 °C. Linker combinations did not appear to influence scFv stability in the various BiTE combinations.

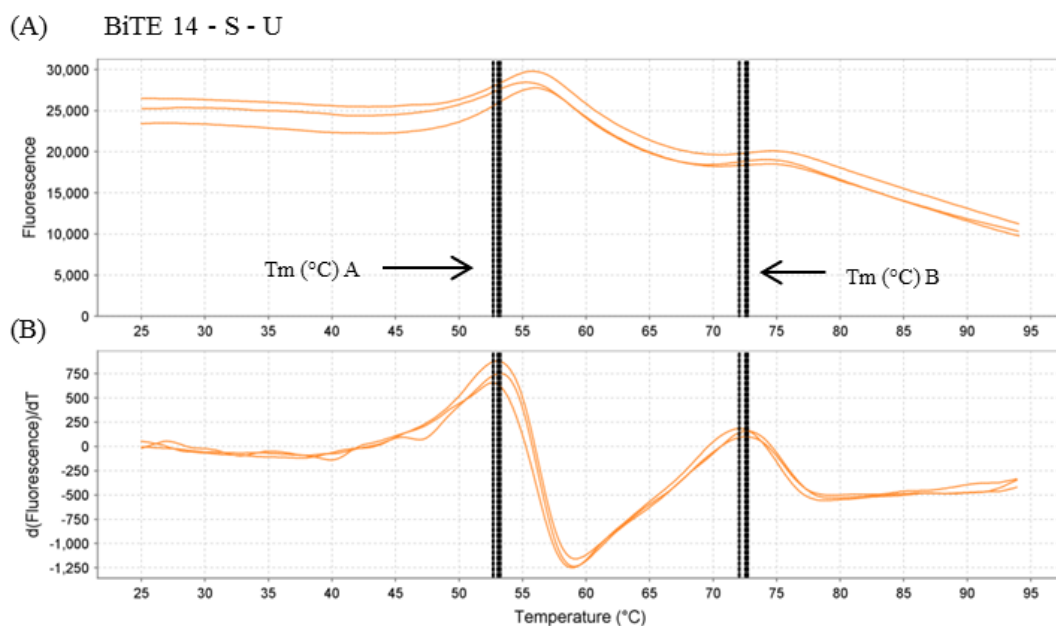


Figure 4.5: Thermal stability of BiTEs by differential scanning fluorimetry.

BiTEs were mixed with SYPRO-Orange dye and fluorescence was monitored using a StepOnePlus quantitative PCR machine with a 1% thermal gradient from 25 to 99°C. Data were analysed using Protein Thermal Shift software to calculate the melting temperature (T_m) using the Derivative method. (A) Representative melt curve and (B) derivative plot to calculate T_m for BiTE 14-S-U. Each scFv of the BiTE correlates to a peak in fluorescence at T_m A and T_m B.

Table 4. 6 Melting temperature of BiTE variants (n=3)

Constructs	GD2 specific	Tm (°C)	CD3 specific	Tm (°C)
	scFv	A	scFv	B
14-S-U	hu14.18	53.1 ± 0.2	huUCHT1	72.5 ± 0.3
14-S-Y	hu14.18	55.7 ± 0.1	huYTH	61.5 ± 0.3
14-H-U	hu14.18	55.6 ± 0.4	huUCHT1	73.0 ± 0.2
14-H-Y	hu14.18	55.8 ± 0.2	huYTH	60.6 ± 0.3
14-C-U	hu14.18	55.0 ± 0.5	huUCHT1	73.9 ± 0.1
14-C-Y	hu14.18	55.0 ± 0.3	huYTH	63.8 ± 0.2
K6-S-U	huK666	49.7 ± 0.4	huUCHT1	71.6 ± 0.2
K6-S-Y	huK666	55.42 ± 0.2	huYTH	57.3 ± 0.1
K6-H-Y	huK666	55.5 ± 0.3	huYTH	56.0 ± 0.3
K6-C-U	huK666	52.3 ± 0.6	huUCHT1	72.6 ± 0.5
K6-C-Y	huK666	55.81 ± 0.2	huYTH	60.1 ± 0.1

4.2.5 BiTEs have specificity for GD2 and CD3 antigens

After the successful production of the BiTE variants, it was necessary to confirm that the BiTEs retained binding to GD2 and CD3. This was determined by measuring BiTE binding to antigen positive and negative cell lines by flow cytometry.

To determine binding specificity for the GD2 antigen, SupT1 cells (GD2⁻) and GD2.SupT1 (GD2⁺) cells were incubated in equal volumes of supernatant from 293T cells transfected to express the BiTE variants. The BiTEs used in this assay were both non-purified and unquantified: paired isogenic SupT1 cells were used as these serve as true positive and negative controls for the antigen of interest. BiTE specificity to GD2 was detected using a penta-his-AF647 antibody (**Figure 4.6**).

All 14 BiTE variants showed specificity for the GD2 antigen, demonstrated by specific binding to GD2.SupT1 cells and not SupT1 cells. Although the MFI in this experiment was not a measure of affinity, the binding appeared to correlate with the respective BiTE yields obtained in **Table 4.5**. BiTE specificity for the CD3 antigen was determined by staining Jurkat cells, which natively express the TCR (CD3⁺) and Jurkat cells with a TCR knock out (ko) (CD3⁻). All 14 BiTE constructs with the different CD3-specific scFvs: huOKT3, huUCHT1 and huYTH showed binding to Jurkat cells (indicated by an increased MFI) and not to Jurkat TCR ko cells (**Figure 4.7**). The binding experiments were performed 3 times.

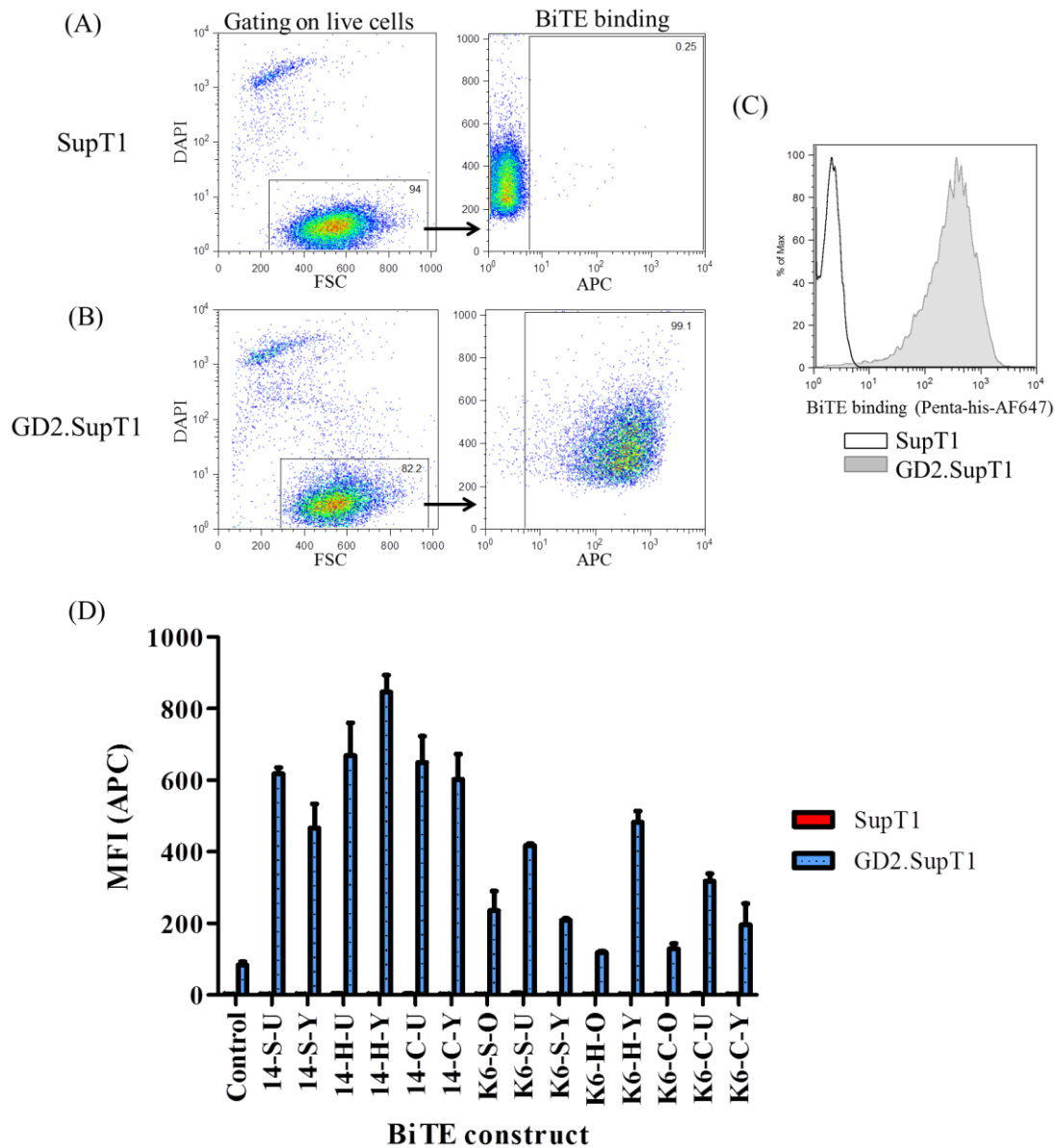


Figure 4.6: Measurement of binding specificity of GD2/CD3 specific BiTEs to GD2. (A) GD2 negative (SupT1) and (B) GD2 positive (GD2.SupT1) cells were incubated for 30 minutes in supernatant from 293T cells transfected to express BiTE protein. Cells were stained with a his-tag specific antibody (Penta-his-AF647) to detect BiTE binding and cells were then analysed by flow cytometry. (C) Overlay plot of staining SupT1 and GD2.SupT1 with BiTE 14-S-U supernatant. (D) Average MFI \pm SD of 14 BiTE variants binding to SupT1 or GD2.SupT1 cell lines (n=3).

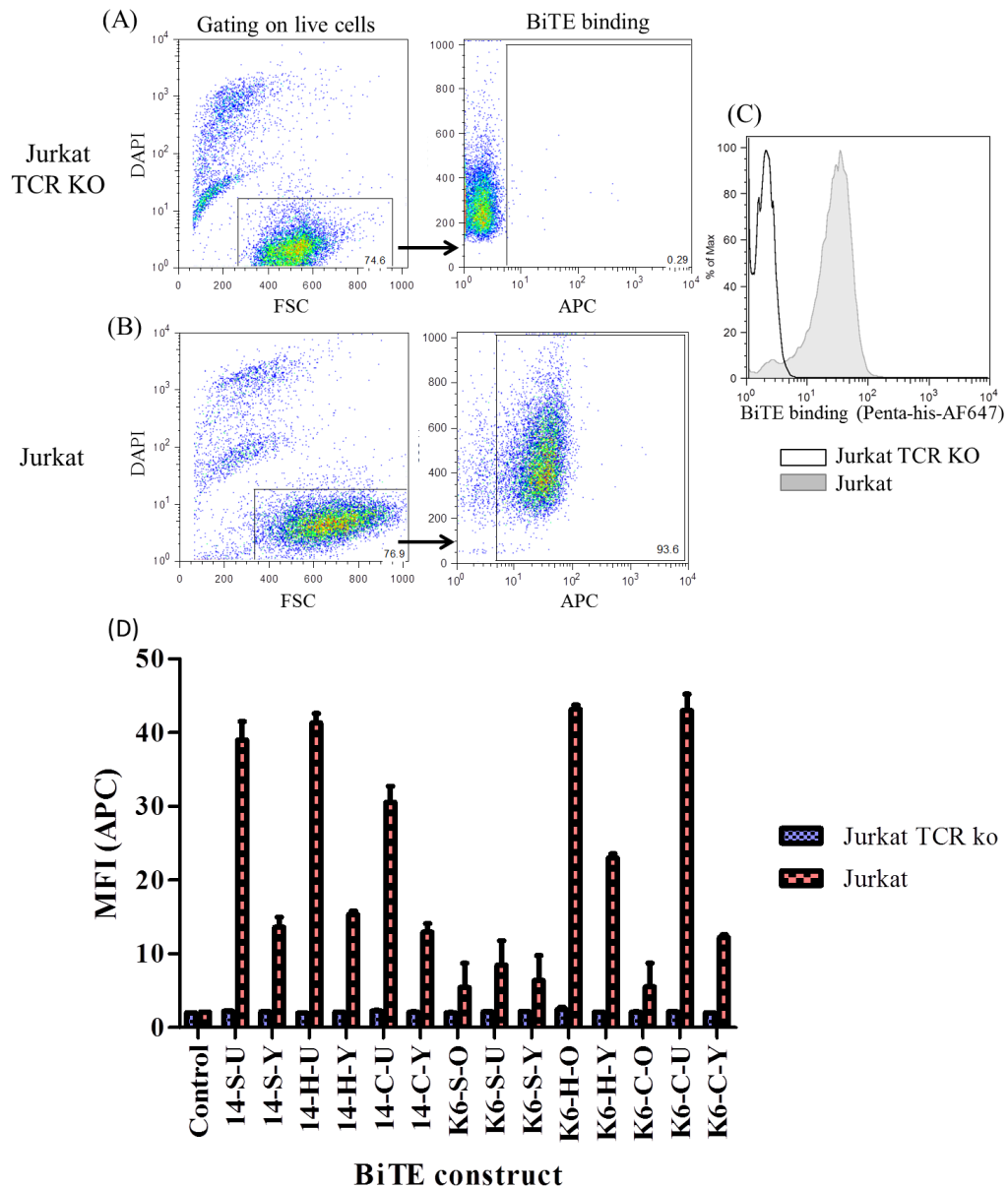


Figure 4.7: Measurement of binding specificity of GD2/CD3 specific BiTEs to CD3. (A) CD3 negative (Jurkat TCR knock out (KO)) and (B) CD3 positive (Jurkat) cells were incubated for 30 minutes in supernatant from 293T cells transfected to express BiTE protein. Cells were stained with a his-tag specific antibody (Penta-his-AF647) to detect BiTE binding and cells were then analysed by flow cytometry. (C) Overlay plot of staining Jurkat and Jurkat TCR KO with BiTE 14-S-U supernatant. (D) Average MFI \pm SD of 14 BiTE variants binding to SupT1 or GD2.SupT1 cell lines (n=3).

4.3 Discussion

This chapter has described the production, purification and characterisation of a series of GD2 and CD3 targeted BiTEs. The BiTEs can be produced using a SFG gamma-retroviral expression system by transfection of 293T cells. Of our 18 designed BiTE formats; 17 were cloned and 14 were successfully produced and purified. The IMAC purification system enabled isolation of BiTE from cell culture supernatant by binding the C-terminal hexa-his tag.

Stability is one of the most important functional requirements for the use of antibodies and antibody fragments in therapeutic and diagnostic applications (Kipriyanov et al., 1999). For this reason we determined the melting temperature of the individual scFvs in the different BiTE formats. Both GD2 binders had a similar melting temperature despite differences in corresponding mAb binding affinities (Mujoo et al., 1987, Nakamura et al., 2001). The melting temperature was also similar to other reported GD2-specific scFvs used in the bsAb format (Cheng et al., 2015).

The CD3-specific huUCHT1 scFv had a higher melting temperature in comparison to huYTH. All BiTE formats containing a huOKT3 specific scFv were either not produced at all or produced with low yield and were omitted from thermal stability comparisons. Two specific amino acid mutations (the substitution of Glu to Gln in position 6 of V_H framework 1 and the substitution of Cys to Ser in the middle of CDR-H3) are reported to induce a high level of production of huOKT3 from bacteria and may be the modification required to improve the production of our constructs containing huOKT3 (Kipriyanov et al., 1997). The combination of short, medium or long linkers did not appear to impact BiTE production or thermal stability.

A limitation for our studies was the low yield of BiTE produced using the small-scale production system: the system utilised 25 mL of BiTE containing supernatant from transfected cells and gave < 200 µg of total protein for all BiTEs produced. This is sufficient for *in vitro* functional experiments, but limiting for larger scale studies (e.g. saturation binding studies and *in vivo* experiments).

All scFvs used in the BiTE formats were able to retain specificity to GD2 or CD3 target antigens. 11 of 18 BiTEs were taken forward for *in vitro* functional testing in chapter 5.

Future directions

The binding affinity for 4/5 mAbs used for the scFv sequence are reported in the literature. The affinity of the scFvs however may differ from that of the whole antibodies, and are important to determine and compare as specific affinities may inform the functional characteristics of the BiTEs. To improve BiTE production a Chinese hamster ovary (CHO) cell expression system can also be used. CHO cells are the industry standard for mAb and bsAb production. These cells are optimised to grow under a high cell concentration and is the system used to produce CD19/CD3 BiTE blinatumomab (Nagorsen et al., 2012).

CHAPTER 5:
RESULTS (III)

***In vitro* functional comparisons of GD2 and CD3 targeted BiTE variants**

5.1 Introduction

In chapter 4, GD2 and CD3 targeted BiTEs were produced, purified and tested for GD2 and CD3 specificity. 11 BiTE variants out of 18 were produced in sufficient quantity and were thermally stable. Next, to determine the optimal BiTE format in redirecting T cells in GD2⁺ tumour cell lysis, these 11 variants have been taken forward for *in vitro* functional comparisons.

Aims

1. To determine the efficacy of different BiTE formats to redirect T cells for lysis of GD2⁺ tumour cell lines. To set up a flow cytometry based cytotoxicity assay to perform these comparative studies.
2. To characterise BiTE mediated redirected T cell function by measuring the release of relevant cytokines: IFN- γ after 24 hours and IL-2, IL-4, IL-10, IFN- γ , TNF α and granzyme B after 72 hours co-culture of T cells with neuroblastoma cells in the presence of different BiTE formats.
3. To measure T cell proliferation capacity in response to co-culture with the different BiTE variants and neuroblastoma cell lines.
4. To confirm BiTEs are able to redirect neuroblastoma patient T cells in GD2⁺ cell lysis.

5.2 Results

5.2.1 Set up of a flow cytometry based cytotoxicity assay

To enable comparisons between our 11 BiTE variants, a flow cytometry based cytotoxicity assay was used to measure T cell cytotoxicity towards (GD2⁺) GD2.SupT1 or (GD2⁻) SupT1 target cells in the presence of individual BiTE variants in a co-culture assay.

T cells were obtained from healthy donor PBMCs; a standard procedure in T cell cytotoxicity assays is prior activation and expansion of T cells using anti-CD3 and anti-CD28 antibodies. In particular, this is performed for CAR-T cell studies and for functional testing of alternative formats of bsAbs (Bohlen et al., 1993, Manzke et al., 1997, Kipriyanov et al., 1999). One of the key features of the BiTE class is the ability to polyclonally redirect T cells in the absence of artificial stimulation (Dreier et al., 2002). Hence, for this assay, to compare T-cell cytolytic function in the presence of different BiTE formats, non-activated T-cells were used to ensure *in vitro* test conditions correspond as much as possible to an *in vivo* setting.

CD4⁺ and CD8⁺ T cells were enriched from healthy donor PBMCs by the removal of B cells and monocytes using a CD3⁺ T cell enrichment column. Efficient removal was indicated by loss of CD19⁺ (B cell) and CD14⁺/CD16⁺ (monocyte) cell populations by flow cytometry (**Figure 5.1**); the column did not remove NK cell populations.

Target cells were labelled with CFSE as to distinguish between T cells and target cells during flow cytometry analysis. Target cells were not irradiated, to try and mimic the natural situation where target cell proliferation may affect the T cell cytotoxic capacity.

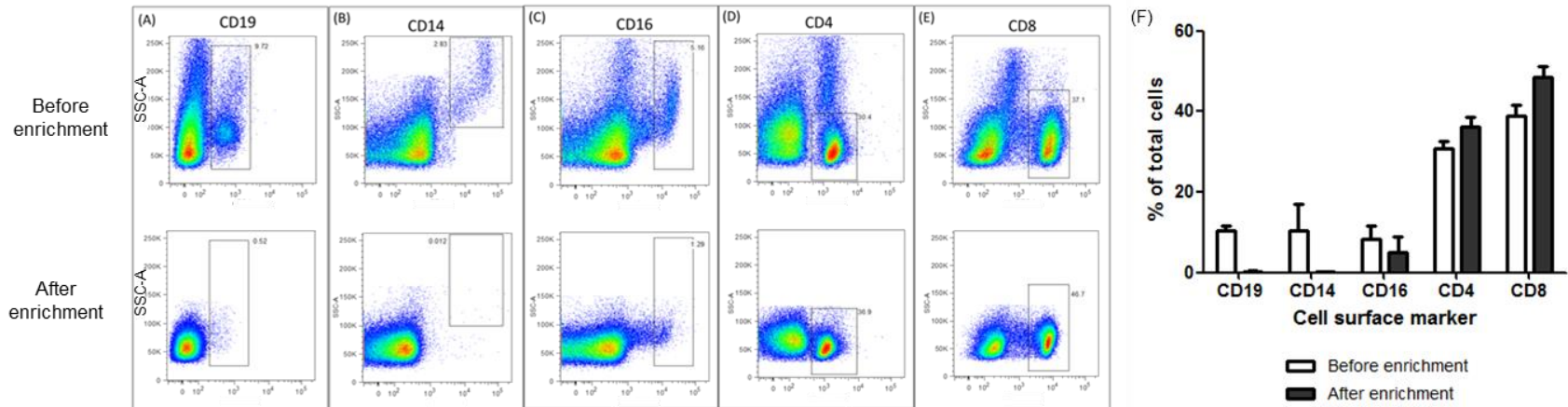


Figure 5.1: T cell enrichment from healthy donor PBMCs. PBMCs were applied to a CD3⁺ T cell enrichment column containing glass beads coated with Ig and anti-Ig for the removal of B cells and monocytes from the sample via high affinity negative selection. PBMCs were stained with antibodies for (A) CD19⁺ B cells (B) CD14⁺ and (C) CD16⁺ monocytes, (D) CD4⁺ and (E) CD8⁺ T cells before and after passing unlabelled PBMCs through the column, staining was analysed by flow cytometry. (F) Mean \pm SD of percentage total cells shown, n = 3.

T cells were co-cultured with SupT1 or GD2.SupT1 target cells at a 5:1 effector: target (E: T) ratio in the presence of 0-1 $\mu\text{g/mL}$ BiTE. A 5:1 E: T ratio was selected based on preliminary studies assessing 1:1, 5:1 and 10:1 E:T ratios, T cell mediated killing was comparable at both 5:1 and 10:1 E: T ratios. **Figure 5.2** is a representative example of a co-culture between T cells and target cells with 0-1 $\mu\text{g/mL}$ BiTE 14-C-Y after 16 hours. Visible loss of GD2.SupT1 cells was observed on visual inspection with a microscope in wells containing BiTE. Loss of GD2.SupT1 cells was not observed in the absence of BiTE or in wells containing SupT1 target cells (**Figure 5.2 A**). Target cell death was measured by flow cytometry after 16 hours co-culture: target cells were determined as the CFSE positive cell population and the numbers of live target cells were determined by exclusion of apoptotic and necrotic cells by staining with annexin and PI (**Figure 5.2 C**). A reduction of viable target cells was detected when GD2.SupT1 cells were co-cultured with T cells and BiTE. Increased cell death was observed with an increased concentration of BiTE (**Figure 5.2 D**).

To determine the appropriate time-point for co-culture read-out, target cell death was measured at four time points: 16, 24, 40 and 48 hours (**Figure 5.3**). The percentage of cell death was similar at each of the different time points. Tumour cell killing after 16 hours was sufficient to detect loss of GD2⁺ target cell number. In addition, a measure of cytotoxicity at the earliest time-point may enable distinctions between the different BiTE formats.

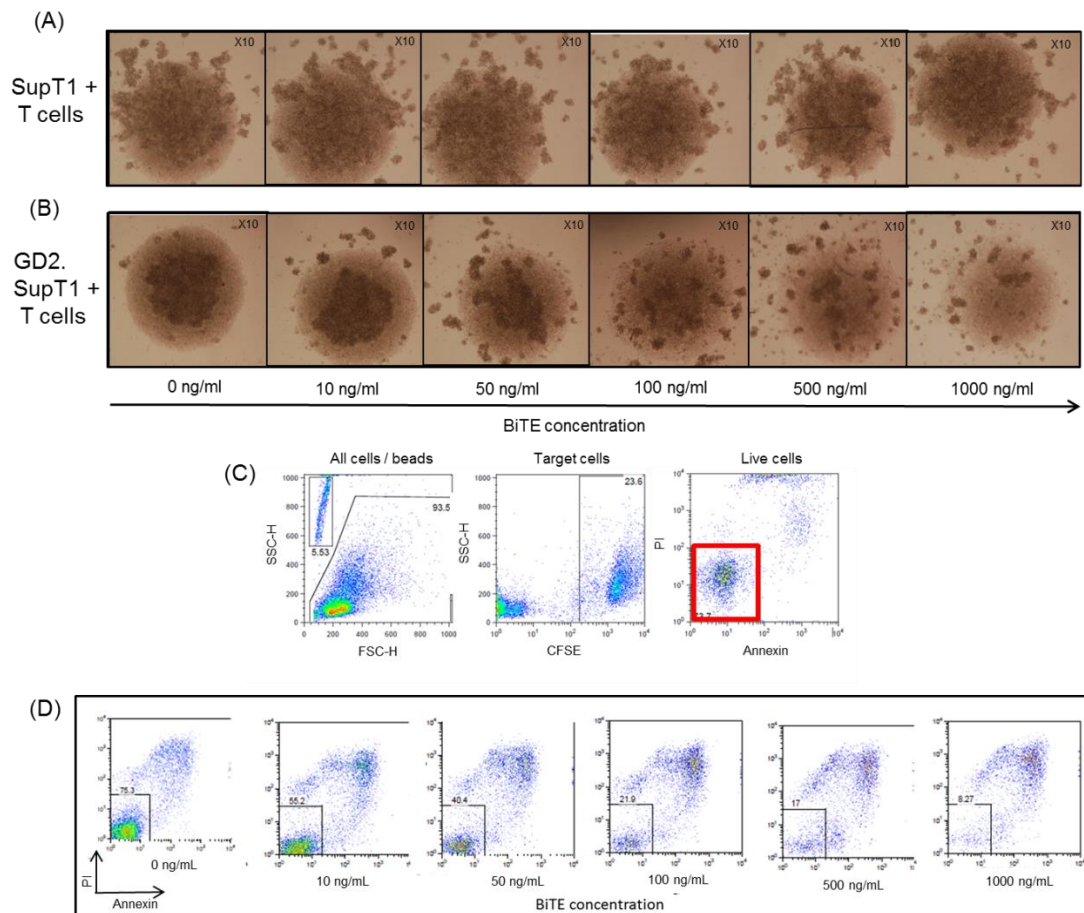


Figure 5.2: Measurement of target cell cytotoxicity by T cells after 16 hours co-culture using flow cytometry. T cells and CFSE-labelled target cells were co-cultured at a 5:1 E:T ratio with 0-1000ng/ml BiTE. **(A – B)** Visual inspection of co-cultures containing SupT1 or GD2.SupT1 target cells and effector T cells with a light microscope (10x objective) after 16 hours of co-culture. **(C)** Measurement of target cell viability by gating on CFSE positive target cells and exclusion of annexin / PI positive cells (red box). **(D)** Measurement of live GD2.SupT1 target cells from **(B)** at 16 hours by flow cytometry. A representative example of 1 experiment is shown.

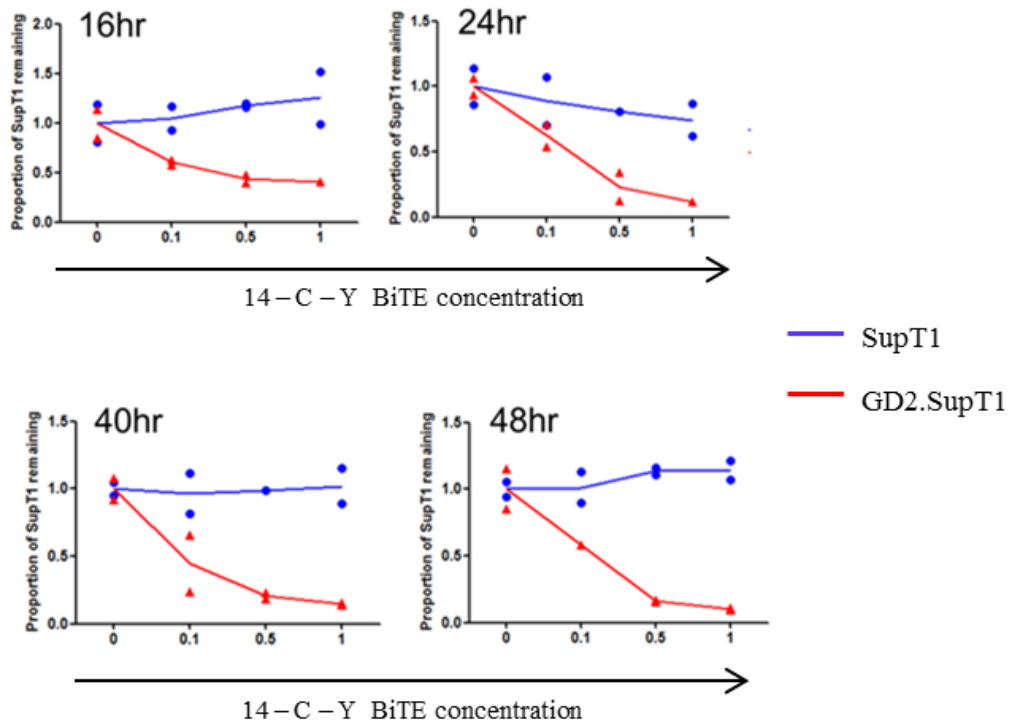


Figure 5.3: Measurement of target cell viability at different time points after co-culture with T cells and 0-1 μg/ml BiTE. SupT1 and GD2.SupT1 target cells were labelled with CFSE and co-cultured with T cells at a 5:1 E:T ratio with increasing BiTE concentration. After 16, 24, 40 and 48 hours, cells were stained with Annexin and PI to determine the number of live CFSE target cells. Viable cell number was quantified using CountBright absolute counting beads. Cell number is plotted as a proportion of cells in co-culture conditions with no BiTE added, n=1.

5.2.2 BiTEs redirect T cells to lyse GD2.SupT1 cells and not SupT1 cells

To compare the 11 BiTE variants in their ability to redirect T cell cytotoxicity to GD2.SupT1 and SupT1 target cells, co-cultures of T cells and target cells at 5:1 E: T ratio were set up for all BiTE variants at concentrations 0 - 1 $\mu\text{g}/\text{mL}$. Target cell death was measured after 16 hours by flow cytometry. Firstly, T cell mediated killing was specific to GD2 positive target cells for all BiTE variants tested; GD2.SupT1 cells were lysed while SupT1 cells were not (**Figure 5.4**). Secondly, T cell mediated lysis of GD2.SupT1 cells did not occur in control conditions with no BiTE, indicating the requirement of BiTEs to co-localise the effector and target cells. In addition, co-culture of target cells with BiTE in the absence of T cells did not lead to target cell death, confirming T cells are mediating the cytotoxicity. Thirdly, of all linker and CD3-specific scFv combinations tested, BiTEs containing a hu14.18 GD2-specific scFv were the most effective at redirecting T cells to kill GD2⁺ targets compared to BiTEs containing a huK666 scFv (**Figure 5.4**). The maximum percentage killing of GD2.SupT1 cells is reported in **Table 5.1**: killing associated with BiTEs containing hu14.18 scFv was greater than 80% in comparison to BiTEs containing huK666 scFvs which achieved a maximum killing of up to approximately 60%.

Table 5. 1 Maximum percentage killing of GD2.SupT1 by T cells at 16 hours incubation (mean \pm SD)

BiTE	% maximum killing	BiTE	% maximum killing
14-S-U	84.7 \pm 2.6	K6-S-U	49.2 \pm 12.3
14-S-Y	88.6 \pm 8.2	K6-S-Y	16.2 \pm 8.7
14-H-U	80.7 \pm 3.9	K6-H-Y	33.7 \pm 16.4
14-H-Y	83.6 \pm 11.4	K6-C-U	55.0 \pm 8.1
14-C-U	87.2 \pm 3.2	K6-C-Y	57.6 \pm 16.2
14-C-Y	83.4 \pm 15.5		

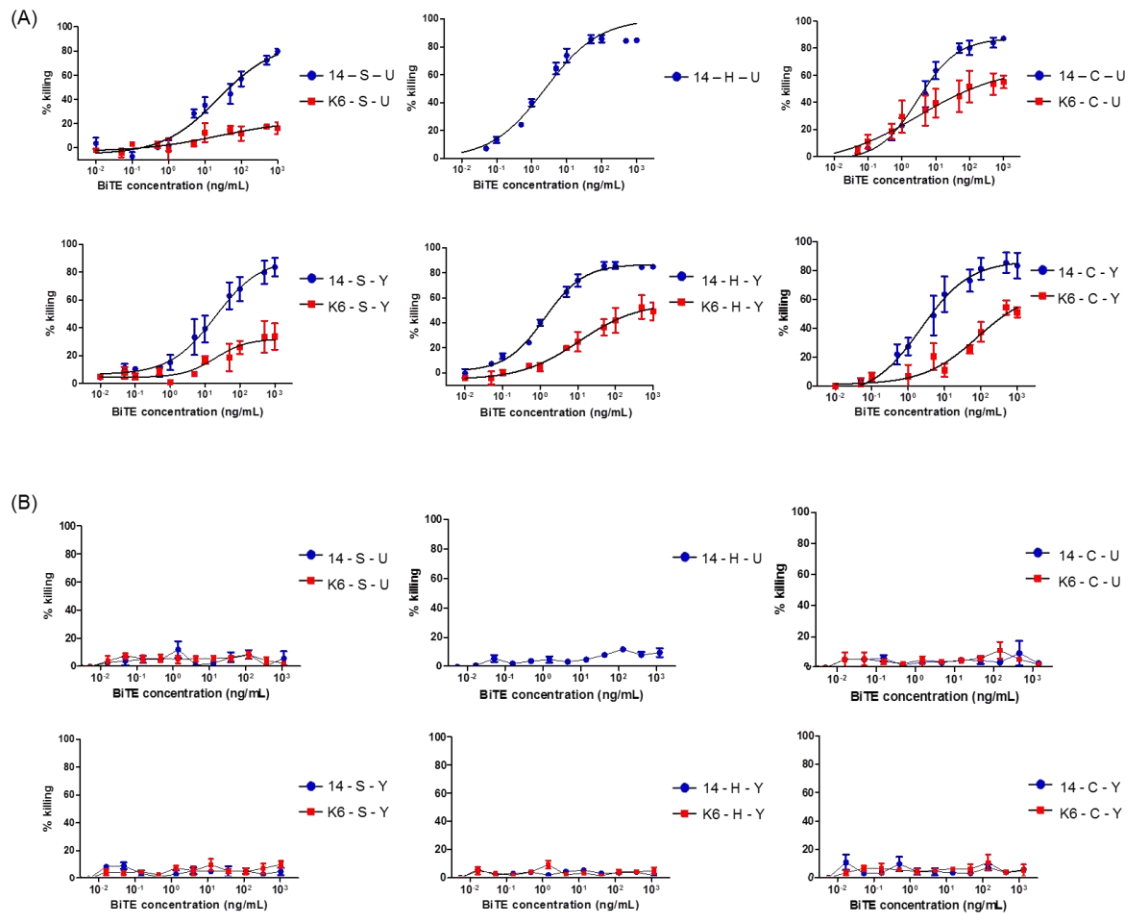


Figure 5.4: Comparison of BiTE variants in mediating target cell death by T cells after 16 hours co-culture. (A) GD2.SupT1 and (B) control SupT1 target cell death measured by percentage of apoptotic and necrotic cells in comparison to control conditions with 0 ng/mL BiTE. Co-cultures were at 5:1 E: T ratio. Hu14.18-based BiTEs: blue line, huK666-based BiTEs: red line. Read out by flow cytometry, graphs show mean \pm SEM (n=3).

EC₅₀ values for hu14.18 scFv-based BiTEs are reported in **Table 5.2**, values were calculated by non-linear regression analysis and compared by the extra sum of squares F-test. BiTEs containing hu14.18 scFv and medium (HNG) or long (CD8-STK) linkers had lower EC₅₀ values in comparison to hu14.18 scFv-based BiTEs with short (G₄S)₃ linkers (p< 0.001). EC₅₀ values for huK666 scFv-based BiTEs were not reported, as maximum killing was < 60% and thus calculated EC₅₀ values at <30% killing were not accurate for comparisons with hu14.18 scFv-based BiTEs.

Table 5. 2 BiTE EC₅₀ values for killing of GD2.SupT1 cells by T cells at 16 hours incubation

BiTE	EC₅₀ [ng/mL]	EC₅₀ (pM)
14-S-U	14.73	263.04
14-S-Y	9.07	161.96
14-H-U	1.20	20.69
14-H-Y	5.50	94.83
14-C-U	3.74	62.33
14-C-Y	3.32	55.33

Both huUCHT1 and huYTH scFv-based BiTEs had a similar potency at redirecting T cells in GD2.SupT1 cell lysis (**Figure 5.5**). In comparison of different linkers: BiTE 14-H-U was more potent than 14-H-Y (BiTE and EC₅₀ ng/mL, 14-H-U: 1.2 ng/mL, 14-H-Y: 5.5 ng/mL, p< 0.001), however there were no significant differences in EC₅₀ values between 14-S-U with 14-S-Y (BiTE and EC₅₀ ng/mL, 14-S-U: 14.73 ng/mL, 14-S-Y: 9.07 ng/mL, p = 0.1447) and 14-C-U with 14-C-Y (BiTE and EC₅₀ ng/mL, 14-C-U: 3.74 ng/mL, 14-C-Y: 3.32 ng/mL, p= 0.3852).

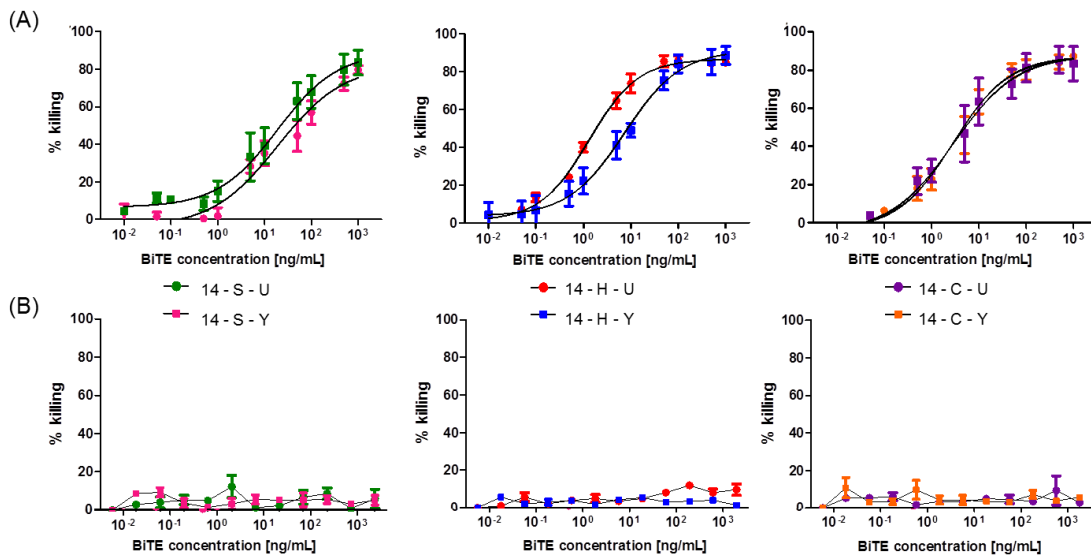


Figure 5.5: Comparison of the activity of BiTEs with different CD3 binders and different linkers. (A) GD2.SupT1 and (B) control SupT1 target cell death measured after co-culture with T cells and hu14.18 scFv-based BiTEs (0-1 μ g/mL). Co-cultures were performed at 5:1 E:T ratio and death measured by percentage of apoptotic and necrotic cells in comparison to control conditions with 0 ng/mL BiTE. Read out performed after 16 hours by flow cytometry. Graphs show mean \pm SEM (n=3).

5.2.3 BiTEs mediate specific killing of neuroblastoma cells

The four BiTEs with the lowest EC₅₀ values at 16 hours co-culture were taken forward for further *in vitro* functional testing. These were:

1. 14-H-U
2. 14-H-Y
3. 14-C-U and
4. 14-C-Y.

After demonstrating the BiTE variants were able to redirect T cells to lyse GD2.SupT1 lymphoma cells which were engineered to express GD2; the next step was to demonstrate specific killing of neuroblastoma cell lines which naturally express GD2: Lan-1, SKNDZ and IMR32. A204 rhabdomyosarcoma cells were used as a GD2⁻ control cell line. Target cell lines were co-cultured at 5:1 E: T ratios with an increasing concentration of BiTE (0-1 µg/mL). After 16 hours co-culture target cell death was measured as described in 5.2.1. All four BiTEs were able to redirect T cells to lyse neuroblastoma cell lines and not A204 cells (**Figure 5.6**).

Comparisons on which BiTE format is most effective at redirecting T-cells to neuroblastoma cell lines cannot yet be made as to date this experiment has only been performed once. Preliminary analysis suggests that BiTEs 14-H-U and 14-H-Y are the only BiTEs that show killing of more than one cell line at the 1 ng/mL concentration.

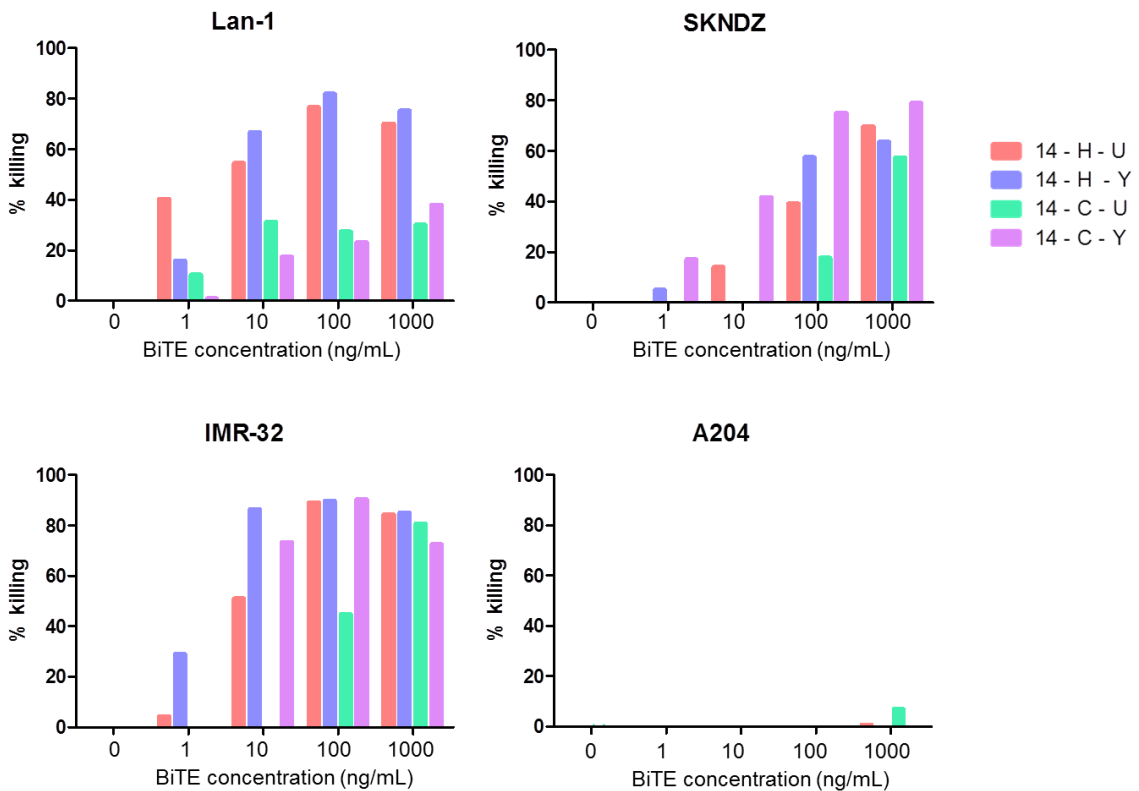


Figure 5.6: GD2/CD3 BiTEs redirect T cell cytotoxicity to neuroblastoma cell lines. Measurement of GD2⁺ neuroblastoma (Lan-1, SKNDZ, IMR-32) target cell killing after 16-hours co-culture with T cells at 5:1 E:T ratio and 0-1 μ g/mL BiTE. Percentage killing was calculated as proportion of annexin/PI positive cells compared to control conditions after 48 hours co-culture using flow cytometry. A204 cells were used as a GD2⁻ control cell lines, n=1.

5.2.4 T cells are activated and secrete IFN- γ upon co-culture with neuroblastoma cells and BiTEs

To measure specific activation of T cells upon engagement with GD2⁺ target cells mediated through the BiTE, the presence of IFN- γ in co-culture supernatant was measured by ELISA after 24 hours co-culture. The presence of IFN- γ was detected when T cells were co-cultured with neuroblastoma cell lines and all BiTE variants tested. IFN- γ was not detected when T cells were co-cultured with GD2⁻ A204 cells (**Figure 5.7**). The level of IFN- γ release increased with an increasing BiTE concentration. IFN- γ production by T cells was significantly higher when Lan-1 cells were incubated with BiTE 14-H-Y in comparison to 14-H-U at 1000 ng/mL (mean concentration \pm SEM: 14-H-U: 30.8 \pm 8.0 pg/mL, 14-H-Y: 56.7 \pm 2.8 pg/mL, n=3, p<0.01). A significant difference in IFN- γ was also seen in conditions containing BiTE 14-C-Y compared to BiTE 14-H-U (mean concentration \pm SEM: 14-C-Y: 79.6 \pm 8.0 pg/mL, 14-H-U: 30.8 \pm 8.0 pg/mL, n=3, p<0.001) and BiTE 14-C-U (mean concentration \pm SEM: 14-C-Y: 79.6 \pm 8.0 pg/mL, 14-C-U: 38.9 \pm 8.9 pg/mL, n=3, p<0.01).

Co-culture of T cells with SKNDZ in presence of BiTE 14-C-Y (100 ng/mL) had a significantly higher IFN- γ production than BiTEs 14-H-Y and 14-C-U (mean concentration \pm SEM: 14-H-Y: 13.6 \pm 2.3 pg/mL, 14-C-U: 6.8 \pm 0.6 pg/mL, 14-C-Y: 35.4 \pm 10 pg/mL, n=3, p<0.01). Co-culture of T cells with IMR32 cells in presence of BiTE 14-C-Y (100 ng/mL) had a significantly higher IFN- γ production than BiTE 14-C-U (mean concentration \pm SEM: 14-H-Y: 65.8 \pm 13.9 pg/mL, 14-C-U: 37.7 \pm 4.4 n=3, p<0.01).

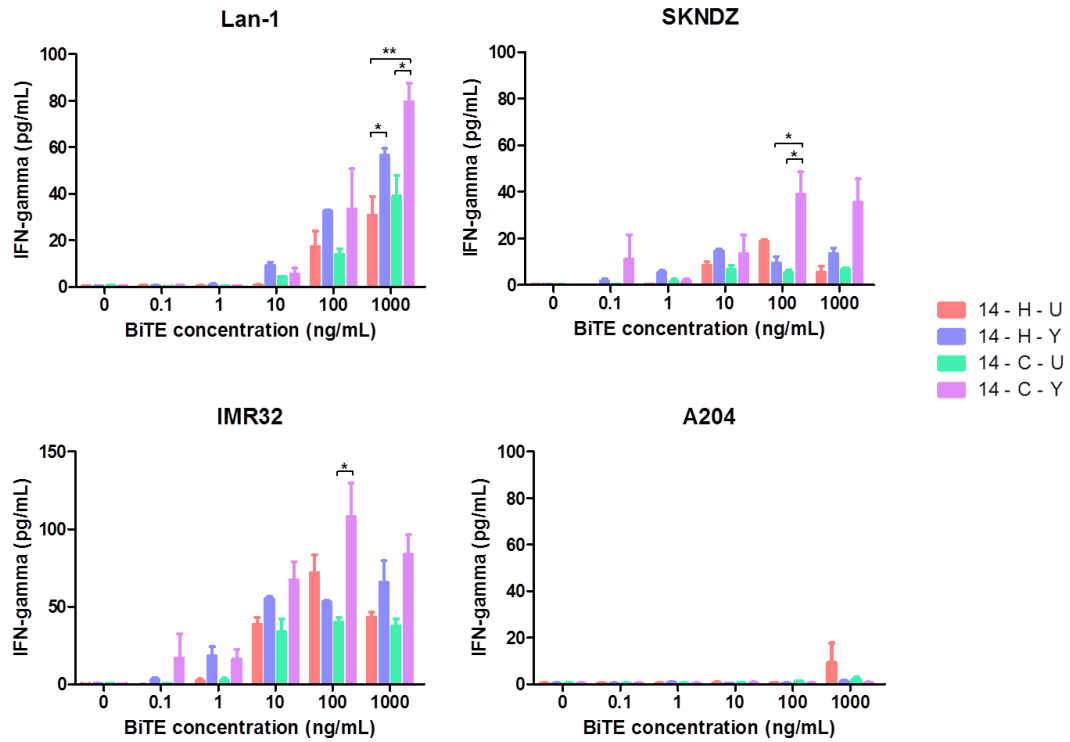


Figure 5.7: Production of IFN- γ by activated T cells in the presence of GD2⁺/GD2⁻ target cells and BiTE. IFN- γ in supernatant measured by ELISA after 24 hour co-culture of T cells and target cells at 5:1 E:T ratio and 0-1 μ g/mL BiTE. Graphs show mean \pm SEM, n=3, * p<0.01, ** p<0.001. Bonferroni post-hoc analysis was performed after one-way ANOVA.

5.2.5 Cytokine production

Differences in cytokine production may have important consequences both for the functionality of the BiTE activated T cells and toxicity when used clinically. To functionally compare the BiTE variants, supernatants were harvested at 72 hours after a 5:1 E: T co-culture with GD2⁺ Lan-1, SKNDZ, IMR32 cells and GD2⁻ A204 cells at 100 ng/mL BiTE concentration and analysed by cytokine bead array analysis. Co-cultures with 0 ng/mL BiTE were used as a control (**Figure 5.8**).

There was a significantly greater production of IL-2 when T cells were co-cultured with Lan-1 cells with 14-H-Y BiTE (Mean concentration \pm SEM: 14-H-U: 4.2 ± 0.5 pg/mL, 14-H-Y: 18.5 ± 3.0 pg/mL, 14-C-U: 4.1 ± 1.7 pg/mL, 14-C-Y: 6.9 ± 0.3 pg/mL, n=3, p<0.001). IL-2 was also significantly greater when T cells were co-cultured with SKNDZ cells and 14-H-Y or 14-C-Y BiTE (Mean concentration \pm SEM: 14-H-U: 20.3 ± 6.8 pg/mL, 14-H-Y: 35.4 ± 4.6 pg/mL, 14-C-U: 1.9 ± 0.8 pg/mL, 14-C-Y: 30.1 ± 5.9 pg/mL, n=3, p=0.072).

T cell activation is associated with the release of pro-inflammatory cytokines as identified by the production of IFN- γ and TNF α . There was a significantly greater production of IFN- γ when T cells were co-cultured with Lan-1 cells and 14-H-Y BiTE (Mean concentration \pm SEM: 14-H-U: 39.1 ± 8.3 pg/mL, 14-H-Y: 86.1 ± 5.8 pg/mL, 14-C-U: 36.2 ± 0.4 pg/mL, 14-C-Y: 59.3 ± 10.1 pg/mL, n=3, p=0.0041). A significant IFN- γ production by T cells was also seen when co-cultured with SKNDZ and 14-H-Y BiTE (Mean concentration \pm SEM: 14-H-U: 35.9 ± 27.6 pg/mL, 14-H-Y: 115.2 ± 4.3 pg/mL, 14-C-U: 0.7 ± 0.2 pg/mL, 14-C-Y: 53.9 ± 21.9 pg/mL, n=3, p=0.0041).

There was a significantly greater production of TNF α upon co-culture of T cells with Lan-1 cells and 14-H-Y BiTE (Mean concentration \pm SEM: 14-H-U: 15.8 ± 1.5 pg/mL, 14-H-Y: 44.2 ± 5.3 pg/mL, 14-C-U: 19.9 ± 3.3 pg/mL, 14-C-Y: 21.5 ± 2.0 pg/mL, n=3, p=0.0014) and in the same condition with SKNDZ cells (Mean concentration \pm SEM: 14-H-U: 15.8 ± 1.5 pg/mL, 14-H-Y: 44.2 ± 5.4 pg/mL, 14-C-U: 19.9 ± 3.3 pg/mL, 14-C-Y: 21.5 ± 2.0 pg/mL, n=3, p=0.0015).

Granzyme B is a serine protease released from the granules of cytotoxic lymphocytes, high levels of granzyme B were detected in supernatants from all three GD2⁺ cell lines. Production of granzyme B was the highest when T cells were co-cultured with SKNDZ and significantly higher for BiTEs containing the HuYTH CD3 binder (Mean concentration \pm SEM: 14-H-U: 2345.2 \pm 931.9 pg/mL, 14-H-Y: 4280.0 \pm 197.0 pg/mL, 14-C-U: 310.1 \pm 83.1 pg/mL, 14-C-Y: 3810.4 \pm 135.4 pg/mL, n=3, p=0.0016).

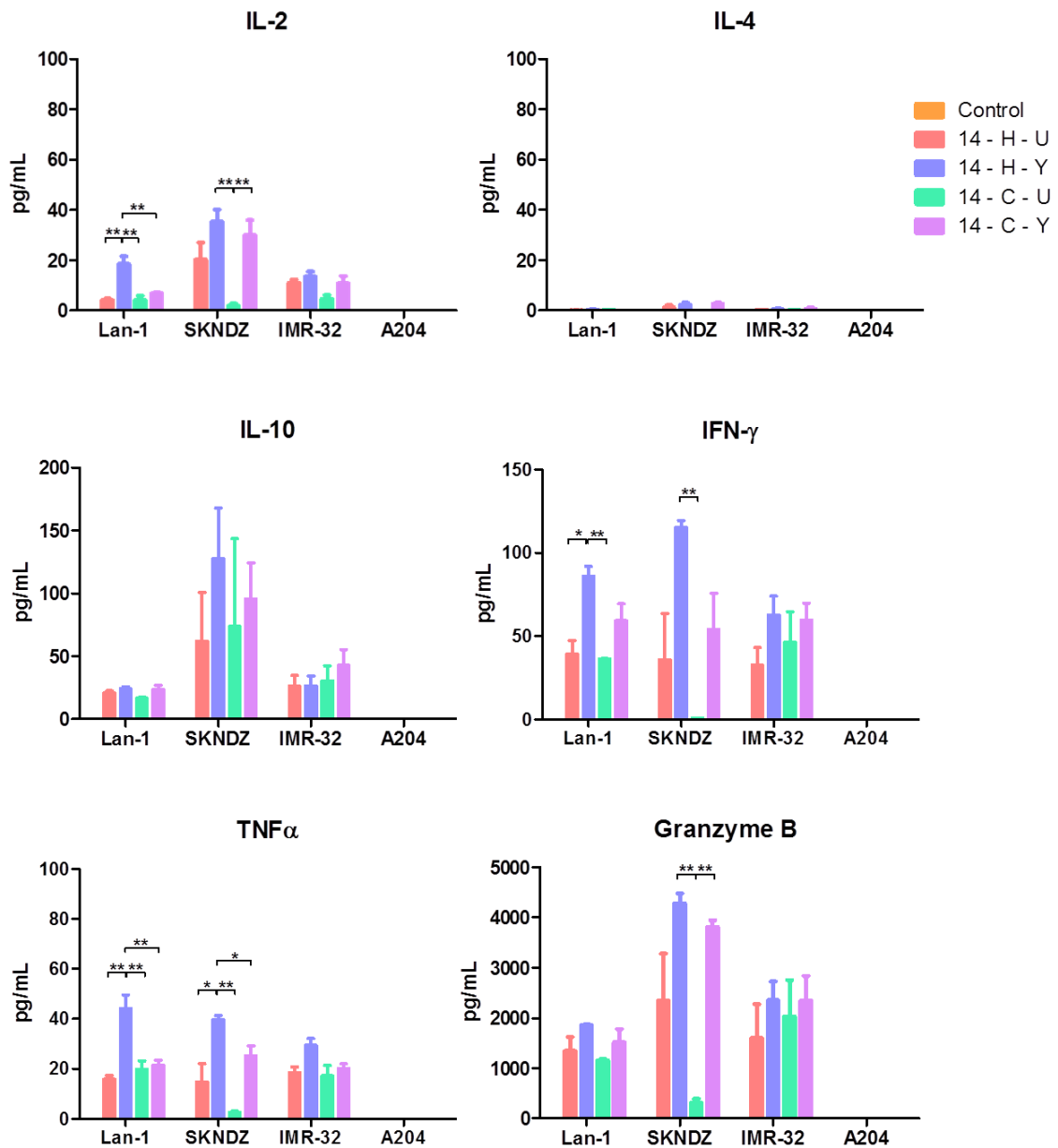


Figure 5.8: Production of cytokines by activated T cells in the presence of GD2⁺/GD2⁻ target cells and BiTE. Cytokines measured by cytokine bead array from supernatants after 72 hour co-culture of T cell and target cells at 5:1 E: T ratio and 100 ng/mL BiTE. Graphs show mean \pm SEM, n=3, * p<0.01, ** p<0.001. Bonferroni post-hoc analysis was performed after one-way ANOVA.

5.2.6 T cells proliferate upon co-culture with neuroblastoma cells and BiTE

One of the important features of a T cell therapeutic is the ability of T cells to proliferate in response to recognition of target antigen. To test the proliferative capacity of CD4⁺ and CD8⁺ T cell subsets in the presence of BiTE, CFSE labelled T cells were co-cultured 5:1 with irradiated Lan-1, SKNDZ, IMR32 or A204 cell lines in the presence of the four BiTE variants (0-1 µg/mL). CFSE fluorescence halves within daughter cells after each cell division and can be used to monitor proliferation.

After 6 days co-culture, CD4⁺ and CD8⁺ T cell proliferation was measured by detecting the percentage of cells that had undergone dilution of CFSE by flow cytometry. Co-cultures containing 0 µg/mL BiTE were used as a control to set the CFSE dilution gate. **Figure 5.9** is a representative example of the flow cytometry read-out of T cells co-cultured with Lan-1 cells and 0-1 µg/mL BiTE 14-H-Y. To determine the fold change in T cell number, the number of gated CD4⁺ or CD8⁺ T cells were compared to the corresponding number of cells in a co-culture condition with 0 ng/mL BiTE.

The percentage proliferation and fold change of CD4⁺ T cells after co-culture with the different target cells and BiTEs are shown in (**Figure 5.10**). CD4⁺ T cells proliferated in co-culture with Lan-1 cells and all BiTE variants tested. A significant difference (measured by Bonferroni post hoc analysis after one-way ANOVA) in CD4⁺ T cell proliferation was seen upon co-culture with 14-H-Y BiTE at 10 ng/ml (mean proliferation ± SEM, 14-H-U: 10.6% ± 0.5, 14-H-Y: 56.9% ± 5.1, 14-C-U: 14.6% ± 7.1, 14-C-Y: 19.3 ± 9.1, n=3, p<0.01). T cells also had a greater fold change when co-cultured with 1000 ng/mL 14-H-Y BiTE (mean fold change ± SEM, 14-H-U: 1.2 ± 0.4, 14-H-Y: 4.0 ± 0.7, 14-C-U: 2.1 ± 0.1, 14-C-Y: 1.2 ± 0.2, n=3, p<0.01). CD4⁺ T cells proliferated in co-culture with SKNDZ cells and the four BiTE variants while proliferation in co-culture with IMR32 cells was minimal and absent in co-culture with A204 cells.

As the main effector T cell population, CD8⁺ T cells had a greater proliferative capacity at a lower BiTE concentration in comparison to CD4⁺ T cells (**Figure 5.11**). Upon co-culture with Lan-1 cells, CD8⁺ T cells had a significantly increased proliferation with 14-H-Y BiTE at 1 ng/mL (mean proliferation \pm SEM, 14-H-U: 3.2% \pm 1.2, 14-H-Y: 56.1% \pm 11.5, 14-C-U: 11.1% \pm 8, 14-C-Y: 15.7 \pm 12.1, n=3, * p<0.01, ** p<0.001). CD8⁺ T cells also had a greater fold change in cell number when co-cultured with 14-H-Y BiTE at 100 ng/mL (mean fold change \pm SEM, 14-H-U: 5.6 \pm 2.4, 14-H-Y: 9.6 \pm 3.0, 14-C-U: 4.8 \pm 1.7, 14-C-Y: 2.9 \pm 1.2, n=3, p<0.01) CD8⁺ T cells proliferated in co-culture with SKNDZ cells and the four BiTE variants while proliferation in co-culture with IMR32 cells was minimal and absent in co-culture with A204 cells. BiTE EC₅₀ values for CD4⁺ and CD8⁺ T cell proliferation demonstrate 14-H-Y BiTE was able to induce proliferation at the lowest BiTE concentrations in cell lines Lan-1 and SKNDZ (**Table 5.3**).

Table 5. 3 BiTE EC₅₀ (ng/mL) values for T cell proliferation after 6 days co-culture with target cells

Cell line / BiTE	14-H-U		14-H-Y		14-C-U		14-C-Y	
	CD4	CD8	CD4	CD8	CD4	CD8	CD4	CD8
Lan-1	34.0	7.7	6.7	0.8	40.1	6.8	28.4	4.9
SKNDZ	175.8	104.6	50.3	8.2	162.2	74.3	123.6	21.0
IMR32	N/A	191.3	N/A	11.3	N/A	N/A	N/A	260.1
A204	N/A	N/A	N/A	N/A	N/A	N/A	N/A	N/A

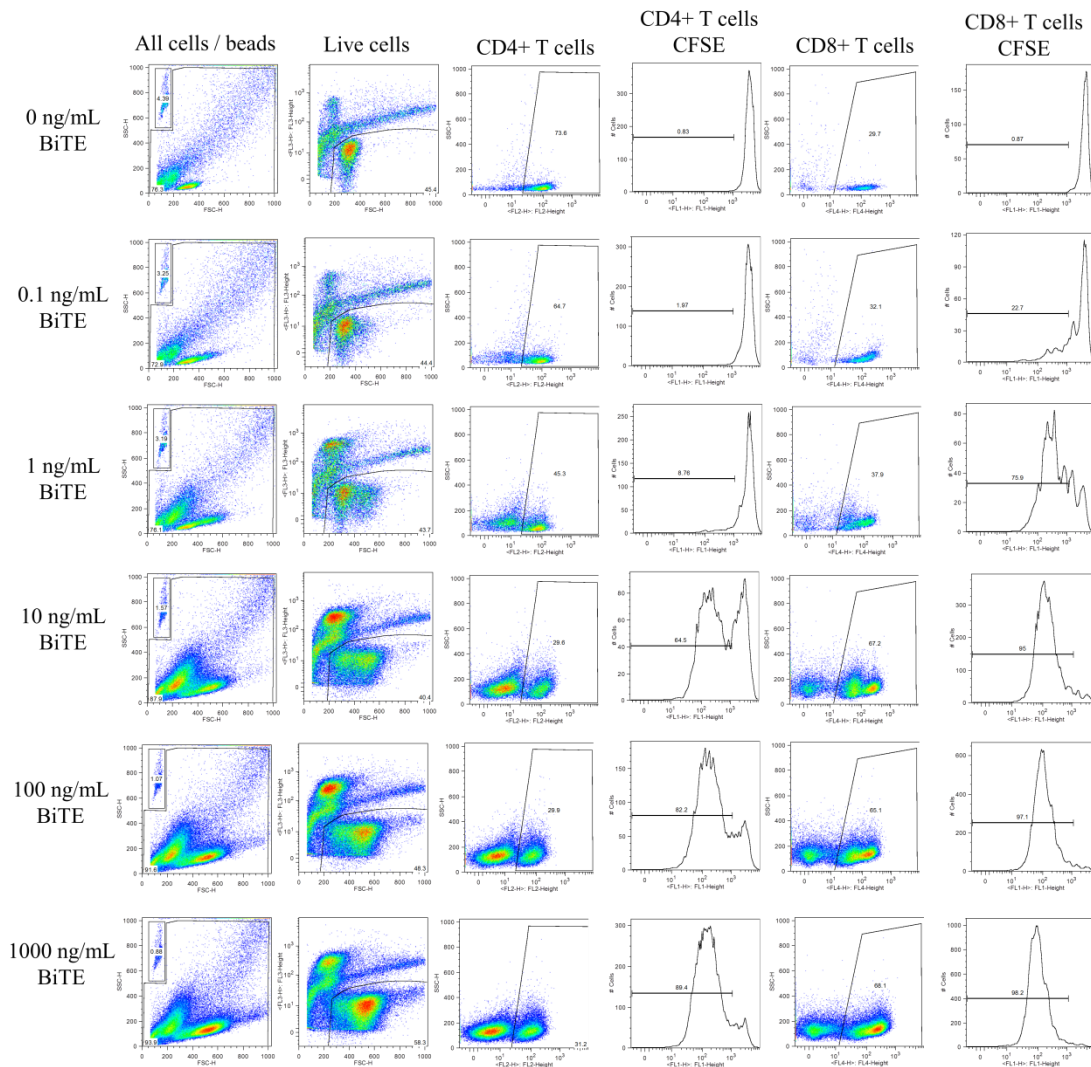


Figure 5.9: Measure of T cell proliferation after co-culture with GD2⁺ Lan-1 cells and BiTE (0-1000 ng/ml). T cells were labelled with CFSE and co-cultured at 5:1 E: T with irradiated target cells for 6 days. Co-cultures were stained with anti-CD4-PE and anti-CD8 APC antibodies to determine CD4 and CD8 T cell proportions by flow cytometry. T cell proliferation was measured by detecting percentage of CD4/CD8 cells with reduced CFSE fluorescence. 0 μ g/mL BiTE condition was used to set a CFSE division gate. Representative experiment shown.

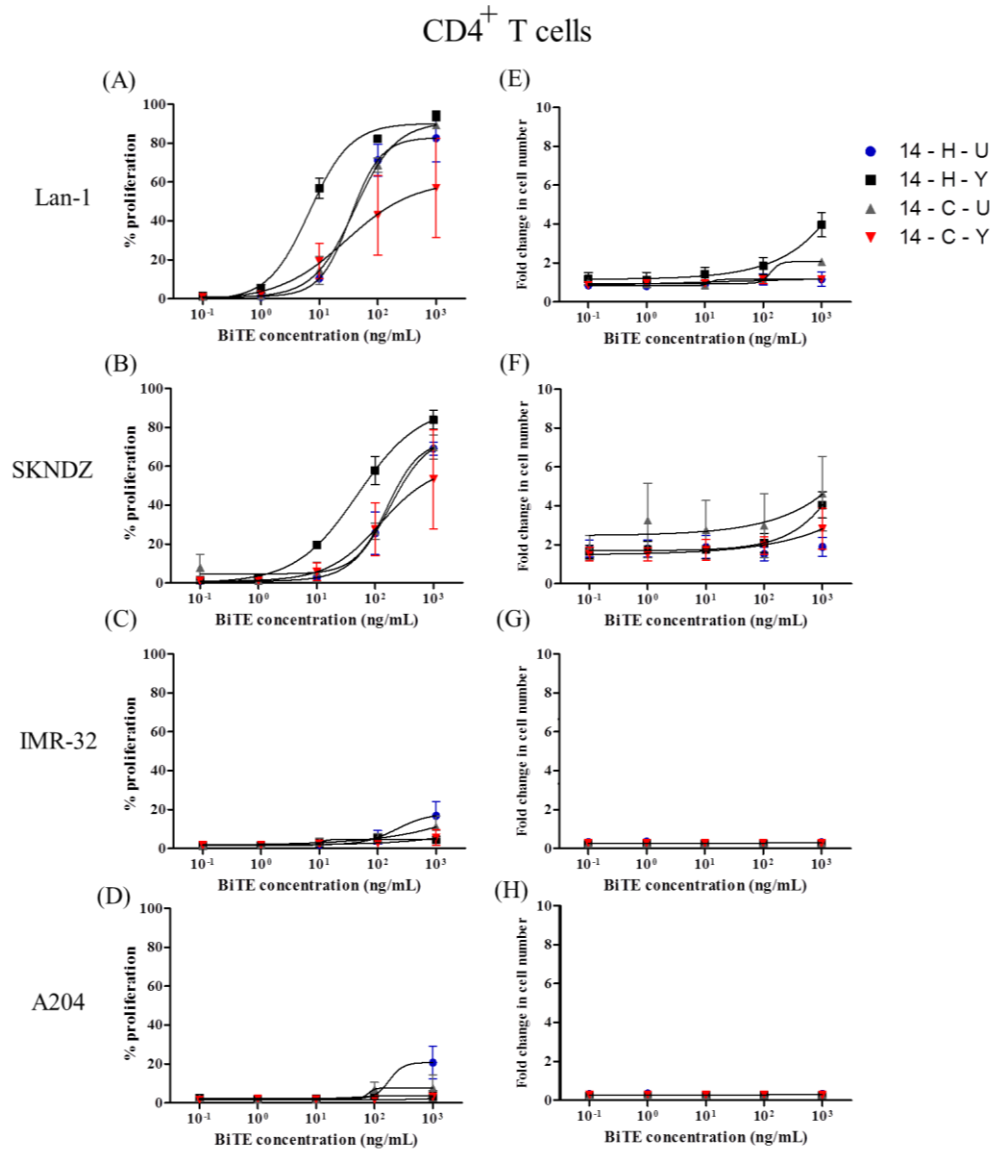


Figure 5.10: $CD4^+$ T cell proliferation in response to co-culture with target cells and BiTE. Read-out of 6 day co-culture between CFSE labelled T cells with $GD2^+/GD2^-$ irradiated target cells at 5:1 E:T and 0-1 $\mu\text{g/mL}$ BiTE by flow cytometry. (A - D) Percentage proliferation determined as percentage of $CD4^+$ T cells with dilution of CFSE compared to 0 ng/mL BiTE control. (E - H) Fold change in $CD4^+$ cell number determined as a proportion of $CD4^+$ T cells in condition with 0 ng/mL BiTE control. Graphs show mean \pm SEM (n=3).

CD8⁺ T cells

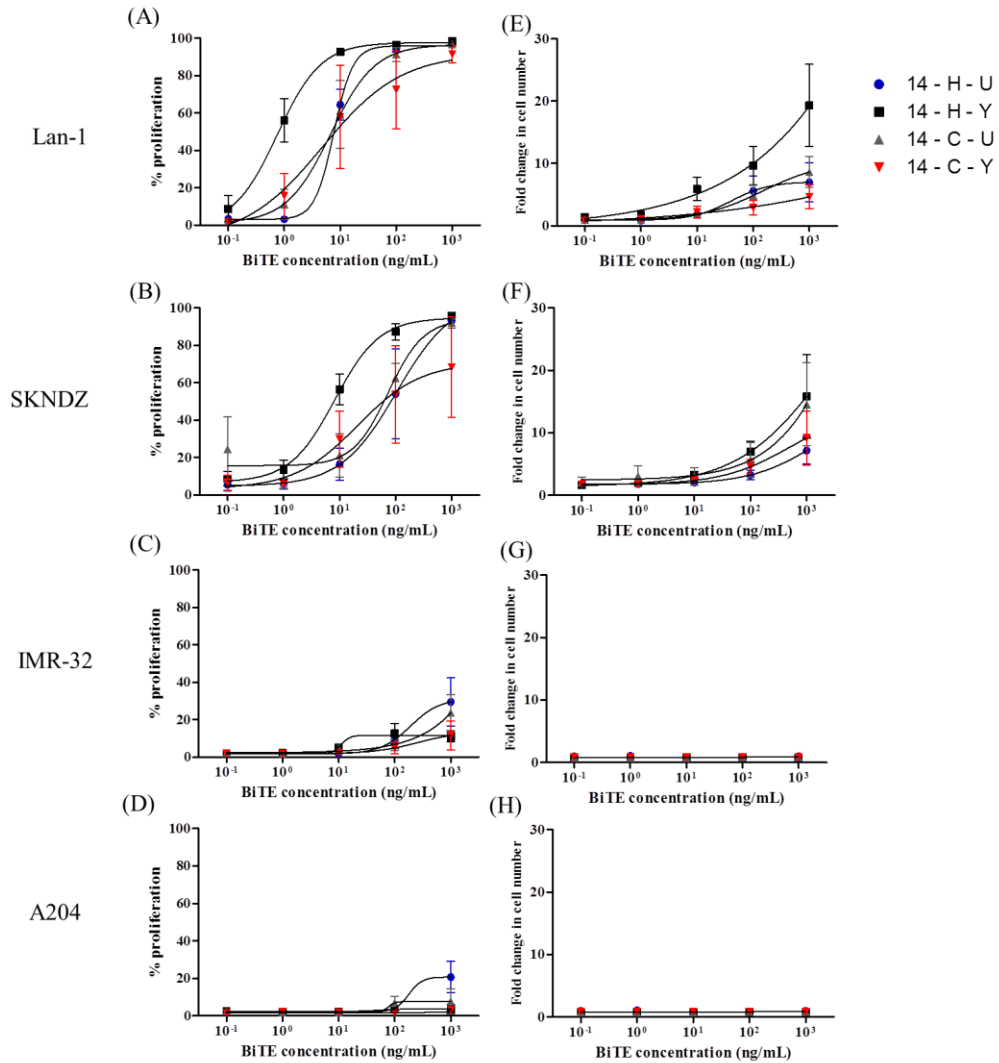


Figure 5.11: CD8⁺ T cell proliferation in response to co-culture with target cells and BiTE. Read-out of 6 day co-culture between CFSE labelled T cells with GD2⁺/GD2⁻ irradiated target cells at 5:1 E:T and 0-1 μ g/mL BiTE by flow cytometry. (A - D) Percentage proliferation determined as percentage of CD8⁺ T cells with dilution of CFSE compared to 0 ng/mL BiTE control. (E - H) Fold change in CD4⁺ cell number determined as a proportion of CD8⁺ T cells in condition with 0 ng/mL BiTE control. Graphs show mean \pm SEM (n=3).

5.2.7 Neuroblastoma patient T cells are able to lyse GD2⁺ targets in the presence of BiTE

Healthy donor T cells have been used in the previous experiments to demonstrate BiTEs are able to redirect their cytotoxic capacity upon co-culture with GD2⁺ targets. This may not be representative of the T cells BiTEs will encounter in an *in vivo* patient setting. Hence, here the ability of BiTE variants to redirect neuroblastoma patient T cells, which can potentially be exposed to an immunosuppressive microenvironment, or function may be impaired due to exposure to chemotherapy agents and/or tumour mediated inhibitory factors, was studied.

T cells from a patient with neuroblastoma were enriched for CD3⁺ cells and co-cultured with GD2.SupT1, Lan-1 and SupT1 target cells in the presence of BiTEs: 14-H-U, 14-C-U and 14-C-Y. BiTE 14-H-Y was not available at the time of the study. All three BiTEs were able to redirect T cell cytotoxicity in co-culture with GD2.SupT1 and Lan-1 cells but not SupT1 cells (**Figure 5.12**). Maximum killing of GD2.SupT1 cells was 60%, 58% and 50%, while for Lan-1 cells 38%, 37% and 39% with BiTEs 14-H-U, 14 -C - U and 14-C-Y respectively. This assay was performed in duplicate (n=1). Killing of GD2.SupT1 cells was greater than Lan-1 cells and may be related to differences in antigen density (GD2.SupT1: ~ 1 million, Lan-1: ~ 0.5 million molecules per cell) or the more suppressive nature of the Lan-1 cell line.

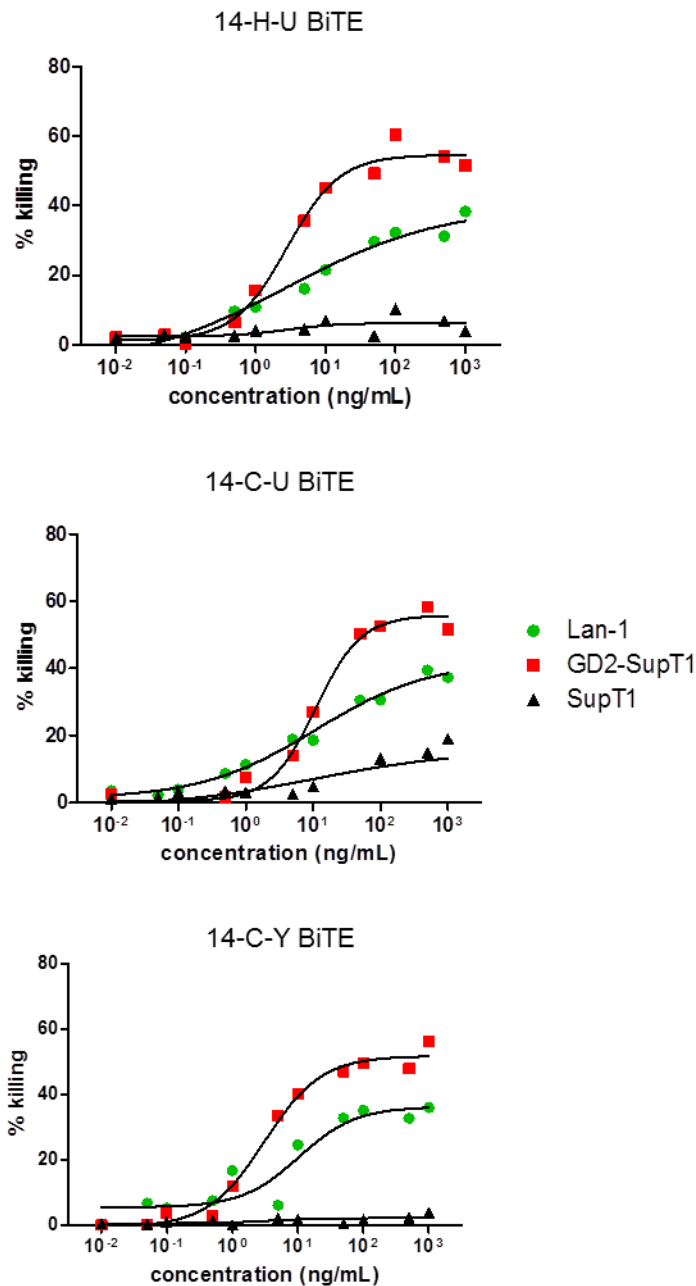


Figure 5.12: Patient T cells are redirected by BiTEs to lyse GD2⁺ tumour cells. Neuroblastoma patient T cells were co-cultured at 5:1 E:T with CFSE labelled (GD2⁺) Lan-1 and GD2.SupT1 or (GD2⁻) SupT1 target cells for 16 hours with 0-1 µg/mL BiTE. Percentage target cell killing was calculated as a proportion of annexin/PI positive target cells compared to conditions with 0 ng/mL BiTE, samples were analysed by flow cytometry, n=1.

5.3 Discussion

GD2/CD3 specific BiTEs with different combinations of scFvs and linkers were functionally compared to determine the optimal format to achieve GD2⁺ tumour directed function. The 11 BiTE variants selected from chapter 4 were able to redirect resting peripheral T cells to induce apoptosis and mediate cell death of GD2.SupT1 target cells. All BiTE variants containing hu14.18 GD2-specific scFvs had an improved ability to redirect T cells compared to BiTEs containing a huK666 scFv. Hu14.18 based BiTEs had EC₅₀ values < 0.3 nM whilst huK666 based BiTEs had EC₅₀ values > 1 nM. This is likely to be associated with the binding affinity of the anti-GD2 scFvs; although the scFv affinity was not measured, the affinity of the 14.18 mAb to GD2 is reported reportedly stronger in comparison to the huK666 mAb (Mujoo et al., 1987, Nakamura et al., 2001). Other studies have also correlated target antigen binding affinity to enhanced bsAb cytotoxicity (McCall et al., 2001, Mazor et al., 2015, Mazor, 2017).

By comparing different linker lengths and CD3 binders; BiTEs containing the medium (HNG) and longer (CD8 STK) linkers were determined to have lower EC₅₀ values when combined with hu14.18 scFvs (BiTE and EC₅₀: 14-H-U: 22.4 pM, 14-H-Y: 127.6 pM, 14-C-U: 55.0 pM, 14-C-Y: 50.0 pM) compared to BiTEs with the short (G₄S)₃ linker (BiTE and EC₅₀: 14-S-U: 263.04 pM and 14-S-Y: 161.96 pM) p<0.001. The optimal distance between a target and effector cell membrane is critical in mediating the efficient formation of an immunological synapse. The distance of an epitope from the target cell membrane has been shown to influence the size of a BiTE mediated immunological synapse (Bluemel, 2010) . As indicated by our data, the small size of GD2 as an extracellular membrane component may require a longer linker length to mediate synapse formation. In contrast, blinatumomab which targets a larger CD19 (95 kDa) antigen, contains a short G₄S linker between the scFvs (Nagorsen et al., 2012). However, the length of the linker itself cannot be directly attributed to BiTE potency as linker sequence and flexibility may also be additional contributing factors and require further study.

The four BiTEs: 14-H-U, 14-H-Y, 14-C-U and 14-C-Y were taken forward for further functional comparisons and demonstrated their ability to activate T cells and induce proliferation. CD8⁺ T cells were shown to be the predominant effector cell population. Detection of cytokines in co-culture supernatant after 24 and 72 hours was observed only in wells containing GD2⁺ cells and BiTE, indicating specificity of the response to GD2. Cytokine production and both CD4⁺ and CD8⁺ T cell proliferation was observed when T cells were co-cultured with BiTE and Lan-1 or SKNDZ cell lines. However, only cytokine production and not an increase in T cell number were apparent upon co-culture of T cells with the IMR32 cell line. CFSE division of T cells is apparent at higher concentrations of BiTE and may be a longer co-culture time is required before an increase in T cell number is apparent.

The comparison of BiTEs containing different CD3 binders showed that 14-H-Y and 14-C-Y (BiTEs containing huYTH) had improved ability to activate T cells and promote T cell proliferation in either Lan-1 or SKNDZ cell lines. Of note, these studies have demonstrated the differences in target cell killing and T cell activation and proliferation when T cells are co-cultured with different cell lines expressing GD2. The huYTH scFv appears to be the lead candidate in the optimal GD2/CD3 specific BiTE.

Future directions

The next steps in developing the optimal GD2 and CD3 specific BiTE for neuroblastoma immunotherapy will be to test the lead BiTE candidates *in vivo*. One approach is a xenograft mouse model, in which the ability of humanised BiTEs to redirect human PBMCs to eliminate neuroblastoma cells can be monitored. This approach has been reported by other groups testing BiTEs antibodies (Dreier et al., 2003, Lutterbuese et al., 2010, Friedrich et al., 2012, Hipp et al., 2017). A limitation to the current study is the absence of a non-specific BiTE control.

To address further questions that will help us understand the effects BiTEs have on T cells, in terms of their ability to persist *in vivo* and proliferate, their response to an immunosuppressive microenvironment and interaction with other immune cells,

studies in an immunocompetent model will be required. For this setting, it will be necessary to test the BiTE constructs in a murine form. This work in a transgenic model for neuroblastoma is described in chapter 7.

CHAPTER 6:
RESULTS (IV)

***O*AcGD2 as a target antigen for CAR T cell therapy of neuroblastoma**

6.1 Introduction

Target selection is a key feature in cancer immunotherapy. In chapters 4 and 5, GD2 was explored as a target antigen for BiTE mediated immunotherapy based on the high level of GD2 expression across neuroblastoma tumours and low level of expression on normal tissues. An alternative approach, which may avoid on-target off-tumour toxicities is targeting novel antigen *O*AcGD2, which has a tumour restricted expression pattern and is present on GD2⁺ tumours. *O*AcGD2 specific immunotherapies have been tested in pre-clinical studies but have not yet progressed to clinical testing. In this chapter, a CAR T cell based approach for targeting *O*AcGD2 is explored.

*O*AcGD2-specific mAb 8B6

MAb 8B6 is currently the only *O*AcGD2 specific mAb described (Cerato et al., 1997, Alvarez-Rueda et al., 2011). To compare the *in vitro* activity of mAb 8B6 to the GD2-specific mAb 14.18, Cochonneau *et al.* demonstrated that in a similar fashion to mAb 14.18, mAb 8B6 was able to inhibit the growth of GD2⁺/*O*AcGD2⁺ tumour cells by inducing cell cycle arrest and apoptosis *in vitro*, through an undetermined mechanism. In an *in vivo* setting, mAb 8B6 was able to induce the regression of GD2⁺/*O*AcGD2⁺ EL4 tumour cells in syngeneic C57BL/6 mice by down regulation of the Ki67 associated proliferation antigen and by inducing apoptosis (Cochonneau et al., 2013).

As *O*AcGD2 has a tumour specific expression pattern, the advantage of developing therapies to target *O*AcGD2 would be to avoid binding to peripheral nerve fibres; a common side effect associated with pain when targeting GD2 in the clinic with mAb therapy. To compare differences in on-target off-tumour binding between chimeric (ch) mAb 8B6 and mAb 14.18, both antibodies were administered in rats to assess

any pain related side effects of targeting peripheral nerve fibres. Allodynia (perceived pain in response to light touch) was assessed by measuring the withdrawal response in rats. The study demonstrated that intravenous ch.8B6 mAb treatment did not induce allodynia in comparison to rats treated with ch14.18 and was due to the absence of *OAcGD2* expression on nerve fibres (Mickaël Terme, 2014).

Considerations of CAR design

CARs are modified T cell receptors constructed by grafting antigen specificity to the intracellular signalling portion of the T cell signalling domain, typically CD3 ζ . In contrast to BiTEs, CAR T cells have the advantage of only needing to identify the tumour cell, whereas BiTEs require co-localisation of both T cells and tumour cells. To determine the optimal format of CAR for a specific tumour antigen, careful selection of the scFv, spacer, transmembrane and activation domains are required.

Antigen binding domain

The choice of scFv used in a CAR design can influence the downstream signalling within a T cell. As mAb 8B6 is the only reported *OAcGD2* specific antibody, the scFv derived from 8B6 was incorporated in the CAR design.

Spacer region

The choice of spacer region directly influences the synapse distance and flexibility between CAR T cell and target cell and plays an important role in building and maintaining the immunological synapse. The choice for a spacer region is target dependent and modifying this region is likely to significantly impact the receptor stability and substrate binding affinity (Guest et al., 2005, Hudecek et al., 2013, Hombach et al., 2000, Moritz and Groner, 1995). The immunoglobulin domain such as the Fc region of IgG is an example of a spacer region. A recent publication confirmed the importance of CAR design by showing that, for a GD2 CAR, the optimal spacer was the IgG Fc spacer (CH₂CH₃) (Thomas et al., 2016). There is however, a theoretical risk of cross-activation between CAR expressing T cells with Fc γ -receptor (Fc γ R) expressing cells resulting in innate immune activation and

activation induced cell death (Clemenceau et al., 2015, Hombach et al., 2010). Hombach *et al.* described two modifications: PELLGG to PPVA and ISR to IAR introduced in the IgG Fc domain to disrupt the binding sites for Fc γ -R expressing cells (Hombach et al., 2010). The IgG1 Fc spacer with disruption of the Fc γ R binding sites was selected for this study.

Transmembrane domain

The transmembrane domain is not only responsible for keeping the CAR membrane bound, but is also important for stable CAR expression. Transmembrane domains can be derived from several transmembrane proteins including CD3 ζ , CD4, CD8 or CD28 molecules. It is not clear which transmembrane domain is optimal for CAR-based therapies and testing distinct versions of this domain in the context of a specific target antigen and various effector cell populations may be necessary.

Activation domain

As described in section 1.3.2.2 the incorporation of costimulatory endodomains into the CAR structure can significantly improve the anti-tumour potential of CAR T cells (Curran et al., 2012). The CD28-CD3 ζ co-stimulatory activation domain was used in this study based on the second-generation CAR format currently being used in a phase I GD2 CAR clinical trial (1RG-CART) taking place at Great Ormond Street Hospital in neuroblastoma patients.

Aims

1. To clone, produce and purify the 8B6 mAb
2. Demonstrate specificity of 8B6 mAb to the *O*AcGD2 antigen
3. To demonstrate *O*AcGD2 specific CAR T cells are activated and produce IFN- γ in response to co-culture with *O*AcGD2⁺ cells.
4. Test the specificity of *O*AcGD2 specific CAR T cells in mediating lysis of *O*AcGD2⁺ and not *O*AcGD2⁻ cells.

6.2 Results

6.2.1 Recombinant mAb 8B6-IgG2a shows similar specificity for *OAcGD2* as the parental mAb 8B6

To validate specific binding of mAb 8B6 to *OAcGD2* and not GD2, the 8B6 mAb sequence was derived from the literature to enable our own production and testing of the mAb. The reported 8B6 mAb V_H and V_L sequence was cloned with a mouse IgG2a Fc portion, in comparison to the parental 8B6 mAb which has a mouse IgG3 Fc, this enables storage of the mAb at -20 °C (Cerato et al., 1997). Firstly, an 8B6-IgG2a mAb producer cell line was made by double transduction of K562 cells with SFG retroviral vectors containing 8B6 mAb heavy or light chains. Double transduced cells underwent fluorescence activated cell sorting by detection of both BFP and GFP, which were co-expressed in the vectors containing heavy and light chains respectively. A homogeneous K562 cell population which stably secreted the 8B6 mAb was obtained by single cell cloning (**Figure 6.1 A**).

Secondly, secreted 8B6-IgG2a mAb was purified from the K562 culture supernatant and purification confirmed by detection of both antibody heavy (50 kDa) and light (25 kDa) chains by Western Blotting analysis and Coomassie Blue staining (**Figure 6.1 B - C**).

To confirm specificity of the re-derived 8B6-IgG2a antibody to *OAcGD2*, binding to IMR5 neuroblastoma cells was determined by thin layer chromatography (TLC), this was performed in comparison to parental mAb 8B6 by Stéphane Birkle's group (Centre de Recherche en Cancérologie de Nantes-Angers, Institut de Recherche en Santé de l'Université de Nantes, Nantes). The re-derived 8B6-IgG2a mAb demonstrated specificity for *OAcGD2* by TLC and had identical staining to the parental 8B6 antibody (**Figure 6.2**).

OAcGD2 expression was confirmed on neuroblastoma cell lines and primary neuroblastoma cell lines using the 8B6 mAb and is reported in Chapter 3, (**Figure 3.3**) and (**Figure 3.5**).

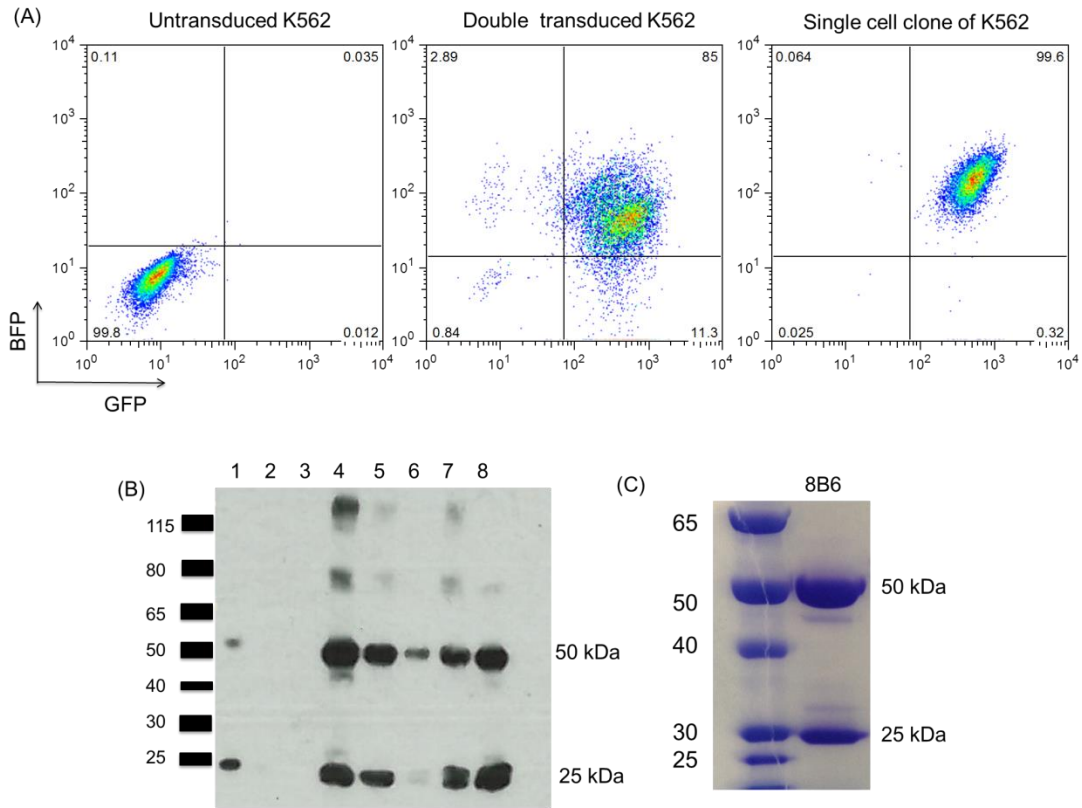


Figure 6.1: Production and purification of *OAcGD2* specific mAb 8B6-IgG2a.

(A) K562 producer cell line transduction efficiency measured by detection of BFP (heavy chain) and GFP (light chain) co-expression using flow cytometry. (B) Western Blotting analysis on samples taken from purified mAb 8B6-IgG2a from K562 supernatant, 1: supernatant, 2: flow through, 3: wash, 4 - 7: fractions 2 - 5. 8: pooled fractions. Detection of 8B6 mAb using goat-anti-mouse-IgG-HRP (1:2000). (C) Coomassie Blue staining of SDS-PAGE gel of purified 8B6-IgG2a mAb.

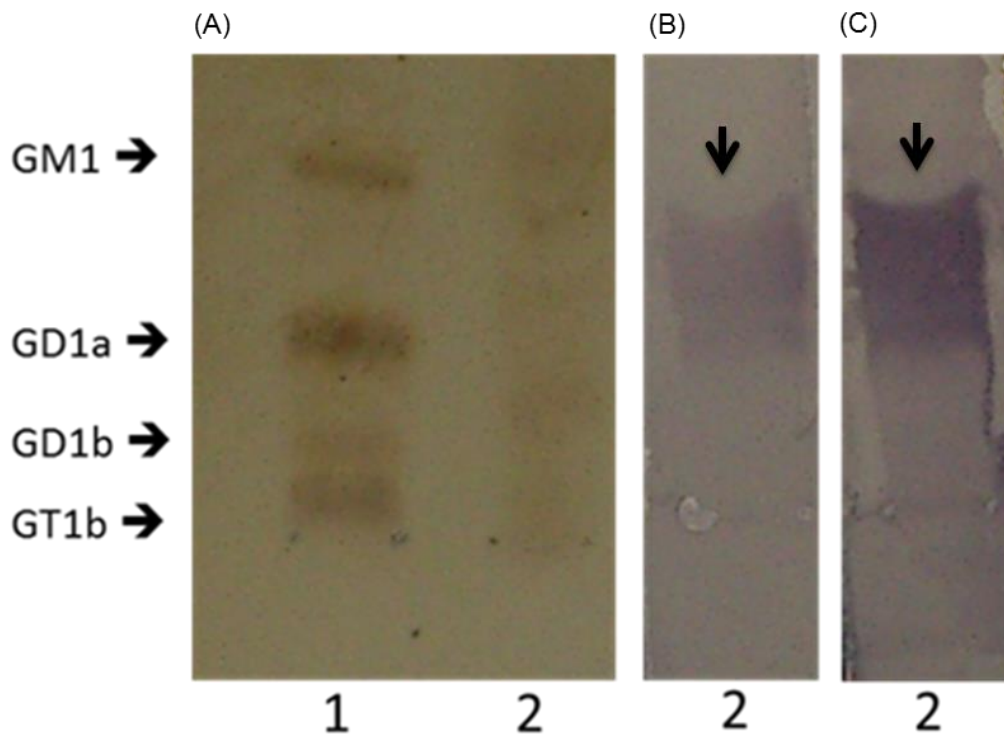


Figure 6.2: 8B6-IgG2a mAb has specificity to *OAcGD2*. Thin layer chromatography-immunostaining of rat brain gangliosides (Lane 1) and IMR5 neuroblastoma gangliosides (Lane 2) with (A) orcinol stain (B) positive control 8B6-IgG3 and (C) 8B6-IgG2a mAb. Primary antibody: 8B6-IgG2a or 8B6-IgG3, detection antibodies: anti-human IgG-biotin (1:2000) and streptavidin-HRP (1:1000). Staining visualised with 4-chloro-1-naphtol solution. *OAcGD2* specific staining indicated by black arrows.

6.2.2 8B6 mAb shows differential binding to GD2.SupT1 cells

One of the important features of an *OAcGD2* specific CAR T cell is absence of cross-reactivity to GD2. In this study we are assuming that 8B6 distinguishes *OAcGD2* from GD2 based on published data (Cerato et al., 1997), in which chromatographic methods were used to distinguish gangliosides and demonstrate specificity of staining. Control cell lines with expression of $GD2^+/OAcGD2^+$ or $GD2^+/OAcGD2^-$ can be used to determine *OAcGD2* specificity. GD2.SupT1 cells are 100% GD2 positive and approx. 50% *OAcGD2* positive, these cells were sorted into $OAcGD2^+$ and $OAcGD2^-$ groups by flow cytometry; both cell lines retain GD2 expression (Figure 6.3).

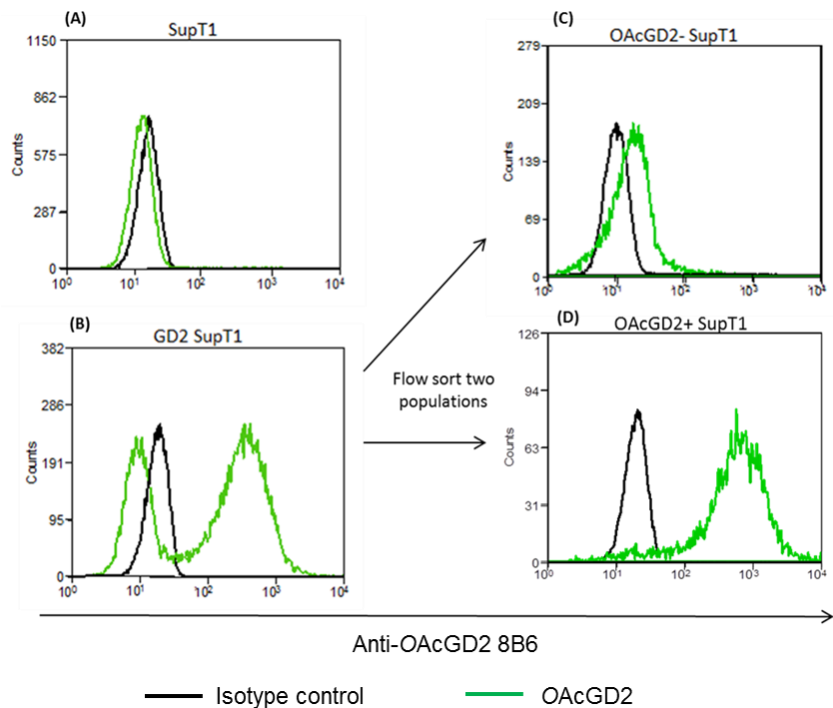


Figure 6.3: *OAcGD2*⁺ and *OAcGD2*⁻ GD2.SupT1 cells obtained by fluorescence activated cell sorting. (A) SupT1 cells (B) GD2.SupT1 cells (C) *OAcGD2*⁻ sorted GD2⁺SupT1 cells and (D) *OAcGD2*⁺ GD2.SupT1 cells.

6.2.3 *OAcGD2* specific CAR T cells secrete IFN- γ and lyse *OAcGD2*⁺ cell lines

An *OAcGD2*-specific CAR was constructed by cloning the 8B6 scFv into a second generation CAR format: 8B6 scFv - CH₂CH₃ - CD28 - CD3 ζ . A GD2-specific CAR was used as a control: HuK666 scFv - CH₂CH₃ - CD28 - CD3 ζ (**Figure 6.4 A**). Healthy donor PBMCs were activated with anti-CD3 and anti-CD28 antibodies and cultured in IL-2 before transduction with the CAR constructs. Transduction efficiency was measured by detection of eBFP2 co-expressed in the vector; transduction efficiencies were measured as 72% and 77% for GD2-specific and *OAcGD2*-specific CARs respectively (**Figure 6.4 B - D**).

To demonstrate *OAcGD2* specificity of the 8B6 CAR and no cross reactivity towards the GD2 antigen, CAR T cells were co-cultured 1:1 with SupT1, GD2.SupT1, *OAcGD2*⁺ GD2.SupT1 and *OAcGD2*⁻ GD2.SupT1 targets. T cell activation was determined after 24 hours by measure of IFN- γ in co-culture supernatant by ELISA. IFN- γ secretion appeared to correlate very well with the presence of *OAcGD2* on target cells. GD2-specific CAR T cells secreted IFN- γ in co-culture with all three GD2⁺ target cell lines, regardless of presence or absence of *OAcGD2* expression (**Figure 6.5 A**).

To measure specific killing of *OAcGD2*⁺ targets by *OAcGD2* specific CAR T cells; T cells and ⁵¹Cr labelled target cells were co-cultured for 4 hours at E:T ratios: 32:1, 16:1, 8:1 and 4:1 in a chromium release assay. GD2.SupT1 and *OAcGD2*⁺GD2.SupT1 cells were lysed by the *OAcGD2*-specific CAR while lysis of *OAcGD2*⁻GD2.SupT1 cells was minimal in comparison to lysis induced by GD2 specific CAR T cells. Although n=1, the results so far demonstrate the *OAcGD2* specific CAR has specificity for *OAcGD2* and does not cross-react with GD2 (**Figure 6.5 B - D**).

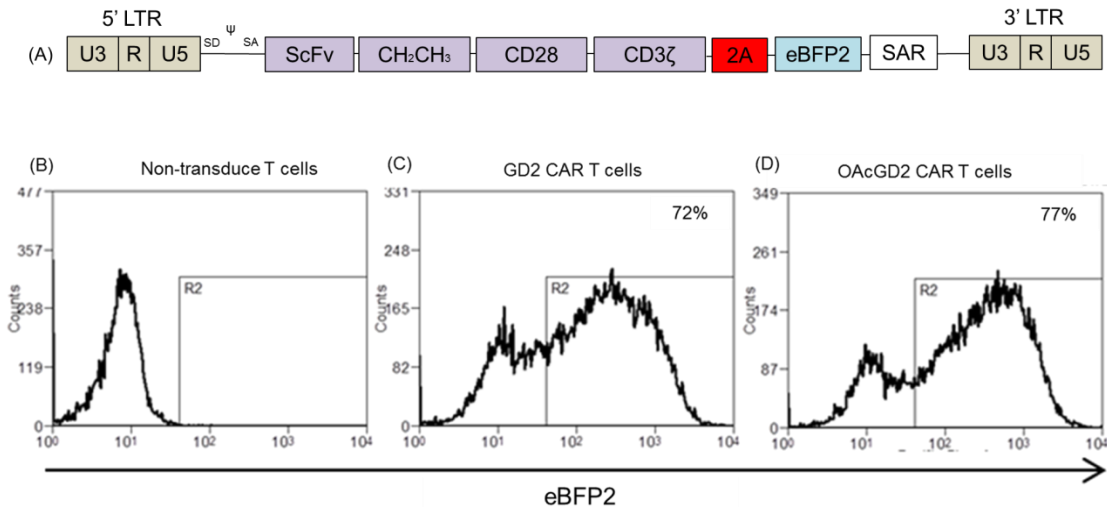


Figure 6.4: Transduction of activated T cells to express CARs. (A) Retroviral expression vector containing second generation CAR (purple) and eBFP2 reporter gene (blue); separated by a cleavable in-frame 2A peptide. Transduction efficiencies measured by detection of eBFP2 in (B) Untransduced (C) GD2 CAR transduced and (D) OAcGD2 CAR transduced T cells (n=1).

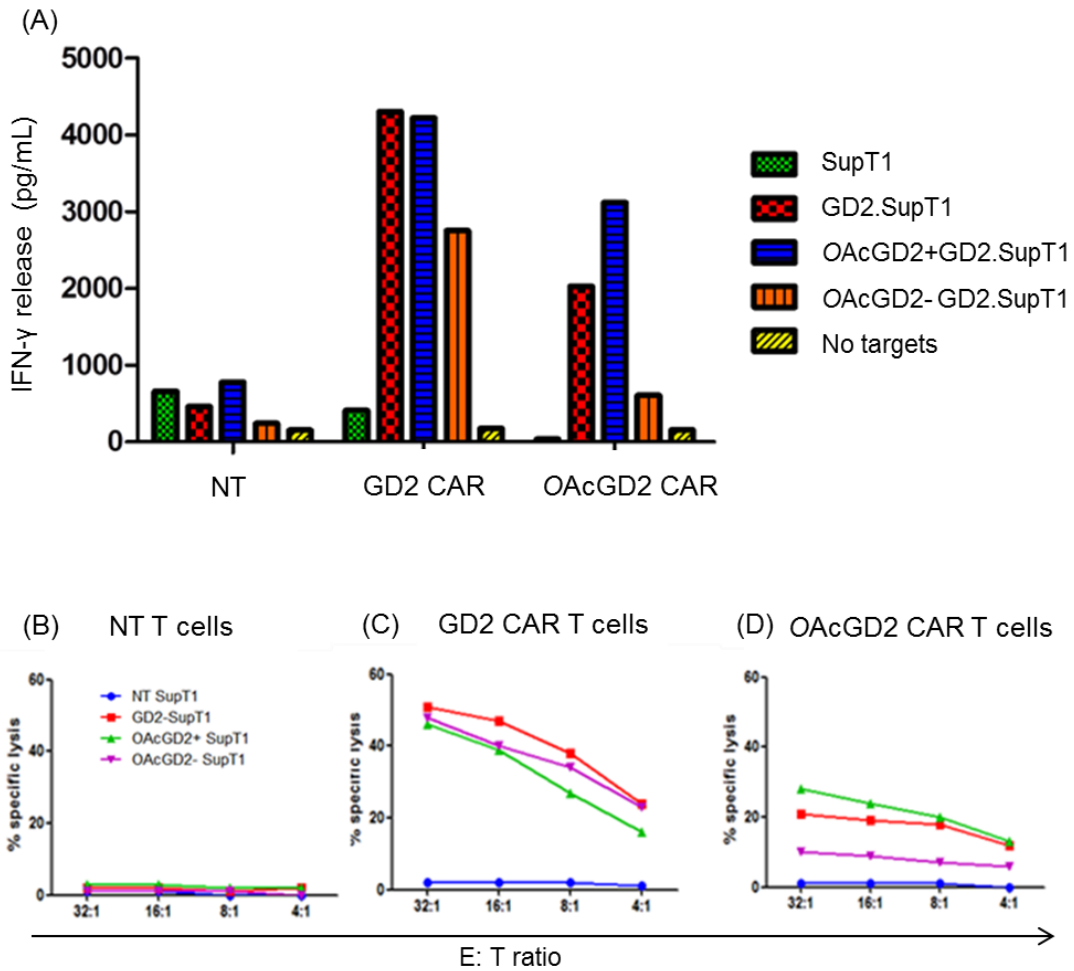


Figure 6.5: *OAcGD2*-specific CAR T cells have specificity to *OAcGD2*. (A) IFN- γ specific ELISA was used to quantitate IFN- γ secreted after 24 hours co-culture of Non-transduced (NT) or CAR T cells 1:1 with GD2/*OAcGD2* target cells. (B - D) NT and CAR transduced T cell cytotoxicity of target cells measured by percentage chromium release after 4 hours co-culture at E: T ratios 32:1, 16:1, 8:1 and 4:1 (n=1).

6.3 Discussion

The data in this chapter has demonstrated specific targeting of *OAcGD2*⁺ cell lines using the 8B6-second generation CAR, this approach has not been previously reported. The main implication of targeting *OAcGD2* would be the avoidance of dose limiting acute toxicities associated with targeting of GD2 on healthy tissues. This data supports the potential of an *OAcGD2*-directed immunotherapy.

Unlike GD2 however, which has been a target in the clinic for more than 20 years; *OAcGD2* remains poorly characterised. Both therapeutic efficacy and potential toxicity profile of targeting the antigen are yet to be determined (Fleurence et al., 2017). In addition, the *O*-acetyl group on GD2 is removed upon alkali treatment, demonstrated by the lack of binding of mAb 8B6 to *OAcGD2* by thin-layer chromatography (Cerato et al., 1997). Thus, *OAcGD2* may not have stable expression as reported for GD2 and may also preclude the generation of further *OAcGD2* specific antibodies (Kramer et al., 1998, Poon et al., 2015). As only one group have reported the tumour restricted expression pattern of *OAcGD2*, it is crucial for further studies to also validate this finding.

With regard to CAR T cell therapy, despite the remarkable success of the CD19 CAR in B cell malignancies, development of CAR T cells in neuroblastoma is challenging due to the paucity of selectively expressed cell surface antigens. In addition, antigen negative tumour escape is well described in B cell malignancies, occurring in greater than 10% of patients with acute lymphoblastic leukaemia treated with a CD19 CAR (Sotillo et al., 2015, Maude et al., 2014). *OAcGD2* may provide an appropriate target antigen for CAR T cell therapy; however regulation of acetylation across tumours is yet to be explored.

Future directions

To determine specific killing of neuroblastoma cell lines with 8B6 CAR T cells and further explore the appropriate CAR format for targeting *OAcGD2*. As the experiments described in this chapter were performed once, it will also be necessary to repeat the assays.

CHAPTER 7:

Results (V)

Testing of immunotherapeutic strategies on an immunocompetent animal model for neuroblastoma

7.1 Introduction

The work described so far has focussed on target selection and the development of BiTE and CAR therapy for neuroblastoma. Both GD2-BiTE and OAcGD2-CAR approaches have demonstrated *in vitro* anti-tumour efficacy. Although both approaches engage T cell effector function; their underlying biology differs significantly (Ruella and Gill, 2015).

The focus of this chapter is to explore the potential use of an immunocompetent animal model of neuroblastoma as a tool to test T cell based immunotherapies *in vivo*. Analysing the *in vivo* anti-tumour response of both BiTEs and CARs is important to direct their best clinical use and apply them to the appropriate disease setting, such as bulky tumours or MRD. Crucial features of both therapies in the context of treating bulky tumours is the requirement of T cells to migrate to the tumour site and overcome an immunosuppressive microenvironment (Beatty and Moon, 2014, Scarfo and Maus, 2017). In addition, to maintain an on-going anti-tumour response, T cells will require the ability to proliferate and persist *in vivo* (Kershaw et al., 2006, Till et al., 2008). These questions cannot be addressed with a xenograft mouse model as there is no interaction with an endogenous immune system. This chapter describes the generation of the required murinised BiTE and CAR constructs and *in vivo* pilot data in an immunocompetent mouse model of neuroblastoma. GD2 was chosen as the target antigen for both murine derived BiTE and CAR constructs.

7.1.1 Mouse model with overexpression of $ALK^{F1174L}/MYCN$ oncogenes

The mouse model for neuroblastoma used in this study has been previously described (Berry et al., 2012). In 1997, Weiss *et al.* created a transgenic mouse model of the *129x1/SvJ* strain in which mice develop neuroblastoma due to overexpression of the *MYCN* oncogene in neuroectodermal cells. This was achieved by placing *MYCN* cDNA downstream of a tyrosine hydroxylase promoter (*Th*) which is active in migrating cells of the neural crest early in development (Banerjee et al., 1992). This tissue specificity resulted in tumours that arose in the sympathetic ganglia and adrenal gland (Weiss et al., 1997). Heterozygote *MYCN* animals developed neuroblastoma within 4 - 5 months, whereas homozygous animals showed increased penetrance and shorter latency of tumours that approached 100% at three months (Weiss et al., 1997).

More recently, Berry *et al.* have described the generation of a C57BL/6J mouse model that overexpressed human ALK^{F1174L} in the neural crest driven by the same *Th* promoter. After crossing the *MYCN* and ALK^{F1174L} expressing mouse strains, approximately a quarter of mice were hemizygous for both ALK^{F1174L} and *MYCN* oncogenes and all of these developed large thoracic and abdominal tumours in locations typically seen in human neuroblastoma. $ALK^{F1174L}/MYCN$ double transgenic mice exhibited high tumour penetrance with rapid lethality greater than that observed for in *MYCN* hemizygotes. $ALK^{F1174L}/MYCN$ tumours were observed to have higher levels of *MYCN* in comparison to *MYCN* alone tumours. Transcriptional profiling indicated a significant upregulation of genes involved in the PI3K, AKT, mTOR and MAPK signal transduction pathways in $ALK^{F1174L}/MYCN$ tumours. The increased activity of the PI3K pathway stabilised *MYCN* by inactivating glycogen synthase kinase 3 β , which mediates the phosphorylation of *MYCN*. Absence of phosphorylation at residue T58 prevented the targeting of *MYCN* for degradation (Otto et al., 2009). Thus, constitutive signalling mediated by ALK^{F1174L} increased *MYCN* dosage and enhanced the aggressive nature of the tumour in the $ALK^{F1174L}/MYCN$ tumour model (Berry et al., 2012).

Aims

1. Determine the expression of antigens GD2, OAcGD2 and ALK on tumours from $ALK^{F1174L}/MYCN$ transgenic mice
2. Develop and test GD2/CD3 specific murine BiTEs *in vitro*
3. Develop and test GD2 specific murine CAR T cells *in vitro*
4. Perform a preliminary *in vivo* experiment to establish optimal settings to:
 - (i) monitor CAR T cell migration by bioluminescence imaging (BLI) and
 - (ii) monitor tumour progression by magnetic resonance imaging (MRI)

7.2 Results

7.2.1 *ALK^{F1174L}/MYCN* tumours express neuroblastoma antigens GD2, *OAcGD2* and ALK

To determine the presence of antigens GD2, *OAcGD2* and ALK on tumours from *ALK^{F1174L}/MYCN* transgenic mice, tumour samples obtained from 35 – 44 day old mice were mechanically disaggregated and stained with anti-GD2-PE, anti-*OAcGD2*-APC or anti-ALK-APC antibodies, followed by analysis with flow cytometry. **Figure 7.1** is a representative example of a tumour specimen and the gating strategy used for flow cytometric analysis. The presence of CD45⁺/CD11b⁻ and CD45⁺/CD11b⁺ cell populations indicates the presence of infiltrating lymphocytes and leukocytes within the tumour sample. CD45⁻/CD11b⁻ cells were gated on to identify the tumour cell population and these cells were analysed for GD2, *OAcGD2* or ALK antigen expression.

Of 8 tumour samples stained, 8/8 samples were positive for both GD2 and ALK expression. MFI values for GD2 expression ranged between 5160 - 70272, indicating overall a high level of GD2 expression but heterogeneity between tumour samples. 6/8 samples had an MFI for ALK of approximately 2000, while 2/8 samples had higher levels of ALK expression with MFI values of 13,090 and 47,806. 5/8 samples stained positive for *OAcGD2* expression; all MFI values were less than 500 apart from 1 sample (MFI: 5,073) (**Figure 7.2**). These staining results indicated that tumours in this transgenic mouse model expressed target antigens that allow for studying GD2, *OAcGD2* and ALK-directed immunotherapy strategies.

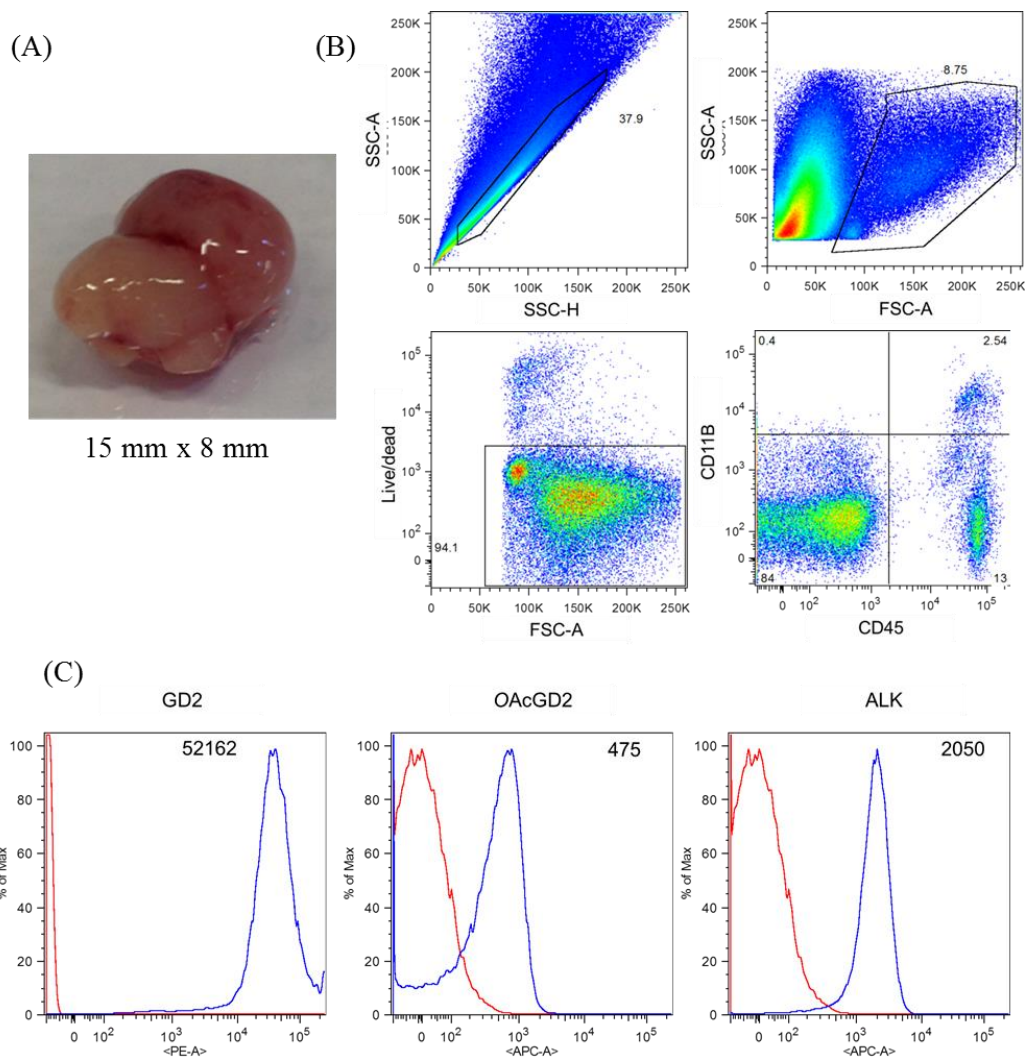


Figure 7.1: Phenotyping of $ALK^{F1174L}/MYCN$ transgenic mouse tumours. (A) Tumour specimen from a mouse bearing the $ALK^{F1174L}/MYCN$ oncogenes. (B) Gating strategy for flow cytometry, top: gating on single cells, bottom: gating on live cells and exclusion of $CD45^+/CD11b^+$ cells. (C) Detection of GD2, OAcGD2 and ALK on tumour cells. Blue graph: antigen expression, red graph: isotype control. MFI values are reported for blue graphs.

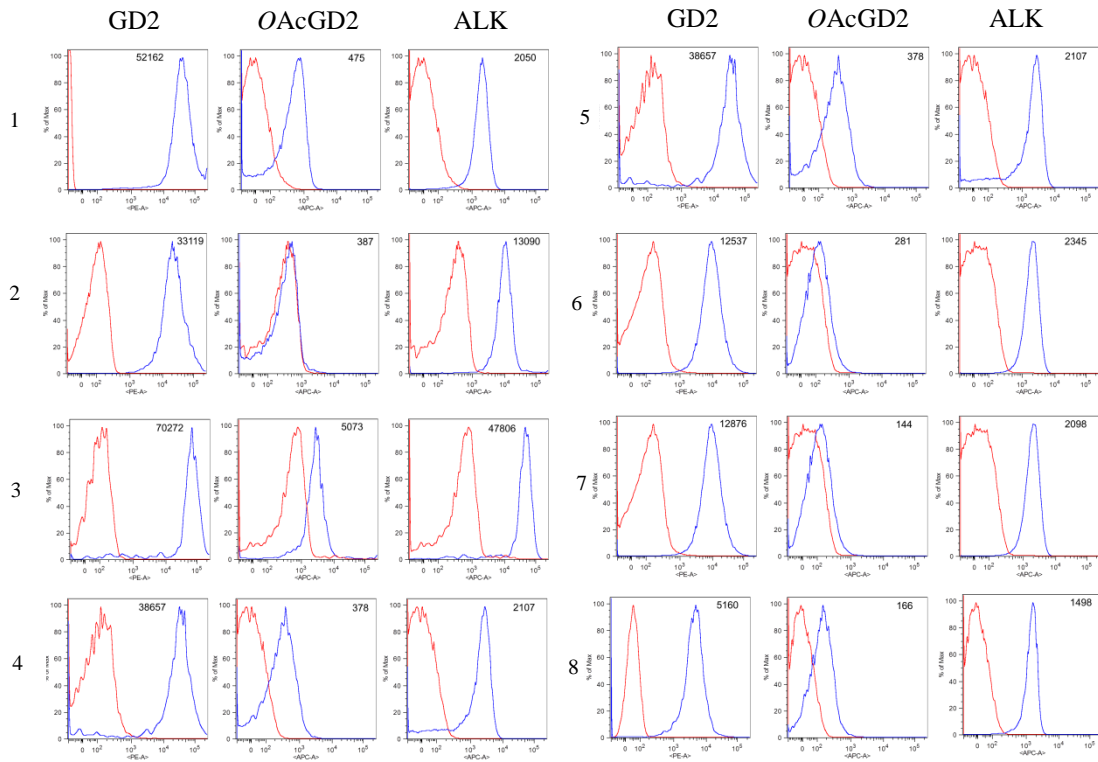


Figure 7.2: GD2, OAcGD2 and ALK antigen expression on tumour samples from $ALK^{F1174L}/MYCN$ transgenic mice. Tumours were removed from 35 – 44 day old mice and mechanically disaggregated followed by staining with anti-GD2-PE, anti-OAcGD2-APC and anti-ALK-APC antibodies. Antibody staining was analysed by flow cytometry. Blue line: antigen expression, red line: isotype control. MFI values are reported for blue graphs, n=8.

7.2.2 Development of GD2 and CD3 specific murine BiTEs

To test GD2/CD3 specific BiTEs in the *MYCN/ALK^{F1174L}* transgenic mouse model, murine versions of BiTEs were generated, a murine sequence is important to minimise immunogenicity within the mouse model. A combination of scFv and linkers were designed to create a panel of 6 murine BiTEs. The GD2 specific scFvs from MuK666 (K6) and 14.18 (14) mAbs were used. The three linkers described for the humanised BiTEs in chapters 4 and 5 were used: a short glycine-serine (S) linker, a medium length IgG1 hinge (H) and a longer linker: murine CD8 stalk region (C). The mouse CD3-specific scFv from 17A2 (17) mAb was used. The final murine BiTE constructs are:

- 1) K6-S-17,
- 2) K6-H-17,
- 3) K6-C-17,
- 4) 14-S-17,
- 5) 14-H-17 and
- 6) 14-C-17.

The BiTEs were co-expressed with the eBFP2 reporter gene in an SFG retroviral vector (**Figure 7.3 A**). BiTEs were produced by transfection of 293T cells and successful transfection measured by the detection of eBFP2 on 293T cells using flow cytometry (n=3). Transfection efficiencies for all constructs were > 50% (**Figure 7.3 B**). To determine if the murine BiTEs had specificity for GD2, non-purified supernatant containing BiTE from transfected 293T cells was incubated with the murine colon carcinoma cell line CT26 or cells transduced to express GD2 (GD2.CT26) (both cell lines were a gift from Dr. Martin Pule, University College London, Cancer Institute). The binding of BiTE to these cell lines was measured by detection of a C-terminal hexa-his tag on the BiTE constructs using a penta-his-AF647 antibody. BiTEs containing the 14G2A scFv showed GD2 specificity by binding the GD2.CT26 cell line and not the CT26 line. BiTEs containing the MuK666 scFv did not show any specific staining; this may be related to a limited protein production (**Figure 7.3 C**). All BiTE formats failed to show binding to mouse

splenic cells (data not shown). Thus, for the development of murine BiTEs, optimisation is required to produce BiTE constructs which bind target antigen and are functional *in vitro* before being tested *in vivo*.

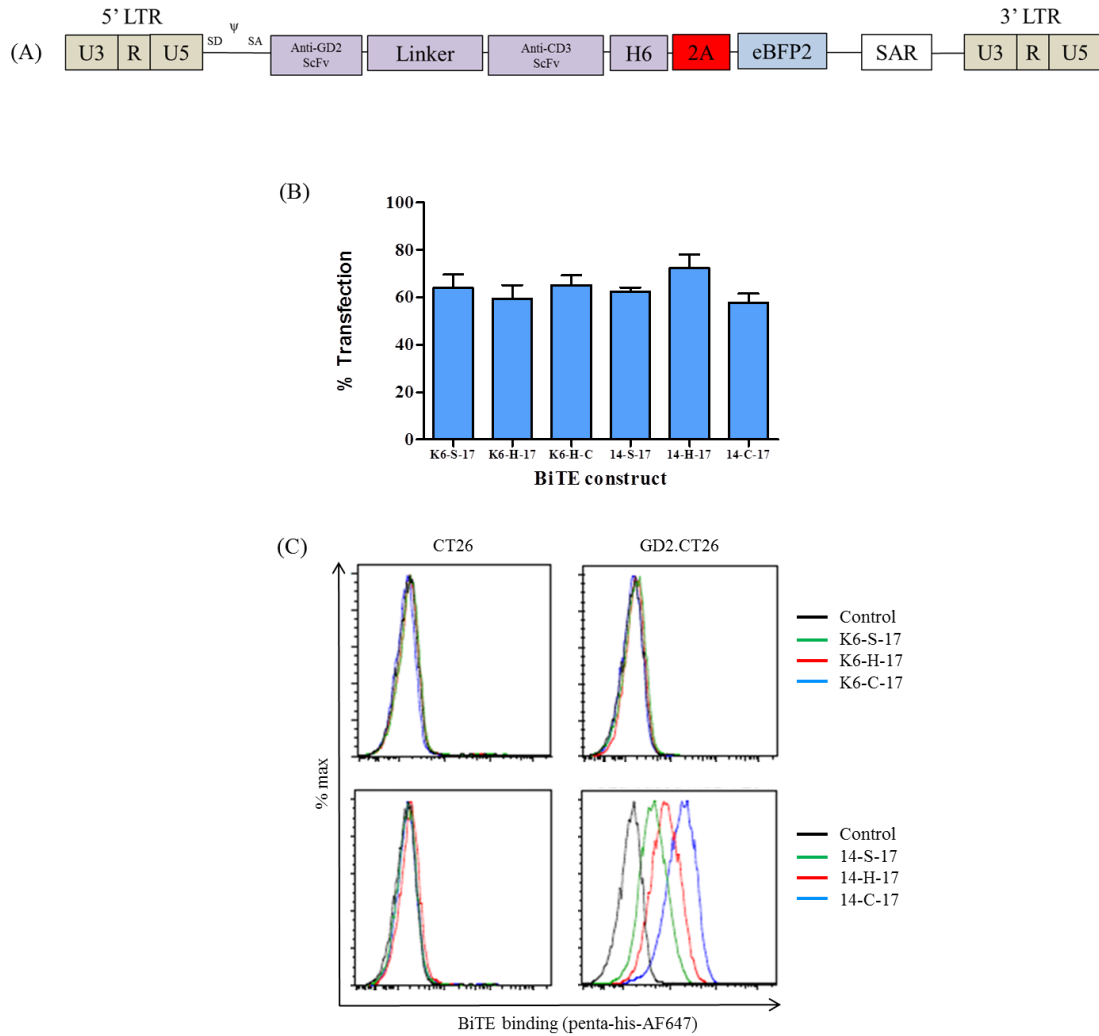


Figure 7.3: Generation of murine BiTE constructs. (A) Structure of the murine BiTE in an SFG retroviral expression vector. BiTEs have a C-terminal hexa-his-tag (H6) and are co-expressed with eBFP2 separated by the cleavable 2A peptide. (B) Transfection efficiency of 293T cells measured by detection of eBFP2 by flow cytometry (n=3). (C) BiTE specificity to GD2 measured by staining of CT26 and GD2.CT26 colon carcinoma cell lines with supernatant from transfected 293T cells and detection of binding measured with penta-his-AF647 antibody, followed by flow cytometric analysis.

7.2.3 Generation of murine CARs targeting GD2

To generate a GD2-specific chimeric antigen receptor, the GD2-specific scFvs from mAbs MuK666 and 14.18 were used (Nakamura et al., 2001, Gillies et al., 1989). A second-generation CAR construct which incorporates a CD8 stalk as the transmembrane domain and CD28-CD3 ζ costimulatory activation domain was used. Murinised CAR components were used to optimise function in mouse splenocytes and minimise immunogenicity. The C-terminal portion of murine CD34 is present upstream of the CAR as a marker gene to allow for *ex vivo* detection of CAR T-cells by flow cytometry or immunohistochemistry. To enable tracking of CAR T cells *in vivo*, a red-shifted firefly luciferase gene is incorporated downstream of the CAR construct, allowing non-invasive serial imaging by bioluminescence (BLI). The three genes are separated by two types of 2A peptide from: *Thosea asigna virus* (T2A) and *Equine rhinitis virus A* (E2A) (Szymczak et al., 2004). A total of four GD2-specific CAR constructs were made with and without firefly luciferase for both MuK666 and 14G2A scFvs (**Figure 7.4 A - B**). The incorporation of luciferase allows for study of homing to the tumour site and persistence of CAR T cells *in vivo*. However there is a risk that co-expression of luciferase in the CAR T cells might induce an anti-CAR T cell immune response and hence impair the *in vivo* persistence of these cells.

7.2.4 Functional testing of GD2-specific murine CARs *in vitro*

To produce CAR transduced T cells, murine splenocytes obtained from BALB/c mice were activated with Concanavalin A and IL-7 for 24 hours and subsequently transduced with ecotropic retroviral vector for stable CAR expression. Transduction efficiency was measured 5 days post transduction by detection of the CD34 marker gene by intracellular staining. In the single *in vitro* experiment performed, CAR transduction efficiency was poor, likely due to poor viral titre. Nevertheless, CD4⁺ and CD8⁺ T cells were transduced, with transduction efficiencies of 21.4% - 29.8% and 7.19% - 13.9% for CD4⁺ and CD8⁺ CAR T cells respectively (**Figure 7.4 C - G**).

To determine GD2-specific cytotoxicity of the CAR transduced T cells; the CT26 and GD2 expressing GD2.CT26 murine colon carcinoma cell lines of BALB/c background were used as targets (**Figure 7.5 A**). CD56 depleted T cells at 6 days

post-transduction and ^{51}Cr labelled target cells were co-cultured for 4 hours at E: T ratios: 32:1, 16:1, 8:1 and 4:1 in a chromium release assay. Both MuK666 and 14G2A based CAR T cells with or without luciferase co-expression demonstrated GD2 specificity by inducing cytotoxicity of GD2.CT26 cells and not CT26 cells. Non-transduced T cells did not have cytotoxicity against either cell line (**Figure 7.5 B - F**).

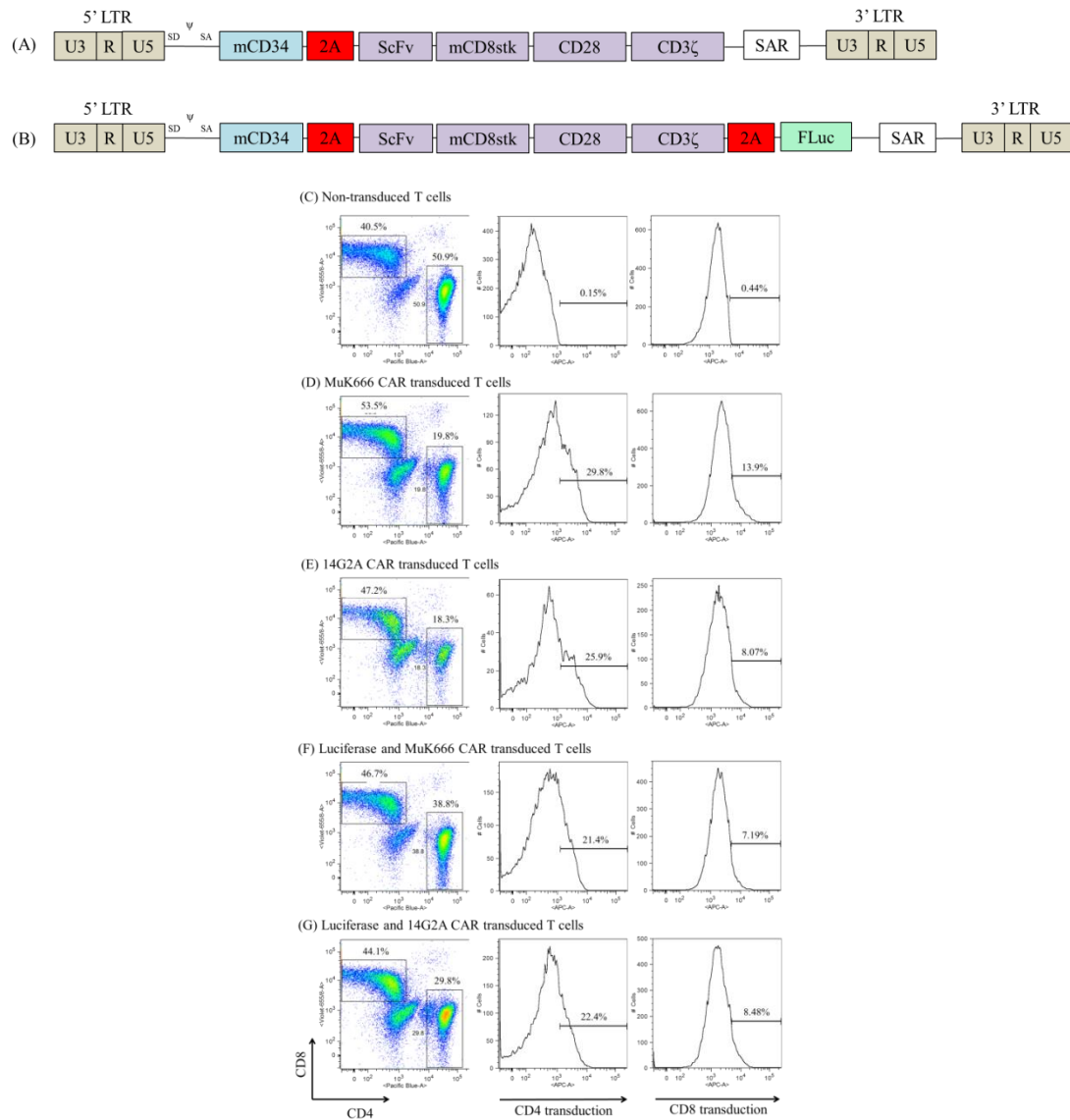


Figure 7.4: Murine CAR expression vectors and transduction efficiencies. (A) Structure of retroviral SFG vector for expression of murine CD34 marker gene and co-expression of second generation murine CAR in murine splenocytes. (B) Structure of retroviral SFG vector for expression of murine CD34 marker gene, co-expression of second generation murine CAR in murine T cells and a firefly luciferase (FLuc) for BLI studies. (C - G) Transduction of conA/IL-7 activated mouse splenocytes with constructs A and B containing either MuK666 or 14G2a GD2-specific scFvs. Shown is the proportion of CD4⁺/CD8⁺ T cells and CAR transduction efficiency measured by detection of CD34 by flow cytometry 6 days post transduction.

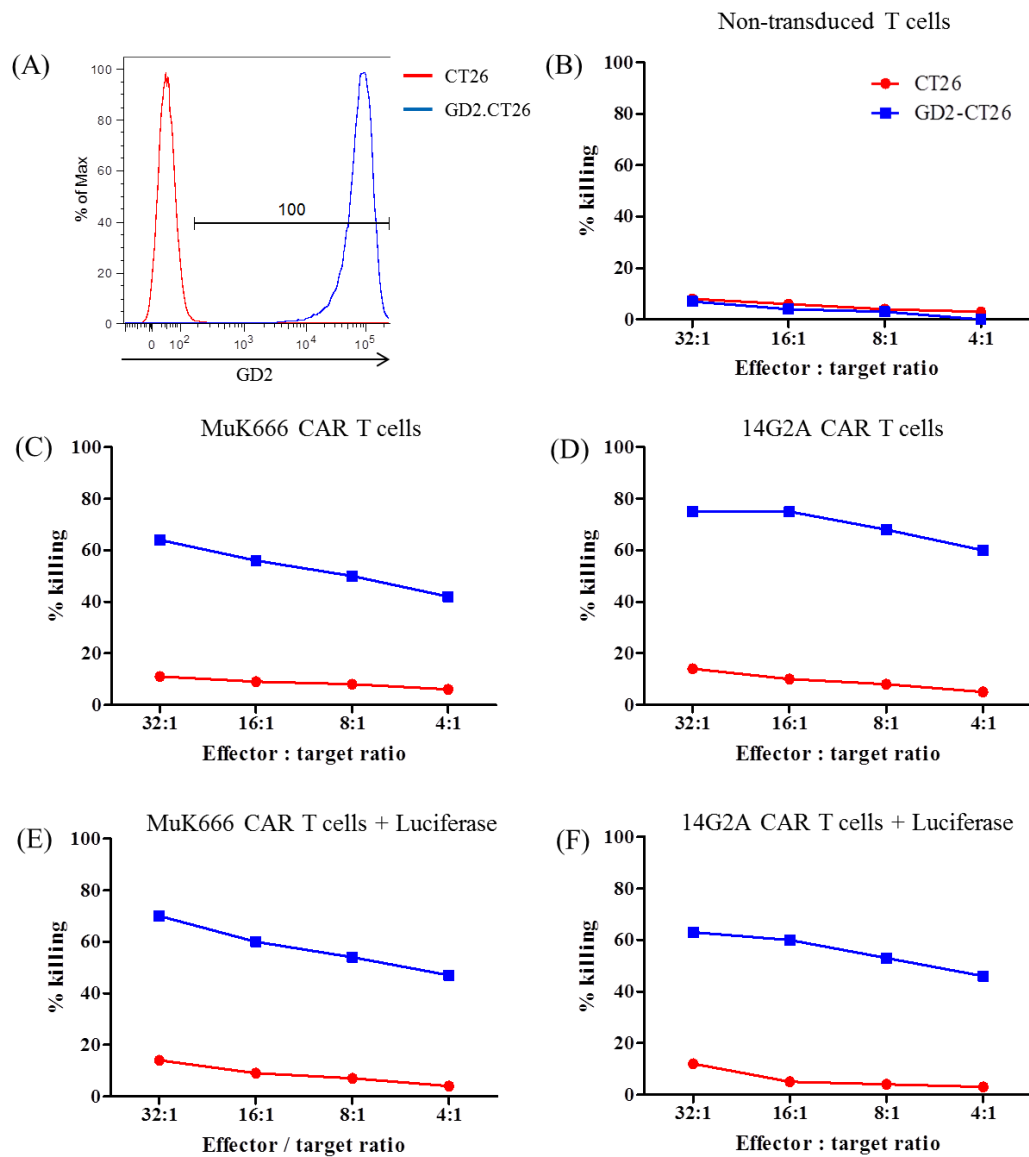


Figure 7.5: GD2-specific CAR T cells are cytotoxic to GD2.CT26 cells. (A) Measure of GD2 expression on CT26 and GD2.CT26 cell lines by flow cytometry with anti-GD2-PE antibody. **(B)** Non-transduced and MuK666 or 14G2a based CAR transduced T cell cytotoxicity to CT26 and GD2.CT26 target cells measured by percentage chromium release from target cells after 4 hours co-culture at E: T ratios 32:1, 16:1, 8:1 and 4:1 (n=1).

7.2.5 GD2-specific CAR T cells migrate to the tumour site *in vivo* in $ALK^{F1174L}/MYCN$ transgenic mice

After demonstrating GD2-specific CAR T cells were functional *in vitro*, CAR T cell migration and anti-tumour efficacy were tested *in vivo* using the $ALK^{F1174L}/MYCN$ transgenic neuroblastoma mouse model. The purpose of this experiment was to determine if luciferase could be reliably detected *in vivo* and if T cells appear to localise to the tumour site. For initial testing, a single CAR construct was selected. Splenocytes from mice with absence of $ALK^{F1174L}/MYCN$ mutations were transduced to express MuK666 specific CARs with co-expression of luciferase. Bulk transduction of both $CD4^+$ and $CD8^+$ T cells was measured as 51.4% (**Figure 7.6**).

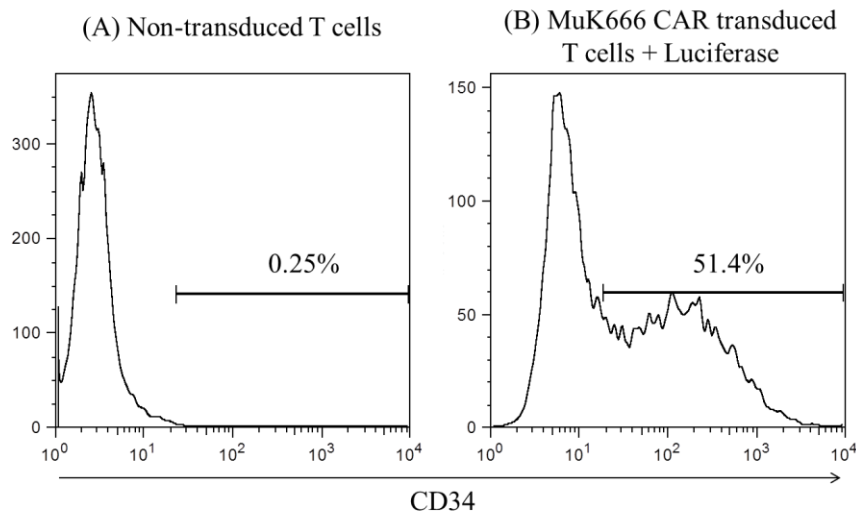


Figure 7.6: Expression of GD2-specific MuK666 CAR in transduced splenocytes. Mouse splenocytes were transduced to express MuK666-CAR 24 hours after activation with conA and IL-7. Transduction efficiency was measured by detection of the CD34 marker gene by flow cytometry in (A) non-transduced splenocytes and (B) muK666 CAR transduced splenocytes 6 days post transduction.

For this study, $ALK^{F1174L}/MYCN$ transgenic mice of age ~ 40 - 45 days were used, as tumours are detectable by palpation at this stage. One of the limitations of using the transgenic model is approximately a quarter of progeny from crossing ALK^{F1174L} heterozygous mice with $MYCN$ heterozygous mice are hemizygous for both oncogenes. For the first study, 4 mice from a cohort of 24 mice had the $ALK^{F1174L}/MYCN$ genotype, thus limiting the number of animals per experimental group. The experimental timeline for the *in vivo* model is shown in **Figure 7.7**. One mouse was used as a non-CAR T cell treated control (mouse 1), and 3 mice were injected with GD2-specific CAR-T cells (mouse 2 - 4).

All four mice aged between 40 - 43 days were palpated regularly to confirm the presence of tumour, 3/4 mice had detectable tumour masses (mouse 1, 2 and 4) in the abdominal region on day -1 of the experimental timeline, this was subsequently confirmed by MRI (**Figure 7.9**). The single mouse which did not have a detectable tumour was likely to develop a tumour at a later stage as the correct genotype was present. Mice in the CAR T cell treated group received 3.1Gy total body irradiation (TBI) and tail vein administration of 6×10^6 day 7 post-transduction bulk splenocytes.

CAR T cell migration was observed in all three CAR T cell treated mice by BLI after 1 day and 3 days CAR T cell administration. Signal localisation was seen in the cervical lymph nodes, spleen and abdominal region corresponding with the tumour location (**Figure 7.8 A - B**). After 7 and 14 days, an increased signal was detectable in the single mouse (mouse 3) which did not have an apparent tumour at the start of the experiment. A signal was also detected on days 21, 28 and 35 of BLI. Signal detection was decreased and subsequently lost in mouse 2 and 4 after day 7 BLI (**Figure 7.8 C - G**).

ALK^{F1174L}/MYCN
Transgenic mouse

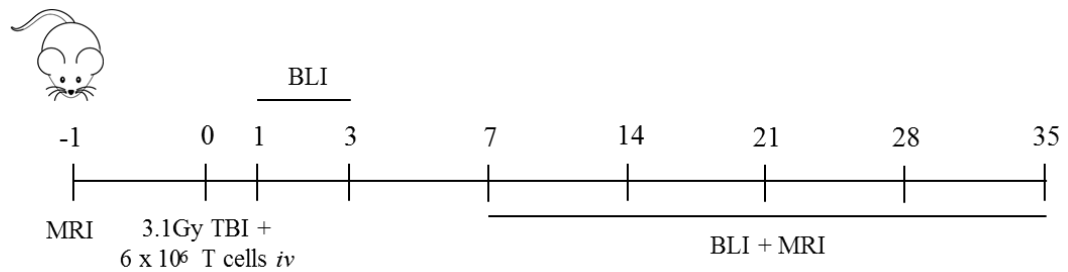


Figure 7.7: Experimental timeline for GD2-specific CAR T cell administration and monitoring. TBI: total body irradiation, BLI: bioluminescence imaging, MRI: magnetic resonance imaging.

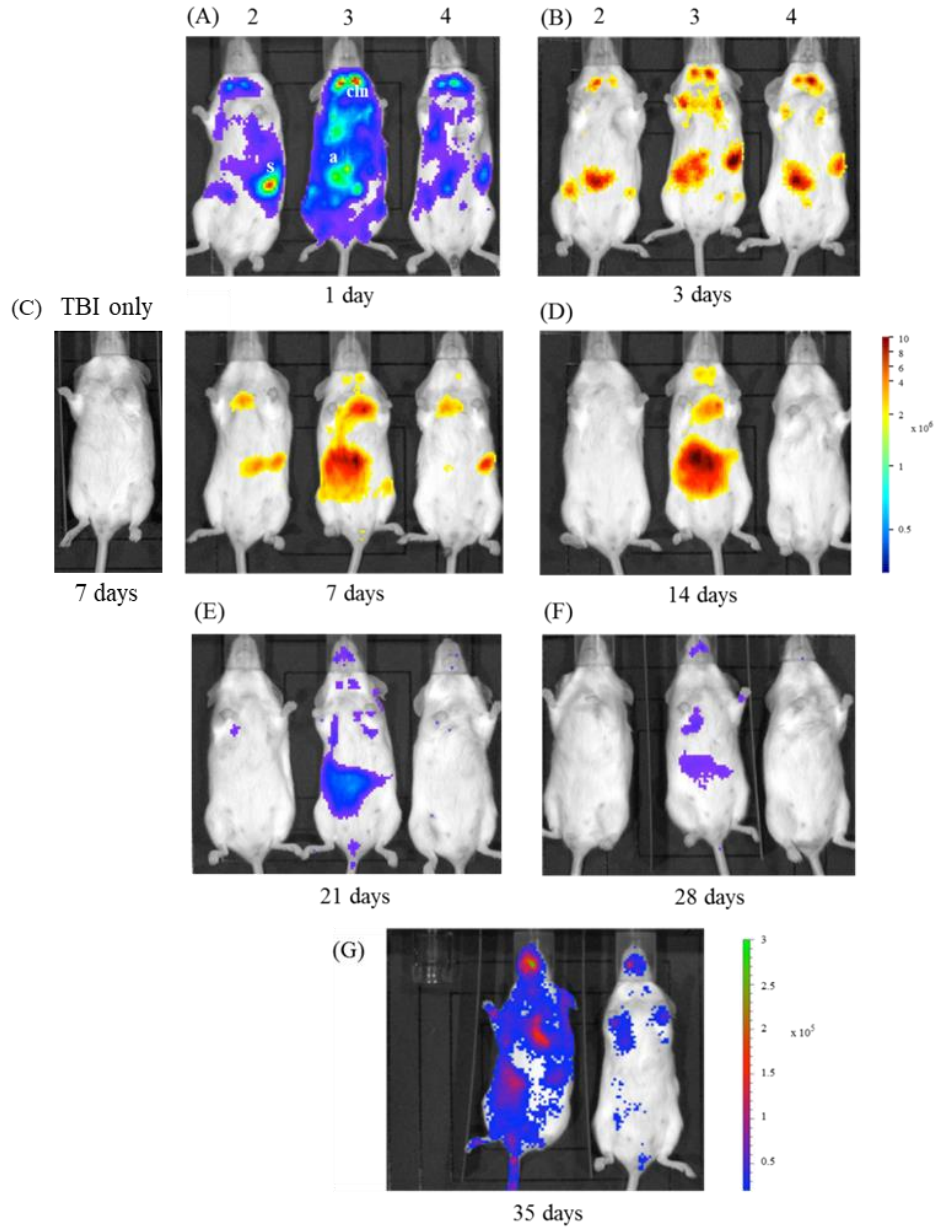


Figure 7.8: Bioluminescence imaging (BLI) of GD2-specific CAR T cell treated mice. *ALK^{F1174L}/MYCN* transgenic mice received 3.1Gy total body irradiation followed by administration of 6×10^6 bulk CAR transduced splenocytes which co-express luciferase. On days (A)1, (B) 3, (C) 7, (D) 14, (E) 21, (F) 28 and (F) 35 post CAR T cell administration, CAR T cell location was monitored by BLI. Mice were anesthetised with isoflurane and given 0.1ml (10mg/ml) Luciferin by intraperitoneal injection. Luminescence intensity was monitored using a PhotonIMAGER optical imaging system. Imaging of treated mice (mouse 2, 3 and 4) shown. TBI only treated control imaging shown for day 7.

7.2.6 Effect of GD2-specific CAR T cells on tumour growth *in vivo*

To determine the feasibility of using this model to evaluate efficacy of GD2-specific CAR T cells *in vivo*, mice were scanned weekly by MRI to monitor tumour size. In the mouse which only received TBI without CAR T cell administration, a reduction in tumour size was apparent after 3 days. This observation indicates that TBI itself has resulted in reduction of tumour size. However, an increased tumour mass was again apparent on MRI by day 14 indicating the TBI mediated effect on tumour growth was transient only (**Figure 7.9 A**).

In mice treated with GD2-specific CAR T cells, the tumour mass was undetectable after 7 days. This persisted at 14 days post CAR T cell infusion potentially demonstrating the elimination of the tumour mass by GD2-specific CAR T cells. A small tumour mass was again detectable on day 21 in both mouse 2 and 4. Tumours continued to increase in size in subsequent MRI scans. No tumour mass was detected in mouse 3 throughout the experiment (**Figure 7.9 B - D**).

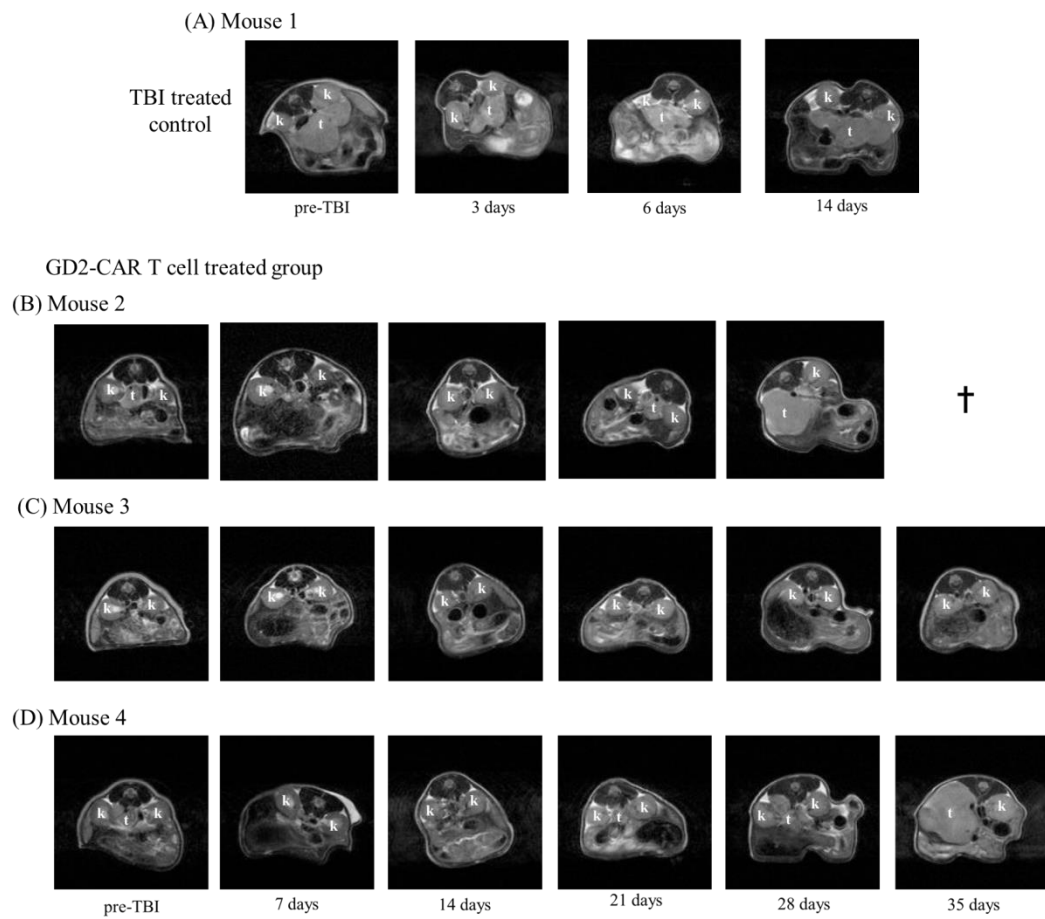


Figure 7.9: *In vivo* imaging of mice by MRI to monitor the effect of GD2-CAR T cell treatment on tumour growth. Abdominal tumour growth in $ALK^{F1174L}/MYCN$ mice monitored by MRI pre-TBI and post-CAR T cell administration. Images acquired using a T2-weighted sequence. (A) TBI treated control mouse (B-D) GD2-specific CAR T cell treated mice. K: kidney, t: tumour.

7.3 Discussion

This chapter has described the use of a transgenic mouse model for neuroblastoma as a potential model to test T cell based immunotherapies on solid tumours. The data presented here suggest that GD2-specific CAR T cells are able to migrate not only to the tumour site but to the spleen and cervical lymph nodes, leading to clearance of the solid tumour for approximately 2 weeks. Tumours reoccurred in 2/3 mice treated with CAR T cells and is likely to be due to lack of persistence of the CAR T cells *in vivo*, indicated by loss of BLI signal. Now that an initial experiment has demonstrated the potential of using the $ALK^{F1174L}/MYCN$ transgenic mouse model to test T cell immunotherapeutic strategies, further experiments can be set up to study the efficacy of CAR T cell and BiTE treatment strategies.

Firstly, larger cohorts of mice will be required to reliably compare treated and non-treated groups. Secondly, relevant controls will help determine the specific effect of a T cell therapy. Use of a non-specific control CAR will determine if T cell migration and tumour size reduction are specific to recognition of GD2 on the tumour surface.

For the development of murine BiTEs, we were unable to produce BiTEs for *in vivo* functional testing. It is likely that optimisation of the BiTE format will be required. This includes scFv $V_H - V_L$ orientation and scFv - linker combinations which may impact protein stability and production.

CHAPTER 8:
DISCUSSION

Final discussion and future directions

There remains an unmet need for therapies that achieve durable disease responses in high-risk neuroblastoma. Current treatment with multi-modal therapies including chemotherapy, radiotherapy and immunotherapy with GD2-specific mAbs are effective but are often followed by relapse of disease. These therapies are frequently associated with dose limiting toxicities which compromise efficacy. To overcome these limitations and achieve a durable disease response, the aim of this study was to investigate the cytolytic activity of T cells through BiTE and CAR T cell mediated immunotherapy of neuroblastoma. Both approaches have demonstrated promise in the treatment of haematological malignancies (Topp et al., 2014, Maude et al., 2014). Based on differences in the individual therapeutic approach, BiTE and CAR T cell therapies hold a unique set of advantages, which may be beneficial for targeting a particular disease setting. Advantages and disadvantages of BiTE and CAR T cell therapies are discussed in chapter 1, section 1.3.2.3.

We explored GD2 as a target for BiTE mediated immunotherapy based on the high level of GD2 expression on neuroblastoma. An advantage of targeting GD2 with BiTE therapy is its short half-life; in the event of treatment related toxicities caused by on-target off-tumour targeting of GD2, the BiTE can readily be titrated (Nagorsen et al., 2012). In our study, we explored the optimal design of a GD2/CD3 BiTE. Our data has demonstrated that careful selection of scFv and linker components in the BiTE design are important to achieve optimal killing of GD2⁺ cells by T cells at low BiTE concentrations.

In a second strategy, we explored *O*AcGD2 as a novel target for T cell therapy of neuroblastoma. *O*AcGD2 has a highly tumour specific expression pattern and may therefore be particularly suitable for targeting with CAR T cells which aims to induce a persistent anti-tumour response and hence any toxicity may be long lasting. In our study we have demonstrated that that a CAR can be generated which specifically targets the *O* acetylated form of GD2 and thus provides an approach which can

potentially avoid on-target off-tumour toxicities associated with the targeting of the GD2 antigen.

Finally, as a pre-clinical approach to develop BiTE and CAR therapy *in vivo*, we were able to demonstrate that the $ALK^{F1174L}/MYCN$ transgenic mouse model for neuroblastoma is a suitable model to test T cell based therapies (Berry et al., 2012).

8.1 Target validation of neuroblastoma antigens

The choice of target antigen is a crucial feature of T cell therapy: ideally the target antigen should be abundantly expressed on the tumour surface with limited or absence of expression on healthy tissues (Cheever et al., 2009). At the onset of this study (chapter 3), we set up an approach to validate the expression of neuroblastoma specific antigens GD2, OAcGD2 and ALK on our available range of neuroblastoma cell lines and primary cells lines by flow cytometry.

GD2 as a therapeutic target in neuroblastoma

We found that GD2 was abundantly and homogeneously expressed on 3/4 neuroblastoma cell lines tested with an average of approx. 5×10^5 - 1×10^6 molecules per cell. We also demonstrated that 10/10 primary cell lines tested had a high level of GD2 expression. This is in line with previous reports which have shown the abundant expression of GD2 across neuroblastoma tumours and other malignancies (Wu et al., 1986, Cheresch et al., 1986, Chang et al., 1992, Lammie et al., 1993, Kramer et al., 1998, Kailayangiri et al., 2012). In normal tissue, the expression of GD2 is restricted to the CNS, peripheral nerve fibres and skin melanocytes (Lammie et al., 1993, Svennerholm et al., 1994, Yuki et al., 1997).

A limitation to our approach was not investigating antigen expression on healthy tissues confirming absence or low level expression. This step is a necessary part of the target validation approach as it confirms the tumour specific nature of the antigen. Normally, antigen expression on tumour samples and healthy tissues is studied by immunohistochemistry on a broad range of fixed tissues. However, specific detection of GD2 by immunohistochemistry is routinely performed using fresh frozen tissue

samples as fixation masks the GD2 epitopes recognised by standard GD2-specific mAbs like 14G2a (Sariola et al., 1991, Alvarez-Rueda et al., 2011).

To address this issue, we have started to study at GD2 expression of frozen cell lines by immunohistochemistry and are building this approach to study antigen expression on fresh tissue samples. Another approach is to use a GD2-specific antibody which is able to detect GD2 on fixed tissue, such as mAb 126 (Schulz et al., 1984).

A further consideration for the selection of a tumour antigen is the maintenance of antigen expression on the tumour surface after therapy. Loss of antigen expression can result in lack of response to a targeted therapy and promote tumour escape and relapse. Loss of GD2 expression on tumour cells after mAb therapy has been reported as a rare event (Kramer et al., 1998, Schumacher-Kuckelkorn et al., 2005). A recent study by Schumacher-Kuckelkorn *et al.* demonstrated that loss of GD2 expression on neuroblastoma cells was in fact underestimated. The study analysed GD2 expression in 474 new or recurrent stage 4 and 4S neuroblastoma cases with bone marrow metastasis by immunostaining. The study found absence of GD2 staining on neuroblastoma cells in bone marrow in a total of 57 cases (12%). 37/474 patients were negative at initial diagnosis, 9/474 during chemotherapy and 11/474 at recurrence (Schumacher-Kuckelkorn et al., 2017). This ultimately has both diagnostic and therapeutic consequences and may require careful monitoring of patients undergoing GD2-directed therapy.

OAcGD2 as a therapeutic target in neuroblastoma

A major limitation of mAb therapy for GD2⁺ tumours is the pain syndrome associated with targeting GD2 on peripheral nerve fibres (Yuki et al., 1997). As a novel therapeutic target with a reported tumour restricted expression pattern, OAcGD2 may be a better target antigen for immunotherapy than GD2 (Alvarez-Rueda et al., 2011). For this reason, we determined OAcGD2 expression alongside GD2 on our neuroblastoma cell lines. Based on our findings, the amount of OAcGD2 molecules present at the cell surface were comparable though lower to that of the GD2 epitope, similar to that reported by others (Kaneko et al., 2010, Alvarez-Rueda et al., 2011).

There were approx. 8×10^4 - 1.5×10^5 OAcGD2 molecules across neuroblastoma cell lines, corresponding to a tenth to a third of GD2 molecules carrying O-acetylation. All 10/10 primary cell lines tested were also positive for OAcGD2 expression.

ALK as a therapeutic target in neuroblastoma

ALK expression was detectable at a low level on 4/4 neuroblastoma cell lines tested with approx. 800 - 5000 molecules per cell while expression was detectable on 2/10 primary neuroblastoma samples tested. One explanation may be that ALK aberrations are reportedly found in 14% (10% mutation, 4% amplification) of high risk neuroblastoma patients (Bresler, 2014), and due to our small sample size, most of our samples did not appear to have ALK mutation or amplification..

Despite the low level of ALK expression on neuroblastoma cells, ALK may still be a suitable target for CAR T cell therapy. CD22 is being explored as a promising target for CAR T cell therapy in haematological malignancies. The median density of CD22 in ALL blasts is 3500 molecules per cell (Haso et al., 2013, Ginaldi et al., 1998) which is in a similar range as ALK. Targeting a low-density antigen will require careful consideration of choice of scFv used to construct the CAR as highlighted in a recent study by Walker *et al.* which explored the potential of targeting ALK using a second generation 41BB-CD3 ζ CAR. The study demonstrated that production of cytokines (such as IL-2, TNF- α and IFN- γ) by ALK CAR T cells was highly dependent on ALK target density. The density of ALK on neuroblastoma cell lines was also insufficient for maximal activation of CAR T cells. In addition, ALK CAR mediated cytotoxicity was regulated by both target antigen and CAR density: low expression of both resulted in limited anti-tumour efficacy of the ALK CAR (Walker et al., 2017). Finally, a detailed study of ALK expression on normal tissues is required to predict any on-target off-tumour toxicities of targeting ALK with CAR T cell therapy.

8.2 Development of GD2/CD3 specific BiTEs

In this study GD2 was selected as the target antigen for the development of a BiTE directed therapy for neuroblastoma. In chapters 4 and 5 we undertook a systematic evaluation of the different components incorporated in the design of a BiTE and considered features from the CD19xCD3 BiTE blinatumomab (Dreier et al., 2002, Nagorsen et al., 2012). We successfully generated a series of BiTE constructs which combined (1) two different humanised GD2-specific scFvs, with (2) three different sized linkers and (3) three different humanised CD3-specific scFvs as described in chapter 4, table 4.1.

Firstly, we demonstrated the successful production and purification of 14 BiTE variants. The production yield of individual variants correlated with the thermal stability of the scFv components within the BiTE. Next, we demonstrated that all variants retained binding specificity to GD2 and CD3 antigens on GD2⁺ or CD3⁺ cell lines, with absence of binding to GD2⁻ and CD3⁻ cell lines. Based on production yield, 11 BiTE variants (excluding BiTEs containing huOKT3 and BiTE K6-H-U) were functionally compared *in vitro*. Step-by-step comparisons were performed to determine the optimal format required to achieve T cell mediated tumour cell lysis response at the lowest BiTE concentration.

Selection of an optimal GD2 specific scFv in the BiTE design

Firstly, to determine the optimal GD2-specific scFv we compared identical BiTE formats with either hu14.18 or huK666 scFvs in a dose response assay. T cells were co-cultured with (GD2⁺) GD2.SupT1 cells or (GD2⁻) SupT1 target cells in the presence of increasing concentrations of BiTE. We demonstrated that BiTEs containing a hu14.18 scFv were able to redirect T cells to lyse GD2.SupT1 cells at a lower concentration in comparison to BiTEs containing a huK666 scFv. Hu14.18-scFv based BiTEs typically had EC₅₀ values less than 263 pM while, huK666-based BiTEs had EC₅₀ values > 500 pM. The improved targeting is likely correlated with affinity of the scFvs to GD2; the 14.18 mAb has a higher affinity to GD2 compared to huK666 (Mujoo et al., 1987, Nakamura et al., 2001).

Other studies have also demonstrated the impact of mAb or bsAb binding affinity on tumour cell killing. Cheng *et al.* tested the importance of structural design on the potency of GD2/CD3 specific BiTEs. The study used several different BiTE constructs with an affinity matured GD2-specific scFv from mAb clone 5F11 and a huOKT3 scFv as the CD3 binder. The study found that the BiTE format containing a disulphide bond stabilised 5F11 scFv ($V_H - V_L$ orientation) and a $(G_4S)_3$ linker had the highest binding affinity to GD2 and was the most efficient at redirecting T cell cytotoxicity to GD2⁺ tumour cells (Cheng et al., 2015). In a follow up study, 5F11 was substituted with the hu3F8 scFv which had a 13-fold higher affinity for GD2. This modification enabled a 5,000-fold higher potency (of femtomolar EC₅₀) compared with the 5F11 BiTE (of picomolar EC₅₀) (Cheng et al., 2016).

This data as well as ours demonstrate the impact of BiTE binding affinity to the GD2 tumour antigen. Other factors that can contribute to enhanced potency include the location of the epitope recognised by the scFv and the distance of the epitope to the target cell membrane (Bluemel, 2010). A suitable additional control for the co-culture assays, which was not included in our study, was a non-specific BiTE control such as a CD19/CD3-targeted BiTE. This would have further confirmed the specific response of the GD2/CD3 specific BiTE and will be considered in future studies.

Selection of an optimal linker in the BiTE design

We subsequently compared the impact of linker size between the GD2 and CD3-specific scFvs. Hu14.18 scFv-based BiTEs containing the medium hinge and longer CD8 stalk linkers had significantly lower EC₅₀ values compared to BiTEs containing shorter $(G_4S)_3$ linkers ($p < 0.01$). This data supports our hypothesis that a longer linker may facilitate improved immunological synapse formation in the context of targeting GD2. However, factors including linker sequence and flexibility were not taken into account and could have influenced the rotation between the two scFv arms in the BiTE format. The optimal linker length depends on the target antigen size and choice of epitope. There are few studies that describe the impact of linker length in the BiTE design (Bluemel, 2010, Cheng et al., 2015). Studies of linker/spacer size in CAR designs have shown that the choice of linker is target dependent and modifying this

region is likely to significantly impact the receptor stability and substrate binding affinity depending on the location of the target epitope (Bridgeman et al., 2010, Hudecek et al., 2013).

The hu14.18 scFv-based BiTEs with the lowest EC₅₀ values (BiTE: EC₅₀, 14-H-U: 20.69, 14-H-Y: 94.83, 14-C-U: 62.33, 14-C-Y: 55.33) were further compared in their ability to activate T cells and induce T cell proliferation. All four BiTE formats were able to stimulate cytokine production from T cells in the presence of GD2⁺ neuroblastoma target cell lines (Lan-1, SKNDZ and IMR32), however significant differences in cytokine production were not seen between BiTEs containing the individual hinge and CD8 stalk linkers.

Selection of an optimal CD3-specific scFv in the BiTE design

One of the desirable features of a CD3-specific scFv in a BiTE format is a weak binding affinity to CD3. This is because the upper limit of TCR affinity correlates to a low dissociation constant of around 1 - 50 μ M (van der Merwe and Davis, 2003, Cole et al., 2007). The affinity of the TCR influences the sensitivity and activation of T cells. Bortoletto *et al.* mutated a CD3 specific scFv (clone TR66) to generate variants that bind to CD3 with higher and lower affinities in comparison to the wild type scFv. The scFv was part of a bispecific antibody with specificity to the tumour associated epithelial cell adhesion molecule (EpCAM). The study showed that a mutant with an increased binding affinity to CD3 showed a lower capacity to target T cells against EpCAM⁺ tumour cells. In contrast, mutants with decreased binding to CD3 efficiently triggered T cell activation and cytotoxicity (Bortoletto et al., 2002). In addition, a low affinity CD3-specific scFv (clone L2K) in the CD19/CD3 specific BiTE blinatumomab mediates the potent activation of T cells at low BiTE concentrations (Dreier et al., 2003). For this reason, CD3-specific scFvs were carefully selected in our study based on 1) low binding affinity and/or 2) previous use in a BiTE antibody format.

GD2/CD3 specific BiTEs containing scFvs huUCHT1 and huYTH demonstrated a similar ability to redirect T cells to lyse GD2.SupT1 cells in co-culture assays. A

superior production of cytokines IL-2, IFN- γ and TNF α by T cells when co-cultured with either Lan-1 or SKNDZ cells in the presence of BiTE 14-H-Y was seen. This cytokine profile is indicative of a Th1 T cell phenotype. It is likely that differences in binding affinity between huUCHT1 and huYTH scFvs may explain the differential activation and proliferation of T cells (Bortoletto et al., 2002).

We were unable to measure the affinity of the CD3-specific scFvs in the BiTE variants due to an insufficient yield of BiTE from our 293T expression system. The affinity of an antibody or scFv for a surface antigen can be determined by performing saturation binding studies. One approach is to label cells expressing the antigen of interest with a range of incrementing antibody concentrations to reach saturation. The level of antibody binding to target cells can be measured by flow cytometry. The MFI values obtained can subsequently be used to determine binding affinity by Scatchard analysis. Scatchard analysis is a method of linearising data from a saturation binding experiment. One creates a secondary plot of specific binding/free ligand concentration (y-axis) vs. specific binding (x-axis). The slope of this line equals $-1/K_D$.

In our attempt to identify the optimal GD2/CD3 specific BiTE format we have shown that the different components in the BiTE design can influence a multitude of factors including T cell activation, T cell proliferation and target cell death. Our approach has demonstrated that it is necessary to screen different scFvs and linkers to identify the optimal BiTE design.

An approach to study BiTE pharmacokinetics in vivo

To further characterise the optimal GD2/CD3 specific BiTE, *in vivo* studies in a xenograft mouse model will help determine the pharmacokinetic properties of the individual BiTE variants. A number of studies have reported the use of xenograft mouse models to test the efficacy of BiTEs *in vivo*. In this model tumour cells positive for the antigen of interest can be implanted subcutaneously, followed by injection of human T cells intravenously after a few days. Intravenous administration of BiTE is then performed daily and tumour growth assessed once a week

(Brischwein et al., 2006, Herrmann et al., 2010, Lutterbuese et al., 2010, Feldmann et al., 2012). An advantage of the xenograft mouse model is the humanised BiTE constructs can be tested *in vivo* without creating an immunogenic response. In addition, reactivity of human T cells against a patient derived neuroblastoma cell line can be measured *in vivo*.

A limitation of the xenograft mouse model is the artificial system is not truly representative of the conditions a BiTE may encounter in a patient with neuroblastoma. The immunosuppressive tumour microenvironment which can efficiently down regulate a T cell response (described in chapter 1, section 1.2.5) will not be assessed in this model. To overcome these limitations, *in vivo* BiTE pharmacokinetic studies can be performed in an immunocompetent mouse model. This model would require the BiTE to be in a murine format to avoid immunogenicity. Our approach to the use of a mouse model for neuroblastoma is further described in section 8.4.

8.3 Novel targeting of *O*AcGD2 with CAR T cells

In an attempt to reduce the on-target off-tumour toxicities associated with targeting of GD2 on peripheral nerves, we explored *O*AcGD2 as a novel antigen to target with T cell based immunotherapy in chapter 6. As *O*AcGD2 has a highly tumour specific expression pattern we hypothesised *O*AcGD2 may be a suitable target for CAR T therapy. Our study demonstrated that *O*AcGD2 specific CAR T cells had selective specificity to *O*AcGD2 and released IFN- γ after co-culture with *O*AcGD2⁺ cell lines, indicating T cell activation. As our experiments were performed once, we are unable to draw final conclusions.

Recently, the sialate O-acetyl transferase CASD1 was identified as the enzyme responsible for *O*-acetylation of sialic acid side chains (Baumann et al., 2015). In future work, the generation of CASD1 knock out cell lines to create *O*AcGD2⁻ cell lines will allow more in depth studies of the *O*AcGD2 specificity of this CAR.

8.4 T cell therapy for solid tumours

As the majority of clinical successes for BiTEs and CARs have been reported for haematological malignancies, it is difficult to directly translate these therapeutic approaches to the treatment of solid tumours. Disappointingly, the clinical outcomes of T cell therapy in solid tumours have not matched pre-clinical results (Kershaw et al., 2006, Huang and Yang, 2016). The three main limitations of targeting solid tumours include 1) the identification of tumour specific antigens, 2) the limited trafficking of adoptively transferred T cells to the tumour site (Kershaw et al., 2006, Ahmed et al., 2015) and 3) the immunosuppressive effect of the tumour microenvironment (Moon et al., 2014).

In chapter 7, we described the use of an immunocompetent transgenic mouse model for neuroblastoma to test a GD2-specific CAR T cell therapy. In the single experiment described we observed that CAR T cells appeared to home to the tumour site and in some of the mice, transient reduction of tumour size was seen. These results suggest the model may be suitable to test BiTE and CAR T cell therapy approaches *in vivo*. In addition, unlike a xenograft mouse model, the advantage of this model is the potential to study the interaction of T cells with the complex and heterogeneous tumour microenvironment. This model can help us improve current approaches which are being developed for the treatment of neuroblastoma.

There are a number of strategies being tested to overcome the limitations of targeting solid tumours with T cell therapies. Some strategies involve targeting the tumour microenvironment in combination with CAR T cell therapy and other approaches aim to optimise the CAR design to improve T cell persistence. Studies on BiTEs in solid tumours exist but are limited in comparison to CAR studies (Fiedler et al., 2012, De Vries et al., 2015). In addition to the therapeutic approach, key considerations in T cell therapy include the choice of target antigen and antigen expression levels. To determine the optimal therapeutic approach for neuroblastoma, we need to learn more about the neuroblastoma tumour microenvironment and explore methods to overcome current limitations to neuroblastoma immunotherapy.

Metabolic stress in the tumour microenvironment is able to modulate T cell metabolism, differentiation and effector functions (Zea et al., 2004, Rodriguez et al., 2007). Kawalekar *et al.* demonstrated the impact of choosing an appropriate co-stimulatory domain in a CAR design on the persistence of CAR T cells. The study demonstrated that CAR T cells with different co-stimulatory domains utilise distinct metabolic pathways which in turn reflect the variable persistence within the tumour microenvironment. CAR T cells with 4-1BB domains utilised a different metabolic pathway to CAR T cells with CD28 domains and had a central memory phenotype. This led to a survival advantage in comparison to CAR T cells with CD28 domains that had an effector memory phenotype. (Kawalekar et al., 2016). Other studies have also demonstrated the impact of costimulatory domain on CAR T cell persistence (Long et al., 2015, Prapa et al., 2015).

A potential option for combination therapy is to induce the local release of stimulatory factors that promote an anti-tumour immune response. Koneru *et al.* designed CAR T cells combining IL-12 secretion with CAR expression. IL-12 is an inflammatory cytokine that is able to improve T cell activation and effector function (Kilinc et al., 2006). The CAR T cells combined with IL-12 were able to completely eradicate an orthotopic ovarian tumour-graft model and showed prolonged persistence of CAR T cells (Koneru et al., 2015).

Combination therapies like this can potentially be tested in our immunocompetent mouse model for neuroblastoma. The model can be used to assess the ability of T cells to mount an anti-tumour response and persist *in vivo*. A major side effect of T cell therapy is cytokine release syndrome (CRS), which is the most common severe toxicity seen after treatment of patients with BiTE or CAR therapy. CRS is characterised by a systemic inflammatory response, marked by the increase of pro-inflammatory cytokines such as IL-2, IFN- γ , IL-6 and IL-10 and is likely to be more pronounced in combination therapies. Thus, it is important that improved therapeutic approaches are balanced and combine novel targeting strategies with minimal toxic side effects.

8.5 Final conclusions

In this study, we have developed and tested a panel of GD2/CD3 targeted BiTEs using an empirical approach to BiTE design. Our work demonstrated that the optimal format of BiTE required to redirect T cell cytotoxicity to GD2⁺ tumour cells required careful selection and testing of different GD2- and CD3-specific scFvs and different linker lengths. We have also shown that the different components of BiTEs heavily influenced BiTE production, yield, stability and binding to target cells. In particular, the choice of CD3-specific scFv in the BiTE design can impact T cell proliferation and the production of cytokines, a key requirement of a T cell therapy. We showed that development of the most effective BiTE for a given antigen required a careful combination of multiple elements and that that the optimal design will likely differ for different antigens.

We also explored the novel antigen *OAcGD2* as a target for CAR therapy, based on its tumour restricted expression pattern. Our study demonstrated that an *OAcGD2*-specific CAR induced highly specific activity against *OAcGD2*⁺ cells. This approach for directing T cell activity via the CAR to *OAcGD2* on tumours had great potential to avoid or limit on-target off-tumour toxicities and hence development of *OAcGD2* CAR T cell therapy merits further development. Lastly, we have demonstrated the potential of using an immunocompetent mouse model which developed neuroblastoma as a suitable model to develop and test T cell-based therapies *in vivo*. We anticipate that this model will further our understanding of the interplay between T cells, tumour cells and the tumour microenvironment in neuroblastoma. Data from studies performed in this model including studies in different disease setting (bulky disease vs minimal residual disease, combination approaches of T-cell therapies with other (immunotherapeutic) agents) can inform the field of BiTE and CAR T cell therapy for neuroblastoma. BiTE and CAR T cell therapies are rapidly advancing fields in cancer immunotherapy. We have used these two technologies and focused on targeting GD2 and *OAcGD2* in neuroblastoma and have identified new opportunities to drive forward the search and clinical development of novel and more effective therapies for neuroblastoma.

REFERENCES

- ADAIR, J. R., ATHWAL, D. S., BODMER, M. W., BRIGHT, S. M., COLLINS, A. M., PULITO, V. L., RAO, P. E., REEDMAN, R., ROTHERMEL, A. L., XU, D. & ET AL. 1994. Humanization of the murine anti-human CD3 monoclonal antibody OKT3. *Hum Antibodies Hybridomas*, 5, 41-7.
- AHMED, M. & CHEUNG, N. K. 2014. Engineering anti-GD2 monoclonal antibodies for cancer immunotherapy. *FEBS Lett*, 588, 288-97.
- AHMED, N., BRAWLEY, V. S., HEGDE, M., ROBERTSON, C., GHAZI, A., GERKEN, C., LIU, E., DAKHOVA, O., ASHOORI, A., CORDER, A., GRAY, T., WU, M. F., LIU, H., HICKS, J., RAINUSSO, N., DOTTI, G., MEI, Z., GRILLEY, B., GEE, A., ROONEY, C. M., BRENNER, M. K., HESLOP, H. E., WELS, W. S., WANG, L. L., ANDERSON, P. & GOTTSCHALK, S. 2015. Human Epidermal Growth Factor Receptor 2 (HER2) -Specific Chimeric Antigen Receptor-Modified T Cells for the Immunotherapy of HER2-Positive Sarcoma. *J Clin Oncol*, 33, 1688-96.
- AI, H. W., SHANER, N. C., CHENG, Z., TSIEN, R. Y. & CAMPBELL, R. E. 2007. Exploration of new chromophore structures leads to the identification of improved blue fluorescent proteins. *Biochemistry*, 46, 5904-10.
- AIFANTIS, I., RAETZ, E. & BUONAMICI, S. 2008. Molecular pathogenesis of T-cell leukaemia and lymphoma. *Nat Rev Immunol*, 8, 380-90.
- ALEGRE, M. L., TSO, J. Y., SATTAR, H. A., SMITH, J., DESALLE, F., COLE, M. & BLUESTONE, J. A. 1995. An anti-murine CD3 monoclonal antibody with a low affinity for Fc gamma receptors suppresses transplantation responses while minimizing acute toxicity and immunogenicity. *J Immunol*, 155, 1544-55.

- ALTAN, M., PELEKANOU, V., SCHALPER, K. A., TOKI, M., GAULE, P., SYRIGOS, K., HERBST, R. S. & RIMM, D. L. 2017. B7-H3 Expression in NSCLC and Its Association with B7-H4, PD-L1 and Tumor-Infiltrating Lymphocytes. *Clin Cancer Res.*
- ALVAREZ-RUEDA, N., DESSELLE, A., COCHONNEAU, D., CHAUMETTE, T., CLEMENCEAU, B., LEPRIEUR, S., BOUGRAS, G., SUPIOT, S., MUSSINI, J. M., BARBET, J., SABA, J., PARIS, F., AUBRY, J. & BIRKLE, S. 2011. A monoclonal antibody to O-acetyl-GD2 ganglioside and not to GD2 shows potent anti-tumor activity without peripheral nervous system cross-reactivity. *PLoS One*, 6, e25220.
- ALVAREZ-RUEDA, N., LEPRIEUR, S., CLEMENCEAU, B., SUPIOT, S., SEBILLE-RIVAIN, V., FAIVRE-CHAUVET, A., DAVODEAU, F., PARIS, F., BARBET, J., AUBRY, J. & BIRKLE, S. 2007. Binding activities and antitumor properties of a new mouse/human chimeric antibody specific for GD2 ganglioside antigen. *Clin Cancer Res*, 13, 5613s-5620s.
- ARAUJO, H., MENEZES, M. & MENDEZ-OTERO, R. 1997. Blockage of 9-O-acetyl gangliosides induces microtubule depolymerization in growth cones and neurites. *Eur J Cell Biol*, 72, 202-13.
- ARGOS, P. 1990. An investigation of oligopeptides linking domains in protein tertiary structures and possible candidates for general gene fusion. *J Mol Biol*, 211, 943-58.
- ARMING, S., WIPFLER, D., MAYR, J., MERLING, A., VILAS, U., SCHAUER, R., SCHWARTZ-ALBIEZ, R. & VLASAK, R. 2011. The human Cas1 protein: a sialic acid-specific O-acetyltransferase? *Glycobiology*, 21, 553-64.

- ARNETT, K. L., HARRISON, S. C. & WILEY, D. C. 2004. Crystal structure of a human CD3-epsilon/delta dimer in complex with a UCHT1 single-chain antibody fragment. *Proc Natl Acad Sci U S A*, 101, 16268-73.
- BANERJEE, S. A., HOPPE, P., BRILLIANT, M. & CHIKARAISHI, D. M. 1992. 5' flanking sequences of the rat tyrosine hydroxylase gene target accurate tissue-specific, developmental, and transsynaptic expression in transgenic mice. *J Neurosci*, 12, 4460-7.
- BAUMANN, A. M., BAKKERS, M. J., BUETTNER, F. F., HARTMANN, M., GROVE, M., LANGEREIS, M. A., DE GROOT, R. J. & MUHLENHOFF, M. 2015. 9-O-Acetylation of sialic acids is catalysed by CASD1 via a covalent acetyl-enzyme intermediate. *Nat Commun*, 6, 7673.
- BEATTY, G. L. & MOON, E. K. 2014. Chimeric antigen receptor T cells are vulnerable to immunosuppressive mechanisms present within the tumor microenvironment. *Oncoimmunology*, 3, e970027.
- BERG, L. J., FINKELSTEIN, L. D., LUCAS, J. A. & SCHWARTZBERG, P. L. 2005. Tec family kinases in T lymphocyte development and function. *Annu Rev Immunol*, 23, 549-600.
- BERRY, T., LUTHER, W., BHATNAGAR, N., JAMIN, Y., POON, E., SANDA, T., PEI, D., SHARMA, B., VETHAROY, W. R., HALLSWORTH, A., AHMAD, Z., BARKER, K., MOREAU, L., WEBBER, H., WANG, W., LIU, Q., PEREZ-ATAYDE, A., RODIG, S., CHEUNG, N. K., RAYNAUD, F., HALLBERG, B., ROBINSON, S. P., GRAY, N. S., PEARSON, A. D., ECCLES, S. A., CHESLER, L. & GEORGE, R. E. 2012. The ALK(F1174L) mutation potentiates the oncogenic activity of MYCN in neuroblastoma. *Cancer Cell*, 22, 117-30.

- BEVERLEY, P. C. & CALLARD, R. E. 1981. Distinctive functional characteristics of human "T" lymphocytes defined by E rosetting or a monoclonal anti-T cell antibody. *Eur J Immunol*, 11, 329-34.
- BIEDLER, J. L., HELSON, L. & SPENGLER, B. A. 1973. Morphology and growth, tumorigenicity, and cytogenetics of human neuroblastoma cells in continuous culture. *Cancer Res*, 33, 2643-52.
- BLUEMEL, C., HAUSMANN, S., FLUHR, P., SRISKANDARAJAH, M., STALLCUP, W.B., KUFER, B.P. 2010. Epitope distance to the target cell membrane and antigen size determine the potency of T cell-mediated lysis by BiTE antibodies specific for a large melanoma surface antigen. *Cancer Immunology Immunotherapy*, 59, 1197-1209.
- BOCHKOV, Y. A. & PALMENBERG, A. C. 2006. Translational efficiency of EMCV IRES in bicistronic vectors is dependent upon IRES sequence and gene location. *Biotechniques*, 41, 283-4, 286, 288 passim.
- BOHLEN, H., MANZKE, O., PATEL, B., MOLDENHAUER, G., DORKEN, B., VON FLIEDNER, V., DIEHL, V. & TESCH, H. 1993. Cytolysis of leukemic B-cells by T-cells activated via two bispecific antibodies. *Cancer Res*, 53, 4310-4.
- BORTOLETTO, N., SCOTET, E., MYAMOTO, Y., D'ORO, U. & LANZAVECCHIA, A. 2002. Optimizing anti-CD3 affinity for effective T cell targeting against tumor cells. *Eur J Immunol*, 32, 3102-7.
- BOSSE, K. R., & MARIS, J. M. 2016. Advances in the translational genomics of neuroblastoma: From improving risk stratification and revealing novel biology to identifying actionable genomic alterations. *Cancer*, 122, 20-33.

- BRANDL, C., HAAS, C., D'ARGOUGES, S., FISCH, T., KUFER, P., BRISCHWEIN, K., PRANG, N., BARGOU, R., SUZICH, J., BAEUERLE, P. A. & HOFMEISTER, R. 2007. The effect of dexamethasone on polyclonal T cell activation and redirected target cell lysis as induced by a CD19/CD3-bispecific single-chain antibody construct. *Cancer Immunol Immunother*, 56, 1551-63.
- BRESLER, S. C., WEISER, D. A., HUWE, P. J. ET AL. 2014. ALK mutations confer differential oncogenic activation and sensitivity to ALK inhibition therapy in neuroblastoma. . *Cancer cell* , 26, 682-694.
- BRIDGEMAN, J. S., HAWKINS, R. E., BAGLEY, S., BLAYLOCK, M., HOLLAND, M. & GILHAM, D. E. 2010. The optimal antigen response of chimeric antigen receptors harboring the CD3zeta transmembrane domain is dependent upon incorporation of the receptor into the endogenous TCR/CD3 complex. *J Immunol*, 184, 6938-49.
- BRISCHWEIN, K., SCHLERETH, B., GULLER, B., STEIGER, C., WOLF, A., LUTTERBUESE, R., OFFNER, S., LOCHER, M., URBIG, T., RAUM, T., KLEINDIENST, P., WIMBERGER, P., KIMMIG, R., FICHTNER, I., KUFER, P., HOFMEISTER, R., DA SILVA, A. J. & BAEUERLE, P. A. 2006. MT110: a novel bispecific single-chain antibody construct with high efficacy in eradicating established tumors. *Mol Immunol*, 43, 1129-43.
- BRODEUR, G. M., SEEGER, R. C., SCHWAB, M., VARMUS, H. E. & BISHOP, J. M. 1984. Amplification of N-myc in untreated human neuroblastomas correlates with advanced disease stage. *Science*, 224, 1121-4.

- BURNS, G. F., BOYD, A. W. & BEVERLEY, P. C. 1982. Two monoclonal anti-human T lymphocyte antibodies have similar biologic effects and recognize the same cell surface antigen. *J Immunol*, 129, 1451-7.
- BYRNE, H., CONROY, P. J., WHISSTOCK, J. C. & O'KENNEDY, R. J. 2013. A tale of two specificities: bispecific antibodies for therapeutic and diagnostic applications. *Trends Biotechnol*, 31, 621-32.
- CERATO, E., BIRKLE, S., PORTOUKALIAN, J., MEZAZIGH, A., CHATAL, J. F. & AUBRY, J. 1997. Variable region gene segments of nine monoclonal antibodies specific to disialogangliosides (GD2, GD3) and their O-acetylated derivatives. *Hybridoma*, 16, 307-16.
- CHAN, A. C., DALTON, M., JOHNSON, R., KONG, G. H., WANG, T., THOMA, R. & KUROSAKI, T. 1995. Activation of ZAP-70 kinase activity by phosphorylation of tyrosine 493 is required for lymphocyte antigen receptor function. *Embo j*, 14, 2499-508.
- CHANG, H. R., CORDON-CARDO, C., HOUGHTON, A. N., CHEUNG, N. K. & BRENNAN, M. F. 1992. Expression of disialogangliosides GD2 and GD3 on human soft tissue sarcomas. *Cancer*, 70, 633-8.
- CHEEVER, M. A., ALLISON, J. P., FERRIS, A. S., FINN, O. J., HASTINGS, B. M., HECHT, T. T., MELLMAN, I., PRINDIVILLE, S. A., VINER, J. L., WEINER, L. M. & MATRISIAN, L. M. 2009. The prioritization of cancer antigens: a national cancer institute pilot project for the acceleration of translational research. *Clin Cancer Res*, 15, 5323-37.
- CHEN, Y., TAKITA, J., CHOI, Y. L., KATO, M., OHIRA, M., SANADA, M., WANG, L., SODA, M., KIKUCHI, A., IGARASHI, T., NAKAGAWARA,

- A., HAYASHI, Y., MANO, H. & OGAWA, S. 2008. Oncogenic mutations of ALK kinase in neuroblastoma. *Nature*, 455, 971-4.
- CHEUNG, M., AHMED, M., XU, H. & CHEUNG, N. K. 2015. Structural design of disialoganglioside GD2 and CD3-bispecific antibodies to redirect T cells for tumor therapy. *Int J Cancer*, 136, 476-86.
- CHEUNG, M., SANTICH, B. H., XU, H., AHMED, M., HUSE, M. & CHEUNG, N. K. 2016. Successful engineering of a highly potent single-chain variable-fragment (scFv) bispecific antibody to target disialoganglioside (GD2) positive tumors. *Oncoimmunology*, 5, e1168557.
- CHERESH, D. A., PIERSCHBACHER, M. D., HERZIG, M. A. & MUJOO, K. 1986. Disialogangliosides GD2 and GD3 are involved in the attachment of human melanoma and neuroblastoma cells to extracellular matrix proteins. *J Cell Biol*, 102, 688-96.
- CHEUNG, N. K., GUO, H., HU, J., TASSEV, D. V. & CHEUNG, I. Y. 2012. Humanizing murine IgG3 anti-GD2 antibody m3F8 substantially improves antibody-dependent cell-mediated cytotoxicity while retaining targeting in vivo. *Oncoimmunology*, 1, 477-486.
- CHEUNG, N. K., SAARINEN, U. M., NEELY, J. E., LANDMEIER, B., DONOVAN, D. & COCCIA, P. F. 1985. Monoclonal antibodies to a glycolipid antigen on human neuroblastoma cells. *Cancer Res*, 45, 2642-9.
- CHMIELEWSKI, M., HOMBACH, A., HEUSER, C., ADAMS, G. P. & ABKEN, H. 2004. T cell activation by antibody-like immunoreceptors: increase in affinity of the single-chain fragment domain above threshold does not increase T cell

activation against antigen-positive target cells but decreases selectivity. *J Immunol*, 173, 7647-53.

CLARK, M., BINDON, C., DYER, M., FRIEND, P., HALE, G., COBBOLD, S., CALNE, R. & WALDMANN, H. 1989. The improved lytic function and in vivo efficacy of monovalent monoclonal CD3 antibodies. *Eur J Immunol*, 19, 381-8.

CLEMENCEAU, B., VALSESIA-WITTMANN, S., JALLAS, A. C., VIVIEN, R., ROUSSEAU, R., MARABELLE, A., CAUX, C. & VIE, H. 2015. In Vitro and In Vivo Comparison of Lymphocytes Transduced with a Human CD16 or with a Chimeric Antigen Receptor Reveals Potential Off-Target Interactions due to the IgG2 CH2-CH3 CAR-Spacer. *J Immunol Res*, 2015, 482089.

COCHONNEAU, D., TERME, M., MICHAUD, A., DORVILLIUS, M., GAUTIER, N., FRIKECHE, J., ALVAREZ-RUEDA, N., BOUGRAS, G., AUBRY, J., PARIS, F. & BIRKLE, S. 2013. Cell cycle arrest and apoptosis induced by O-acetyl-GD2-specific monoclonal antibody 8B6 inhibits tumor growth in vitro and in vivo. *Cancer Lett*, 333, 194-204.

COLE, D. K., PUMPHREY, N. J., BOULTER, J. M., SAMI, M., BELL, J. I., GOSTICK, E., PRICE, D. A., GAO, G. F., SEWELL, A. K. & JAKOBSEN, B. K. 2007. Human TCR-binding affinity is governed by MHC class restriction. *J Immunol*, 178, 5727-34.

COSSET, F. L., TAKEUCHI, Y., BATTINI, J. L., WEISS, R. A. & COLLINS, M. K. 1995. High-titer packaging cells producing recombinant retroviruses resistant to human serum. *J Virol*, 69, 7430-6.

- CURRAN, K. J., PEGRAM, H. J. & BRENTJENS, R. J. 2012. Chimeric antigen receptors for T cell immunotherapy: current understanding and future directions. *J Gene Med*, 14, 405-15.
- DE BROUWER, S., DE PRETER, K., KUMPS, C., ZABROCKI, P., PORCU, M., WESTERHOUT, E. M., LAKEMAN, A., VANDESOMPELE, J., HOEBEECK, J., VAN MAERKEN, T., DE PAEPE, A., LAUREYS, G., SCHULTE, J. H., SCHRAMM, A., VAN DEN BROECKE, C., VERMEULEN, J., VAN ROY, N., BEISKE, K., RENARD, M., NOGUERA, R., DELATTRE, O., JANOUeix-LEROSEY, I., KOGNER, P., MARTINSSON, T., NAKAGAWARA, A., OHIRA, M., CARON, H., EGGERT, A., COOLS, J., VERSTEEG, R. & SPELEMAN, F. 2010. Meta-analysis of neuroblastomas reveals a skewed ALK mutation spectrum in tumors with MYCN amplification. *Clin Cancer Res*, 16, 4353-62.
- DE VRIES, E., HEINEMANN, V., FIEDLER, W. M., SEUFFERLEIN, T., VERHEUL, H. M., DE GROOT, D., REN, S., CHEUNG, K., RASMUSSEN, E., VOLKLAND, J., MEANS, G., KRATZER, A., WOLDF, A. & STIENEN, S. 2015. Phase I study of AMG 211/MEDI-565 administered as continuous intravenous infusion for relapsed/refractory gastrointestinal (GI) adenocarcinoma. *J Clin Oncol*, 33.
- DEPPISCH, N., RUF, P., EISSLER, N., NEFF, F., BUHMANN, R., LINDHOFER, H. & MOCIKAT, R. 2015. Efficacy and Tolerability of a GD2-Directed Trifunctional Bispecific Antibody in a Preclinical Model: Subcutaneous Administration Is Superior to Intravenous Delivery. *Mol Cancer Ther*, 14, 1877-83.
- DING, Y. Y., PANZER, J., MARIS, J. M., CASTANEDA, A., GOMEZ-CHIARI, M. & MORA, J. 2017. Transverse myelitis as an unexpected complication

following treatment with dinutuximab in pediatric patients with high-risk neuroblastoma: A case series.

DONG, L., LIU, Y., COLBERG-POLEY, A. M., KAUCIC, K. & LADISCH, S. 2011. Induction of GM1a/GD1b synthase triggers complex ganglioside expression and alters neuroblastoma cell behavior; a new tumor cell model of ganglioside function. *Glycoconj J*, 28, 137-47.

DREIER, T., BAEUERLE, P. A., FICHTNER, I., GRUN, M., SCHLERETH, B., LORENCZEWSKI, G., KUFER, P., LUTTERBUSE, R., RIETHMULLER, G., GJORSTRUP, P. & BARGOU, R. C. 2003. T cell costimulus-independent and very efficacious inhibition of tumor growth in mice bearing subcutaneous or leukemic human B cell lymphoma xenografts by a CD19-/CD3- bispecific single-chain antibody construct. *J Immunol*, 170, 4397-402.

DREIER, T., LORENCZEWSKI, G., BRANDL, C., HOFFMANN, P., SYRING, U., HANAKAM, F., KUFER, P., RIETHMULLER, G., BARGOU, R. & BAEUERLE, P. A. 2002. Extremely potent, rapid and costimulation-independent cytotoxic T-cell response against lymphoma cells catalyzed by a single-chain bispecific antibody. *Int J Cancer*, 100, 690-7.

DUNN, G. P., BRUCE, A. T., IKEDA, H., OLD, L. J. & SCHREIBER, R. D. 2002. Cancer immunoediting: from immunosurveillance to tumor escape. *Nat Immunol*, 3, 991-8.

DURBEN, M., SCHMIEDEL, D., HOFMANN, M., VOGT, F., NUBLING, T., PYZ, E., BUHRING, H. J., RAMMENSEE, H. G., SALIH, H. R., GROSSE-HOVEST, L. & JUNG, G. 2015. Characterization of a bispecific FLT3 X CD3 antibody in an improved, recombinant format for the treatment of leukemia. *Mol Ther*, 23, 648-55.

- ERDMANN, M., WIPFLER, D., MERLING, A., CAO, Y., CLAUS, C., KNIEP, B., SADICK, H., BERGLER, W., VLASAK, R. & SCHWARTZ-ALBIEZ, R. 2006. Differential surface expression and possible function of 9-O- and 7-O-acetylated GD3 (CD60 b and c) during activation and apoptosis of human tonsillar B and T lymphocytes. *Glycoconj J*, 23, 627-38.
- FELDMANN, A., ARNDT, C., TOPFER, K., STAMOVA, S., KRONE, F., CARTELLIERI, M., KORISTKA, S., MICHALK, I., LINDEMANN, D., SCHMITZ, M., TEMME, A., BORNHAUSER, M., EHNINGER, G. & BACHMANN, M. 2012. Novel humanized and highly efficient bispecific antibodies mediate killing of prostate stem cell antigen-expressing tumor cells by CD8+ and CD4+ T cells. *J Immunol*, 189, 3249-59.
- FIEDLER, W. M., WOLF, M., KEBENKO, M., GOEBELER, M., RITTER, B., VIESER, E., HIJAZI, Y., PATZAC, I., FRIEDRICH, M., KUFER, P., STANLEY, F., SEGGEWISS-BERNHARDT, R. & KAUBITZSCH, S. 2012. A phase I study of EpCAM/CD3-bispecific antibody (MT110) in patients with advanced solid tumors. *J Clin Oncol* 30, 2504.
- FINNEY, H. M., LAWSON, A. D., BEBBINGTON, C. R. & WEIR, A. N. 1998. Chimeric receptors providing both primary and costimulatory signaling in T cells from a single gene product. *J Immunol*, 161, 2791-7.
- FLEURENCE, J., COCHONNEAU, D., FOUGERAY, S., OLIVER, L., GERALDO, F., TERME, M., DORVILLIUS, M., LOUSSOUARN, D., VALLETTE, F., PARIS, F. & BIRKLE, S. 2016. Targeting and killing glioblastoma with monoclonal antibody to O-acetyl GD2 ganglioside. *Oncotarget*.
- FLEURENCE, J., FOUGERAY, S., BAHRI, M., COCHONNEAU, D., CLEMENCEAU, B., PARIS, F., HECZEY, A. & BIRKLE, S. 2017.

Targeting O-Acetyl-GD2 Ganglioside for Cancer Immunotherapy. 2017, 5604891.

FRIEDMANN-MORVINSKI, D., BENDAVID, A., WAKS, T., SCHINDLER, D. & ESHHAR, Z. 2005. Redirected primary T cells harboring a chimeric receptor require costimulation for their antigen-specific activation. *Blood*, 105, 3087-93.

FRIEDRICH, M., RAUM, T., LUTTERBUESE, R., VOELKEL, M., DEEGEN, P., RAU, D., KISCHEL, R., HOFFMANN, P., BRANDL, C., SCHUHMACHER, J., MUELLER, P., FINNERN, R., FUERGUT, M., ZOPF, D., SLOOTSTRA, J. W., BAEUERLE, P. A., RATTEL, B. & KUFER, P. 2012. Regression of human prostate cancer xenografts in mice by AMG 212/BAY2010112, a novel PSMA/CD3-Bispecific BiTE antibody cross-reactive with non-human primate antigens. *Mol Cancer Ther*, 11, 2664-73.

FURUKAWA, K., HAMAMURA, K., OHKAWA, Y., OHMI, Y. & FURUKAWA, K. 2012. Disialyl gangliosides enhance tumor phenotypes with differential modalities. *Glycoconj J*, 29, 579-84.

FURUKAWA, K., TAKAMIYA, K. & FURUKAWA, K. 2002. Beta1,4-N-acetylgalactosaminyltransferase--GM2/GD2 synthase: a key enzyme to control the synthesis of brain-enriched complex gangliosides. *Biochim Biophys Acta*, 1573, 356-62.

GALON, J., COSTES, A., SANCHEZ-CABO, F., KIRILOVSKY, A., MLECNIK, B., LAGORCE-PAGES, C., TOSOLINI, M., CAMUS, M., BERGER, A., WIND, P., ZINZINDOHOUE, F., BRUNEVAL, P., CUGNENC, P. H., TRAJANOSKI, Z., FRIDMAN, W. H. & PAGES, F. 2006. Type, density, and

location of immune cells within human colorectal tumors predict clinical outcome. *Science*, 313, 1960-4.

GARGETT, T., YU, W., DOTTI, G., YVON, E. S., CHRISTO, S. N., HAYBALL, J. D., LEWIS, I. D., BRENNER, M. K. & BROWN, M. P. 2016. GD2-specific CAR T Cells Undergo Potent Activation and Deletion Following Antigen Encounter but can be Protected From Activation-induced Cell Death by PD-1 Blockade. *Mol Ther*, 24, 1135-49.

GILLIES, S. D., LO, K. M. & WESOLOWSKI, J. 1989. High-level expression of chimeric antibodies using adapted cDNA variable region cassettes. *J Immunol Methods*, 125, 191-202.

GINALDI, L., DE MARTINIS, M., MATUTES, E., FARAHAT, N., MORILLA, R. & CATOVSKY, D. 1998. Levels of expression of CD19 and CD20 in chronic B cell leukaemias. *J Clin Pathol*, 51, 364-9.

GOEBELER, M., VIARDOT, A., KUFER, P., TOPP, M., KNOP, S., MACKENSEN, A. & AL., E. 2013. Final results from a phase 1 study of blinatumomab in patients with relapsed/refractory non-Hodgkin's lymphoma. *Hematol Oncol.*, 31, 302.

GOLDBERGER, O., VOLOVITZ, I., MACHLENKIN, A., VADAI, E., TZEHOVAL, E. & EISENBACH, L. 2008. Exuberated numbers of tumor-specific T cells result in tumor escape. *Cancer Res*, 68, 3450-7.

GRAZIANO, R. F. & GUPTILL, P. 2004. Chemical production of bispecific antibodies. *Methods Mol Biol*, 283, 71-85.

- GRUEN, M., BOMMERT, K. & BARGOU, R. C. 2004. T-cell-mediated lysis of B cells induced by a CD19xCD3 bispecific single-chain antibody is perforin dependent and death receptor independent. *Cancer Immunol Immunother.*, 53, 625-632.
- GUAN, J., UMAPATHY, G., YAMAZAKI, Y., WOLFSTETTER, G., MENDOZA, P., PFEIFER, K., MOHAMMED, A., HUGOSSON, F., ZHANG, H., HSU, A. W., HALENBECK, R., HALLBERG, B. & PALMER, R. H. 2015. FAM150A and FAM150B are activating ligands for anaplastic lymphoma kinase. 4, e09811.
- GUEST, R. D., HAWKINS, R. E., KIRILLOVA, N., CHEADLE, E. J., ARNOLD, J., O'NEILL, A., IRLAM, J., CHESTER, K. A., KEMSHEAD, J. T., SHAW, D. M., EMBLETON, M. J., STERN, P. L. & GILHAM, D. E. 2005. The role of extracellular spacer regions in the optimal design of chimeric immune receptors: evaluation of four different scFvs and antigens. *J Immunother*, 28, 203-11.
- HAAGEN, I. A., GEERARS, A. J., DE LAU, W. B., BAST, B. J. & DE GAST, B. C. 1995. The efficacy of CD3 x CD19 bispecific monoclonal antibody (BsAb) in a clonogenic assay: the effect of repeated addition of BsAb and interleukin-2. *Blood*, 85, 3208-12.
- HAAGEN, I. A., VAN DE GRIEND, R., CLARK, M., GEERARS, A., BAST, B. & DE GAST, B. 1992. Killing of human leukaemia/lymphoma B cells by activated cytotoxic T lymphocytes in the presence of a bispecific monoclonal antibody (alpha CD3/alpha CD19). *Clin Exp Immunol*, 90, 368-75.
- HASO, W., LEE, D. W., SHAH, N. N., STETLER-STEVENSON, M., YUAN, C. M., PASTAN, I. H., DIMITROV, D. S., MORGAN, R. A., FITZGERALD,

- D. J., BARRETT, D. M., WAYNE, A. S., MACKALL, C. L. & ORENTAS, R. J. 2013. Anti-CD22-chimeric antigen receptors targeting B-cell precursor acute lymphoblastic leukemia. *Blood*, 121, 1165-74.
- HERRMANN, I., BAEUERLE, P. A., FRIEDRICH, M., MURR, A., FILUSCH, S., RUTTINGER, D., MAJDOUB, M. W., SHARMA, S., KUFER, P., RAUM, T. & MUNZ, M. 2010. Highly efficient elimination of colorectal tumor-initiating cells by an EpCAM/CD3-bispecific antibody engaging human T cells. *PLoS One*, 5, e13474.
- HERSEY, P., JAMAL, O., HENDERSON, C., ZARDAWI, I. & D'ALESSANDRO, G. 1988. Expression of the gangliosides GM3, GD3 and GD2 in tissue sections of normal skin, naevi, primary and metastatic melanoma. *Int J Cancer*, 41, 336-43.
- HEUSEL, J. W., WESSELSCHMIDT, R. L., SHRESTA, S., RUSSELL, J. H. & LEY, T. J. 1994. Cytotoxic lymphocytes require granzyme B for the rapid induction of DNA fragmentation and apoptosis in allogeneic target cells. *Cell*, 76, 977-87.
- HEXHAM, J. M., DUDAS, D., HUGO, R., THOMPSON, J., KING, V., DOWLING, C., NEVILLE, D. M., JR., DIGAN, M. E. & LAKE, P. 2001. Influence of relative binding affinity on efficacy in a panel of anti-CD3 scFv immunotoxins. *Mol Immunol*, 38, 397-408.
- HIGA, H. H., BUTOR, C., DIAZ, S. & VARKI, A. 1989. O-acetylation and de-O-acetylation of sialic acids. O-acetylation of sialic acids in the rat liver Golgi apparatus involves an acetyl intermediate and essential histidine and lysine residues--a transmembrane reaction? *J Biol Chem*, 264, 19427-34.

- HIPP, S., TAI, Y. T., BLANSET, D., DEEGEN, P., WAHL, J., THOMAS, O., RATTEL, B., ADAM, P. J., ANDERSON, K. C. & FRIEDRICH, M. 2017. A novel BCMA/CD3 bispecific T-cell engager for the treatment of multiple myeloma induces selective lysis in vitro and in vivo. *Leukemia*.
- HOFFMANN, P., HOFMEISTER, R., BRISCHWEIN, K., BRANDL, C., CROMMER, S., BARGOU, R., ITIN, C., PRANG, N. & BAEUERLE, P. A. 2005. Serial killing of tumor cells by cytotoxic T cells redirected with a CD19-/CD3-bispecific single-chain antibody construct. *Int J Cancer*, 115, 98-104.
- HOGAN, P. G., CHEN, L., NARDONE, J. & RAO, A. 2003. Transcriptional regulation by calcium, calcineurin, and NFAT. *Genes Dev*, 17, 2205-32.
- HOMBACH, A., HEUSER, C., GERKEN, M., FISCHER, B., LEWALTER, K., DIEHL, V., POHL, C. & ABKEN, H. 2000. T cell activation by recombinant FcepsilonRI gamma-chain immune receptors: an extracellular spacer domain impairs antigen-dependent T cell activation but not antigen recognition. *Gene Ther*, 7, 1067-75.
- HOMBACH, A., HOMBACH, A. A. & ABKEN, H. 2010. Adoptive immunotherapy with genetically engineered T cells: modification of the IgG1 Fc 'spacer' domain in the extracellular moiety of chimeric antigen receptors avoids 'off-target' activation and unintended initiation of an innate immune response. *Gene Ther*, 17, 1206-13.
- HUANG, M., & WEISS, W. A. 2013. Neuroblastoma and MYCN. *Cold Spring Harbor Perspectives in Medicine*, 3.

- HUANG, X. & YANG, Y. 2016. Driving an improved CAR for cancer immunotherapy. *J Clin Invest*, 126, 2795-8.
- HUDECEK, M., LUPO-STANGHELLINI, M. T., KOSASIH, P. L., SOMMERMEYER, D., JENSEN, M. C., RADER, C. & RIDDELL, S. R. 2013. Receptor affinity and extracellular domain modifications affect tumor recognition by ROR1-specific chimeric antigen receptor T cells. *Clin Cancer Res*, 19, 3153-64.
- HUEHLS, A. M., COUPET, T. A., SENTMAN, C. L. 2015. Bispecific T cell engagers for cancer immunotherapy. *Immunol Cell Biol*, 93, 290-296.
- HUSTON, J. S., LEVINSON, D., MUDGETT-HUNTER, M., TAI, M. S., NOVOTNY, J., MARGOLIES, M. N., RIDGE, R. J., BRUCCOLERI, R. E., HABER, E., CREA, R. & ET AL. 1988. Protein engineering of antibody binding sites: recovery of specific activity in an anti-digoxin single-chain Fv analogue produced in *Escherichia coli*. *Proc Natl Acad Sci U S A*, 85, 5879-83.
- IWAHARA, T., FUJIMOTO, J., WEN, D., CUPPLES, R., BUCAY, N., ARAKAWA, T., MORI, S., RATZKIN, B. & YAMAMOTO, T. 1997. Molecular characterization of ALK, a receptor tyrosine kinase expressed specifically in the nervous system. *Oncogene*, 14, 439-49.
- JACOBS, N., MAZZONI, A., MEZZANZANICA, D., NEGRI, D. R., VALOTA, O., COLNAGHI, M. I., MOUTSCHEN, M. P., BONIVER, J. & CANEVARI, S. 1997. Efficiency of T cell triggering by anti-CD3 monoclonal antibodies (mAb) with potential usefulness in bispecific mAb generation. *Cancer Immunol Immunother*, 44, 257-64.

JANEWAY, C., A., TRAVERS, P., WALPORT, M., SHLOMCHIK, M.J., 2001. Immunobiology. *Garland Science*.

JANOUEIX-LEROSEY, I., LEQUIN, D., BRUGIERES, L., RIBEIRO, A., DE PONTUAL, L., COMBARET, V., RAYNAL, V., PUISIEUX, A., SCHLEIERMACHER, G., PIERRON, G., VALTEAU-COUANET, D., FREBOURG, T., MICHON, J., LYONNET, S., AMIEL, J. & DELATTRE, O. 2008. Somatic and germline activating mutations of the ALK kinase receptor in neuroblastoma. *Nature*, 455, 967-70.

KAILAYANGIRI, S., ALTVATER, B., MELTZER, J., PSCHERER, S., LUECKE, A., DIERKES, C., TITZE, U., LEUCHTE, K., LANDMEIER, S., HOTFILDER, M., DIRKSEN, U., HARDES, J., GOSHEGER, G., JUERGENS, H. & ROSSIG, C. 2012. The ganglioside antigen G(D2) is surface-expressed in Ewing sarcoma and allows for MHC-independent immune targeting. *Br J Cancer*, 106, 1123-33.

KAMERLING, J. P., SCHAUER, R., SHUKLA, A. K., STOLL, S., VAN HALBEEK, H. & VLIEGENTHART, J. F. 1987. Migration of O-acetyl groups in N,O-acetylneuraminic acids. *Eur J Biochem*, 162, 601-7.

KANEKO, T., OKITA, H., NAKAJIMA, H., IJIMA, K., OGASAWARA, N., MIYAGAWA, Y., KATAGIRI, Y. U., NAKAGAWA, A., KIYOKAWA, N., SATO, T. & FUJIMOTO, J. 2010. Neuroblastoma cells can be classified according to glycosphingolipid expression profiles identified by liquid chromatography-tandem mass spectrometry. *Int J Oncol*, 37, 1279-88.

KANTARJIAN, H., STEIN, A., GOKBUGET, N., FIELDING, A. K., SCHUH, A. C., RIBERA, J. M., WEI, A., DOMBRET, H., FOA, R., BASSAN, R., ARSLAN, O., SANZ, M. A., BERGERON, J., DEMIRKAN, F., LECH-

MARANDA, E., RAMBALDI, A., THOMAS, X., HORST, H. A., BRUGGEMANN, M., KLAPPER, W., WOOD, B. L., FLEISHMAN, A., NAGORSEN, D., HOLLAND, C., ZIMMERMAN, Z. & TOPP, M. S. 2017. Blinatumomab versus Chemotherapy for Advanced Acute Lymphoblastic Leukemia. *N Engl J Med*, 376, 836-847.

KAWALEKAR, O. U., O'CONNOR, R. S., FRAIETTA, J. A., GUO, L., MCGETTIGAN, S. E., POSEY, A. D., JR., PATEL, P. R., GUEDAN, S., SCHOLLER, J., KEITH, B., SNYDER, N. W., BLAIR, I. A., MILONE, M. C. & JUNE, C. H. 2016. Distinct Signaling of Coreceptors Regulates Specific Metabolism Pathways and Impacts Memory Development in CAR T Cells. *Immunity*, 44, 380-90.

KERSH, G. J., KERSH, E. N., FREMONT, D. H. & ALLEN, P. M. 1998. High- and low-potency ligands with similar affinities for the TCR: the importance of kinetics in TCR signaling. *Immunity*, 9, 817-26.

KERSHAW, M. H., WESTWOOD, J. A., PARKER, L. L., WANG, G., ESHHAR, Z., MAVROUKAKIS, S. A., WHITE, D. E., WUNDERLICH, J. R., CANEVARI, S., ROGERS-FREEZER, L., CHEN, C. C., YANG, J. C., ROSENBERG, S. A. & HWU, P. 2006. A phase I study on adoptive immunotherapy using gene-modified T cells for ovarian cancer. *Clin Cancer Res*, 12, 6106-15.

KILINC, M. O., AULAKH, K. S., NAIR, R. E., JONES, S. A., ALARD, P., KOSIEWICZ, M. M. & EGILMEZ, N. K. 2006. Reversing tumor immune suppression with intratumoral IL-12: activation of tumor-associated T effector/memory cells, induction of T suppressor apoptosis, and infiltration of CD8+ T effectors. *J Immunol*, 177, 6962-73.

- KIM, C. H., AXUP, J. Y., DUBROVSKA, A., KAZANE, S. A., HUTCHINS, B. A., WOLD, E. D., SMIDER, V. V. & SCHULTZ, P. G. 2012. Synthesis of bispecific antibodies using genetically encoded unnatural amino acids. *J Am Chem Soc*, 134, 9918-21.
- KIPRIYANOV, S. M., MOLDENHAUER, G., MARTIN, A. C., KUPRIYANOVA, O. A. & LITTLE, M. 1997. Two amino acid mutations in an anti-human CD3 single chain Fv antibody fragment that affect the yield on bacterial secretion but not the affinity. *Protein Eng*, 10, 445-53.
- KIPRIYANOV, S. M., MOLDENHAUER, G., SCHUHMACHER, J., COCHLOVIUS, B., VON DER LIETH, C. W., MATYS, E. R. & LITTLE, M. 1999. Bispecific tandem diabody for tumor therapy with improved antigen binding and pharmacokinetics. *J Mol Biol*, 293, 41-56.
- KONERU, M., PURDON, T. J., SPRIGGS, D., KONERU, S. & BRENTJENS, R. J. 2015. IL-12 secreting tumor-targeted chimeric antigen receptor T cells eradicate ovarian tumors in vivo. *Oncoimmunology*, 4, e994446.
- KRAMER, K., GERALD, W. L., KUSHNER, B. H., LARSON, S. M., HAMEED, M. & CHEUNG, N. K. 1998. Disialoganglioside G(D2) loss following monoclonal antibody therapy is rare in neuroblastoma. *Clin Cancer Res*, 4, 2135-9.
- KRISHNAN, C., TWIST, C. J., FU, T. & ARBER, D. A. 2009. Detection of isolated tumor cells in neuroblastoma by immunohistochemical analysis in bone marrow biopsy specimens: improved detection with use of beta-catenin. *Am J Clin Pathol*, 131, 49-57.

- LADENSTEIN, R., POTSCHEGER, U., PEARSON, A. D. J., BROCK, P., LUKSCH, R., CASTEL, V., YANIV, I., PAPADAKIS, V., LAUREYS, G., MALIS, J., BALWIERZ, W., RUUD, E., KOGNER, P., SCHROEDER, H., DE LACERDA, A. F., BECK-POPOVIC, M., BICIAN, P., GARAMI, M., TRAHAIR, T., CANETE, A., AMBROS, P. F., HOLMES, K., GAZE, M., SCHREIER, G., GARAVENTA, A., VASSAL, G., MICHON, J. & VALTEAU-COUANET, D. 2017. Busulfan and melphalan versus carboplatin, etoposide, and melphalan as high-dose chemotherapy for high-risk neuroblastoma (HR-NBL1/SIOPEN): an international, randomised, multi-arm, open-label, phase 3 trial. *Lancet Oncol*, 18, 500-514.
- LAMANT, L., PULFORD, K., BISCHOF, D., MORRIS, S. W., MASON, D. Y., DELSOL, G. & MARIAME, B. 2000. Expression of the ALK tyrosine kinase gene in neuroblastoma. *Am J Pathol*, 156, 1711-21.
- LAMMIE, G., CHEUNG, N., GERALD, W., ROSENBLUM, M. & CORDONCARDO, C. 1993. Ganglioside gd(2) expression in the human nervous-system and in neuroblastomas - an immunohistochemical study. *Int J Oncol*, 3, 909-15.
- LEEVEERS, S. J. & MARSHALL, C. J. 1992. Activation of extracellular signal-regulated kinase, ERK2, by p21ras oncoprotein. *Embo j*, 11, 569-74.
- LEUPIN, O., ZARU, R., LAROCHE, T., MULLER, S. & VALITUTTI, S. 2000. Exclusion of CD45 from the T-cell receptor signaling area in antigen-stimulated T lymphocytes. *Curr Biol*, 10, 277-80.
- LI, R., GAGE, D., MCKALLIP, R. & LADISCH, S. 1996. Structural characterization and in vivo immunosuppressive activity of neuroblastoma GD2. *Glycoconj J*, 13, 385-9.

- LIU, D., SONG, L., WEI, J., COURTNEY, A. N., GAO, X., MARINOVA, E., GUO, L., HECZEY, A., ASGHARZADEH, S., KIM, E., DOTTI, G. & METELITSA, L. S. 2012. IL-15 protects NKT cells from inhibition by tumor-associated macrophages and enhances antimetastatic activity. *J Clin Invest*, 122, 2221-33.
- LODE, H. N., REISFELD, R. A., HANDGRETINGER, R., NICOLAOU, K. C., GAEDICKE, G. & WRASIDLO, W. 1998. Targeted therapy with a novel enediyene antibiotic calicheamicin theta(I)1 effectively suppresses growth and dissemination of liver metastases in a syngeneic model of murine neuroblastoma. *Cancer Res*, 58, 2925-8.
- LONG, A. H., HASO, W. M., SHERN, J. F., WANHAINEN, K. M., MURGAI, M., INGARAMO, M., SMITH, J. P., WALKER, A. J., KOHLER, M. E., VENKATESHWARA, V. R. & KAPLAN, R. N. 2015. 4-1BB costimulation ameliorates T cell exhaustion induced by tonic signaling of chimeric antigen receptors. 21, 581-90.
- LONGEE, D. C., WIKSTRAND, C. J., MANSSON, J. E., HE, X., FULLER, G. N., BIGNER, S. H., FREDMAN, P., SVENNERHOLM, L. & BIGNER, D. D. 1991. Disialoganglioside GD2 in human neuroectodermal tumor cell lines and gliomas. *Acta Neuropathol*, 82, 45-54.
- LOUIS, C. U., SAVOLDO, B., DOTTI, G., PULE, M., YVON, E., MYERS, G. D., ROSSIG, C., RUSSELL, H. V., DIOUF, O., LIU, E., LIU, H., WU, M. F., GEE, A. P., MEI, Z., ROONEY, C. M., HESLOP, H. E. & BRENNER, M. K. 2011. Antitumor activity and long-term fate of chimeric antigen receptor-positive T cells in patients with neuroblastoma. *Blood*, 118, 6050-6.

- LUTTERBUESE, R., RAUM, T., KISCHEL, R., HOFFMANN, P., MANGOLD, S., RATTEL, B., FRIEDRICH, M., THOMAS, O., LORENCZEWSKI, G., RAU, D., SCHALLER, E., HERRMANN, I., WOLF, A., URBIG, T., BAEUERLE, P. A. & KUFER, P. 2010. T cell-engaging BiTE antibodies specific for EGFR potently eliminate KRAS- and BRAF-mutated colorectal cancer cells. *Proc Natl Acad Sci U S A*, 107, 12605-10.
- MAETZIG, T., GALLA, M., BAUM, C. & SCHAMBACH, A. 2011. Gammaretroviral vectors: biology, technology and application. *Viruses*, 3, 677-713.
- MANZKE, O., TITZER, S., TESCH, H., DIEHL, V. & BOHLEN, H. 1997. CD3 x CD19 bispecific antibodies and CD28 costimulation for locoregional treatment of low-malignancy non-Hodgkin's lymphoma. *Cancer Immunol Immunother*, 45, 198-202.
- MARCONI, S., DE TONI, L., LOVATO, L., TEDESCHI, E., GAETTI, L., ACLER, M. & BONETTI, B. 2005. Expression of gangliosides on glial and neuronal cells in normal and pathological adult human brain. *J Neuroimmunol*, 170, 115-21.
- MARIS, J. M. 2010. Recent advances in neuroblastoma. *N Engl J Med*, 362, 2202-11.
- MARIS, J. M., HOGARTY, M. D., BAGATELL, R. & COHN, S. L. 2007. Neuroblastoma. *Lancet*, 369, 2106-20.
- MATSUMOTO, R., WANG, D., BLONSKA, M., LI, H., KOBAYASHI, M., PAPPU, B., CHEN, Y., WANG, D. & LIN, X. 2005. Phosphorylation of CARMA1 plays a critical role in T Cell receptor-mediated NF-kappaB activation. *Immunity*, 23, 575-85.

- MATSUSHITA, H., VESELY, M. D., KOBOLDT, D. C., RICKERT, C. G., UPPALURI, R., MAGRINI, V. J., ARTHUR, C. D., WHITE, J. M., CHEN, Y. S., SHEA, L. K., HUNDAL, J., WENDL, M. C., DEMETER, R., WYLIE, T., ALLISON, J. P., SMYTH, M. J., OLD, L. J., MARDIS, E. R. & SCHREIBER, R. D. 2012. Cancer exome analysis reveals a T-cell-dependent mechanism of cancer immunoediting. *Nature*, 482, 400-4.
- MAUDE, S. L., FREY, N., SHAW, P. A., APLENC, R., BARRETT, D. M., BUNIN, N. J., CHEW, A., GONZALEZ, V. E., ZHENG, Z., LACEY, S. F., MAHNKE, Y. D., MELENHORST, J. J., RHEINGOLD, S. R., SHEN, A., TEACHEY, D. T., LEVINE, B. L., JUNE, C. H., PORTER, D. L. & GRUPP, S. A. 2014. Chimeric antigen receptor T cells for sustained remissions in leukemia. *N Engl J Med*, 371, 1507-17.
- MAZOR, Y., HANSEN, A., YANG, C., CHOWDHURY, P. S., WANG, J., STEPHENS, G., WU, H. & DALL'ACQUA, W. F. 2015. Insights into the molecular basis of a bispecific antibody's target selectivity. *MAbs*, 7, 461-9.
- MAZOR, Y., SACHSENMEIER, K. F., YANG, C. ET AL. 2017. Enhanced tumor-targeting selectivity by modulating bispecific antibody binding affinity and format valence. . *Scientific Reports*, 7.
- MCCALL, A. M., SHAHIED, L., AMOROSO, A. R., HORAK, E. M., SIMMONS, H. H., NIELSON, U., ADAMS, G. P., SCHIER, R., MARKS, J. D. & WEINER, L. M. 2001. Increasing the affinity for tumor antigen enhances bispecific antibody cytotoxicity. *J Immunol*, 166, 6112-7.
- MEDZHITOV, R. & JANEWAY, C. A., JR. 2002. Decoding the patterns of self and nonself by the innate immune system. *Science*, 296, 298-300.

- MEITAR, D., CRAWFORD, S. E., RADEMAKER, A. W. & COHN, S. L. 1996. Tumor angiogenesis correlates with metastatic disease, N-myc amplification, and poor outcome in human neuroblastoma. *J Clin Oncol*, 14, 405-14.
- MERRY, A. H., GILBERT, R. J., SHORE, D. A., ROYLE, L., MIROSHNYCHENKO, O., VUONG, M., WORMALD, M. R., HARVEY, D. J., DWEK, R. A., CLASSON, B. J., RUDD, P. M. & DAVIS, S. J. 2003. O-glycan sialylation and the structure of the stalk-like region of the T cell co-receptor CD8. *J Biol Chem*, 278, 27119-28.
- MICHAELSON, J. S., DEMAREST, S. J., MILLER, B., AMATUCCI, A., SNYDER, W. B., WU, X., HUANG, F., PHAN, S., GAO, S., DOERN, A., FARRINGTON, G. K., LUGOVSKOY, A., JOSEPH, I., BAILLY, V., WANG, X., GARBER, E., BROWNING, J. & GLASER, S. M. 2009. Anti-tumor activity of stability-engineered IgG-like bispecific antibodies targeting TRAIL-R2 and LTbetaR. *MAbs*, 1, 128-41.
- MICKAËL TERME, M. D., DENIS COCHONNEAU, TANGUY CHAUMETTE, WENHUA XIAO, MITCHELL B. DICCIANNI, JACQUES BARBET, ALICE L. YU, FRANÇOIS PARIS, LINDA S. SORKIN, STÉPHANE BIRKLÉ 2014. Chimeric Antibody c.8B6 to O-Acetyl-GD2 Mediates the Same Efficient Anti-Neuroblastoma Effects as Therapeutic ch14.18 Antibody to GD2 without Antibody Induced Allodynia. *PLoS One*, 9, e87210.
- MILSTEIN, C. & CUELLO, A. C. 1983. Hybrid hybridomas and their use in immunohistochemistry. *Nature*, 305, 537-40.
- MONKS, C. R., FREIBERG, B. A., KUPFER, H., SCIAKY, N. & KUPFER, A. 1998. Three-dimensional segregation of supramolecular activation clusters in T cells. *Nature*, 395, 82-6.

- MOON, E. K., WANG, L. C., DOLFI, D. V., WILSON, C. B., RANGANATHAN, R., SUN, J., KAPOOR, V., SCHOLLER, J., PURE, E., MILONE, M. C., JUNE, C. H., RILEY, J. L., WHERRY, E. J. & ALBELDA, S. M. 2014. Multifactorial T-cell hypofunction that is reversible can limit the efficacy of chimeric antigen receptor-transduced human T cells in solid tumors. *Clin Cancer Res*, 20, 4262-73.
- MORITZ, D. & GRONER, B. 1995. A spacer region between the single chain antibody- and the CD3 zeta-chain domain of chimeric T cell receptor components is required for efficient ligand binding and signaling activity. *Gene Ther*, 2, 539-46.
- MORRIS, S. W., KIRSTEIN, M. N., VALENTINE, M. B., DITTMER, K., SHAPIRO, D. N., LOOK, A. T. & SALTMAN, D. L. 1994. Fusion of a kinase gene, ALK, to a nucleolar protein gene, NPM, in non-Hodgkin's lymphoma. *Science*, 267, 316-7.
- MOSSE, Y. P., LAUDENSLAGER, M., LONGO, L., COLE, K. A., WOOD, A., ATTIYEH, E. F., LAQUAGLIA, M. J., SENNETT, R., LYNCH, J. E., PERRI, P., LAUREYS, G., SPELEMAN, F., KIM, C., HOU, C., HAKONARSON, H., TORKAMANI, A., SCHORK, N. J., BRODEUR, G. M., TONINI, G. P., RAPPAPORT, E., DEVOTO, M. & MARIS, J. M. 2008. Identification of ALK as a major familial neuroblastoma predisposition gene. *Nature*, 455, 930-5.
- MUJOO, K., CHERESH, D. A., YANG, H. M. & REISFELD, R. A. 1987. Disialoganglioside GD2 on human neuroblastoma cells: target antigen for monoclonal antibody-mediated cytotoxicity and suppression of tumor growth. *Cancer Res*, 47, 1098-104.

- MUJOO, K., KIPPS, T. J., YANG, H. M., CHERESH, D. A., WARGALLA, U., SANDER, D. J. & REISFELD, R. A. 1989. Functional properties and effect on growth suppression of human neuroblastoma tumors by isotype switch variants of monoclonal antiganglioside GD2 antibody 14.18. *Cancer Res*, 49, 2857-61.
- MUKHERJEE, K., CHOWDHURY, S., MONDAL, S., MANDAL, C., CHANDRA, S., BHADRA, R. K. & MANDAL, C. 2007. 9-O-acetylated GD3 triggers programmed cell death in mature erythrocytes. *Biochem Biophys Res Commun*, 362, 651-7.
- MUSSAI, F., EGAN, S., HUNTER, S., ET AL. 2015. Neuroblastoma arginase activity creates an immunosuppressive microenvironment that impairs autologous and engineered immunity. . *Cancer research.*, 75, 3043-3053.
- NAGORSEN, D., KUFER, P., BAEUERLE, P. A. & BARGOU, R. 2012. Blinatumomab: a historical perspective. *Pharmacol Ther*, 136, 334-42.
- NAITO, T., TANAKA, H., NAOE, Y. & TANIUCHI, I. 2011. Transcriptional control of T-cell development. *Int Immunol*, 23, 661-8.
- NAITO, Y., SAITO, K., SHIIBA, K., OHUCHI, A., SAIGENJI, K., NAGURA, H. & OHTANI, H. 1998. CD8+ T cells infiltrated within cancer cell nests as a prognostic factor in human colorectal cancer. *Cancer Res*, 58, 3491-4.
- NAKAMURA, K., TANAKA, Y., SHITARA, K. & HANAI, N. 2001. Construction of humanized anti-ganglioside monoclonal antibodies with potent immune effector functions. *Cancer Immunol Immunother*, 50, 275-84.

- NIESEN, F. H., BERGLUND, H. & VEDADI, M. 2007. The use of differential scanning fluorimetry to detect ligand interactions that promote protein stability. *Nat Protoc*, 2, 2212-21.
- OFFRINGA, R. 2009. Antigen choice in adoptive T-cell therapy of cancer. *Curr Opin Immunol*, 21, 190-9.
- ORSI, G., BARBOLINI, M. & FICARRA, G. E. A. 2017. GD2 expression in breast cancer. *Oncotarget*, 8.
- OTTO, T., HORN, S., BROCKMANN, M., EILERS, U., SCHUTTRUMPF, L., POPOV, N., KENNEY, A. M., SCHULTE, J. H., BEIJERSBERGEN, R., CHRISTIANSEN, H., BERWANGER, B. & EILERS, M. 2009. Stabilization of N-Myc is a critical function of Aurora A in human neuroblastoma. *Cancer Cell*, 15, 67-78.
- PASTORINO, F., BRIGNOLE, C., LOI, M., DI PAOLO, D., DI FIORE, A., PERRI, P., PAGNAN, G. & PONZONI, M. 2013. Nanocarrier-mediated targeting of tumor and tumor vascular cells improves uptake and penetration of drugs into neuroblastoma. *Front Oncol*, 3, 190.
- PEREZ-PINERA, P., ZHANG, W., CHANG, Y., VEGA, J.A., DEUEL, T.F. 2007. Anaplastic lymphoma kinase is activated through the pleiotrophin/receptor protein-tyrosine phosphatase beta/zeta signaling pathway: an alternative mechanism of receptor tyrosine kinase activation. *J Biol Chem*, 282, 28683-90.
- POON, V. I., ROTH, M., PIPERDI, S., GELLER, D., GILL, J., RUDZINSKI, E. R., HAWKINS, D. S. & GORLICK, R. 2015. Ganglioside GD2 expression is

maintained upon recurrence in patients with osteosarcoma. *Clin Sarcoma Res*, 5, 4.

PRAPA, M., CALDRER, S., SPANO, C., BESTAGNO, M., GOLINELLI, G., GRISENDI, G., PETRACHI, T., CONTE, P., HORWITZ, E. M., CAMPANA, D., PAOLUCCI, P. & DOMINICI, M. 2015. A novel anti-GD2/4-1BB chimeric antigen receptor triggers neuroblastoma cell killing. *Oncotarget*, 6, 24884-94.

PULE, M. A., SAVOLDO, B., MYERS, G. D., ROSSIG, C., RUSSELL, H. V., DOTTI, G., HULS, M. H., LIU, E., GEE, A. P., MEI, Z., YVON, E., WEISS, H. L., LIU, H., ROONEY, C. M., HESLOP, H. E. & BRENNER, M. K. 2008. Virus-specific T cells engineered to coexpress tumor-specific receptors: persistence and antitumor activity in individuals with neuroblastoma. *Nat Med*, 14, 1264-70.

RAFFAGHELLO, L., PRIGIONE, I., AIROLDI, I., CAMORIANO, M., LEVRERI, I., GAMBINI, C., PENDE, D., STEINLE, A., FERRONE, S. & PISTOIA, V. 2004. Downregulation and/or release of NKG2D ligands as immune evasion strategy of human neuroblastoma. *Neoplasia*, 6, 558-68.

RAFFAGHELLO, L., PRIGIONE, I., AIROLDI, I., CAMORIANO, M., MORANDI, F., BOCCA, P., GAMBINI, C., FERRONE, S. & PISTOIA, V. 2005. Mechanisms of immune evasion of human neuroblastoma. *Cancer Lett*, 228, 155-61.

RIVIERE, I., BROSE, K. & MULLIGAN, R. C. 1995. Effects of retroviral vector design on expression of human adenosine deaminase in murine bone marrow transplant recipients engrafted with genetically modified cells. *Proc Natl Acad Sci U S A*, 92, 6733-7.

- RODRIGUEZ, P. C., QUICENO, D. G. & OCHOA, A. C. 2007. L-arginine availability regulates T-lymphocyte cell-cycle progression. *Blood*, 109, 1568-73.
- ROUTLEDGE, E. G., LLOYD, I., GORMAN, S. D., CLARK, M. & WALDMANN, H. 1991. A humanized monovalent CD3 antibody which can activate homologous complement. *Eur J Immunol*, 21, 2717-25.
- ROUX, K. H., STRELETS, L. & MICHAELSEN, T. E. 1997. Flexibility of human IgG subclasses. *J Immunol*, 159, 3372-82.
- RUELLA, M. & GILL, S. 2015. How to train your T cell: genetically engineered chimeric antigen receptor T cells versus bispecific T-cell engagers to target CD19 in B acute lymphoblastic leukemia. *Expert Opin Biol Ther*, 15, 761-6.
- RUF, P., SCHAFER, B., EISSLER, N., MOCIKAT, R., HESS, J., PLOSCHER, M., WOSCH, S., SUCKSTORFF, I., ZEHETMEIER, C. & LINDHOFER, H. 2012. Ganglioside GD2-specific trifunctional surrogate antibody Surek demonstrates therapeutic activity in a mouse melanoma model. *J Transl Med*, 10, 219.
- SARIOLA, H., TERAHA, H., RAPOLA, J. & SAARINEN, U. M. 1991. Cell-surface ganglioside GD2 in the immunohistochemical detection and differential diagnosis of neuroblastoma. *Am J Clin Pathol*, 96, 248-52.
- SATO, E., OLSON, S. H., AHN, J., BUNDY, B., NISHIKAWA, H., QIAN, F., JUNGBLUTH, A. A., FROSINA, D., GNJATIC, S., AMBROSONE, C., KEPNER, J., ODUNSI, T., RITTER, G., LELE, S., CHEN, Y. T., OHTANI, H., OLD, L. J. & ODUNSI, K. 2005. Intraepithelial CD8+ tumor-infiltrating lymphocytes and a high CD8+/regulatory T cell ratio are associated with

favorable prognosis in ovarian cancer. *Proc Natl Acad Sci U S A*, 102, 18538-43.

SCARFO, I. & MAUS, M. V. 2017. Current approaches to increase CAR T cell potency in solid tumors: targeting the tumor microenvironment. *J Immunother Cancer*, 5, 28.

SCHREIBER, R. D., OLD, L. J. & SMYTH, M. J. 2011. Cancer immunoediting: integrating immunity's roles in cancer suppression and promotion. *Science*, 331, 1565-70.

SCHULZ, G., CHERESH, D. A., VARKI, N. M., YU, A., STAFFILENO, L. K. & REISFELD, R. A. 1984. Detection of ganglioside GD2 in tumor tissues and sera of neuroblastoma patients. *Cancer Res*, 44, 5914-20.

SCHUMACHER-KUCKELKORN, R., HERO, B., ERNESTUS, K. & BERTHOLD, F. 2005. Lacking immunocytological GD2 expression in neuroblastoma: report of 3 cases. *Pediatr Blood Cancer*, 45, 195-201.

SCHUMACHER-KUCKELKORN, R., VOLLAND, R., GRADEHANDT, A., HERO, B., SIMON, T. & BERTHOLD, F. 2017. Lack of immunocytological GD2 expression on neuroblastoma cells in bone marrow at diagnosis, during treatment, and at recurrence. *Pediatr Blood Cancer*, 64, 46-56.

SCHWARTZBERG, P. L., FINKELSTEIN, L. D. & READINGER, J. A. 2005. TEC-family kinases: regulators of T-helper-cell differentiation. *Nat Rev Immunol*, 5, 284-95.

SCIMONE, M. L., AIFANTIS, I., APOSTOLOU, I., VON BOEHMER, H. & VON ANDRIAN, U. H. 2006. A multistep adhesion cascade for lymphoid

progenitor cell homing to the thymus. *Proc Natl Acad Sci U S A*, 103, 7006-11.

SCOTT, A. M., WOLCHOK, J. D. & OLD, L. J. 2012. Antibody therapy of cancer. *Nat Rev Cancer*, 12, 278-87.

SEEGER, R. C., BRODEUR, G. M., SATHER, H., DALTON, A., SIEGEL, S. E., WONG, K. Y. & HAMMOND, D. 1985. Association of multiple copies of the N-myc oncogene with rapid progression of neuroblastomas. *N Engl J Med*, 313, 1111-6.

SEIMETZ, D., LINDHOFER, H. & BOKEMEYER, C. 2010. Development and approval of the trifunctional antibody catumaxomab (anti-EpCAM x anti-CD3) as a targeted cancer immunotherapy. *Cancer Treat Rev*, 36, 458-67.

SEN, M., WANKOWSKI, D. M., GARLIE, N. K., SIEBENLIST, R. E., VAN EPPS, D., LEFEVER, A. V. & LUM, L. G. 2001. Use of anti-CD3 x anti-HER2/neu bispecific antibody for redirecting cytotoxicity of activated T cells toward HER2/neu+ tumors. *J Hematother Stem Cell Res*, 10, 247-60.

SHALABY, M. R., SHEPARD, H. M., PRESTA, L., RODRIGUES, M. L., BEVERLEY, P. C., FELDMANN, M. & CARTER, P. 1992. Development of humanized bispecific antibodies reactive with cytotoxic lymphocytes and tumor cells overexpressing the HER2 protooncogene. *J Exp Med*, 175, 217-25.

SHIBUYA, H., HAMAMURA, K., HOTTA, H., MATSUMOTO, Y., NISHIDA, Y., HATTORI, H., FURUKAWA, K., UEDA, M. & FURUKAWA, K. 2012. Enhancement of malignant properties of human osteosarcoma cells with disialyl gangliosides GD2/GD3. *Cancer Sci*, 103, 1656-64.

- SIEBERT, H. C., LIETH, C., DONG, X ET AL. 1996. Molecular dynamics-derived conformation and intramolecular interaction analysis of the N-acetyl-9-O-acetylneuraminic acid-containing ganglioside GD1a and NMR-based analysis of its binding to a human polyclonal immunoglobulin G fraction with selectivity for O-acetylated sialic acids. *Glycobiology*, 6, 561-572.
- SJOBERG, E. R., MANZI, A. E., KHOO, K. H., DELL, A. & VARKI, A. 1992. Structural and immunological characterization of O-acetylated GD2. Evidence that GD2 is an acceptor for ganglioside O-acetyltransferase in human melanoma cells. *J Biol Chem*, 267, 16200-11.
- SMITH, M. A., SEIBEL, N. L., ALTEKRUSE, S. F., RIES, L. A. G., MELBERT, D. L., O'LEARY, M., REAMAN, G. H. 2010. Outcomes for Children and Adolescents With Cancer: Challenges for the Twenty-First Century. *Journal of Clinical Oncology*, 28, 2625-2634.
- SODA, M., CHOI, Y. L., ENOMOTO, M., TAKADA, S., YAMASHITA, Y., ISHIKAWA, S., FUJIWARA, S., WATANABE, H., KURASHINA, K., HATANAKA, H., BANDO, M., OHNO, S., ISHIKAWA, Y., ABURATANI, H., NIKI, T., SOHARA, Y., SUGIYAMA, Y. & MANO, H. 2007. Identification of the transforming EML4-ALK fusion gene in non-small-cell lung cancer. *Nature*, 448, 561-6.
- SONAWANE, P., CHO, H. E., TAGDE, A., VERLEKAR, D., YU, A. L., REYNOLDS, C. P., & KANG, M. H. 2014. Metabolic characteristics of 13-cis-retinoic acid (isotretinoin) and anti-tumour activity of the 13-cis-retinoic acid metabolite 4-oxo-13-cis-retinoic acid in neuroblastoma. *British Journal of Pharmacology*, 171, 5330-5344.

SORKIN, L. S., OTTO, M., BALDWIN, W. M., 3RD, VAIL, E., GILLIES, S. D., HANDGRETINGER, R., BARFIELD, R. C., MING YU, H. & YU, A. L. 2010. Anti-GD(2) with an FC point mutation reduces complement fixation and decreases antibody-induced allodynia. *Pain*, 149, 135-42.

SOTILLO, E., BARRETT, D. M., BLACK, K. L., BAGASHEV, A., OLDRIDGE, D., WU, G., SUSSMAN, R., LANAUZE, C., RUELLA, M., GAZZARA, M. R., MARTINEZ, N. M., HARRINGTON, C. T., CHUNG, E. Y., PERAZZELLI, J., HOFMANN, T. J., MAUDE, S. L., RAMAN, P., BARRERA, A., GILL, S., LACEY, S. F., MELENHORST, J. J., ALLMAN, D., JACOBY, E., FRY, T., MACKALL, C., BARASH, Y., LYNCH, K. W., MARIS, J. M., GRUPP, S. A. & THOMAS-TIKHONENKO, A. 2015. Convergence of Acquired Mutations and Alternative Splicing of CD19 Enables Resistance to CART-19 Immunotherapy. *Cancer Discov*, 5, 1282-95.

STONE, J. D., AGGEN, D. H., SCHIETINGER, A., SCHREIBER, H. & KRANZ, D. M. 2012. A sensitivity scale for targeting T cells with chimeric antigen receptors (CARs) and bispecific T-cell Engagers (BiTEs). *Oncoimmunology*, 1, 863-873.

SUZUKI, M. & CHEUNG, N. K. 2015. Disialoganglioside GD2 as a therapeutic target for human diseases. *Expert Opin Ther Targets*, 19, 349-62.

SVENNERHOLM, L., BOSTROM, K., FREDMAN, P., JUNGBJER, B., LEKMAN, A., MANSSON, J. E. & RYNMARK, B. M. 1994. Gangliosides and allied glycosphingolipids in human peripheral nerve and spinal cord. *Biochim Biophys Acta*, 1214, 115-23.

SVENNERHOLM, L., BOSTROM, K., FREDMAN, P., MANSSON, J. E., ROSENGREN, B. & RYNMARK, B. M. 1989. Human brain gangliosides:

developmental changes from early fetal stage to advanced age. *Biochim Biophys Acta*, 1005, 109-17.

SZYMCZAK, A. L., WORKMAN, C. J., WANG, Y., VIGNALI, K. M., DILIOGLOU, S., VANIN, E. F. & VIGNALI, D. A. 2004. Correction of multi-gene deficiency in vivo using a single 'self-cleaving' 2A peptide-based retroviral vector. *Nat Biotechnol*, 22, 589-94.

TEMIN, H. M. & MIZUTANI, S. 1970. RNA-dependent DNA polymerase in virions of Rous sarcoma virus. *Nature*, 226, 1211-3.

THOMAS, P. B., DELATTE, S. J., SUTPHIN, A., FRANKEL, A. E. & TAGGE, E. P. 2002. Effective targeted cytotoxicity of neuroblastoma cells. *J Pediatr Surg*, 37, 539-44.

THOMAS, S., STRAATHOF, K., HIMOUDI, N., ANDERSON, J. & PULE, M. 2016. An Optimized GD2-Targeting Retroviral Cassette for More Potent and Safer Cellular Therapy of Neuroblastoma and Other Cancers. *PLoS One*, 11, e0152196.

TILL, B. G., JENSEN, M. C., WANG, J., CHEN, E. Y., WOOD, B. L., GREISMAN, H. A., QIAN, X., JAMES, S. E., RAUBITSCHKE, A., FORMAN, S. J., GOPAL, A. K., PAGEL, J. M., LINDGREN, C. G., GREENBERG, P. D., RIDDELL, S. R. & PRESS, O. W. 2008. Adoptive immunotherapy for indolent non-Hodgkin lymphoma and mantle cell lymphoma using genetically modified autologous CD20-specific T cells. *Blood*, 112, 2261-71.

TOPP, M. S., GOKBUGET, N., ZUGMAIER, G., KLAPPERS, P., STELLJES, M., NEUMANN, S., VIARDOT, A., MARKS, R., DIEDRICH, H., FAUL, C., REICHLER, A., HORST, H. A., BRUGGEMANN, M., WESSIEPE, D.,

- HOLLAND, C., ALEKAR, S., MERGEN, N., EINSELE, H., HOELZER, D. & BARGOU, R. C. 2014. Phase II trial of the anti-CD19 bispecific T cell-engager blinatumomab shows hematologic and molecular remissions in patients with relapsed or refractory B-precursor acute lymphoblastic leukemia. *J Clin Oncol*, 32, 4134-40.
- TWEDDLE, D. A., MALCOLM, A. J., COLE, M., PEARSON, A. D. & LUNEC, J. 2001. p53 cellular localization and function in neuroblastoma: evidence for defective G(1) arrest despite WAF1 induction in MYCN-amplified cells. *Am J Pathol*, 158, 2067-77.
- VALITUTTI, S. 2012. The Serial Engagement Model 17 Years After: From TCR Triggering to Immunotherapy. *Front Immunol*, 3, 272.
- VAN DER MERWE, P. A. & DAVIS, S. J. 2003. Molecular interactions mediating T cell antigen recognition. *Annu Rev Immunol*, 21, 659-84.
- VAN HOUT, I. S., SLUIJTER, B. J., MOESBERGEN, L. M., VOS, W. M., DE GRUIJL, T. D., MOLENKAMP, B. G., VAN DEN EERTWEGH, A. J., HOOIJBERG, E., VAN LEEUWEN, P. A., MEIJER, C. J. & OUDEJANS, J. J. 2008. Favorable outcome in clinically stage II melanoma patients is associated with the presence of activated tumor infiltrating T-lymphocytes and preserved MHC class I antigen expression. *Int J Cancer*, 123, 609-15.
- VAN WAUWE, J. P., DE MEY, J. R. & GOOSSENS, J. G. 1980. OKT3: a monoclonal anti-human T lymphocyte antibody with potent mitogenic properties. *J Immunol*, 124, 2708-13.
- VAN WAUWE, J. P., GOOSSENS, J. G. & BEVERLEY, P. C. 1984. Human T lymphocyte activation by monoclonal antibodies; OKT3, but not UCHT1,

triggers mitogenesis via an interleukin 2-dependent mechanism. *J Immunol*, 133, 129-32.

VARMA, R., CAMPI, G., YOKOSUKA, T., SAITO, T. & DUSTIN, M. L. 2006. T cell receptor-proximal signals are sustained in peripheral microclusters and terminated in the central supramolecular activation cluster. *Immunity*, 25, 117-27.

VERNERSSON, E., KHOO, N. K., HENRIKSSON, M. L., ROOS, G., PALMER, R. H. & HALLBERG, B. 2006. Characterization of the expression of the ALK receptor tyrosine kinase in mice. *Gene Expr Patterns*, 6, 448-61.

VON BOEHMER, H. & FEHLING, H. J. 1997. Structure and function of the pre-T cell receptor. *Annu Rev Immunol*, 15, 433-52.

VON BOEHMER, H., TEH, H. S. & KISIELOW, P. 1989. The thymus selects the useful, neglects the useless and destroys the harmful. *Immunol Today*, 10, 57-61.

VON BOEHMER, L., MATTLE, M., BODE, P., LANDSHAMMER, A., SCHAFFER, C., NUBER, N., RITTER, G., OLD, L., MOCH, H., SCHAFFER, N., JAGER, E., KNUTH, A. & VAN DEN BROEK, M. 2013. NY-ESO-1-specific immunological pressure and escape in a patient with metastatic melanoma. *Cancer Immun*, 13, 12.

WALKER, A. J., MAJZNER, R. G., ZHANG, L., WANHAINEN, K., LONG, A. H., NGUYEN, S. M., LOPOMO, P., VIGNY, M., FRY, T. J., ORENTAS, R. J. & MACKALL, C. L. 2017. Tumor Antigen and Receptor Densities Regulate Efficacy of a Chimeric Antigen Receptor Targeting Anaplastic Lymphoma Kinase. *Mol Ther*.

- WEIJTENS, M. E., HART, E. H. & BOLHUIS, R. L. 2000. Functional balance between T cell chimeric receptor density and tumor associated antigen density: CTL mediated cytotoxicity and lymphokine production. *Gene Ther*, 7, 35-42.
- WEISS, W. A., ALDAPE, K., MOHAPATRA, G., FEUERSTEIN, B. G. & BISHOP, J. M. 1997. Targeted expression of MYCN causes neuroblastoma in transgenic mice. *Embo j*, 16, 2985-95.
- WELLSTEIN, A. & TORETSKY, J. A. 2011. Hunting ALK to feed targeted cancer therapy. *Nat Med*, 17, 290-1.
- WILLUDA, J., HONEGGER, A., WAIBEL, R., SCHUBIGER, P. A., STAHEL, R., ZANGEMEISTER-WITTKE, U. & PLUCKTHUN, A. 1999. High thermal stability is essential for tumor targeting of antibody fragments: engineering of a humanized anti-epithelial glycoprotein-2 (epithelial cell adhesion molecule) single-chain Fv fragment. *Cancer Res*, 59, 5758-67.
- WU, L., BERNARD-TRIFILO, J. A., LIM, Y., LIM, S. T., MITRA, S. K., URYU, S., CHEN, M., PALLEEN, C. J., CHEUNG, N. K., MIKOLON, D., MIELGO, A., STUPACK, D. G. & SCHLAEPFER, D. D. 2008. Distinct FAK-Src activation events promote alpha5beta1 and alpha4beta1 integrin-stimulated neuroblastoma cell motility. *Oncogene*, 27, 1439-48.
- WU, Z. L., SCHWARTZ, E., SEEGER, R. & LADISCH, S. 1986. Expression of GD2 ganglioside by untreated primary human neuroblastomas. *Cancer Res*, 46, 440-3.
- YAMASHIRO, S., RUAN, S., FURUKAWA, K., TAI, T., LLOYD, K. O., SHIKU, H. & FURUKAWA, K. 1993. Genetic and enzymatic basis for the differential

expression of GM2 and GD2 gangliosides in human cancer cell lines. *Cancer Res*, 53, 5395-400.

YANKELEVICH, M., KONDADASULA, S. V., THAKUR, A., BUCK, S., CHEUNG, N. K. & LUM, L. G. 2012. Anti-CD3 x anti-GD2 bispecific antibody redirects T-cell cytolytic activity to neuroblastoma targets. *Pediatr Blood Cancer*, 59, 1198-205.

YE, J. N. & CHEUNG, N. K. 1992. A novel O-acetylated ganglioside detected by anti-GD2 monoclonal antibodies. *Int J Cancer*, 50, 197-201.

YOSHIDA, S., FUKUMOTO, S., KAWAGUCHI, H., SATO, S., UEDA, R. & FURUKAWA, K. 2001. Ganglioside G(D2) in small cell lung cancer cell lines: enhancement of cell proliferation and mediation of apoptosis. *Cancer Res*, 61, 4244-52.

YOSHIDA, S., KOBAYASHI, T., MATSUOKA, H., SEKI, C., GOSNELL, W. L., CHANG, S. P. & ISHII, A. 2003. T-cell activation and cytokine production via a bispecific single-chain antibody fragment targeted to blood-stage malaria parasites. *Blood*, 101, 2300-6.

YU, A. L., GILMAN, A. L., OZKAYNAK, M. F., LONDON, W. B., KREISSMAN, S. G., CHEN, H. X., SMITH, M., ANDERSON, B., VILLABLANCA, J. G., MATTHAY, K. K., SHIMADA, H., GRUPP, S. A., SEEGER, R., REYNOLDS, C. P., BUXTON, A., REISFELD, R. A., GILLIES, S. D., COHN, S. L., MARIS, J. M. & SONDEL, P. M. 2010. Anti-GD2 antibody with GM-CSF, interleukin-2, and isotretinoin for neuroblastoma. *N Engl J Med*, 363, 1324-34.

- YUAN, H., WEI, X., ZHANG, G., LI, C., ZHANG, X. & HOU, J. 2011. B7-H3 over expression in prostate cancer promotes tumor cell progression. *J Urol*, 186, 1093-9.
- YUKI, N., YAMADA, M., TAGAWA, Y., TAKAHASHI, H. & HANDA, S. 1997. Pathogenesis of the neurotoxicity caused by anti-GD2 antibody therapy. *J Neurol Sci*, 149, 127-30.
- ZAIZEN, Y., TANIGUCHI, S., NOGUCHI, S. & SUITA, S. 1993. The effect of N-myc amplification and expression on invasiveness of neuroblastoma cells. *J Pediatr Surg*, 28, 766-9.
- ZEA, A. H., RODRIGUEZ, P. C., CULOTTA, K. S., HERNANDEZ, C. P., DESALVO, J., OCHOA, J. B., PARK, H. J., ZABALETA, J. & OCHOA, A. C. 2004. L-Arginine modulates CD3zeta expression and T cell function in activated human T lymphocytes. *Cell Immunol*, 232, 21-31.
- ZHOU, J., CHEN, J., ZHONG, R., MOKOTOFF, M., SHULTZ, L. D. & BALL, E. D. 2006. Targeting gastrin-releasing peptide receptors on small cell lung cancer cells with a bispecific molecule that activates polyclonal T lymphocytes. *Clin Cancer Res*, 12, 2224-31.